Transfert d'électrons dans le photosystème II

Arezki Sedoud

THESE DE DOCTORAT DE L'UNIVERSITE PARIS SUD - 11

Ecole Doctorale de Chimie Paris Sud

Présentée par

Arezki SEDOUD

Pour obtenir le grade de DOCTEUR de L'UNIVERSITE PARIS SUD 11

Transfert d'électrons dans le photosystème II

24 mars 2011, jury composé de :

Dr. Fabrice RAPPAPORT	Rapporteur
Dr. Wolfgang A. NITSCHKE	Rapporteur
Dr. Yiannis DELIGIANNAKIS	Examinateur
Prof. Pierre SEBBAN	Examinateur
Prof. Ally AUKAULOO	Examinateur
Dr. Alfred W. RUTHERFORD	Directeur de thèse

Laboratoire de Bioénergétique Moléculaire et Photosynthèse

CEA-Saclay, iBiTec-S/SB^{2}SM, CNRS, UMR2096

Remerciements:

Bill merci pour Tout. Ecrire ce que tu as fait pour moi dépassera le nombre de pages de cette thèse. Je te dis donc mille mercis.

Merci à Diana de m'avoir accueilli et encadré lors de mon stage M2. Merci pour tout ce que tu m'as appris et conseillé.

Merci à Alain d'avoir Toujours été présent lorsque j'en avais besoin, merci pour toutes les explications et toutes les discussions sur le PSII.

Merci à vous Anja et Sun : J'ai vraiment beaucoup appris avec vous. De la science à la vie. C'était très enrichissant d'écouter vos discussions, même si souvent je ne disais rien. Vos conseils me sont très chers.

Je remercie tout le personnel du SB^2SM qui m'ont connu et soutenu, je me dois de citer quelques noms : Sandrine Cot, Gérard, Véronique, Anabella, Léandro, Francis, Pierre Sétif et Dorlet, Jérôme, Bernard, Hervé, Klaus, Martin B, Claire, Philippe Champeil, Marc Lemaire, Ghada, Violaine et Bruno Robert. Merci pour tout. Je sais qu'il me manque des noms, c'est pourquoi je vous remercie plus spécialement, si votre nom est manquant.

Un clin d'œil à notre équipe de foot: Pierre, Guillaume, Elympe, Amine, Anis et notre entraineur François. On n'a jamais été champion, il faut donc changer d'équipe. C'est pourquoi je vous quitte pour laisser la place au plus jeunes.

Merci à tous les amis que j'ai rencontré pendant ces trois ans: Adjélé, Clémence, Thanh (^_^), Cédric, Lisa. K, Naoko (^_^), Tiona (^_^), Christine. G, Maria, Eiri, Nando, Denis, Michael. G, Tanai, Benedikt, Lucie, Laure (en plus pour les corrections), Thomas (l'anglais), Christian. H, Alberto. M, Nadjimé, Jo, Winfried, Ally, Sandrine et Nick. Merci aussi à tous les amis Irtelis et Maiot.

Merci à l'administration qui a toujours essayé de faciliter les démarches : Karin, Jocelyne, Sophie, Soizick, Isabelle. G et Romano.

Je remercie tout particulièrement toute ma famille qui est toujours derrière moi.

Un dernier merci à Bill.

Résumé:

Le photosystème II (PSII) est un complexe multi-protéique qui utilise l'énergie lumineuse solaire pour oxyder l'eau et réduire les quinones. Le site catalytique d'oxydation de l'eau est localisé sur le coté (lumen) du complexe, alors, que le site de réduction comprenant deux quinones (Q_A et Q_B) et un fer non-hémique est localisé sur l'autre coté du complexe membranaire. Dans cette thèse j'ai étudié les deux cotés accepteur et donneur d'électrons du PSII.

$Q_A^{\bullet-}$ et $Q_B^{\bullet-}$ sont couplés magnétiquement au fer non-hémique donnant de faibles signaux RPE. Le fer non-hémique possède quatre ligands histidines et un ligand (bi)carbonate échangeable. Le formate peut échanger le ligand (bi)carbonate en causant un ralentissement dans le transfert d'électrons. Ici, je décris une modification du signal RPE de $Q_B^{\bullet-}$ Fe^{2+} lorsque le formate substitue le (bi)carbonate. J'ai aussi découvert un second signal RPE du à la présence du formate à la place du (bi)carbonate lorsque Q_B est réduit deux fois. De plus, j'ai trouvé que les signaux RPE *natifs* de $Q_A^{\bullet-}$ Fe^{2+} and $Q_B^{\bullet-}$ Fe^{2+} possèdent une caractéristique intense jamais détecté. Tous ces signaux RPE rapportées dans cette thèse devraient faciliter le titrage redox de Q_B par RPE.

J'ai aussi observé que $Q_B^{\bullet-}$ peut oxyder le fer non-hémique à l'obscurité en anaérobie. Cette observation implique qu'au moins dans une fraction des centres, le couple $Q_B^{\bullet-}/Q_BH_2$ possède un potentiel redox plus haut que suppose. La quantification du nombre de centres où cette oxydation du fer se produit par le couple $Q_B^{\bullet-}/Q_BH_2$ reste à faire.

La réduction du PSII par le dithionite génère un signal modifié de $Q_A^{\bullet-}Fe^{2+}$, un changement structurale du PSII obsérvé sur gel de protéine. Cela peut indiquer une réduction d'un pont disulfure à l'interieur du PSII.

Concernant le côté de l'oxydation de l'eau, j'ai étudié la première étape de l'assemblage du site catalytique (Mn_4Ca), en étudiant l'oxydation du Mn^{2+} par RPE classique et haut champ. J'ai mis au point des conditions expérimentales permettant le piégeage du premier intermédiaire, et j'ai aussi trouvé une incohérence avec des travaux publié dans la littérature. J'ai aussi trouvé que le dithionite pouvait réduire le site catalytique Mn_4Ca, en formant des états sur-réduits qui peuvent correspondre aux intermédiaires de l'assemblage du cluster Mn_4Ca.

Mots clés: Photosystème II, RPE, transfert d'électrons, quinones, semiquinones, manganèse, photoactivation, formate, bicarbonate.

Abstract:

Photosystem II (PSII) uses light energy to oxidise water and reduce quinone. The water oxidation site is a Mn_4Ca cluster located on the luminal side of the membrane protein complex, while the quinone reduction site is made up of two quinones (Q_A and Q_B) and a non-heme Fe^{2+} located on the stromal side of the membrane protein. In this thesis I worked on both oxidation and reduction functions of the enzyme.

$Q_A^{\bullet-}$ and $Q_B^{\bullet-}$ are magnetically couple to the Fe^{2+} giving weak and complex EPR signals. The distorted octahedral Fe^{2+} has four histidines ligands and an exchangeable (bi)carbonate ligand. Formate can displace the exchangeable (bi)carbonate ligand, slowing electron transfer out of the PSII reaction centre. Here I report the formate-modified $Q_B^{\bullet-}$ Fe^{2+} EPR signal, and this shows marked spectral changes and has a greatly enhanced intensity. I also discovered a second new EPR signal from formate-treated PSII that is attributed to formate-modified $Q_A^{\bullet-}$ Fe^{2+} in the presence of a 2-electron reduced form of Q_B. In addition, I found that the *native* $Q_A^{\bullet-}$ Fe^{2+} and $Q_B^{\bullet-}$ Fe^{2+} EPR signals have a strong feature that had been previously missed because of overlapping signals (mainly the stable tyrosyl radical $TyrD^{\bullet}$). These previously unreported EPR signals should allow for the redox potential of this cofactor to be directly determined for the first time.

I also observed that when $Q_B^{\bullet-}$Fe was formed; it was able to oxidise the iron slowly in the dark. This occurred in samples pumped to remove O_2. This observation implies that at least in some centres, the $Q_B^{\bullet-}/Q_BH_2$ couple has a higher potential then is often assumed and thus that the protein-bound semiquinone is thermodynamically less stable expected. It has yet to be determined if this represents a situation occurring in the majority of centres. Treatment of the system with dithionite generated a modified form of $Q_A^{\bullet-}Fe^{2+}$ state and a change in the association of the proteins on gels. This indicates a redox induced modification of the protein, possibly structurally important cysteine bridge in PSII.

On the water oxidation side of the enzyme, I studied the first step in the assembly of the Mn_4Ca cluster looking at Mn^{2+} oxidation using kinetic EPR and high field EPR. Conditions were found for stabilising the first oxidised state and some discrepancies with the literature were observed. I also found that dithionite could be used to reduce the Mn_4Ca, forming states that are formally equivalent to those that exist during the assembly of the enzyme.

Keywords: Photosytem II, EPR, electron transfer, quinones, semiquinones, manganese, photoactivation, formate, bicarbonate.

Table des matières

INTRODUCTION

et

MATERIELS ET METHODES

1. La photosynthèse

La photosynthèse est le plus important mécanisme biologique de conversion d'énergie solaire en énergie chimique nécessaire pour tous les êtres vivants. En effet, la photosynthèse convertit efficacement l'énergie solaire en énergie électrochimique essentielle pour les réactions d'oxydo-réduction (redox). L'excitation des pigments photosynthétiques par des photons (lumière solaire) provoque une séparation de charge et un transfert d'électrons à travers une longue chaine de transporteurs jusqu'au dernier accepteur, le CO_2. L'électron perdu est ensuite récupéré par l'extraction d'un électron à partir d'un donneur final. Il existe deux types de photosynthèse selon le donneur final d'électrons. Si le donneur final d'électrons est une molécule d'eau, alors on parle de photosynthèse oxygénique, car une molécule d'oxygène est produite comme "déchet". Si le donneur final d'électrons n'est pas une molécule d'eau, on parle alors de photosynthèse non-oxygénique.

La photosynthèse oxygénique a lieu dans les membranes photosynthétiques : les thylacoïdes. Chez les plantes et les algues, les thylacoïdes se trouvent dans les chloroplastes. Elles sont empilées en grana interconnectées par des lamelles simples plus exposées au stroma. Chez les procaryotes (eg. cyanobactéries), cette différenciation est absente, les thylacoïdes sont distribuées dans le cytoplasme cellulaire.

La réaction globale de la photosynthèse oxygénique est comme suit :

$$CO_2 + 2H_2O \text{ ---> } (CH_2O) + O_2 + H_2O.$$

La photosynthèse non-oxygénique est considérée comme l'ancêtre de la photosynthèse oxygénique. Dans ce cas, le donneur d'électrons est autre que l'eau, il peut s'agir par exemple de H_2S. Certains bactéries pourpres, les bactéries sulfureuse vertes, les heliobactéries peuvent effectuer cette réaction. Dans cette thèse je serai mené a comparer le centre réactionnel des organismes photosynthètiques non-oxygéniques tels que les bactéries pourpres, pour lequel de nombreux données sont diponible dans la littérature, avec celui d'organismes photosynthétiques oxygéniques tels que celui des plantes supérieures et plus souvent de cyanobactéries thermophiles (*Thermosynechococcus elongatus*).

Deux phases caractérisent la photosynthèse oxygénique : i) Une phase lumineuse où l'énergie solaire est transformée en énergie chimique. ii) Une phase "obscure" où l'énergie chimique est utilisée pour fixer le CO_2 en produisant les glucides (cycle de Calvin-Benson).

Les acteurs principaux de la phase lumineuse sont : (1) Des complexes protéiques transmembranaires contenant des chlorophylles photoactives (le photosystème I; PSI, le photosystème II; PSII), ainsi que le cytochrome b_6f et l'ATP synthase. (2) Un transporteur d'électron membranaire liposoluble : la plastoquinone. (3) Des transporteurs d'électrons solubles : la plastocyanine ou le cytochrome *c6* chez certaines espèces, la ferrédoxine (Fd) et la FNR (Ferrédoxine-$NADP^+$-oxydoréductase). Voir la Figure 1.

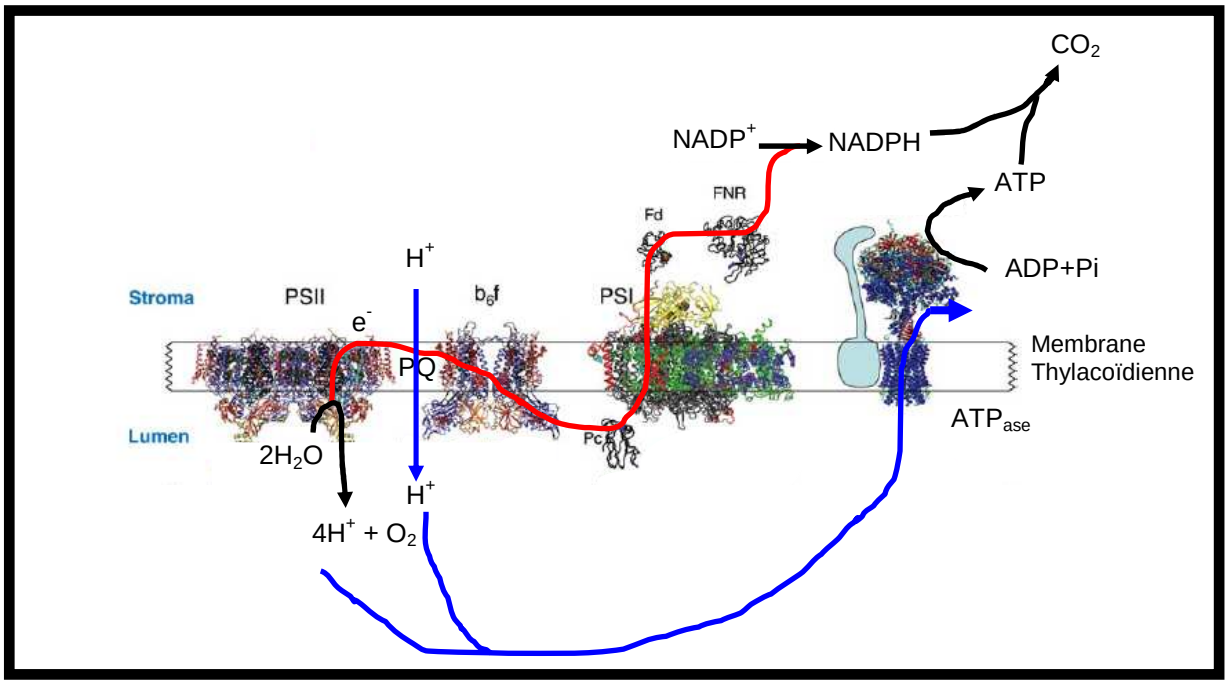

Figure 1: Organisation et structure des complexes intervenant dans la phase lumineuse de la photosynthèse au niveau de la membrane thylacoïdale. Les quatre complexes membranaires sont présentés : Photosystème II (PSII), Cytochrome b_6f (b_6f), photosystème I (PSI) et l'ATP synthase (ATP_{ase}) ainsi que les protéines solubles impliquées, la plastocyanine (Pc), la ferrédoxine (Fd) ainsi que la FNR (Ferrédoxin-$NADP^+$-oxidoreductase). Les électrons sont transférés de l'eau au $NADP^+$ (trait rouge), ce transfert d'électrons génère un gradient de protons au niveau de la membrane. Ce gradient de protons est utilisé pour la synthèse d'ATP par l'ATP synthase (flèche en bleu). L'ATP et le NADPH sont utilisés pour fixer le CO_2 afin de produire les composés organiques (cycle de Calvin-Benson). Figure modifiée à partir de la référence [1].

2. Les centres réactionnels

Les centres réactionnels peuvent être classés en deux types. Les centres réactionnels (CR) de type I (PSI) utilisent des centres fer-soufre (FeS) comme accepteurs finaux d'électrons, alors que les centres réactionnels de type II (PSII) utilisent une quinone comme accepteurs finaux d'électrons. Les bactéries pourpres et les bactéries vertes non-sulfureuses contiennent le CR type II, alors que les bactéries vertes sulfureuses et les héliobactéries

contiennent le CR type I. Les organismes contenants les deux types de CRs sont capables de réaliser la photosynthèse oxygénique, tel que les algues, les cyanobactéries et les plantes.

Selon la théorie de l'endosymbiose sur l'origine des chloroplastes présents dans le cytoplasme des plantes et des algues, une cyanobactérie a été endocytée par une cellule hôte eucaryotique non photosynthétique [2]. Cela justifie la grande ressemblance des CRs de plantes, des algues et de cyanobactéries.

Une grande partie du travail présenté ici a été obtenue en utilisant du PSII isolé à partir d'une cyanobactérie thermophile, *Thermosynechococcus elongatus* BP1, anciennement appelée *Synechococcus elongatus* BP1. Cette souche a été isolée dans les sources d'eau chaude à Beppu au Japon [3]. Les avantages de l'utilisation de cette espèce sont: une grande stabilité à température ambiante et une homogénéité du PSII isolé, un génome totalement séquencé (disponible dans la banque de donnée *Cyanobase*) et des conditions de culture à haute température minimisant le risque de contamination lors de la culture. De plus, le PSII peut être isolé à l'aide d'une étiquette histidines [4].

3. La chaine de transfert d'électrons (les électrons de l'eau à la Fd)

L'absorption de la lumière par les centres réactionnels chlorophylliens du PSI et du PSII induit une séparation de charge et un transfert d'électrons. Au niveau du PSII, la séparation de charge est suivie par un transfert d'électrons qui finit par la réduction de l'accepteur final d'électrons du PSII (une quinone nommée Q_B, voir ci-dessous). Q_B peut accepter deux électrons et deux protons pour former Q_BH_2. Q_BH_2 migre au travers de la membrane thylacoïdale pour réduire le cytochrome b_6f. Le cytochrome b_6f réduit à son tour un transporteur d'électrons soluble, la plastocyanine (ou le cytochrome *c6* dans certain cas) (Fig. 1). La chlorophylle du PSII qui a perdu son électron après la séparation de charge oxyde une tyrosine, qui à son tour oxyde le site catalytique d'oxydation de l'eau (pour plus de détails voir ci-dessous). Au niveau du PSI, la séparation de charges est aussi suivie par un transfert d'électrons. Dans ce cas, la ferrédoxine est réduite à la fin de la réaction. La ferrédoxine est un carrefour métabolique de réactions redox, l'une des voies majeures est celle de la réduction de la ferrédoxine-$NADP^+$ réductase (FNR) qui produit le NADPH. La chlorophylle du PSI oxydée est réduite par la plastocyanine. Cette chaine de transfert d'électrons est dite linéaire (i.e les électrons de l'eau sont transféré vers NADPH). Cependant, il existe un autre type de transfert d'électrons non-linéaire, voir par exemple [5]. Le transfert d'électrons linéaire (et

cyclique) génère un gradient de protons au niveau de la membrane thylacoïdale qui va servir à la synthèse d'ATP à partir d'ADP et de phosphate inorganique grâce au complexe multi-protéique de l'ATP synthase. L'ATP et le NADPH sont utilisés pour la fixation du CO_2 et la production de composés organiques tels que les sucres pendant cycle de Calvin et Benson.

4. Le PSII

4.1 La structure

Le PSII est le siège de l'oxydation de l'eau et de la réduction des molécules de plastoquinone, le nom exacte de cette enzyme est : eau/plastoquinone :photooxydoréductase. Le PSII catalyse la réaction suivante:

$$2H_2O + 2PQ + 4H^+ \text{----> } O_2 + 2PQH_2 + 4H^+$$

Les premiers modèles du repliement des sous unités protéiques du PSII ont été pendant longtemps inspirés par analogie à la structure des centres réactionnels des bactéries pourpres, résolue dans les années 80s par [6]. Par la suite, les résultats spectroscopiques n'ont cessé de confirmer ces analogies [7-8]. L'analogie ensuite était validée dans les années 2000, par la première publication de la structure cristallographique à une résolution de 3.8 Ådu PSII [9]. Depuis ce jour, la résolution n'a cessé d'être améliorée. La résolution était améliorée à 3.5Å, ce qui a permis pour la première fois le raffinement de la structure et la résolution des acides aminés par [10], ensuite à 3Å puis 2.9Å [11] (voir la structure à 2.9Å sur la Fig. 2). Une nouvelle résolution à un niveau atomique cette fois-ci (1.9Å) est en cours d'achèvement, cette structure est supposée être moins affectée par les radiations lors de l'acquisition des données de diffractions aux rayons X (Shen et al, en préparation).

Le PSII est un homodimère (de dimension 105x200x110 Å) inséré dans la membrane des thylacoïdes, composé de protéines transmembranaires et de protéines extrinsèques attachées du côté lumen protégeant le site catalytique d'oxydation de l'eau. Selon la structure la plus récente [11], le PSII est formé de 20 sous-unités peptidiques et d'un grand nombre de cofacteurs par monomère (35 chlorophylles, 12 caroténoïdes, 2 phéophytines, un fer non-hémique, deux ions calcium, dont un contenu dans le cluster de manganèse, quatre ions manganèse (formant le cluster de Mn_4Ca), deux ions Cl^-, 2-3 quinones, 2 hèmes et 25 lipides). Le noyau enzymatique du monomère (le centre réactionnel) est constitué de

l'hétérodimère D1/D2 et du cytochrome *b559*. Ce noyau est entouré par deux protéines antennes CP43 et CP47 qui capturent l'énergie lumineuse grâce aux chlorophylles qu'elles contiennent, et la transfèrent au centre réactionnel. L'hétérodimère D1/D2 lie les cofacteurs nécessaires à la séparation de charges et à leur stabilisation.

Le PSII peut être vu en trois parties: un côté donneur d'électrons qui se situe du côté du lumen et qui possède le site catalytique du cluster de Mn_4Ca protégé par les protéines extrinsèques, un côté accepteur d'électrons qui contient les quinones, qui se situe sur l'autre côté de la membrane i.e. stroma; et la partie centrale possédant les acteurs impliqués dans le transfert d'électrons du côté donneur au côté accepteur d'électrons.

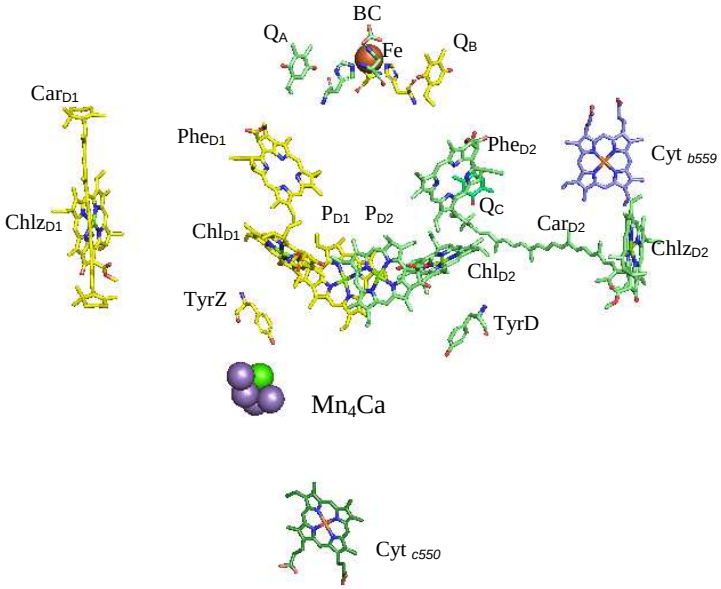

Fig. 2: Les principaux cofacteurs du PSII intervenant dans le transfert d'électrons. (PDB:3BZ1) [11]. Figure réalisée par Pymol.

4.2 Le transfert d'électrons dans le PSII

L'absorption de l'énergie d'un photon induit une excitation puis une séparation de charge au niveau de la Chl_{D1}. Le cation est stabilisé sur la P_{680}, formant ainsi P_{680}^+ et réduisant le premier accepteur d'électron la phéophitine D1 ($Pheo_{D1}$). La vitesse de formation de $P_{680}^+Pheo^-$ est estimée à $t_{1/2}$~ 2-20 ps. La $Pheo^-$ réduit Q_A ($t_{1/2}$ ~ 250-650 ps) avec une perte d'énergie qui stabilise la paire de charges. P_{680}^+ oxyde la tyrosine Z (Y_Z) avec une vitesse multiphasique, la phase majoritaire avec un $t_{1/2}$ ~20 ns pour les états S_0 et S_1, et un $t_{1/2}$ ~250-300 ns pour les états S_2 et S_3 [12]. La tyrosine oxydé cède un proton à l'His191 de D1 formant ainsi un radical neutre $Y_Z^{\bullet}$ [12]. $Y_Z^{\bullet}$ oxyde le cluster de Mn_4Ca avec des vitesses dépendant de

l'état S, $t_{1/2}$ ≤3-250 µs pour la transition S_0-S_1, $t_{1/2}$~30-140 µs pour la transition S_1-S_2, $t_{1/2}$ 100-600 µs pour la transition S_2-S_3 et $t_{1/2}$ 1-4.5 ms pour la transition S_3-S_0 [12]. Q_A^- réduit Q_B (voir ci-dessous pour plus de détail concernant le transfert d'électrons entre les deux quinones Q_A et Q_B) [12-13]. L'absorption de deux photons induit deux séparations de charges, et donc une double réduction de Q_B. Q_B réduit deux fois accepte deux protons, formant Q_BH_2, qui se détache de son site de fixation, une autre molécule quinonique (Q_B) venant du pool membranaire le remplace.

Le PSII accumule 4 équivalents de charges positives, avec 4 déprotonations afin de compenser cette accumulation de charges avant l'oxydation de 2 molécules d'eau et le dégagement d'oxygène [14].

4.3 Les protéines extrinsèques :

Le mécanisme catalytique et l'architecture du PSII ont été conservés de manière remarquable à travers l'évolution depuis les cyanobactéries jusqu'aux plantes. Il n'existe qu'un seul type de centre réactionnel PSII quelque soit l'organisme photosynthétique dont il est issu. Néanmoins, des différences existent au niveau des protéines extrinsèques qui protègent le site catalytique de l'oxydation de l'eau. Il existe cinq protéines extrinsèques (PsbO, PsbP, PsbQ, PsbU et la PsbV) qui s'associent avec des combinaisons différentes dans chaque organisme photosynthétique. Les principales protéines extrinsèques chez les plantes sont les protéines PsbO, PsbP et PsbQ. Chez les cyanobactéries, nous trouvons les protéines PsbO, PsbU, PsbV (cytochrome *c550*) et aussi PsbP et PsbQ avec des combinaisons différentes, les algues rouges et les diatomées possèdent aussi la PsbO, PsbP, PsbV et une PsbQ-like (PsbQ') [15-18].

- **PsbO**

La protéine PsbO (33kDa) est la seule protéine extrinsèque ubiquiste des organismes faisant la photosynthèse oxygénique. Son principal rôle semble être de stabiliser et protéger le cluster de Mn_4Ca des agents réducteurs [19]. Son absence empêche la croissance photo-autotrophique des plantes et des algues vertes, alors que chez les cyanobactéries son absence ne fait que baisser le taux de croissance photo-auto trophique [20-21]. Récemment, il a été proposé que la protéine PsbO puisse avoir des canaux d'acheminement de l'eau du lumen vers le site catalytique et des canaux de dégagement de protons et d'oxygène [22].

- **Psb Q, P, U et V**

Les protéines PsbQ et PsbP (17 kDa et 23 kDa) sont présentes chez les plantes et algues vertes [23], et les protéines PsbU et PsbV (12 kDa, 15 kDa) sont trouvées chez les cyanobactéries, les algues rouges et les diatomées. Ses protéines stabilisent la fixation des ions Ca^{2+} et Cl^-, essentiels pour l'activité de dégagement de l'oxygène [24]. La protéine PsbV pourrait avoir une fonction redox inconnue du fait qu'elle contienne un hème [25].

Récemment, des protéines homologues aux protéines PsbP et PsbQ des plantes ont été identifiées chez les cyanobactéries [17, 26-27]. Ces protéines extrinsèques ne sont pas présentes dans la structure cristallographique du PSII obtenue chez *T. elongatus*.

Il a été montré que les mutants de *Synechocystis* dépourvues de PsbP ou PsbQ poussent plus lentement que la souche sauvage en absence des ions Ca^{2+} et/ou Cl^-. Ces résultats suggèrent que ces protéines ont un rôle dans la fixation des ions Ca^{2+} et/ou Cl^-. Le PSII a pu être isolé grâce à une étiquette hisitidine présente sur la sous-unité PsbQ de *Synechocystis* [28], la structure cristallographique de PsbQ isolée de *Synechocystis* a été résolue récemment par [29]. Le nombre de PsbP par PSII ne semble pas être stœchiométrique chez *T. elongatus* [17]. Récemment aussi, la structure de la PsbP de *T. elongatus* a été obtenue [30].

- **Cas unique de la PsbV (Cyt *c550*)**

La protéine extrinsèque PsbV (15 kDa) est un cytochrome de type c (Cyt *c550*). C'est la seule protéine extrinsèque possédant un hème, ce qui la rend assez unique. Le Cyt *c550* est un composé du PSII trouvé chez les cyanobactéries, les algues rouges, les diatomées et quelques autres algues. Son rôle demeure inconnu. Cela dit, plusieurs travaux montrent que cette protéine n'est pas impliquée dans les réactions photochimiques du PSII. Son potentiel redox a été mesuré par plusieurs laboratoires, et s'avère sensible aux traitements subis par le PSII.

5. La photoactivation

Le photoassemblage (*photoactivation*) du cluster de Mn_4Ca est un mécanisme à bas rendement quantique qui se fait de manière naturelle en présence d'ions Mn^{2+}, Ca^{2+} et Cl^- en lumière faible. La photoactivation passe au moins par deux intermédiaires instables séparés

par une étape de réarrangement [31-32]. Il est décrit dans la littérature que le premier Mn^{2+} se lie à un site de haute affinité. Ce Mn^{2+} est ensuite oxydé en Mn^{3+} par la $Tyr_Z^{\bullet}$ générée lorsque le PSII réalise une séparation de charge. La liaison d'un deuxième ion Mn^{2+} pourrait constituée l'étape limitante correspondant à une étape de réarrangement structural. Ce deuxième Mn^{2+} est photo-oxydé, 2 autres ions Mn^{2+} se lient et sont photo-oxydés et un ion Ca^{2+} se lie au cours de la photoactivation. Au final le cluster de Mn_4Ca est assemblé [32]. Le mécanisme exact de l'assemblage du cluster de Mn_4Ca reste inconnu.

Le Ca^{2+} et le Cl^- sont nécessaires pour le dégagement d'oxygène. Il est proposé que le Ca^{2+} a un rôle dans l'étape de réarrangement structural du PSII. Le rôle du Cl^- dans la photoactivation reste inconnu, mais sa présence est nécessaire à la photoactivation *in-vitro* et aussi au fonctionnement du PSII. Une grande quantité (de l'ordre du molaire) de Cl^- est nécessaire pour maintenir le dégagement d'oxygène lorsque les protéines extrinsèques sont enlevées [33].

Le mécanisme ci-dessous (Fig. 3) représente le modèle communément admis dans la littérature [31-32, 34-35].

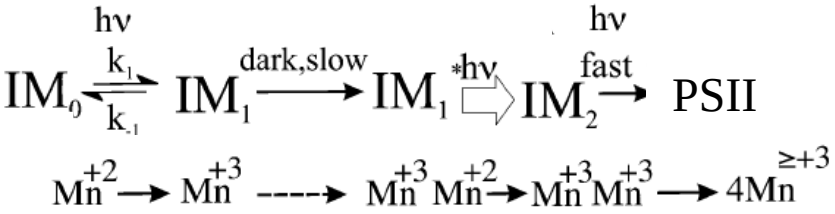

Fig. 3: Mécanisme de photoactivation tiré de la référence [32]. IM : intermédiaire. L'apo-PSII lie le Mn^{2+} à son site de haute affinité (IM_0). Ce Mn^{2+} est photo-oxydé en Mn^{3+} (IM_1). Cette étape est suivie d'une étape lente, indépendante de la lumière, au cours de laquelle un second Mn^{2+} est supposé se lié (IM_1^*). Ce deuxième Mn^{2+} est photo-oxydé en Mn^{3+} (IM_2). Deux autres Mn^{2+} sont liés et photo-oxydés pour former le complexe Mn_4Ca, après liaison de Ca^{2+}.

La première étape de la photoactivation consiste à lier un ion Mn^{2+} à un site de liaison de haute affinité. Cette étape peut être piégée soit par une congélation sous éclairement [36] ou par éclairement à -20°C [37]. Il est supposé qu'à -20°C, seul un Mn^{2+} lié au site de haute affinité puisse subir une photo-oxydation [37]. Cette hypothèse a été à la base de plusieurs articles [37-40]. Un problème majeur de tous les travaux cités précédemment, est que seule la RPE classique (X-band) a été utilisée, alors que le Mn^{2+} n'est pas quantifiable en utilisant cette méthode.

6. Le côté donneur d'électrons :

6.1 Le cluster de Mn_4Ca et les états S

L'oxydation de deux molécules d'eau générant une molécule d'oxygène, est une réaction à quatre électrons ($2H_2O \rightarrow 4H^+ + O_2 + 4e^-$). Le cluster de Mn_4Ca doit pour réaliser cette réaction stocker 4 équivalents de charges positives. Joliot et al, [41] ont observé une périodicité de quatre dans le dégagement d'oxygène. L'explication de cette observation a été proposée par Kok et al, [42]. Dans ce modèle, le cluster de Mn_4Ca passe par cinq états S, désignés par S_n, où n= 0 à 4 (Fig. 4). Chaque état S_n représente un état d'oxydation différent du complexe d'oxydation de l'eau. L'enzyme est ainsi capable de stocker quatre équivalents de charges positives, avant d'oxyder 2 molécules d'H_2O et de dégager de l'O_2. L'état S_1 est celui qui est le plus stable à l'obscurité. Le Ca^{2+} est un cofacteur nécessaire pour le dégagement d'oxygène [33, 43]. Les études spectroscopiques et structurelles ainsi que son échange par le Sr^{2+} ont clairement déterminé que le Ca^{2+} faisait partie du cluster de Mn [11, 44]. Quant au Cl^-, il est évident que c'est un cofacteur important pour le dégagement d'oxygène, et dans la photoactivation. Les résultats récents venant des expériences d'échanges biosynthétiques, de mesures EXAFS ainsi que de la cristallographies ont montré qu'il existerait deux sites de liaison de Cl^- à environs 6-7 Å du cluster de Mn_4Ca [45].

L'état d'oxydation de chaque état S n'est encore pas totalement résolu. Néanmoins, l'utilisation de la technique Résonance Paramagnétique Electronique (RPE) a montré que les états S_0 et S_2 sont paramagnétiques, montrant des signaux multilignes, et que l'état S_1 a aussi un signal RPE (en polarisation parallèle) (Fig. 4). Le modèle de structure du cluster de Mn_4Ca à l'état S_2 le plus accepté de nos jours est celui d'un arrangement en trimère/monomère de trois Mn^{IV} et un Mn^{III} [46]. Actuellement, les états de valences les plus favorables pour les états S sont : $Mn^{III}{}_3Mn^{IV}$ pour S_0, $Mn^{III}{}_2Mn^{IV}{}_2$ pour S_1 et $Mn^{III}Mn^{IV}{}_3$ pour S_2, (voir la revue [47]).

S_0: L'état S_0 donne un signal multiligne centré autour de g = 2 [48-51]. Il est réparti sur environ 2380 G et est constitué d'environ 25 lignes résolues espacées de 65-95 G. Il provient du cluster de Mn4Ca en spin ½. Le signal multiligne S0 a été observé chez les plantes en présence de méthanol [48, 51] et sans méthanol chez T. elongatus [50]. Bien que la présence de méthanol ne soit pas requise pour observer le signal S_0 chez T. elongatus, son addition améliore la résolution du signal RPE S0. L'état S_0 peut être formé par la réduction avec l'hydroxylamine [48, 51] ou encore après une série de flashs à température ambiante [49-50].

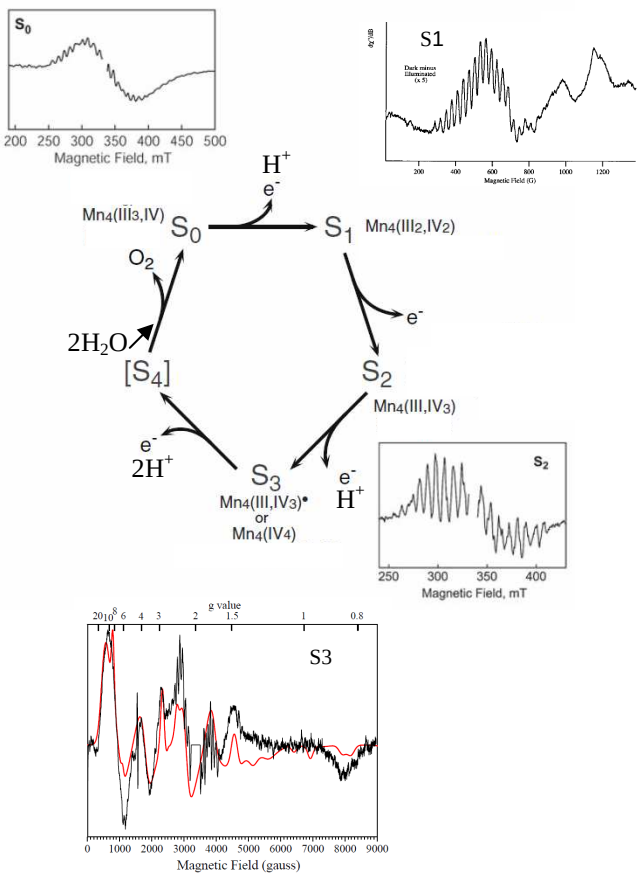

Fig. 4 : Etats S avec les signaux RPE du cluster de Mn_4Ca identifiés jusqu'à présent. Figure modifiée à partir de la réf [63]. Le spectre S1 est pris de la référence [54], Le spectre S3 est pris de la référence [60]. L'état S_4 reste toujours inconnu.

S_1: C'est l'état le plus stable dans le noir. Invisible en RPE classique car son état de spin est intègre (S=1). Cela dit, l'utilisation de la RPE en mode parallèle a permis la détection de signaux attribués à l'état S_1 à haut champ [52-54]. Le signal RPE en polarisation parallèle obtenu pour S_1 est supposé être compatible avec un motif de $Mn^{III}_2Mn^{IV}_2$ [55].

S_2: Le signal RPE de l'état S_2 caractérisé par un spin ½ donne lieu à un signal multiligne centré autour de g=2 et s'étend sur 1800 G, il est composé de 18 raies séparées d'environs 87 G [56-57]. Un autre signal correspondant à des formes moins résolues du cluster de Mn_4Ca haut spin a été identifié en hauts champs [33, 58-59].

S_3: L'état S_3 est l'état le plus élevé en valence proprement détectable en RPE, le spectre complet de cet état observé par RPE à été simulé. Le spectre est simulé avec un *fit* ayant un spin=3 [60].

S_4: C'est l'étape où la molécule d'eau est oxydée et la molécule d'oxygène dégagée. Cet état est jusqu'à présent inaccessible. Aucune méthode ne permet de le piéger et de le suivre. L'élucidation de cet état permettra de faire progresser nos connaissances sur la réaction d'oxydation de l'eau et permettra le développement de catalyseurs chimiques inspirés de l'oxydation de l'eau par le PSII.

S_{-1}, S_{-2} et S_{-3}: Ces états sur-réduits non détectés dans les conditions physiologiques peuvent être générés par réduction du PSII par le NO, l'hydroxylamine ou l'hydrazine [61-62].

- **La Tyr Z**

Le PSII contient deux tyrosines (Y_Z et Y_D) qui sont oxydo-réductibles. Ces deux tyrosines Y_Z et Y_D sont localisées de manière symétrique aux positions 161 et 162 des protéines D1 et D2 (160, 161 chez *Synechocystis*), respectivement dans le PSII. Y_Z est un cofacteur très important qui intervient dans le mécanisme d'oxydation de l'eau. En effet, après la séparation de charge et la formation du P_{680}^+, la Y_Z réduit P_{680}^+ afin d'empêcher la recombinaison de charge dans un temps de demi-vie $t_{1/2}$ de 50-300 ns (dépendant de l'état S, voir ci-dessus), formant ainsi $Y_Z^{\bullet}$. $Y_Z^{\bullet}$ oxyde le cluster de Mn_4Ca (voir la revue de Diner et Britt [12]).

L'oxydoréduction de la Y_Z est couplée à un transfert de proton avec le résidu D1-H190. L'oxydation de la Y_Z chez le mutant délaité du résidu D1-His190, a montré un sévère ralentissement du transfert d'électrons; ce ralentissement peut être accéléré par l'addition de l'histidine dans l'échantillon [64]. De plus, les structures cristallines ont confirmé la proximité de D1-His190 avec la Y_Z.

- **La Tyr D**

Y_D n'est pas impliquée directement dans le processus d'oxydation de l'eau. Cependant, Y_D peut être oxydée par la lumière et former $Y_D^{\bullet}$. $Y_D^{\bullet}$ est beaucoup plus stable que $Y_Z^{\bullet}$ (heures vs µs respectivement). Le rôle exact de cet acide aminé reste à définir [65]. Cela dit, $Y_D^{\bullet}$ peut oxyder l'état S_0, ce qui permet le maintien de l'enzyme dans l'état le plus stable S_1 [65-66]. Ce rôle d'oxydant peut être bénéfique durant la photoactivation du cluster de Mn_4Ca comme suggéré dans [65, 67].

Comme dans le cas de Y_Z, l'oxydoréduction de Y_D est couplée à un transfert d'un proton [12]. Le proton généré par l'oxydation de Y_D est pris par le résidu D2-His189. Il est proposé que le proton ainsi généré influence le potentiel redox et/ou la localisation de la charge positive sur P_{680}^+ [12, 65].

6.2 Les voies secondaires de transfert d'électrons

Dans les conditions physiologiques, le donneur d'électrons à la P_{680}^+ est majoritairement l'eau. Cependant, dans certaines conditions non physiologiques, telles que le PSII dépourvu du cluster de Mn_4Ca, ou éclairé à basse température (≤100K), la réduction du P_{680}^+ par la Y_Z est en grande partie inhibée. Des donneurs d'électrons secondaires peuvent remplir le rôle de réducteurs de P_{680}^+ avec un faible rendement quantique. Ces donneurs secondaires sont: le caroténoïde situé sur la sous-unité D2 (Car_{D2}), le Cyt *b559* ou encore la $Chl_{Z\ D2}$ (voir la structure Fig. 2). Le Car_{D2} est oxydé par la P_{680}^+ générant $Car_{D2}^{\bullet+}$, ce radical est ensuite soit réduit par le Cyt *b559* si il est disponible ou par la $Chl_{Z\ D2}$ [68]. Il est souvent considéré que les voies secondaires de transfert d'électrons sont des mécanismes protecteurs qui visent à réduire le cation P_{680}^+ [69], Faller et al, [68] ont proposé un autre rôle de ces donneurs secondaires, il s'agirait en fait, d'un cycle photoprotecteur visant à réduire le $Car^{\bullet+}$, ce qui lui permettra ensuite de jouer son rôle de quencheur d'oxygène singulet.

7. Le cytochrome *b559* (Cyt *b559*)

Le Cyt *b559* fait partie intégrante du centre réactionnel du PSII [70-71]. En effet, il a été montré que les sous unités nécessaires à la réalisation d'une séparation de charge sont les protéines D1, D2 et le Cyt *b559* [72]. Le Cyt *b559* peut être photo-oxydé ou photo-réduit [71, 73]. Le Cyt *b559* peut être aussi réduit ou oxydé chimiquement, par exemple par l'ascorbate ou le ferricyanure, respectivement.

Trois formes avec des potentiels redox (E_m) différents existent pour le Cyt *b559* (voir la revue [70]). À pH 6,5, dans le PSII intact, la forme haut potentiel (E_m=390-400 mV) est la plus dominante (70% des centres), le reste des centres possèdent un potentiel redox entre 200-250 mV (Potentiel intermédiaire) ou entre 50-100 mV (bas potentiel). La forme haut potentiel est associé à l'intégralité du PSII, plus le PSII est intact, plus la forme haut potentiel est trouvée. Dans *T. elongatus*, la forme bas potentiel n'est pas présente [74].

Plusieurs rôles sont proposés pour le Cyt *b559*. Il a été proposé que le Cyt *b559* soit impliqué dans les premiers événements de photoactivation ou dans l'assemblage du PSII [75-77]. Le rôle le plus attribué au Cyt *b559* est l'implication dans la voie du transfert cyclique d'électrons, qui contribue à la protection du PSII contre la photoinhibition. Dans ce mécanisme de protection, le Cyt *b559* oxydé peut jouer le rôle d'accepteur d'électrons soit du pool de la plastoquinol membranaire ou de la semiquinone $Q_B^{\bullet -}$ ou encore de Q_BH_2 [78-81].

Dans la thèse présentée ici, le Cyt *b559* réduit est souvent utilisé comme donneur d'électrons à la P_{680}^+ après un éclairement à des températures cryogéniques.

8. Le côté accepteur d'électrons

Le PSII et le centre réactionnel des bactéries pourpres lient deux quinones, Q_A et Q_B (dans le cas du PSII, il s'agit de plastoquinones), qui sont des accepteurs d'électrons fonctionnant de manière séquentielle, un fer non-hémique se localise entre ces deux quinones. Les propriétés physicochimiques de ces deux quinones sont différentes. Q_A est fortement liée et fonctionne comme un transporteur à un électron, alors que Q_B peut accepter deux électrons. Q_B est faiblement liée sous ses formes quinone et quinol, mais fortement liée sous la forme semiquinone [14]. Dans le PSII intact, l'état Q_A^- à une demie vie de l'ordre de 200 µs-1 ms (selon les conditions expérimentaux), aucun proton n'est associé à cette espèce. Lors du transfert d'électron de Q_A^- à Q_B, Q_B^- se forme. Q_B^- est fortement liée, et il semble qu'elle reste non protonée. Cependant, la charge négative est partiellement compensée par une prise de proton par les résidus voisins de Q_B^-. Après une deuxième séparation de charge, Q_B^- accepte un deuxième électron. Ce dernier événement est couplé à une réaction de protonation formant Q_BH_2. Q_BH_2 se détache de son site de fixation, une nouvelle molécule de plastoquinone venant du pool de la membrane le remplace [82-84]. Les vitesses de transfert d'électrons entre Q_A et Q_B sont rassemblées dans le tableau. 1

Tableau 1: Vitesses de transfert d'électrons entre Q_A et Q_B

	$Q_A^-\rightarrow Q_B$	$Q_A^-\rightarrow Q_B^-$	$Q_A^-\rightarrow Q_BH_2$
PSII intact	200-400 µs[1*]	600-800 µs[1*]	2-3 ms[1]

[1] vitesses tirées de la référence [85]

[*] Ces valeurs confirment celles publiées précédemment par [86-87].

Le centre réactionnel des bactéries pourpres est l'un des modèles le plus étudié en terme de transfert d'électrons couplé aux protons [88-89]. Du fait de (i) disponibilité de la structure (*Rb. sphaeroides*) plus de 30 ans [90], (ii) de l'accès à un grand nombre de mutants, (iii) de la grande stabilité du matériel biochimique (iv) du fonctionnement de l'enzyme à basse température dans certaines conditions, et enfin (v) de la présence de seulment 6 pigments chlorophylliens présentant des propriété spectroscopiques différentes.

Dans les centres réactionnels des bactéries pourpres, le transfert d'électron entre Q_A^- et Q_B est dépendant de la conformation et du réarrangement du CR. Le transfert d'un électron entre Q_A^- et Q_B^- est précédé par un événement de protonation rapide et réversible puis s'en suit le transfert d'électron [88-89].

Dans le PSII, peu de choses sont connues concernant les événements de protonation. En revanche, la sensibilité du transfert d'électrons entre Q_A et Q_B aux changements au niveau du ligand du fer non-hémique, le bicarbonate, est bien établie [14]. Ce qui est souvent interprété dans la littérature comme une possible implication du bicarbonate dans le transfert de protons.

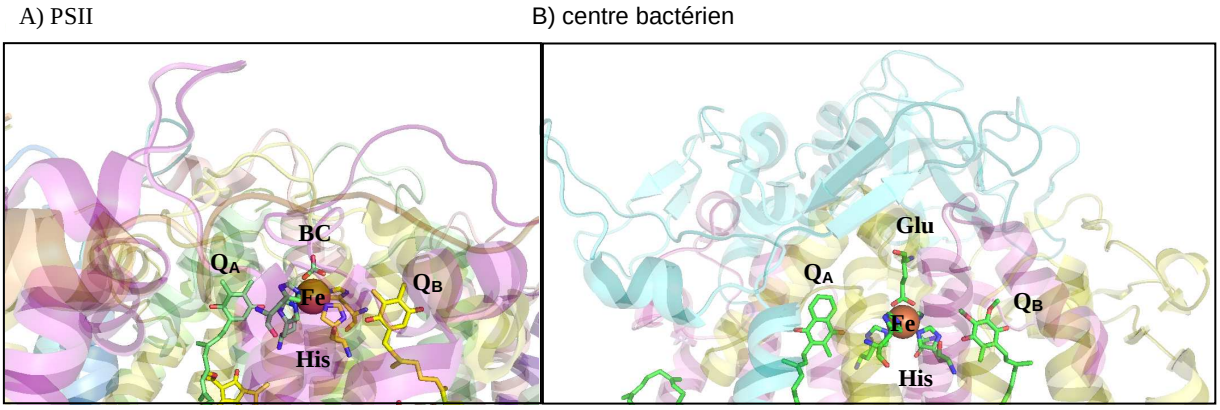

Fig. 5: Structure du côté accepteur d'électrons dans le PSII *T. elongatus* (PDB:3BZ1) [11] et dans le centre réactionnel bactérien *Blastochloris viridis* (PDB:1VRN) [91]. BC: bicarbonate, His: ligands histidines, Glu: résidu glutamate 232. Figure réalisée avec le logiciel Pymol.

8.1 Le fer non-hémique

Un atome de fer non-hémique est localisé symétriquement entre les deux quinones Q_A et Q_B (voir la structure Fig. 5). Ce fer est coordonné par quatre histidines ; deux de la protéine D1 (H215 et H272) et deux de la protéine D2 (H214 et H268). Dans les centres réactionnels des bactéries pourpres, la cinquième et la sixième coordination viennent d'un groupement

glutamate [7]. Dans le PSII, en revanche, une molécule labile remplit les coordinations cinq et six: il s'agit du bicarbonate [7-8, 92-93]. Dans les centres réactionnels des bactéries pourpres, le fer peut être échangé par d'autres métaux, tels que : le Mn^{2+}, Co^{2+}, Ni^{2+} et le Cu^{2+}, dans ce cas le transfert d'électrons entre Q_A et Q_B n'est ralenti que de moitié [94]. Des centres contenant naturellement le Mn^{2+} à la place deu fer ont été identifiés [95]. Ces études ont suggéré que ce fer a un rôle marginal dans le transfert d'électrons entre Q_A et Q_B dans le centre réactionnel des bactéries pourpres.

En revanche, dans le PSII, le transfert d'électron en Q_A et Q_B est nettement plus sensible à l'environnement du Fe^{2+}. Le bicarbonate labile est le ligand du Fe^{2+} dans le PSII, ce ligand peut être échangé facilement par plusieurs molécules de nature différentes comme par exemple : le cyanure, NO et plusieurs acides carboxyliques (glycolate, formate…etc.) [14]. Dans le cas de ces changements, le transfert d'électrons entre Q_A et Q_B est ralenti.

Il a été observé que le fer pouvait être oxydé chimiquement par oxydation avec le ferricyanure [96], ensuite Zimmermann et al ont montré que le fer pouvait être photo-oxydé en présence de quinone [97].

Le potentiel redox du couple Fe^{2+}/Fe^{3+} mesuré à pH 7 est de 400 mV (avec une variation de -60 mV par unité le pH dans la zone pH 6 à 8,5) [96]. Le fer non-hémique peut être oxydé par Q_B^-/Q_BH_2 lors de l'utilisation de quinones exogènes (PPBQ) qui possèdent un plus haut potentiel redox que le couple Q_B^-/Q_BH_2 [96-97]. Il a été montré récemment que l'addition à l'obscurité de l'inhibiteur DCMU au PSII en présence de Q_B^- induit l'oxydation du fer non-hémique dans une fraction des centres de PSII [98]. Ishikita et Knapp, 2005, ont proposé à l'aide de calcules théoriques que la formation de Q_BH_2 à partir de l'oxydation du fer non-hémique par Q_B^- fait intervenir la deprotonation de l'acide aminé D1-His252. Ce même groupe a vérifié que le potentiel redox du fer non-hémique est influencé par l'états des quinones Q_A et Q_B ; à pH 6,5, en présence de Q_A^-, le potentiel redox du fer est estimé à +313 mV, alors qu'en présence de Q_B^- son potentiel est de +207 mV.

8.2 Le (bi)carbonate et l'effet du formate

Le rôle du bicarbonate a longtemps été discuté dans la littérature, les auteurs ont souvent interprété les données d'inhibition du transfert d'électrons après une déplétion du

bicarbonate (phénomène connu sous le nom de l'effet bicarbonate) à un effet du bicarbonate sur le côté donneur ou sur le côté accepteur [99]. L'effet du bicarbonate direct sur le côté donneur est controversé [100]. Une autre théorie a été établie par Klimov et al, [101] afin de prouver l'effet du bicarbonate sur le côté donneur. Cette théorie implique le bicarbonate dans le processus de photoactivation du cluster de Mn_4Ca [39, 102]. L'effet du bicarbonate sur le côté accepteur est en revanche plus accepté [99, 103]. La substitution du bicarbonate par le formate, permettant d'enlever le bicarbonate, a longtemps été utilisée [99].

La substitution du bicarbonate par le formate induit un ralentissement du transfert d'électron de Q_A^- à Q_B et à Q_B^- par un facteur de cinq et dix fois respectivement, cette inhibition peut être levée par simple addition de bicarbonate [86, 104-106]. L'échange de Q_BH_2 est inhibé par un facteur 100 [105, 107-108]. Certaines de ces inhibitions sont pourraient être dues à l'inhibition ou à la perturbation des réactions de protonation qui sont couplées aux transferts d'électrons [92]. Une explication claire de cet effet du formate (ou de déplétion du bicarbonate) est encore manquante [99, 109]. Dans un travail récent, il a été montré que le ligand du fer pourrait être le carbonate au lieu du bicarbonate [110]. La charge négative supplémentaire sur le carbonate comparé au bicarbonate est supposée avoir une importance pour le transfert d'électrons couplé aux protons.

8.3 Le potentiel redox de Q_A et de Q_B

Le potentiel redox de Q_A dans le PSII a été mesuré. Krieger et al, 1995 ont recensé plus de 35 valeurs pour le potentiel redox du couple Q_A/Q_A^- [111]. Ce large panel de valeurs a été rationalisé par l'état (ou la structure) du PSII et par la méthode utilisée. Chez les plantes, dans le cas où le cluster de Mn_4Ca était présent, la valeur du potentiel de demi-réduction pour le couple Q_A/Q_A^- était basse (-80 mV), alors qu'en l'absence de ce cluster une valeur haute à été mesurée (+65 mV) [112-113]. Le même résultat a été trouvé si le Ca^{2+} était enlevé tout en laissant le Mn_4 en place [114-115]. Le remplacement du Ca^{2+} par le Sr^{2+} provoque un ralentissement dans la réoxydation de Q_A^- par Q_B [116]. Le potentiel redox a récemment été mesuré dans un échantillon contenant le Sr^{2+} à la place du Ca^{2+}. Les auteurs ont trouvé que le potentiel redox du couple $Q_A/Q_A^{\bullet-}$ est moins réducteur en présence de Sr^{2+} (Kato, Boussac et Sugiura, communication personnelle). Le changement de potentiel redox de $Q_A/Q_A^{\bullet-}$ est donc probablement due à la présence ou l'absence de Ca^{2+} qui perturbe la structure du cluster de Mn_4 et influence le côté accepteur du PSII qui se situe à ~45Å.

Le potentiel redox du couple Q_A/Q_A^- peut être influencé par l'occupation de la poche de Q_B par des inhibiteurs tels que le DCMU (le potentiel du couple Q_A/Q_A^- devient plus oxydant) ou le bromoxynil (le potentiel du couple Q_A/Q_A^- devient plus réducteur) [98, 117], voir [118]. L'effet de la liaison des inhibiteurs sur le potentiel redox du couple Q_A/Q_A^- est peut-être dû aux changements du réseau de liaisons hydrogène entre le résidu D2-His214 et Q_A ; la nature de ce changement est très probablement différente de celui induit par l'absence du cluster de Mn_4Ca [118-119].

Le changement de potentiel de demi-réduction de Q_A/Q_A^- en fonction de l'état du cluster de Mn_4Ca pourrait avoir un grand rôle sur les réactions de recombinaison de charges qui peuvent générer l'état de triplet des Chl ($^3P_{680}$) pouvant interagir avec l'oxygène à l'état de triplet et produire ainsi de l'oxygène singulet extrêmement réactif et dangereux pour le PSII [112, 118, 120].

Récemment, le potentiel de demi-réduction de Q_A/Q_A^- a aussi été mesuré chez *T. elongatus*, le même phénomène a été observé concernant les valeurs du potentiel redox du couple Q_A/Q_A^-. -140 mV et +20 mV ont été trouvées pour la forme active et la forme sans cluster de Mn_4Ca, respectivement [121]. Ces valeurs sont plus négatives que celle trouvées chez les plantes.

Le potentiel redox de la plastoquinone du pool membranaire (PQ/PQH_2) est de ~ +130 mV à pH 6,5 [122]. Le potentiel redox des couples Q_B/Q_B^- et Q_B^-/Q_BH_2 ont été jusqu'à présent très peu mesurés dans le PSII. Un potentiel redox de +60 mV a été mesuré directement pour le couple Q_B/Q_B^- chez une cyanobactérie (*Phormidium laminosum*). Ensuite, il a été proposé une valeur de 0 mV pour le couple Q_B^-/Q_BH_2 [123]. Cette valeur a été obtenue après une seule vague non réversible de titration, ce qui remet en cause la validité de ces valeurs.

La force motrice entre Q_A/Q_A^- et Q_B/Q_B^- est estimée entre 70 mV et 83 mV [124-127]. Ces valeurs sont en harmonie avec la constante d'équilibre qui est de ~20 à pH7 pour les couples $Q_A^-Q_B \leftrightarrow Q_AQ_B^-$ [124, 128].

La mesure du potentiel redox de Q_B/Q_B^- et Q_B^-/Q_BH_2 est d'une importance primordiale. Malheureusement, la titration de Q_B s'avère très difficile. En effet, Q_B/Q_B^- n'a pas de signal facilement mesurable comparé à l'état Q_A/Q_A^- qui peut être suivie par fluorescence. L'utilisation de méthodes optiques est compliquée pour suivre et titrer Q_B/Q_B^-. Les signaux RPE de Q_B^- sont très petits et élargis.

8.4 Diagramme énergétique du transfert d'électrons dans le PSII

Pour l'instant, seul le potentiel redox des couples Pheo/Pheo$^-$ et Q_A/Q_A^- sont mesurés directement. En effet, le potentiel redox de Pheo/Pheo$^-$ a été mesuré il ya plus de 30 ans. Klimov et al, et Rutherford et al, ont trouvé une valeur proche de -605 mV [129-130]. Cette valeur a été pendant longtemps acceptée et utilisé dans la littérature. Kato et el, [131] ont récemment remesuré cette valeur, et ont trouvé -505 mV (100 mV de différence), ce qui a permis de réconcilier les cinétiques et les résultats de titrations redox [132-133]. La différence d'énergie libre entre P_{680}^*/Pheo et P_{680}^+/Pheo$^-$ est estimé entre -150 mV [134] et -165 mV [135] ce qui permet de déduire la valeur du couple P_{680}^*/P_{680}^+ entre -620 mV et -660 mV. Le potentiel du couple P_{680}/P_{680}^+ est estimé entre 1170 mV et 1210 mV [121, 132-133].

En se basant sur les connaissances expérimentales et théoriques, le diagramme énergétique du transfert d'électrons dans le PSII est proposé (Fig. 6). Le diagramme des potentiels redox des différents cofacteurs présents dans le PSII, mesurés dans le PSII *T. elongatus* sont présentés.

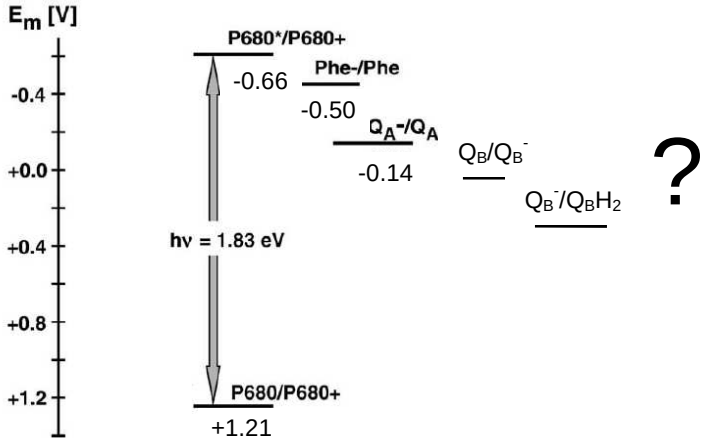

Figure 6: Les potentiels redox estimés impliqués dans le transfert d'électron primaire et secondaire selon Shibamoto et al, [121], dans ce model, le potentiel de Tyr_Z/Tyr_Z^+ est estimé être inferieur au potentiel redox du couple P_{680}/P_{680}^+. Les potentiels redox liés à Q_B sont inconnu jusqu'à présent.

9. Objectifs et résumé de ma thèse

Les signaux RPE de Q_B^- sont couplés magnétiquement au fer non-hémique. Ces signaux sont petits et souvent difficilement différenciables des signaux de $Q_A^-Fe^{2+}$. J'ai dans un premier temps cherché à générer un signal plus grand et différent de celui de $Q_A^-Fe^{2+}$, et

cela par l'utilisation du formate. Le formate a la capacité de substituer le ligand naturel (le bicarbonate) du fer non-hémique et il a été montré depuis plus de 30 ans que lorsque le formate lie le fer non-hémique, le signal RPE de $Q_A^-Fe^{2+}$ devient dix fois plus grand que la normale. J'ai donc cherché à générer pour la première fois le signal $Q_B^-Fe^{2+}$ en présence de formate. Les résultats sont présentés dans l'article 1. L'effet du formate sur le transfert d'électrons entre Q_A et Q_B est aussi étudié en utilisant la thermoluminescence, les résultats sont présentés dans l'article 2.

Durant la réalisation de ce projet, j'ai résolu pour la première fois des signaux complets d'RPE appartenant à $Q_A^-Fe^{2+}$ et $Q_B^-Fe^{2+}$. Les résultats sont présentés dans l'article 3. Ces nouveaux signaux s'avèrent encore plus grands que les signaux générés par le formate. En collaboration avec le Dr. Nicholas Cox, les simulations théoriques ont été réalisées afin de renforcer nos connaissances et simuler nos résultats expérimentaux. J'ai participé à la formation des spectres de $Q_A^-Fe^{2+}$, $Q_B^-Fe^{2+}$ et $Q_A^-Fe^{2+}Q_B^-$ qui ont ensuite été utilisés pour les simulations, les résultats sont présentés dans l'article 10 en annexes.

Dans l'article 4 de cette thèse, j'ai mis en évidence que le fer pouvait être oxydé par Q_B^-/Q_BH_2 de manière naturelle dans une fraction des centres de PSII et cela, dans le PSII WT, dans le mutant PsbA3 ou encore dans le mutant sans TyrD.

L'effet de la réduction du PSII par le dithionite est étudié. J'ai trouvé que le dithionite pouvait réduire le cluster de Mn_4Ca et produire l'état S_0. De plus que le dithionite pouvait réduire le coté accepteur d'électrons. J'ai trouvé que le signal RPE de QA-Fe2+ évolue avec l'incubation à température ambiante. La discussion sur l'origine de ce phénoméne est présentée dans l'article 5.

En collaboration avec le Dr. Roncel Mercédes, j'ai participé à la mise en évidence d'un haut potentiel redox du cytochrome *c550*, cela remet en question le rôle rempli par cette sous unité. Les résultats sont présentés dans l'article 6.

En collaboration avec le Dr. Krieger-Liszkay Anja, j'ai participé au projet de mesure du potentiel redox de Q_A dans *T. elongatus*, par la réalisation des préparations de PSII. Au cours de cette collaboration, nous avons testé l'hypothèse du changement de structure du PSII

en l'absence du cluster de Mn_4Ca, en utilisant un *cross-linker* capable de bloquer la structure dans une conformation donnée. Ces résultats sont présentés dans l'article 7.

Dans la dernière partie de ma thèse, je me suis focalisé sur la caractérisation de la première étape de photoactivation. Les résultats seront présentés dans l'article 8 en cours de préparation. Je me suis intéressé dans un premier temps à la mise au point d'un protocole semblable de photo-oxydation du Mn^{2+} à -20°C chez *T. elongatus*, puis dans un second temps, à la vérification du nombre d'ions Mn^{2+} oxydés par l'apo-PSII à -20°C. Le résultat est contradictoire comparé à ce qui avait été proposé dans la littérature. Plusieurs Mn^{2+} (jusqu'à 10 Mn^{2+} sont photo-oxydés à -20°C). J'ai mis au point de nouvelles méthodes de piégeage d'intermédiaires au cours de la photoactivation dans le PSII de *T. elongatus*. J'ai aussi mis en évidence que lorsque le Mn^{2+} lie un ion Cl^-, le signal haut champ RPE est influencé, ce qui permettra la distinction en un Mn^{2+} en interaction avec une protéine ou bien "libre" en interaction avec le Cl^- présent dans le tampon. L'effet du Cl^- sur le spectre du Mn^{2+} mesuré en RPE haut champs est présenté dans l'article 9 en annexes.

MATERIELS ET METHODES

Souches utilisées

Souches *T. elongatus* :

PSII CP43 WT : contenant une étiquette histidine sur le coté C-terminal de la sous unité CP43 [4].
PSII CP43 (PsbA3) : contenant une étiquette histidine le coté C-terminal de la sous unité CP43, exprimant que la copie du gène *psbA3* [98, 136].
PSII TyrD less : contenant une étiquette histidine le coté C-terminal de la sous unité CP43, la tyrosine D est muté par une phénylalanine [137].
PSII CP47 : contenant une étiquette histidine le coté C-terminal de la sous unité CP47 [138].

Epinards:
Achetés au marché de Daumesnil à Paris.

Milieux de croissance (*T. elongatus*)

DTN + $NaHCO_3$. Solution (stock concentrée 20x) dans 1 L d'eau stérile : 3,8 g EDTA Na_2 ; 2 g $MgSO_4$, $7H_2O$; 2g KNO_3 ;14 g $NaNO_3$; 2,8 g $NaHPO_4.2H_2O$; 1,09 g $CaCl_2.H_2O$; 0,16 g NaCl ; pH7,5.

Isolation du PSII

Les cellules des différentes souches de *T. elongatus* sont ensemencées dans des erlens-mayers de 3 l contenant 1 à 1,5 l de culture en présence de milieu DTN, décrit par [139]. Les cultures sont incubées sous agitation rotative de 120 rpm à 45°C dans une atmosphère enrichie en CO_2 (5%) et éclairées continuellement par des lampes fluorescentes à lumière blanche ayant une intensité de 80 µmoles photons $m^{-2}.s^{-1}$. Les souches mutantes sont maintenues par ajout de l'antibiotique approprié. La concentration cellulaire est mesurée par spectroscopie à 800 nm. La correspondance entre la $DO_{800\ nm}$ et la concentration cellulaire a été établie par numération de cellules viables sur milieu DTN solide (0,5 u. $DO_{800\ nm} \approx 6.10^8$ cellules /mL).

Les complexes PSII sont préparés selon la méthode améliorée dans notre laboratoire selon [44], protocole inspiré de [4]. Les cellules de *T. elongatus* (16 l) sont cultivées jusqu'à atteindre une DO de 0,6 - 0.8. Les cellules sont centrifugées à 22°C pendant 5 minutes à 6500

rpm (rotor JA10) puis lavées par tampon TP1 (40 mM MES pH 6,5 ; 15 mM $MgCl_2$; 15 mM $CaCl_2$, 10% glycerol et 1 M Bétaine) et sont centrifugées 10 minutes à 7000 rpm et 4°C. A partir de cette étape il est nécessaire de travailler dans le noir, au froid et être le plus rapide que possible. Le culot contenant les cellules est remis en suspension et sa concentration en chlorophylle est ajustée à 0.8 – 1.2 mg/ml en chlorophylles dans le tampon TP1. Des inhibiteurs de protéases sont ajoutés : 1 mM benzamidine, 1 mM acide caproïque et 50 µg/ml DNAase I en présence de 0,2% BSA. Puis les cellules sont cassées avec une Presse de French à une pression de 700 PSI. Les cellules entières sont éliminées par une centrifugation de 5 minutes à 3500 rpm (rotor JA20) et 4°C. Le surnageant contenant la phase cytoplasmique ainsi que les membranes est récupéré. Les membranes sont isolées par centrifugation de 40 min à 4°C et 50000 rpm (70 Ti Beckman rotor). Les thylakoïdes sont lavées par le TP1 et centrifugées 40 minutes à 4°C et 50000 rpm (70 Ti Beckman rotor). Le culot est remis en suspension dans le TP1 à une concentration en chlorophylle de 1 mg/ml. Les membranes sont solubilisées dans 1% de β-maltosyl- dodecyl et 100 mM de NaCl en concentration final et précipitées par centrifugation de 15 min à 50000 rpm (70 Ti Beckman rotor) à 4°C. Le surnageant est mélangé au même volume de résine d'affinité nickel Probond^{TM} (Invitrogen, Groningen, Pays-Bas) équilibré avec le tampon TP1 et agité doucement pendant 2 minutes à l'obscurité et 4°C. Le mélange est déposé sur colonne et lavé avec 5 – 6 volumes de tampon de lavage TP3 (50 mM MES pH 6,5 ; 15 mM $MgCl_2$; 15 mM $CaCl_2$; 100 mM NaCl ; 15 mM Imidazole ; 10% glycérol ; 1 M Bétaine), le débit de lavage est régler de façon suffisante pour toute la nuit. Le lendemain, le PSII est élué par le tampon d'élution TP4 (150 mM MES pH 6,5 ; 15 mM $MgCl_2$; 300 mM Imidazole ; 200 mM NaCl ; 15 mM $CaCl_2$; 0,1% Dodecyl maltosyl ; 10% glycérol, 1 M Bétaine). Les fractions d'élutions sont collectées et mélangées puis concentrées sur tubes Amicons (100 kDa). Le précipité est remis en suspension dans le tampon TP1 et la concentration en chlorophylle est mesurée. Le PSII isolé est conservé dans l'azote liquide.

Mesure de la concentration en chlorophylle : Diluer 5 µl de l'échantillon PSII purifié dans 1 ml de méthanol. L'échantillon est vortexé et centrifugé 1 min à 14000 rpm puis l'absorbance de la chlorophylle est mesurée à 665 nm. La relation suivante nous donne la concentration en chlorophylle dans le PSII purifié : [chlorophylle] = $DO_{665\ nm}$ x d/ε ($\varepsilon_{chlorophylle}$ = 74,5 ml/mg cm^{-1}. d : dilution de la chlorophylle)

Mesure de l'activité d'émission d'oxygène du PS II : L'activité d'émission d'oxygène du PSII est mesurée (5 µg Chlorophylle/ml de PS II) dans le tampon TP1 en présence de 0,5 mM DBCQ (2,6, dichloro-p-benzoquinone, dissout dans l'éthanol) qui joue le rôle d'accepteur

d’électrons. Les mesures sont réalisées à 25°C au moyen de l’électrode à oxygène (électrode de Clark) avec une lumière blanche saturante.

Mesure RPE

Les mesures RPE sont enregistrées sur Bruker Elexsys 500 X-band spectrometer équipé d’un résonateur standard ER 4102 et d’un cryostat Oxford Instruments ESR 900. Les réglages de l’instrument sont : 9,4 GHz pour la fréquence micro-onde avec une modulation de 100 kHz. Les autres paramètres, se referer aux différents chapitres. En général, un volume final de 120-150 µL d’échantillon est utilisé pour les mesures RPE. Les échantillons sont mis dans des tubes RPE en quartz d'un diamètre externe de 4 mm. Les échantillons sont d’abords congeler dans un bain d’éthanol refroidi au CO_2 solide à 200 K. Tous les échantillons sont dégazés à cette température. Les tubes RPE sont ensuite transvasés dans un bain d’azote liquide avant la mesure RPE.

Thermoluminescence

La thermoluminescence est mesurée par l’utilisation de l’appareillage construit par Ducruet [140]. Les échantillons d’une concentration de 10 µg Chl/ml de PSII sont incubés dans le noir à température ambiante durant 30 min. Les échantillons sont éclairés à 5°C par l’utilisation de flashs saturants produits par une lampe xénon (PerkinElmer Optoelectronics). Les échantillons sont ensuite congelés à -10°C dans les 5 secondes. Après 5 sec supplémentaire d’incubation à -10°C, les échantillons sont chauffés jusqu'à 80°C avec une constante de chauffage de (0,33°C/s).

Références:

[1] N. Nelson, C.F. Yocum, Structure and function of photosystems I and II, Annu Rev Plant Biol, 57 (2006) 521-565.
[2] L.O. Bjorn, Govindjee, The evolution of photosynthesis and chloroplasts, Curr. Sci., 96 (2009) 1466-1474.
[3] T. Yamaoka, K. Satoh, S. Katoh, Photosynthetic activities of a thermophilic blue-green-alga, Plant Cell Physiol, 19 (1978) 943-954.
[4] M. Sugiura, Y. Inoue, Highly purified thermo-stable oxygen-evolving photosystem II core complex from the thermophilic cyanobacterium *Synechococcus elongatus* having his-tagged CP43, Plant Cell Physiol, 40 (1999) 1219-1231.
[5] G. DalCorso, P. Pesaresi, S. Masiero, E. Aseeva, D.S. Nemann, G. Finazzi, P. Joliot, R. Barbato, D. Leister, A complex containing PGRL1 and PGR5 is involved in the switch between linear and cyclic electron flow in Arabidopsis, Cell, 132 (2008) 273-285.
[6] J. Deisenhofer, O. Epp, K. Miki, R. Huber, H. Michel, X-ray structure-analysis of a membrane-protein complex - electron-density map at 3A resolution and a model of the chromophores of the photosynthetic reaction center from *Rhodopseudomonas viridis*, J Mol Biol, 180 (1984) 385-398.
[7] H. Michel, J. Deisenhofer, Relevance of the photosynthetic reaction center from purple bacteria to the structure of Photosystem II, Biochemistry, 27 (1988) 1-7.
[8] A.W. Rutherford, Photosystem-II, the water-splitting enzyme, Trends Biochem Sci, 14 (1989) 227-232.
[9] A. Zouni, H.T. Witt, J. Kern, P. Fromme, N. Krauss, W. Saenger, P. Orth, Crystal structure of photosystem II from *Synechococcus elongatus* at 3.8 angstrom resolution, Nature, 409 (2001) 739-743.
[10] K.N. Ferreira, T.M. Iverson, K. Maghlaoui, J. Barber, S. Iwata, Architecture of the photosynthetic oxygen-evolving center, Science, 303 (2004) 1831-1838.
[11] A. Guskov, J. Kern, A. Gabdulkhakov, M. Broser, A. Zouni, W. Saenger, Cyanobacterial photosystem II at 2.9-angstrom resolution and the role of quinones, lipids, channels and chloride, Nat Struct Mol Biol, 16 (2009) 334-342.
[12] B.A. Diner, R.D. Britt, The redox-active tyrosines Y_Z and Y_D, in: T. Wydrzynski, K. Satoh (Eds.) Photosystem II. The light-driven water: plastoquinone oxidoreductase, Springer, Dordecht, The Netherlands, 2005, pp. 207-233.
[13] A.W. Rutherford, A. Boussac, Water photolysis in biology, Science, 303 (2004) 1782-1784.
[14] V. Petrouleas, A.R. Crofts, The iron-quinone acceptor complex, in: T. Wydrzynski, K. Satoh (Eds.) Photosystem II. The light-driven water: plastoquinone oxidoreductase, Springer, Dordecht, The Netherlands, 2005, pp. 177-206.
[15] B. Hankamer, E. Morris, J. Nield, A. Carne, J. Barber, Subunit positioning and transmembrane helix organisation in the core dimer of photosystem II, Febs Lett, 504 (2001) 142-151.
[16] I. Enami, M. Iwai, A. Akiyama, T. Suzuki, A. Okumura, T. Katoh, O. Tada, H. Ohta, J.R. Shen, Comparison of binding and functional properties of two extrinsic components, Cyt c_{550} and a 12 kDa protein, in cyanobacterial PSII with those in red algal PSII, Plant Cell Physiol, 44 (2003) 820-827.
[17] L.E. Thornton, H. Ohkawa, J.L. Roose, Y. Kashino, N. Keren, H.B. Pakrasi, Homologs of plant PsbP and PsbQ proteins are necessary for regulation of photosystem II activity in the cyanobacterium Synechopystis 6803, Plant Cell, 16 (2004) 2164-2175.
[18] R. Nagao, A. Moriguchi, T. Tomo, A. Niikura, S. Nakajima, T. Suzuki, A. Okumura, M. Iwai, J.R. Shen, M. Ikeuchi, I. Enami, Binding and functional properties of five extrinsic

proteins in oxygen-evolving Photosystem II from a marine centric diatom, *Chaetoceros gracilis*, J Biol Chem, 285 (2010) 29191-29199.
[19] A.K. Williamson, Structural and functional aspects of the MSP (PsbO) and study of its differences in thermophilic versus mesophilic organisms, Photosynth Res, 98 (2008) 365-389.
[20] S.P. Mayfield, P. Bennoun, J.D. Rochaix, Expression of the nuclear encoded OEE1 protein is required for oxygen evolution and stability of Photosystem II particles in *Chlamydomonas reinhardtii*, EMBO J, 6 (1987) 313-318.
[21] X.P. Yi, M. McChargue, S. Laborde, L.K. Frankel, T.M. Bricker, The manganese-stabilizing protein is required for photosystem II assembly/stability and photoautotrophy in higher plants, J Biol Chem, 280 (2005) 16170-16174.
[22] J.W. Murray, J. Barber, Structural characteristics of channels and pathways in photosystem II including the identification of an oxygen channel, J Struct Biol, 159 (2007) 228-237.
[23] D.F. Ghanotakis, G.T. Babcock, C.F. Yocum, Calcium reconstitutes high-rates of oxygen evolution in polypeptide depleted Photosystem II preparations, Febs Lett, 167 (1984) 127-130.
[24] J.L. Roose, K.M. Wegener, H.B. Pakrasi, The extrinsic proteins of photosystem II, Photosynth Res, 92 (2007) 369-387.
[25] F. Guerrero, A. Sedoud, D. Kirilovsky, A.W. Rutherford, J.M. Ortega, M. Roncel, A high redox potential form of cytochrome c550 in Photosystem II from Thermosynechococcus elongatus, J. Biol. Chem, (2010).
[26] Y. Kashino, W.M. Lauber, J.A. Carroll, Q.J. Wang, J. Whitmarsh, K. Satoh, H.B. Pakrasi, Proteomic analysis of a highly active photosystem II preparation from the cyanobacterium Synechocystis sp PCC 6803 reveals the presence of novel polypeptides, Biochemistry, 41 (2002) 8004-8012.
[27] T.C. Summerfield, J.A. Shand, F.K. Bentley, J.J. Eaton-Rye, PsbQ (Sll1638) in Synechocystis sp PCC 6803 is required for photosystem II activity in specific mutants and in nutrient-limiting conditions, Biochemistry, 44 (2005) 805-815.
[28] J.L. Roose, Y. Kashino, H.B. Pakrasi, The PsbQ protein defines cyanobacterial Photosystem II complexes with highest activity and stability, Proc. Natl. Acad. Sci. U. S. A., 104 (2007) 2548-2553.
[29] S.A. Jackson, R.D. Fagerlund, S.M. Wilbanks, J.J. Eaton-Rye, Crystal structure of PsbQ from Synechocystis sp PCC 6803 at 1.8 angstrom: implications for binding and function in cyanobacterial Photosystem II, Biochemistry, 49 (2010) 2765-2767.
[30] F. Michoux, K. Takasaka, M. Boehm, P.J. Nixon, J.W. Murray, Structure of CyanoP at 2.8 angstrom: implications for the evolution and function of the PsbP subunit of Photosystem II, Biochemistry, 49 (2010) 7411-7413.
[31] R. Radmer, G.M. Cheniae, Photoactivation of manganese catalyst of O2 evolution .2. 2-Quantum mechanism, Biochim Biophys Acta, 253 (1971) 182-&.
[32] N. Tamura, G. Cheniae, Photoactivation of the water-oxidizing complex in Photosystem-II membranes depleted of Mn and extrinsic proteins .1. Biochemical and kinetic characterization, Biochim Biophys Acta, 890 (1987) 179-194.
[33] R.J. Debus, The manganese and calcium-ions of photosynthetic oxygen evolution, Biochim Biophys Acta, 1102 (1992) 269-352.
[34] A.F. Miller, G.W. Brudvig, Manganese and calcium requirements for reconstitution of oxygen-evolution activity in manganese-depleted Photosystem II membranes, Biochemistry, 28 (1989) 8181-8190.
[35] T. Ono, Metallo-radical hypothesis for photoassembly of Mn_4-cluster of photosynthetic oxygen evolving complex, Biochim Biophys Acta, 1503 (2001) 40-51.
[36] K.A. Campbell, D.A. Force, P.J. Nixon, F. Dole, B.A. Diner, R.D. Britt, Dual-mode EPR detects the initial intermediate in photoassembly of the photosystem II mn cluster: The

influence of amino acid residue 170 of the D1 polypeptide on Mn coordination, J Am Chem Soc, 122 (2000) 3754-3761.
[37] A.M. Tyryshkin, R.K. Watt, S.V. Baranov, J. Dasgupta, M.P. Hendrich, G.C. Dismukes, Spectroscopic evidence for Ca^{2+} involvement in the assembly of the Mn_4Ca cluster in the photosynthetic water-oxidizing complex, Biochemistry, 45 (2006) 12876-12889.
[38] J. Dasgupta, A.M. Tyryshkin, G.C. Dismukes, ESEEM spectroscopy reveals carbonate and an N-donor protein-ligand binding to Mn^{2+} in the photoassembly reaction of the Mn4Ca cluster in photosystem II, Angew Chem Int Edit, 46 (2007) 8028-8031.
[39] J. Dasgupta, G.M. Ananyev, G.C. Dismukes, Photoassembly of the water-oxidizing complex in photosystem II, Coordin. Chem. Rev, 252 (2008) 347-360.
[40] J. Dasgupta, A.M. Tyryshkin, S.V. Baranov, G.C. Dismukes, Bicarbonate coordinates to Mn^{3+} during photo-assembly of the catalytic Mn_4Ca core of photosynthetic water oxidation: EPR characterization, Appl. Magn. Reson., 37 (2010) 137-150.
[41] P. Joliot, G. Barbieri, R. Chabaud, A new model of photochemical centers in system-2, Photochem Photobiol, 10 (1969) 309-&.
[42] B. Kok, B. Forbush, M. Mcgloin, Cooperation of charges in photosynthetic O2 evolution .1. A linear 4 step mechanism, Photochem Photobiol, 11 (1970) 457-&.
[43] M. Miqyass, H.J. van Gorkom, C.F. Yocum, The PSII calcium site revisited, Photosynth Res, 92 (2007) 275-287.
[44] A. Boussac, F. Rappaport, P. Carrier, J.M. Verbavatz, R. Gobin, D. Kirilovsky, A.W. Rutherford, M. Sugiura, Biosynthetic Ca^{2+}/Sr^{2+} exchange in the photosystem II oxygen-evolving enzyme of *Thermosynechococcus elongatus*, J Biol Chem, 279 (2004) 22809-22819.
[45] J.W. Murray, K. Maghlaoui, J. Kargul, N. Ishida, T.L. Lai, A.W. Rutherford, M. Sugiura, A. Boussac, J. Barber, X-ray crystallography identifies two chloride binding sites in the oxygen evolving centre of Photosystem II, Energ Environ Sci, 1 (2008) 161-166.
[46] J.M. Peloquin, K.A. Campbell, D.W. Randall, M.A. Evanchik, V.L. Pecoraro, W.H. Armstrong, R.D. Britt, Mn-55 ENDOR of the S_2 state multiline EPR signal of photosystem II: Implications on the structure of the tetranuclear Mn cluster, J Am Chem Soc, 122 (2000) 10926-10942.
[47] A. Haddy, EPR spectroscopy of the manganese cluster of photosystem II, Photosynth Res, 92 (2007) 357-368.
[48] J. Messinger, J.H. Robblee, W.O. Yu, K. Sauer, V.K. Yachandra, M.P. Klein, The S-0 state of the oxygen-evolving complex in photosystem II is paramagnetic: Detection of EPR multiline signal, J Am Chem Soc, 119 (1997) 11349-11350.
[49] K.A. Ahrling, S. Peterson, S. Styring, An oscillating manganese electron paramagnetic resonance signal from the S-0 state of the oxygen evolving complex in photosystem II, Biochemistry, 36 (1997) 13148-13152.
[50] A. Boussac, H. Kuhl, E. Ghibaudi, M. Rogner, A.W. Rutherford, Detection of an electron paramagnetic resonance signal in the S_0 state of the manganese complex of photosystem II from *Synechococcus elongatus*, Biochemistry, 38 (1999) 11942-11948.
[51] J. Messinger, J.H.A. Nugent, M.C.W. Evans, Detection of an EPR multiline signal for the S_0 state in photosystem II, Biochemistry, 36 (1997) 11055-11060.
[52] S.L. Dexheimer, M.P. Klein, Detection of a paramagnetic intermediate in the S1-state of the photosynthetic oxygen-evolving complex, J Am Chem Soc, 114 (1992) 2821-2826.
[53] T. Yamauchi, H. Mino, T. Matsukawa, A. Kawamori, T. Ono, Parallel polarization electron paramagnetic resonance studies of the S_1 state manganese cluster in the photosynthetic oxygen-evolving system, Biochemistry, 36 (1997) 7520-7526.
[54] K.A. Campbell, J.M. Peloquin, D.P. Pham, R.J. Debus, R.D. Britt, Parallel polarization EPR detection of an S_1 state "multiline" EPR signal in photosystem II particles from *Synechocystis sp*. PCC 6803, J Am Chem Soc, 120 (1998) 447-448.

[55] W.Y. Hsieh, K.A. Campbell, W. Gregor, R.D. Britt, D.W. Yoder, J.E. Penner-Hahn, V.L. Pecoraro, The first spectroscopic model for the S_1 state multiline signal of the OEC, Biochim Biophys Acta, 1655 (2004) 149-157.
[56] G.C. Dismukes, Y. Siderer, Intermediates of a polynuclear manganese center involved in photosynthetic oxidation of water, Proc. Natl. Acad. Sci. U. S. A., 78 (1981) 274-278.
[57] O. Hansson, L.E. Andreasson, EPR-detectable magnetically interacting manganese ions in the photosynthetic oxygen-evolving system after continuous illumination, Biochim Biophys Acta, 679 (1982) 261-268.
[58] A. Boussac, S. Un, O. Horner, A.W. Rutherford, High-spin states (S >= 5/2) of the photosystem II manganese complex, Biochemistry, 37 (1998) 4001-4007.
[59] A. Boussac, H. Kuhl, S. Un, M. Rogner, A.W. Rutherford, Effect of near-infrared light on the S_2 state of the manganese complex of photosystem II from *Synechococcus elongatus*, Biochemistry, 37 (1998) 8995-9000.
[60] A. Boussac, M. Sugiura, A.W. Rutherford, P. Dorlet, Complete EPR spectrum of the S_3 state of the oxygen-evolving Photosystem II, J Am Chem Soc, 131 (2009) 5050-+.
[61] J. Messinger, G. Seaton, T. Wydrzynski, U. Wacker, G. Renger, S_{-3} state of the water oxidase in photosystem II, Biochemistry, 36 (1997) 6862-6873.
[62] G. Schansker, C. Goussias, V. Petrouleas, A.W. Rutherford, Reduction of the Mn cluster of the water-oxidizing enzyme by nitric oxide: Formation of an S_{-2} state, Biochemistry, 41 (2002) 3057-3064.
[63] J. Yano, V.K. Yachandra, Oxidation state changes of the Mn_4Ca cluster in Photosystem II, Photosynth Res, 92 (2007) 289-303.
[64] A.M.A. Hays, I.R. Vassiliev, J.H. Golbeck, R.J. Debus, Role of D1-His190 in proton-coupled electron transfer reactions in photosystem II: A chemical complementation study, Biochemistry, 37 (1998) 11352-11365.
[65] A.W. Rutherford, A. Boussac, P. Faller, The stable tyrosyl radical in Photosystem II: why D?, Biochim Biophys Acta, 1655 (2004) 222-230.
[66] S. Styring, A.W. Rutherford, In the oxygen-evolving complex of Photosystem II the S_0 state is oxidized to the S_1 State by D^+ (Signal-II slow), Biochemistry, 26 (1987) 2401-2405.
[67] G.A. Ananyev, I. Sakiyan, B.A. Diner, G.C. Dismukes, A functional role for tyrosine-D in assembly of the inorganic core of the water oxidase complex of photosystem II and the kinetics of water oxidation, Biochemistry, 41 (2002) 974-980.
[68] P. Faller, C. Fufezan, A.W. Rutherford, Side-path electrondonnors: cytochrom b_{559}, chlorophyll Z and beta-caroten, in: T.J. Wydrzynski, K. Satoh (Eds.) Photosystem II: The light-driven water: plastoquinone oxidoreductase, Springer, Dordecht, the Netherlands, 2005, pp. 347-365.
[69] L.K. Thompson, G.W. Brudvig, Cytochrome b-559 may function to protect Photosystem II from photoinhibition, Biochemistry, 27 (1988) 6653-6658.
[70] J. Whitmarsh, H.B. Pakrasi, Form and function of cytochrome *b-559*, in: D.R. Ort, C.F. Yocum (Eds.) Oxygenic photosynthesis: The light reactions, Kluwer Academic Publishers, The Netherlands, 1996, pp. 249-564.
[71] D.H. Stewart, G.W. Brudvig, Cytochrome b_{559} of photosystem II, Biochim Biophys Acta, 1367 (1998) 63-87.
[72] O. Nanba, K. Satoh, Isolation of a photosystem II reaction center consisting of D1 and D2 polypeptides and cytochrome b_{559}, Proc. Natl. Acad. Sci. U. S. A., 84 (1987) 109-112.
[73] D.B. Knaff, D.I. Arnon, Light-induced oxidation of a chloroplast b-type cytochrome at -189°C, Proc. Natl. Acad. Sci. U. S. A., 63 (1969) 956-&.
[74] M. Roncel, A. Boussac, J.L. Zurita, H. Bottin, M. Sugiura, D. Kirilovsky, J.M. Ortega, Redox properties of the photosystem II cytochromes *b*559 and *c*550 in the cyanobacterium *Thermosynechococcus elongatus*, J. Biol. Inorg. Chem., 8 (2003) 206-216.

[75] A. Magnuson, M. Rova, F. Mamedov, P.O. Fredriksson, S. Styring, The role of cytochrome b_{559} and $tyrosine_D$ in protection against photoinhibition during in vivo photoactivation of photosystem II, Biochim Biophys Acta, 1411 (1999) 180-191.
[76] F. Morais, J. Barber, P.J. Nixon, The chloroplast-encoded alpha subunit of cytochrome b-559 is required for assembly of the photosystem two complex in both the light and the dark in Chlamydomonas reinhardtii, J Biol Chem, 273 (1998) 29315-29320.
[77] N. Mizusawa, T. Yamashita, M. Miyao, Restoration of the high-potential form of cytochrome b559 of photosystem II occurs via a two-step mechanism under illumination in the presence of manganese ions, Biochim Biophys Acta, 1410 (1999) 273-286.
[78] C.A. Buser, B.A. Diner, G.W. Brudvig, Photooxidation of cytochrome b_{559} in oxygen-evolving Photosystem II, Biochemistry, 31 (1992) 11449-11459.
[79] N. Bondarava, L. De Pascalis, S. Al-Babili, C. Goussias, J.R. Golecki, P. Beyer, R. Bock, A. Krieger-Liszkay, Evidence that cytochrome b_{559} mediates the oxidation of reduced plastoquinone in the dark, J Biol Chem, 278 (2003) 13554-13560.
[80] N. Bondarava, C.M. Gross, M. Mubarakshina, J.R. Golecki, G.N. Johnson, A. Krieger-Liszkay, Putative function of cytochrome b_{559} as a plastoquinol oxidase, Physiol. Plantarum, 138 (2010) 463-473.
[81] J. Kruk, K. Strzalka, Redox changes of cytochrome b_{559} in the presence of plastoquinones, J Biol Chem, 276 (2001) 86-91.
[82] B. Bouges-Bouquet, Electron transfer between the two photosystems in spinach chloroplasts, Biochim Biophys Acta, 314 (1973) 250-256.
[83] B.R. Velthuys, J. Amesz, Charge accumulation at reducing side of system 2 of photosynthesis, Biochim Biophys Acta, 333 (1974) 85-94.
[84] C.A. Wraight, Oxidation-reduction physical-chemistry of the acceptor quinone complex in bacterial photosynthetic reaction centers - evidence for a new model of herbicide activity, Isr. J. Chem., 21 (1981) 348-354.
[85] R. de Wijn, H.J. van Gorkom, Kinetics of electron transfer from Q_A to Q_B in photosystem II, Biochemistry, 40 (2001) 11912-11922.
[86] H.H. Robinson, J.J. Eaton Rye, J.J.S. van Rensen, Govindjee, The effects of bicarbonate depletion and formate incubation on the kinetics of oxidation-reduction reactions of the Photosystem II quinone acceptor complex., Z.Naturforsch.(C), 39 (1984) 382-385.
[87] W. Weiss, G. Renger, UV-spectral characterization in tris-washed chloroplasts of the redox component-D1 which functionally connects the reaction center with the water-oxidizing enzyme system-Y in photosynthesis, Febs Lett, 169 (1984) 219-223.
[88] M.Y. Okamura, M.L. Paddock, M.S. Graige, G. Feher, Proton and electron transfer in bacterial reaction centers, Biochim Biophys Acta, 1458 (2000) 148-163.
[89] C.A. Wraight, Proton and electron transfer in the acceptor quinone complex of photosynthetic reaction centers from *Rhodobacter sphaeroides*, Front Biosci, 9 (2004) 309-337.
[90] J.P. Allen, G. Feher, Crystallization of reaction center from Rhodopseudomonas sphaeroides - preliminary characterization, Proc. Natl. Acad. Sci. U. S. A., 81 (1984) 4795-4799.
[91] R.H.G. Baxter, B.L. Seagle, N. Ponomarenko, J.R. Norris, Cryogenic structure of the photosynthetic reaction center of Blastochloris viridis in the light and dark, Acta Crystallogr. Sect. D-Biol. Crystallogr., 61 (2005) 605-612.
[92] J.J.S. van Rensen, W.J.M. Tonk, S.M. Debruijn, Involvement of bicarbonate in the protonation of the secondary quinone electron-acceptor of Photosystem-II via the non-heme Iron of the quinone-iron acceptor complex, Febs Lett, 226 (1988) 347-351.
[93] R. Hienerwadel, C. Berthomieu, Bicarbonate binding to the non-heme iron of photosystem II investigated by Fourier transform infrared difference spectroscopy and C-13-labeled bicarbonate, Biochemistry, 34 (1995) 16288-16297.

[94] R.J. Debus, G. Feher, M.Y. Okamura, Iron-depleted reaction centers from Rhodopseudomonas sphaeroides R-26.1 - Characterization and reconstitution with Fe2+, Mn2+, Co2+, Ni2+, Cu2+, and Zn2+, Biochemistry, 25 (1986) 2276-2287.
[95] A.W. Rutherford, I. Agalidis, F. Reisshusson, Manganese-quinone interactions in the electron-acceptor region of bacterial photosynthetic reaction centers, Febs Lett, 182 (1985) 151-157.
[96] B.A. Diner, V. Petrouleas, Q_{400}, the non-heme iron of the Photosystem-II iron-quinone complex - a spectroscopic probe of quinone and inhibitor binding to the reaction center Biochim Biophys Acta, 895 (1987) 107-125.
[97] J.L. Zimmermann, A.W. Rutherford, Photoreductant-induced oxidation of Fe^{2+} in the electron-acceptor complex of Photosystem-II, Biochim Biophys Acta, 851 (1986) 416-423.
[98] A. Boussac, M. Sugiura, F. Rappaport, Probing the quinone binding site of Photosystem II from *Thermosynechococcus elongatus* containing either PsbA1 or PsbA3 as the D1 protein through the binding characteristics of herbicides, Biochim Biophys Acta, 1807 (2011) 119-129.
[99] J.J.S. van Rensen, V.V. klimov, Role of bicarbonate in Photosystem II, in: T.J. Wydrzynski, K. Satoh (Eds.) Advances in Photosynthesis and Respiration Oxygenic Photosynthesis: Photosystem II. The light driven water: Plastoquinone oxidoreductase, Springer, Dordrecht, 2005, pp. 329-346.
[100] A.J. Stemler, The bicarbonate effect, oxygen evolution, and the shadow of Otto Warburg, Photosynth Res, 73 (2002) 177-183.
[101] V.V. Klimov, S.V. Baranov, Bicarbonate requirement for the water-oxidizing complex of photosystem II, Biochim Biophys Acta, 1503 (2001) 187-196.
[102] S.V. Baranov, G.M. Ananyev, V.V. Klimov, G.C. Dismukes, Bicarbonate accelerates assembly of the inorganic core of the water-oxidizing complex in manganese-depleted photosystem II: A proposed biogeochemical role for atmospheric carbon dioxide in oxygenic photosynthesis, Biochemistry, 39 (2000) 6060-6065.
[103] J.J.S. van Rensen, Role of bicarbonate at the acceptor side of Photosystem II, Photosynth Res, 73 (2002) 185-192.
[104] P. Jursinic, J. Warden, Govindjee, Major site of bicarbonate effect in system-II reaction evidence from ESR signal-II_{vf}, fast fluorescence yield changes and delayed light-emission, Biochim Biophys Acta, 440 (1976) 322-330.
[105] U. Siggel, R. Khanna, G. Renger, Govindjee, Investigation of the absorption changes of the plasto-quinone system in broken chloroplasts. The effect of bicarbonate-depletion, Biochim Biophys Acta, 462 (1977) 196-207.
[106] J.J. Eaton-Rye, Govindjee, Electron-transfer through the quinone acceptor complex of Photosystem-II after one or 2 actinic flashes in bicarbonate-depleted spinach thylakoid membranes, Biochim Biophys Acta, 935 (1988) 248-257.
[107] M.P.J. Pulles, H.J. Van Gorkom, J.G. Willemsen, Absorbance changes due to charge-accumulating species in system 2 of photosynthesis, Biochim Biophys Acta, 449 (1976) 536-540.
[108] J. Farineau, P. Mathis, Effect of bicarbonate on electron transfer between plastoquinones in Photosystem II, in: Y. Inoue, A.R. Crofts, Govindjee, N. Murata, G. Renger, K. Satoh (Eds.) The oxygen evolving system of photosynthesis, Academic Press, Inc., 1983, pp. 317-325.
[109] D.J. Blubaugh, Govindjee, The molecular mechanism of the bicarbonate effect at the plastoquinone reductase site of photosynthesis, Photosynth Res, 19 (1988) 85-128.
[110] N. Cox, L. Jin, A. Jaszewski, P.J. Smith, E. Krausz, A.W. Rutherford, R. Pace, The semiquinone-iron complex of Photosystem II: structural insights from ESR and theoretical simulation; evidence that the native ligand to the non-heme iron is carbonate, Biophys. J., 97 (2009) 2024-2033.

[111] A. Krieger, A.W. Rutherford, G.N. Johnson, On the determination of redox midpoint potential of the primary quinone electron-acceptor, Q_A, in Photosystem-II, Biochim Biophys Acta, 1229 (1995) 193-201.
[112] G.N. Johnson, A.W. Rutherford, A. Krieger, A change in the midpoint potential of the quinone Q_A in Photosystem-II associated with photoactivation of oxygen evolution, Biochim Biophys Acta, 1229 (1995) 202-207.
[113] A. Krieger, E. Weis, Energy-dependent quenching of chlorophyll-a-fluorescence - the involvement of proton-calcium exchange at Photosystem 2, Photosynthetica, 27 (1992) 89-98.
[114] A. Krieger, E. Weis, S. Demeter, Low-pH-induced Ca2+ ion release in the water-splitting system is accompanied by a shift in the midpoint redox potential of the primary quinone acceptor QA, Biochim Biophys Acta, 1144 (1993) 411-418.
[115] A. Krieger, A.W. Rutherford, Comparison of chloride-depleted and calcium-depleted PSII: The midpoint potential of Q(A) and susceptibility to photodamage, Biochim Biophys Acta, 1319 (1997) 91-98.
[116] J. Kargul, K. Maghlaoul, J.W. Murray, Z. Deak, A. Boussac, A.W. Rutherford, I. Vass, J. Barber, Purification, crystallization and X-ray diffraction analyses of the T-elongatus PSII core dimer with strontium replacing calcium in the oxygen-evolving complex, Biochim Biophys Acta, 1767 (2007) 404-413.
[117] C. Fufezan, C.M. Gross, M. Sjodin, A.W. Rutherford, A. Krieger-Liszkay, D. Kirilovsky, Influence of the redox potential of the primary quinone electron acceptor on photoinhibition in photosystem II, J Biol Chem, 282 (2007) 12492-12502.
[118] A.W. Rutherford, A. Krieger-Liszkay, Herbicide-induced oxidative stress in photosystem II, Trends Biochem Sci, 26 (2001) 648-653.
[119] A. Takano, R. Takahashi, H. Suzuki, T. Noguchi, Herbicide effect on the hydrogen-bonding interaction of the primary quinone electron acceptor QA in photosystem II as studied by Fourier transform infrared spectroscopy, Photosynth Res, 98 (2008) 159-167.
[120] A. Krieger-Liszkay, C. Fufezan, A. Trebst, Singlet oxygen production in photosystem II and related protection mechanism, Photosynth Res, 98 (2008) 551-564.
[121] T. Shibamoto, Y. Kato, M. Sugiura, T. Watanabe, Redox potential of the primary plastoquinone electron acceptor Q_A in Photosystem II from *Thermosynechococcus elongatus* determined by spectroelectrochemistry, Biochemistry, 48 (2009) 10682-10684.
[122] J.H. Golbeck, B. Kok, Redox titration of electron-acceptor Q and the plastoquinone pool in Photosystem II, Biochim Biophys Acta, 547 (1979) 347-360.
[123] A.R. Corrie, J.H.A. Nugent, M.C.W. Evans, Identification of EPR Signals from the States $Q_A^{\cdot-}Q_B^{\cdot-}$ and $Q_B^{\cdot-}$ in Photosystem-II from *Phormidium laminosum*, Biochim Biophys Acta, 1057 (1991) 384-390.
[124] H.H. Robinson, A.R. Crofts, Kinetics of the oxidation reduction reactions of the Photosystem II quinone acceptor complex, and the pathway for deactivation, Febs Lett, 153 (1983) 221-226.
[125] A.R. Crofts, C.A. Wraight, The electrochemical domain of photosynthesis, Biochim Biophys Acta, 726 (1983) 149-185.
[126] J. Minagawa, Y. Narusaka, Y. Inoue, K. Satoh, Electron transfer between Q_A and Q_B in photosystem II is thermodynamically perturbed in phototolerant mutants of *Synechocystis sp*. PCC 6803, Biochemistry, 38 (1999) 770-775.
[127] F. Rappaport, J. Lavergne, Thermoluminescence: theory, Photosynth Res, 101 (2009) 205-216.
[128] W.F.J. Vermaas, G. Renger, G. Dohnt, The reduction of the oxygen-evolving system in chloroplasts by thylakoid components, Biochim Biophys Acta, 764 (1984) 194-202.
[129] V.V. Klimov, S.I. Allakhverdiev, S. Demeter, A.A. Krasnovskii, Photo-reduction of pheophytin in the Photosystem 2 of chloroplasts depending on the oxidation-reduction potential of the medium, Doklady Akademii Nauk Sssr, 249 (1979) 227-230.

[130] A.W. Rutherford, J.E. Mullet, A.R. Crofts, Measurement of the midpoint potential of the pheophytin acceptor of Photosystem II, Febs Lett, 123 (1981) 235-237.
[131] Y. Kato, M. Sugiura, A. Oda, T. Watanabe, Spectroelectrochemical determination of the redox potential of pheophytin a, the primary electron acceptor in photosystem II, Proc. Natl. Acad. Sci. U. S. A., 106 (2009) 17365-17370.
[132] F. Rappaport, M. Guergova-Kuras, P.J. Nixon, B.A. Diner, J. Lavergne, Kinetics and pathways of charge recombination in photosystem II, Biochemistry, 41 (2002) 8518-8527.
[133] M. Grabolle, H. Dau, Energetics of primary and secondary electron transfer in Photosystem II membrane particles of spinach revisited on basis of recombination-fluorescence measurements, Biochim Biophys Acta, 1708 (2005) 209-218.
[134] S. Vasil'ev, A. Bergmann, H. Redlin, H.J. Eichler, G. Renger, On the role of exchangeable hydrogen bonds for the kinetics of P680•+ QA•- formation and P680•+ Pheo•- recombination in photosystem II, Biochim Biophys Acta, 1276 (1996) 35-44.
[135] K. Gibasiewicz, A. Dobek, J. Breton, W. Leibl, Modulation of primary radical pair kinetics and energetics in photosystem II by the redox state of the quinone electron acceptor Q(A), Biophys. J., 80 (2001) 1617-1630.
[136] M. Sugiura, Y. Kato, R. Takahashi, H. Suzuki, T. Watanabe, T. Noguchi, F. Rappaport, A. Boussac, Energetics in Photosystem II from *Thermosynechococcus elongatus* with a D1 protein encoded by either the *psbA1* or *psbA3* gene, Biochim Biophys Acta, 1797 (2010) 1491-1499.
[137] M. Sugiura, F. Rappaport, K. Brettel, T. Noguchi, A.W. Rutherford, A. Boussac, Site-directed mutagenesis of *Thermosynechococcus elongatus* photosystem II: the O2-evolving enzyme lacking the redox-active tyrosine D, Biochemistry, 43 (2004) 13549-13563.
[138] A. Sedoud, L. Kastner, N. Cox, S. El-Alaoui, D. Kirilovsky, A.W. Rutherford, Effects of formate binding on the quinone-iron electron acceptor complex of photosystem II, Biochim Biophys Acta, 1807 (2011) 216-226.
[139] U. Muhlenhoff, F. Chauvat, Gene transfer and manipulation in the thermophilic cyanobacterium *Synechococcus elongatus*, Mol Gen Genet, 252 (1996) 93-100.
[140] J.M. Ducruet, Chlorophyll thermoluminescence of leaf discs: simple instruments and progress in signal interpretation open the way to new ecophysiological indicators, J Exp Bot, 54 (2003) 2419-2430.

RESULTATS

ARTICLE 1

Effect of formate binding on the quinone-iron acceptor complex of photosystem II

Biochimica et Biophysica Acta xxx (2010) xxx–xxx

Contents lists available at ScienceDirect

Biochimica et Biophysica Acta

journal homepage: www.elsevier.com/locate/bbabio

Effects of formate binding on the quinone–iron electron acceptor complex of photosystem II

Arezki Sedoud [a], Lisa Kastner [a], Nicholas Cox [b], Sabah El-Alaoui [a], Diana Kirilovsky [a], A. William Rutherford [a,*]

[a] iBiTec-S, CNRS URA 2096, CEA Saclay, 91191 Gif-sur-Yvette, France
[b] MPI für Bioanorganische Chemie, Stiftstrasse 34-36/D-45470 Mülheim an der Ruhr, Germany

ARTICLE INFO

Article history:
Received 4 August 2010
Received in revised form 1 October 2010
Accepted 25 October 2010
Available online xxxx

Keywords:
Photosystem II
Quinone
Non-heme iron
Formate
Bicarbonate
EPR

ABSTRACT

EPR was used to study the influence of formate on the electron acceptor side of photosystem II (PSII) from *Thermosynechococcus elongatus*. Two new EPR signals were found and characterized. The first is assigned to the semiquinone form of Q_B interacting magnetically with a high spin, non-heme-iron (Fe^{2+}, $S=2$) when the native bicarbonate/carbonate ligand is replaced by formate. This assignment is based on several experimental observations, the most important of which were: (i) its presence in the dark in a significant fraction of centers, and (ii) the period-of-two variations in the concentration expected for $Q_B^{\bullet-}$ when PSII underwent a series of single-electron turnovers. This signal is similar but not identical to the well-know formate-modified EPR signal observed for the $Q_A^{\bullet-}Fe^{2+}$ complex (W.F.J. Vermaas and A.W. Rutherford, FEBS Lett. 175 (1984) 243–248). The formate-modified signals from $Q_A^{\bullet-}Fe^{2+}$ and $Q_B^{\bullet-}Fe^{2+}$ are also similar to native semiquinone–iron signals ($Q_A^{\bullet-}Fe^{2+}/Q_B^{\bullet-}Fe^{2+}$) seen in purple bacterial reaction centers where a glutamate provides the carboxylate ligand to the iron. The second new signal was formed when $Q_A^{\bullet-}$ was generated in formate-inhibited PSII when the secondary acceptor was reduced by two electrons. While the signal is reminiscent of the formate-modified semiquinone–iron signals, it is broader and its main turning point has a major sub-peak at higher field. This new signal is attributed to the $Q_A^{\bullet-}Fe^{2+}$ with formate bound but which is perturbed when Q_B is fully reduced, most likely as Q_BH_2 (or possibly $Q_BH^{\bullet-}$ or $Q_B^{2\bullet-}$). Flash experiments on formate-inhibited PSII monitoring these new EPR signals indicate that the outcome of charge separation on the first two flashes is not greatly modified by formate. However on the third flash and subsequent flashes, the modified $Q_A^{\bullet-}Fe^{2+}Q_BH_2$ signal is trapped in the EPR experiment and there is a marked decrease in the quantum yield of formation of stable charge pairs. The main effect of formate then appears to be on Q_BH_2 exchange and this agrees with earlier studies using different methods.

1. Introduction

Photosystem II (PSII) is a chlorophyll-containing membrane-bound enzyme that uses the energy of light to take electrons from water and reduce plastoquinone (reviewed in [1,2]). The protein has two bound plastoquinones, Q_A and Q_B, which act as sequential electron acceptors. Although both are plastoquinones, their physical and chemical properties differ. Q_A is tightly bound and acts as a one-electron carrier while Q_B undergoes two sequential one-electron reduction steps. Q_B is weakly bound in its quinone and quinol form but tightly bound in its one-electron reduced semiquinone form (reviewed in [3]).

Excitation of the chlorophylls in PSII by light results in a charge separation forming a radical pair made up of a chlorophyll radical cation ($P_{680}^{\bullet+}$) and a pheophytin radical anion ($Ph^{\bullet-}$). The pheophytin radical anion subsequently reduces Q_A to $Q_A^{\bullet-}$. The $Q_A^{\bullet-}$ state is relatively short-lived (<1 ms) and undergoes no observable protonation events during its lifetime. $Q_A^{\bullet-}$ then reduces Q_B, forming $Q_B^{\bullet-}$, a tightly bound semiquinone that is thought to remain unprotonated. However, the negative charge is partially compensated by proton uptake by protein residues in close proximity to the semiquinone. After a second photochemical turnover, $Q_B^{\bullet-}$ undergoes a further one-electron reduction step. This event is coupled to protonation reactions forming Q_BH_2. Q_BH_2 leaves the Q_B site and is replaced by plastoquinone from the pool in the membrane, this gives rise to the characteristic two-electron gate phenomena associated with Q_B function [4–7].

The acceptor side electron and proton transfer reactions occurring in PSII are poorly understood compared to the related reactions occurring in the purple bacterial reaction center [8,9]. As a result the

Abbreviations: ANT2p, 2-(3-chloro-4-trifluoromethyl) aniline-3,5-dinitrothiophene; Cyt b_{559}, Cytochrome b_{559}; DAD, 2,3,5,6 tetramethyl-p-phenylenediamine; DCMU, 3-(3,4-dichlorophenyl)-1,1-dimethylurea; EPR, electron paramagnetic resonance; PSII, photosystem II; Q_A and Q_B, primary and secondary quinone electron acceptor of PSII

* Corresponding author. Tel.: +33 1 69 08 2940; fax: +33 1 69 08 87 17.
E-mail address: alfred.rutherford@cea.fr (A.W. Rutherford).

0005-2728/$ – see front matter © 2010 Elsevier B.V. All rights reserved.
doi:10.1016/j.bbabio.2010.10.019

working model for PSII is greatly influenced by insights from the purple bacterial reaction center [3]. The close structural similarity between the purple bacterial reaction center and PSII was indicated by the similar spectroscopic signatures from the semiquinone iron complex (reviewed in [10]). The crystallographic model from the purple bacterial reaction center [11] thus provided a good model for PSII [11,12], this was supported by amino acid sequence comparisons [13], mutagenesis [14,15], molecular modeling [16] and biochemistry [17,18]. The model was verified by extensive biophysical studies (e.g. [19,20]) and eventually by crystallography of PSII [21–23].

A high spin non-heme iron (Fe^{2+}, $S=2$) is located between the two bound quinones Q_A and Q_B. It is coordinated by four histidines, two from the D1 subunit (H215 and H272) and two from the D2 subunit (H214 and H268). In the bacterial reaction center, the fifth and sixth ligand to the iron is a bidentate carboxylate ligand from the glutamate M-E232 [11]. In PSII an exchangeable, bidentate bicarbonate/carbonate is the non-histidine ligand [10,11,24,25].

The depletion of bicarbonate/carbonate or its substitution by formate results in a slowing of the electron transfer rate from $Q_A^{\bullet-}$ to Q_B and to $Q_B^{\bullet-}$ by factors of five and ten, respectively [26–29]. The exchange of the Q_BH_2 with the plastoquinone pool is slowed down by more than a two orders of magnitude [27,30,31]. Some of these inhibitory effects maybe due to the perturbation and/or inhibition of the protonation reactions that are coupled to electron transfer [24]. A specific chemical model explaining how depletion of bicarbonate affects electron transfer in the quinone–iron complex has not yet been established (reviewed in [32,33]). Recent observations have suggested that carbonate rather than bicarbonate is the native ligand to the non-heme iron in PSII [34]. The additional negative charge on the carbonate ion compared to bicarbonate would be expected to be relevant to its purported roles in the proton-coupled electron transfer.

The existence of an exchangeable ligand on the iron that strongly affects the rate of electrons leaving PSII could reflect a regulatory mechanism of some kind. The natural ligand (CO_3^{2-}/HCO_3^-) is in equilibrium with CO_2, the terminal electron acceptor of photosynthesis. A role for CO_2 in regulating electron input into the electron transfer chain seems plausible. If however the slow down in electron transfer occurs simply upon protonation of carbonate (forming bicarbonate) [34], then the regulatory factor could be pH or the binding of another carboxylic acid.

The semiquinone radicals $Q_A^{\bullet-}$ and $Q_B^{\bullet-}$ in PSII and purple bacteria are magnetically coupled to the non-heme iron Fe^{2+} ($S=2$). This interaction strongly perturbs the radical signals as seen by EPR. Semiquinones generally appear as sharp structureless signals centered at $g\sim2.004$ but in PSII and purple bacterial reaction centers they interact with the Fe^{2+} leading to a broadening of their EPR lineshape. In PSII, the $Q_{A/B}^{\bullet-}Fe^{2+}$ complexes have turning points around $g\sim1.8$ and 1.9 [35–39], reviewed in [3,10]. The signal at $g=1.9$ is the native form [37] while the $g=1.8$ form is seen when formate or other carboxylic acids replace the bicarbonate/carbonate ion [38]. In PSII isolated from the cyanobacterium, *Thermosynechococcus elongatus*, the same phenomenology is observed [40,41]. The presence of the $g=1.8$ form in samples that have not been treated with a carboxylic acid [35–37] presumably reflects those (non-native) centers: (i) in which the (bi) carbonate ion is absent, or (ii) in which the native carbonate is replaced by bicarbonate (see [34]). In either case, the $g=1.8$ form probably represents non-functional centers [42]. The addition of formate to PSII significantly increased the amplitude of the $Q_A^{\bullet-}Fe^{2+}$ EPR signal by converting the weak $g=1.9$ signal to a well resolved $g=1.8$ signal [38]. This simple biochemical procedure is routinely employed to allow $Q_A^{\bullet-}Fe^{2+}$ to be monitored (e.g. [40,41]). Some other carboxylic acids have been shown to have smaller effects on the $Q_A^{\bullet-}Fe^{2+}$ in plant PSII showing competitive binding effects with the much more pronounced formate effect [43].

$Q_B^{\bullet-}Fe^{2+}$ EPR signals have been the subject of less study. This is because the detergent treatment used to isolate PSII in plants and the low pH used to stabilized Mn_4Ca cluster [44] appears to be detrimental to Q_B. It is possible that the low pH procedure could result in the loss of the native carbonate/bicarbonate ligand to the iron (the pKa of bicarbonate/carbonic acid is 6.4). Nevertheless, $Q_B^{\bullet-}Fe^{2+}$ signals have been reported in plant PSII on rare occasions in which Q_B integrity is conserved in standard preparations [10,39,45], and when efforts were made to conserve bicarbonate [46]. In the cyanobacteria however, $Q_B^{\bullet-}Fe^{2+}$ EPR signals are routinely detected, thus, Q_B seems more stable to both the detergent used and the pH [47,48]. The native $Q_B^{\bullet-}Fe^{2+}$ EPR signal has a very similar line shape to that observed for the native $Q_A^{\bullet-}Fe^{2+}$ [48].

Fufezan et al. noted the presence of an additional functional quinone in *T. elongatus* PSII core preparations [48]. An additional quinone was also reported in quinone quantification studies in similar preparations [49] and was detected in the most recent crystallographic model of PSII and designated Q_C [23]. Mechanistic evidence for an additional quinone binding site in PSII from plants had already been obtained from studies of Cytochrome b559 (Cyt b_{559}) [50,51].

In the present work we have used EPR to study the effect of formate binding on PSII using cyanobacterial preparations that have functional Q_B and Q_C prior to formate addition.

2. Materials and methods

2.1. Culture conditions

A strain of *T. elongatus* with a histidine tag on the CP47 protein of PSII was engineered as described in supplementary information. Cells of the transformed strain were grown in a rotary shaker (120 rpm) at 45 °C under continuous illumination using fluorescent white lamps of intensity of about 80 μmoles photons m^{-2} s^{-1}. Cells were grown in a DTN-medium [52] in a CO_2-enriched atmosphere. For maintenance, the cells were grown in the presence of kanamycin (40 μg ml^{-1}). For PSII preparations, the cells were grown in 3 L flasks (1 L culture).

2.2. PSII preparation

PSII core complexes were prepared as described in [53] using a protocol based on [54] with the following modifications. The concentrations of betaine in all buffers used here was 1 M instead of 1.2 M and the concentration of *n*-dodecyl-β-maltoside used in the elution buffer "buffer 3" was 0.06% (w/v) instead of 0.10% (w/v). The eluted fraction from the nickel column was concentrated and washed using Millipore Ultrafree-15 centrifugal filters. Oxygen evolution was measured under continuous light at 27 °C in a Clark-type oxygen electrode (Hansatech) with saturating white light. The oxygen evolution activity of the PSII core complexes was ~3500 μmol $O_2\cdot mg^{-1}\cdot Chl/h$. Samples were stored in liquid nitrogen in the storage buffer (10% glycerol, 40 mM MES pH 6.5, 1 M betaine, 15 mM $MgCl_2$ and 15 mM $CaCl_2$).

2.3. Formate treatments

For EPR experiments the formate treatment was performed as follows. 120 μL aliquots of PSII (~1 mg Chl/ml) were dark-adapted for the time specified in the figure legends (either 1 or 12 h), then 160 mM final concentration of sodium formate in the storage buffer was added in the dark and the sample allowed to incubate for 30 min incubation at room temperature. Experiments in which the concentration and incubation time were varied demonstrated that these conditions were optimal for generating ~100% of the modified semiquinone–iron EPR signals (not shown). For oxygen evolution measurements 160 mM of sodium formate was added to PSII at 5 μg Chl/ml, and the sample was then incubated for 30 min at room temperature. The O_2 evolving activity decreased to 20% under these conditions and was restored to 60% by addition of 50 mM bicarbonate.

Please cite this article as: A. Sedoud, et al., Effects of formate binding on the quinone–iron electron acceptor complex of photosystem II, Biochim. Biophys. Acta (2010), doi:10.1016/j.bbabio.2010.10.019

These formate-induced changes in activity are reported in the literature (e.g. [55]). The addition of 160 mM NaCl had no affect on oxygen evolution. In all the experiments shown here sodium formate was added as a 1 M stock in storage buffer.

2.4. Chemical reduction treatments

Chemical reduction of the 120 μL aliquots of PSII (~1 mg Chl/ml) with ascorbate was performed using two methods (see figure legends). (1) Sodium ascorbate in storage buffer (300 mM stock) was added to the sample in the EPR tube in darkness to give a final concentration of 10 mM. The sample was then incubated for 10 min at room temperature prior to freezing. (2) DAD in DMSO (30 mM stock solution) was added to the sample in the EPR tube in darkness to give a final concentration of 1 mM and then sodium ascorbate in storage buffer was added to give a final concentration of 10 mM. The sample was then incubated for 30 min at room temperature before freezing the sample (see below). Dithionite reduction was performed by addition of sodium dithionite to the sample in the EPR tube to give a final concentration of 30 mM using a 500 mM stock solution made up in degassed storage buffer.

2.5. EPR measurements

EPR spectra were recorded using a Bruker Elexsys 500 X-band spectrometer equipped with standard ER 4102 resonator and Oxford Instruments ESR 900 cryostat. Instrument settings were: microwave frequency 9.4 GHz, modulation frequency 100 kHz. All other settings were as indicated in the figure legends. 120 μl aliquots of PSII cores (~1 mg Chl/ml) in the same buffer used for storage were loaded into 4 mm outer diameter quartz EPR tubes. The samples were manipulated under dim-green light and then incubated in complete darkness for 1 h (short-dark adaptation) or 12 h (long-dark adaptation). The EPR samples were frozen in a dry-ice/ethanol bath at 200 K. Samples were degassed by pumping at 200 K and then filled with helium gas. EPR tubes were then transferred to liquid nitrogen prior to the EPR measurements being made. Samples were handled in darkness.

2.6. Illumination conditions

Flashes were performed using a frequency-doubled Nd:YAG laser (Spectra Physics, 7 ns fwhm, 550 mJ, 532 nm) at room temperature. After flashing, samples were rapidly frozen (1-2 s) in a dry-ice/ethanol bath at 200 K followed by storage in liquid nitrogen. The laser flash used was saturating under these conditions.

Low-temperature red-light illuminations were performed in an unsilvered dewar using either liquid nitrogen (77 K) or a dry-ice/ethanol bath at 200 K. 77 K illuminations were performed for 30 min in order to reduce $Q_A^{\bullet-}Fe^{2+}$ and oxidize Cyt b_{559} to near completion, as verified by EPR. Illuminations at 200 K for ~20 sec generated ~100% S_2 manganese multiline signal. Continuous illuminations were performed using an 800 W halogen lamp. The light was filtered through 3 cm of water, Calflex IR heat filters and a long-band pass filter (RG-670 nm).

For multiple photochemical turnover experiments, separate samples were used for 0, 1, 2 and 3 turnovers. The samples were treated with sodium ascorbate after a long dark adaptation (see above). A photochemical turnover was performed by illuminating a sample for 30 min at 77 K. Samples were then thawed and incubated for 10 min at room temperature, this allowed: (i) electron transfer to be completed on the electron acceptor side, i.e. $Q_A^{\bullet-}$ to Q_B, or $Q_A^{\bullet-}$ to $Q_B^{\bullet-}$, associated protonation reactions and the exchange of Q_BH_2 when possible; and (ii) the reduction of the oxidized Cyt b_{559} by ascorbate as verified by EPR. When a second or third turnover was required, further low temperature illumination/thawing cycles were given. Sodium formate (final concentration 160 mM) was added to samples which had undergone 0, 1, 2 and 3 turnovers and then incubated for 30 min at room temperature in darkness. Samples were then frozen and their EPR spectra recorded.

2.7. EPR simulations

Spectral simulations were performed as described in [34]. The Spin Hamiltonian (10 x 10 matrix) was solved numerically using: (i) Scilab-4.4.1, an open source vector-based linear algebra package (www.scilab.org); and (ii) the EasySpin package [56] in MATLAB. To broaden the comparison we also simulated $Q_A^{\bullet-}Fe^{2+}$ and $Q_B^{\bullet-}Fe^{2+}$ signals from wild type of *Rhodopseudomonas viridis* chromatophores. Biochemical preparation and EPR conditions for the *R. viridis* were as described in Ref. [57]

3. Results

3.1. The formate-modified $Q_B^{\bullet-}Fe^{2+}$ EPR signal

Fig. 1A shows the EPR spectrum measured at 4.5 K of untreated PSII core complexes isolated from *T. elongatus* after short dark-adaption. A weak broad signal was observed at $g=1.73$ that is characteristic of the $Q_B^{\bullet-}Fe^{2+}$ complex [48]. The $Q_B^{\bullet-}Fe^{2+}$ complex has a second turning point at $g=1.95$ that is not readily observed at this temperatures (see [34]) but which can be seen more easily at higher temperatures [48] (see Fig. 6). The addition of sodium formate alters the $Q_B^{\bullet-}Fe^{2+}$ signal (Fig. 1B). The native signal as described above is replaced by a new signal centered at g~1.84 that is similar to semiquinone–iron signals observed in purple bacteria reaction centers [58,59]. A similar signal has also been observed for the formate-modified $Q_A^{\bullet-}Fe^{2+}$ complex in plant and cyanobacterial PSII [38,40,41,60].

Under the experimental conditions used here, no $Q_A^{\bullet-}$ is expected to be reduced prior to the addition of formate. In contrast, $Q_B^{\bullet-}$ is expected to be present in a significant fraction of centers (~40%) after a short-period of dark-adaptation in *T. elongatus* [48]. Thus it is probable that this new signal (Fig. 1B) arises from the formate-modified $Q_B^{\bullet-}Fe^{2+}$, where formate has displaced the exogenous bicarbonate/carbonate ligand of the Fe^{2+}. The new semiquinone–

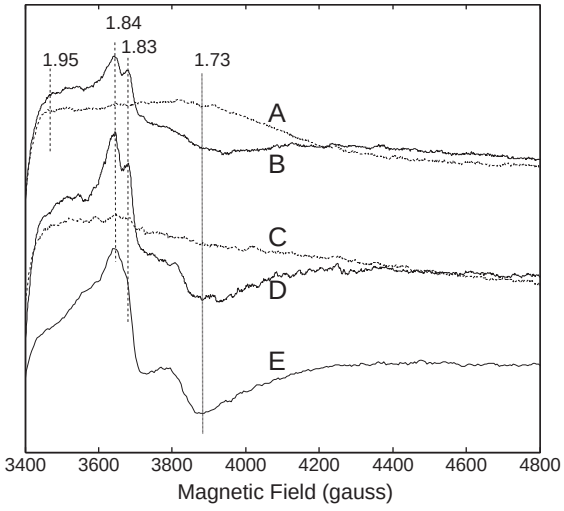

Fig. 1. EPR signals present in formate-treated PSII from *T. elongatus*. (A) Short-dark adapted (1 h) PSII. (B) After formate addition to the sample shown in A. (C) Formate added to a long-dark adapted PSII. (D) One saturating laser flash at room temperature given to the long dark-adapted sample shown in C. (E) Spectrum attributed to formate-modified $Q_A^{\bullet-}Fe^{2+}$ generated by 30 min illumination at 77 K in a long-dark adapted PSII sample. Some g-values of features mentioned in the text are shown. Instrument settings: microwave power: 20 mW, modulation amplitude: 25 gauss, temperature: 4.5 K.

Please cite this article as: A. Sedoud, et al., Effects of formate binding on the quinone–iron electron acceptor complex of photosystem II, Biochim. Biophys. Acta (2010), doi:10.1016/j.bbabio.2010.10.019

iron signal described above was absent when formate was added to a sample that had been dark-adapted for 12 h (Fig. 1C). Incubation for 12 h in the dark at room temperature is known to result in the almost complete loss of $Q_B^{\bullet-}$ Fe^{2+} [48]. This result is consistent with the assignment of the signal in Fig. 1B to a formate-modified form of $Q_B^{\bullet-}Fe^{2+}$.

Fig. 1D shows the EPR signal obtained after a single saturating flash was given to a long dark-adapted sample (Fig. 1C) at room temperature. The photo-induced signal is similar to that seen in Fig. 1B. Excitation of dark-adapted PSII by a single saturating flash is expected to generate the $S_2Q_B^{\bullet-}$ state. This result further supports the assignment of this new signal to the formate-modified $Q_B^{\bullet-}Fe^{2+}$ complex. The size of the $Q_B^{\bullet-}Fe^{2+}$ signal in Fig. 1D is approximately double that of the signal seen for the short dark-adapted sample (Fig. 1B). This suggests that formate does not affect the yield of $Q_B^{\bullet-}$ formation on the first flash and is consistent with earlier studies of bicarbonate depletion/formate addition (e.g. [28–33]). In this experiment the contribution from the overlapping S = ½ multiline signal from S_2 is minimized by the choice of EPR conditions used for the measurement (low temperature and high microwave power). When S_2 is formed in centers containing TyrD, the S_2 state is reduced back to the S_1 state and $TyrD^{\bullet}$ is formed [61]. This occurs in the seconds timescale through the equilibrium between the intervening electron carriers (P_{680}, TyrZ) (reviewed in [62]). This also contributes to the low intensity of the S_2 signal in Fig. 1D.

Control measurements (see Fig. S2 in supporting information) showed that the addition of formate did not significantly alter the electron donor side function on the first photochemical turnover. The S_2 multiline signal [63] generated by 200 K illumination [64] had almost the same amplitude in control and formate-treated samples, ±20% (Fig. S2 in supporting information). This is in marked contrast to the situation in plant PSII where it was concluded that acceptor side effects of formate were matched by donor side inhibition [65,66] but see however [67]. The discrepancy is most likely due to species differences and/or biochemical conditions.

Fluorescence yield experiments were performed on samples before and after the addition of formate to rule out the possibility that formate addition led to $Q_A^{\bullet-}$ reduction in the short dark-adapted samples, perhaps by a change in the $Q_AQ_B^{\bullet-} \leftrightarrow Q_A^{\bullet-}Q_B$ equilibrium. The addition of formate increased the F_0 level by less than 1% of the F_{max} (see Table 1 in supporting information). In addition, thermoluminescence experiments in the presence of formate indicated that $S_2Q_B^{\bullet-}$ recombination occurs on the first flash; no evidence for $S_2Q_A^{\bullet-}$ recombination was seen (not shown). These results show that formate addition does not generate formation of a significant fraction of $Q_A^{\bullet-}$ from $Q_B^{\bullet-}$ and further support the assignment of the new EPR signal (Fig. 1B) to formate-modified $Q_B^{\bullet-}Fe^{2+}$.

Fig. 1E shows the EPR signal generated by illumination of a long dark-adapted PSII sample at 77 K for 30 min. Illumination at this temperature is known to generate $Q_A^{\bullet-}$ in most centers [68]. The observed $Q_A^{\bullet-}Fe^{2+}$ signal (Fig. 1E) has the same *g*-values (a peak at $g = 1.84$ and a trough at $g \sim 1.73$) and line-shape as seen in PSII from higher plants [38] and as reported earlier in *T. elongatus* [40,41]. The signal generated after one flash (Fig. 1D), which is attributed to $Q_B^{\bullet-}Fe^{2+}$, is similar to that of $Q_A^{\bullet-}Fe^{2+}$ (Fig. 1E) but it has an additional resolved secondary peak at $g \sim 1.83$. These small changes in the line-shape of the two signals are reminiscent of those that distinguish the $Q_A^{\bullet-}Fe^{2+}$ and $Q_B^{\bullet-}Fe^{2+}$ signals in purple bacteria [59,69,70].

3.2. Formate-treated PSII illuminated by a series of flashes

The left panel of Fig. 2 shows the effect of a series of flashes on long dark-adapted PSII that was subsequently treated with formate. Fig. 2A, the zero flash sample showed no signal. After one flash (Fig. 2B) the $Q_B^{\bullet-}Fe^{2+}$ was formed in the majority of the centers (~80%, this is obtained from an estimate of the miss factor derived from the size of the signal present after the second flash). Fig. 2C shows the sample that was excited by two flashes. In this case, the EPR signal was significantly smaller than that seen after 1 flash (Fig. 2B). The residual $Q_B^{\bullet-}Fe^{2+}$ observed maybe attributed to: (i) the centers that did not turnover on the first flash because of photochemical misses but which did turnover on the second flash; and (ii) those centers that did turnover on the first flash but not on the second flash, again because of misses. The marked decrease in amplitude on the second flash is similar to that expected for untreated PSII. This indicates that the yield of electron transfer from $Q_A^{\bullet-}$ to Q_B and from $Q_A^{\bullet-}$ to $Q_B^{\bullet-}$ is not greatly affected by formate treatment. In contrast on the third and subsequent flashes the EPR spectra indicate the gradual accumulation of an EPR signal with peaks at $g = 1.84$ with additional features at $g = 1.81$ and $g = 1.68$ (Fig. 2D and E).

In the right panel of Fig. 2 each of the samples that had been flashed at room temperature (Fig. 2 left panel), were then illuminated at 77 K. Under these conditions the final electron donors are the chlorophyll(s), the carotenoid(s) or Cyt b_{559}, known collectively as the side-pathway donors [71]. Fig. 2F shows the one flash sample (Fig. 2B) after illumination at 77 K. The EPR signal intensity of the

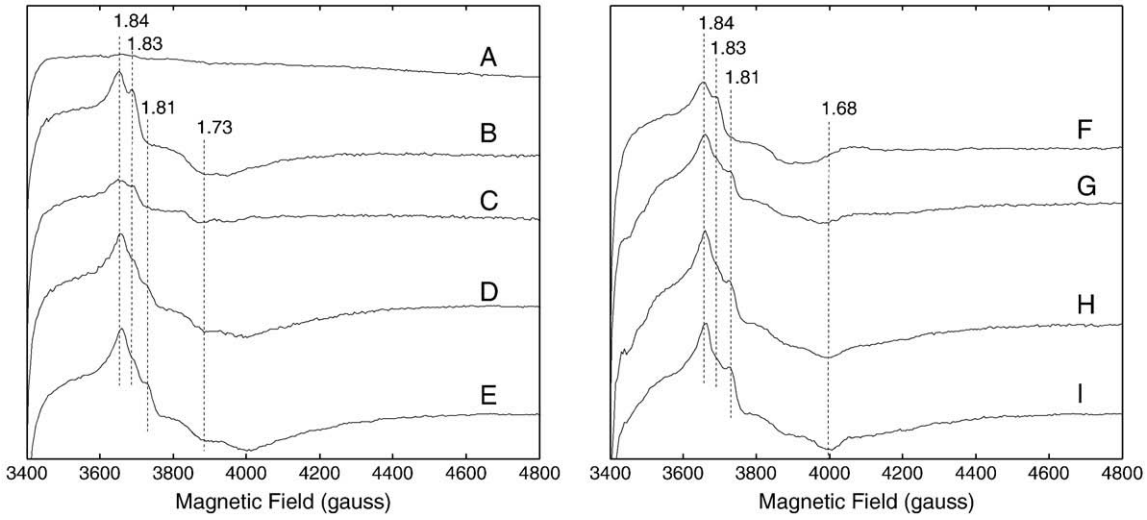

Fig. 2. The effect of a flash series on the formate-treated PSII. PSII samples were dark-adapted for 12 h. A series of 0, 1, 2, 3, 4 flashes were then given. The corresponding spectra are shown in the left panel and labeled as A, B, C, D and E respectively. In the right panel, the spectra labeled F, G, H and I correspond to the samples used to obtain spectra B, C, D and E, respectively, but after a 77 K illumination. Instrument settings were the same as in Fig. 1.

Please cite this article as: A. Sedoud, et al., Effects of formate binding on the quinone–iron electron acceptor complex of photosystem II, Biochim. Biophys. Acta (2010), doi:10.1016/j.bbabio.2010.10.019

semiquinone–iron signal decreased upon 77 K illumination. This effect is more marked under comparable conditions in Fig. 3 (see below). This is attributed to the formation of a $Q_A^{\bullet-}Fe^{2+}Q_B^{\bullet-}$ biradical species that does not show an EPR signal in this region. A similar situation occurs in purple bacterial centers when the same state is formed [69,72]. The theoretical rationale for this will be discussed elsewhere (Cox et al., in preparation).

In Fig. 2F the remaining signal is a mixture of $Q_A^{\bullet-}Fe^{2+}$ and $Q_B^{\bullet-}Fe^{2+}$ present in separate centers. Illumination of samples that had been pre-flashed by 2, 3 or 4 flashes prior to low temperature illumination (Fig. 2G, H and I) showed an increase in the EPR intensities and the signal formed is broad and has features at $g=1.84$, $g=1.81$ and $g=1.68$. This is the same signal which appeared after 3 and 4 flashes prior to low temperature illumination (Fig. 2D and E). Given that this signal is formed at low temperature, it seems likely that it arises from $Q_A^{\bullet-}$ even though it is unlike the well-known formate-modified $Q_A^{\bullet-}Fe^{2+}$ signal (Fig. 1E) [38]. In Fig. 2 this new signal is seen when three or more turnovers have occurred: i.e. after 3 or more flashes at room temperature or after 2 or more flashes at room temperature plus an illumination at 77 K.

3.3. EPR signals formed after a series of photochemical turnovers at low temperature

In Fig. 2 it was shown that in formate-treated PSII the typical period-of-two flash dependence in the $Q_B^{\bullet-}$ concentration could be observed for the first two flashes but its reappearance on the third flash was inhibited. To demonstrate more extensive period of two amplitude oscillations in the $Q_B^{\bullet-}Fe^{2+}$ signal we performed experiments in which the $Q_A^{\bullet-}$ to $Q_B/Q_B^{\bullet-}$ electron transfer steps were allowed to occur *before* adding the formate. Fig. 3 (left panel) shows variations in the size of the $Q_B^{\bullet-}Fe^{2+}$ EPR signal depending on the number of photochemical turnovers when formate was added *after* the turnovers had occurred. Because of the long incubation time needed for formate to bind and the occurrence of charge recombination during this time, this experiment could not be done by addition of formate after a series of flashes. Instead photochemical turnovers were generated using a protocol involving low temperature illumination (77 K) of ascorbate-reduced PSII followed by thawing (for details, see material and methods). The increase in the size of the signal on turnovers 1 and 3 (Fig. 3B and D) is characteristic of Q_B function and further supports the assignment of the signal to the formate-modified $Q_B^{\bullet-}Fe^{2+}$ state.

The right panel of Fig. 3 shows EPR spectra obtained from the same samples used for the experiments used for the multiple turnover experiments (Fig. 3 left panel) but recorded directly after an additional illumination at 77 K. Fig. 3E shows the formation of a formate-modified $Q_A^{\bullet-}Fe^{2+}$ signal in a dark-adapted sample. Fig. 3F shows the effect of illumination at 77 K of a sample that already contained the formate-modified $Q_B^{\bullet-}Fe^{2+}$ state in a significant fraction of centers. The resulting signal has a smaller amplitude (i.e. $Q_B^{\bullet-}Fe^{2+}$ signal is lost) (Fig. 3F) and is more reminiscent of a residual formate-modified $Q_A^{\bullet-}Fe^{2+}$ signal. These effects can be explained in the same way as those in Fig. 2F: the $Q_A^{\bullet-}Fe^{2+}Q_B^{\bullet-}$ biradical state was formed in those centers in which $Q_B^{\bullet-}Fe^{2+}$ was present prior to the 77 K illumination and this state exhibits no (or a small) EPR signal in this region. The remaining signal seen upon illumination represents formation of $Q_A^{\bullet-}Fe^{2+}$ in those centers lacking $Q_B^{\bullet-}$ prior to 77 K illumination. By comparison to the $Q_A^{\bullet-}Fe^{2+}$ signal in Fig. 3E, this fraction is estimated to represent ~25% of centers.

Fig. 3G shows the result of a 77 K illumination given to a sample that had undergone two turnovers and should have passed two electrons already to Q_B in the majority of centers. Because of inefficiencies in the turnover protocol some centers do show formate-modified $Q_B^{\bullet-}Fe^{2+}$ prior to the 77 K illumination, however this is in a small minority of centers. As seen earlier (Fig. 2), instead of the standard formate-modified $Q_A^{\bullet-}Fe^{2+}$ EPR signal (e.g. Fig. 3E), a new broader signal (with peaks at $g=1.84$, and $g=1.81$ and a trough at $g=1.68$) is observed (see Fig. 2). A similar signal was seen after 77 K illumination of a sample that had undergone three turnovers (Fig. 3H). The data in Fig. 3 confirm the association of the new signal with a formate-modified $Q_A^{\bullet-}Fe^{2+}$ state in centers in which two (or more) electrons have already arrived at the secondary acceptor.

3.4. The new formate modified $Q_A^{\bullet-}Fe^{2+}$ signal: effects of light, reductants and inhibitors

The new broad signal was also seen when a formate-treated sample was frozen under illumination (Fig. 4B) or frozen in the dark immediately after illumination (not shown). This treatment should fully reduce Q_B, Q_C (when present and if reducible) and trap $Q_A^{\bullet-}$ in the reduced form. Fig. 4B shows that the new signal formed does not resemble the usual $Q_A^{\bullet-}Fe^{2+}$ signal (trace 4A). It has a significantly

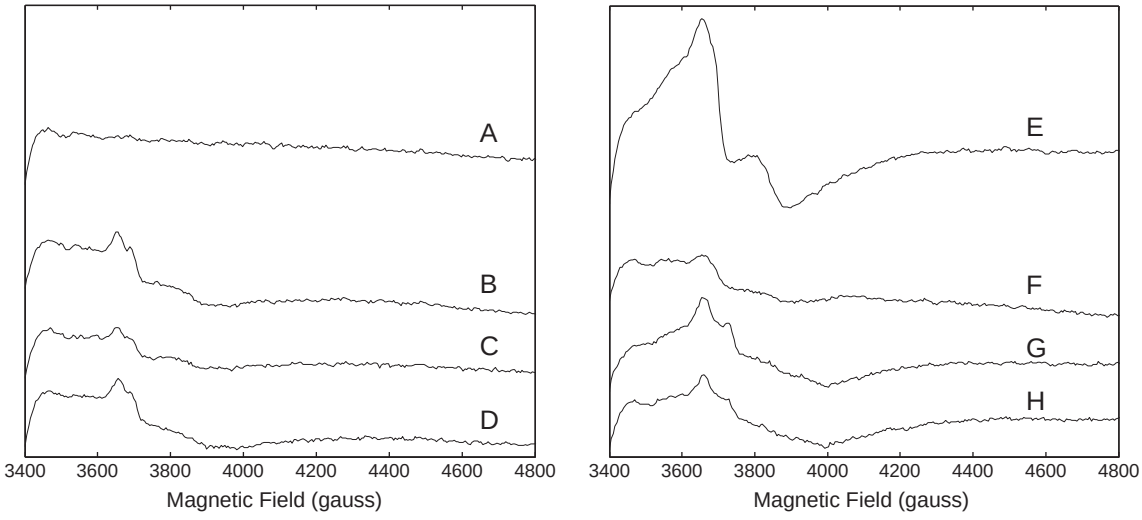

Fig. 3. The formate-modified signal monitored with different $Q_B^{\bullet-}$ concentrations induced by 0, 1, 2 or 3 photochemical turnovers occurring *prior* to formate addition. See the text and material and methods for more experimental details. In the left panel, A, B, C and D represent the formate-induced EPR signal after 0, 1, 2 and 3 photochemical turnovers respectively. In the right panel, E, F, G and H show the samples shown in the left panel, A, B, C and D, respectively, but after a 77 K illumination. Instrument settings were the same as in Fig. 1.

Please cite this article as: A. Sedoud, et al., Effects of formate binding on the quinone–iron electron acceptor complex of photosystem II, Biochim. Biophys. Acta (2010), doi:10.1016/j.bbabio.2010.10.019

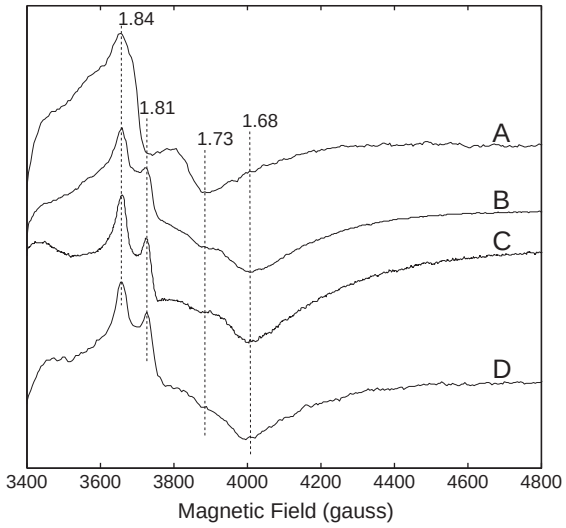

Fig. 4. The formate-modified $Q_A^{\bullet-}Fe^{2+}$ EPR signals generated in formate-treated PSII under a range of conditions: (A) illumination at 77 K of the 12 h dark-adapted PSII showing the usual $Q_A^{\bullet-}Fe^{2+}$ formate-induced signal as reference; (B) freezing under illumination; (C) dithionite reduction in the dark; (D) 77 K illumination of a sample reduced by DAD/ascorbate. Instrument settings were the same as in Fig. 1.

different line-shape with a peak at $g=1.81$ and a trough at $g=1.68$. The same signal is formed in formate-treated samples when reduced with dithionite in the dark (Fig. 4C) and also when pre-reduced by DAD and sodium ascorbate and then illuminated at 77 K (Fig. 4D). Dithionite is expected to fully reduce Q_B to Q_BH_2 and singly reduce Q_A in the dark. Similarly, DAD/ascorbate treatment is able to doubly reduce Q_B to Q_BH_2 in fraction of centers, and subsequent illumination at 77 K is expected to result in formation of $Q_A^{\bullet-}$. Hence, both of these chemically modified samples represent the $Q_A^{\bullet-}Fe^{2+}Q_BH_2$ state (or possibly one of its deprotonated forms $Q_A^{\bullet-}Fe^{2+}Q_BH^{\bullet-}$ or $Q_A^{-}Fe^{2+}Q_B^{2\bullet-}$).

Fig. 5B and C show the signals generated in formate-treated PSII in the presence of DCMU after freezing under illumination or reduced by dithionite, respectively. Both conditions should give rise to $Q_A^{\bullet-}Fe^{2+}$. These signals are virtually indistinguishable from each other and similar to that formed by low temperature illumination in the absence

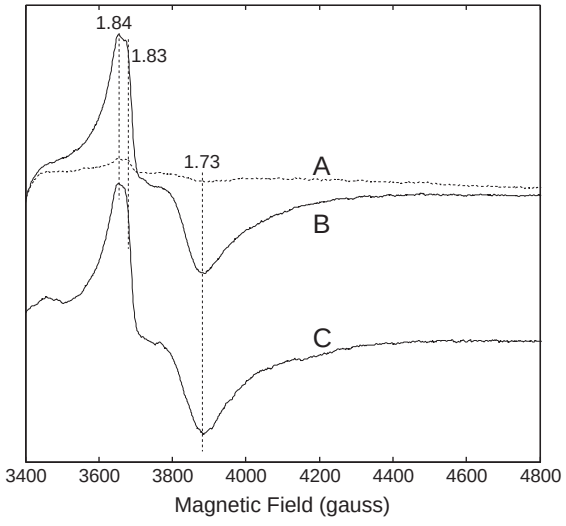

Fig. 5. Effect of DCMU on formate-treated, long dark-adapted PSII. (A) The signal present in the dark. (B) The signal formed after freezing under illumination. (C) The signal formed by reduction with dithionite. DCMU was prepared in DMSO (the concentration of the stock solution was 1 mM) was added to the sample in the EPR tube in darkness to give a final concentration of 50 μM. Instrument settings were the same as in Fig. 1.

of DCMU (Fig. 1E). These results indicate that occupation of the Q_B site by the inhibitor DCMU prevents the formation of the new broad signal.

When the PSII was treated with dithionite in the presence of ANT2p the modified $Q_A^{\bullet-}Fe^{2+}$ broad signal was converted to the unmodified $Q_A^{\bullet-}Fe^{2+}$ signal (Fig. S3). Similarly when the redox mediator indigodisulfonate ($E_m=-125$ mV), or the anion, azide, were added to dithionite reduced PSII, the modified signal showed partial reversion to the usual $Q_A^{\bullet-}Fe^{2+}$ signal (Fig. S3).

Fig. 6 shows an experiment in which DAD and sodium ascorbate were used as a reducing treatment. In the control sample without formate, the $Q_B^{\bullet-}$ was present in the majority of centers as indicated by the large $Q_A^{\bullet-}Fe^{2+}Q_B^{\bullet-}$ signal generated at $g=1.66$ upon illumination at 77 K [47,48]. This spectrum of the native $Q_A^{\bullet-}Fe^{2+}Q_B^{\bullet-}$ state (Fig. 6B) shows almost no overlap from the typical $Q_A^{\bullet-}Fe^{2+}$ signal at $g=1.95$, indicating that $Q_B^{\bullet-}$ was present in nearly all the centers prior to illumination at 77 K.

In the right panel the formate-modified $Q_B^{\bullet-}Fe^{2+}$ signal was formed in the presence of DAD/ascorbate (Fig. 6C). While the size of the signal seems to vary from experiment to experiment, illumination at 77 K resulted in formation of the new broad $Q_A^{\bullet-}Fe^{2+}$ signal. This was the case even when the formate-modified $Q_B^{\bullet-}Fe^{2+}$ signal was small. Given the assignment of the new signal to $Q_A^{\bullet-}Fe^{2+}$ in the presence of a two-electron reduced form of Q_B, this observation indicates that DAD/ascorbate is capable of doubly reducing Q_B in at least a fraction of the formate-treated PSII, while the untreated PSII was reduced only to the $Q_B^{\bullet-}$ level. This may indicate that the potentials of the redox couples associated with Q_B are shifted in the presence of formate, resulting in a less thermodynamically stable $Q_B^{\bullet-}$ state. Redox titrations are planned to test this.

We note that in the spectrum of native $Q_B^{\bullet-}Fe^{2+}$ in Fig. 6B there is a strong sharp feature at $g\sim2.00$, in addition to the typical features at $g=1.95$ and a broad signal at $g=1.71$ [48]. This new feature arises from $Q_B^{\bullet-}Fe^{2+}$ and is detected here because the TyrD$^{\bullet}$ signal is absent due to reduction by the DAD/ascorbate. This, and a corresponding signal in $Q_A^{\bullet-}Fe^{2+}$ will be the subject of a future publication. The $g=2.00$ signal from $Q_B^{\bullet-}Fe^{2+}$ can also be seen in the TyrD-less mutant (Boussac et al. personal communication).

3.5. Simulations of the semiquinone–iron EPR signals

Spectral simulations of the semiquinone–iron signal seen in formate treated PSII were performed using the Spin Hamiltonian formalism. The semiquinone–iron signal seen in purple bacteria is well understood from a theoretical standpoint [59]. The strong turning point at $g\sim1.8$ can be considered the intersection of two signals that arise from the two lowest Kramer's doublets of the quinone–iron spin manifold (for full discussion see [59]). The interaction of the non-heme iron ($S=2$) and semi-quinone, $Q_A^{\bullet-}$ ($S=½$) was described as follows. A basis set that describes the Fe-semiquinone ($Q^{\bullet}$, $S_Q=½$) spin manifold can be built from the product of the eigenstates of the two interacting spins. These are expressed in terms of three quantum numbers, $|S,\ m,\ s\rangle$. Where S is the total spin of the ground iron manifold ($S=2$), m is the iron magnetic sublevel ($m=-S,-S+1,\ldots,S-1,S$) and s is the semi-quinone sublevel ($s=-½,½$). Thus 10 basis vectors are required to span the spin manifold.

The Spin Hamiltonian appropriate for the $Q_A^{\bullet-}Fe^{2+}$ system, includes zero field (D, E), Zeeman (g_{Fe}, g_Q) and anisotropic exchange (J):

$$\mathcal{H} = D\left[\left(S_{FeZ}^2 - 1/3S_{Fe}(S_{Fe}+1)\right) + (E/D)\left(S_{FeX}^2 - S_{FeY}^2\right)\right] + \beta H\cdot g_{Fe}\cdot S_{Fe} + g_Q\beta H\cdot S - S_{Fe}\cdot J\cdot S_Q \quad (1)$$

Subsequent calculations assume the zero-field, Zeeman–iron and exchange tensors to be co-linear and g_Q to be scalar as in [59].

Please cite this article as: A. Sedoud, et al., Effects of formate binding on the quinone–iron electron acceptor complex of photosystem II, Biochim. Biophys. Acta (2010), doi:10.1016/j.bbabio.2010.10.019

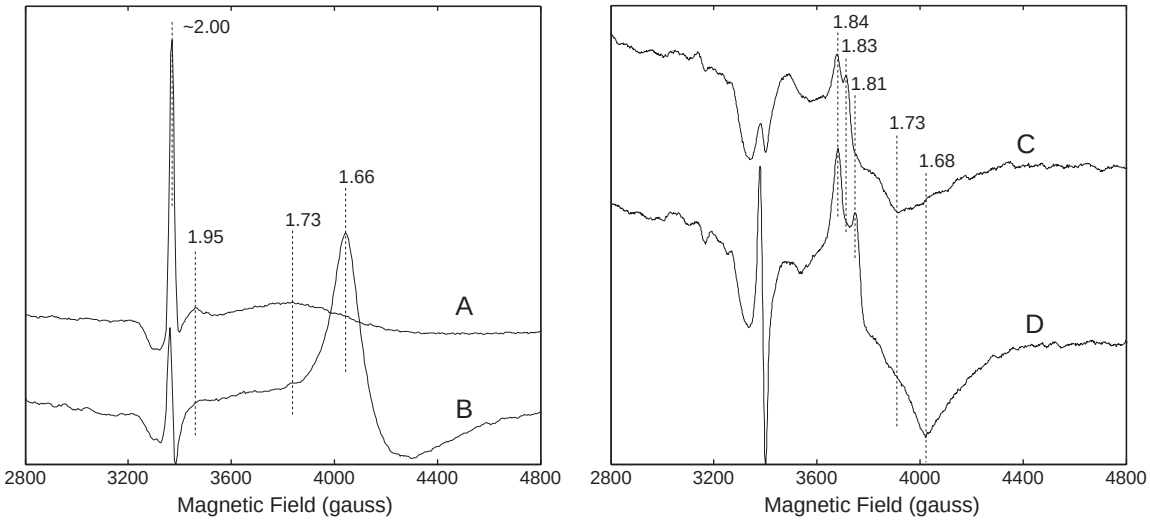

Fig. 6. Effect of DAD/ascorbate reduction on PSII in the presence and absence of formate. Left panel shows untreated PSII, (A) in the dark and (B) after illumination at 77 K. Right panel shows formate-treated PSII, (C) in the dark and (D) after illumination at 77 K. Instrument settings were the same as in Fig. 1, except for the temperature (5 K).

Estimates for all the Spin Hamiltonian parameters (D, E, g_{Fe}, g_Q and J) have been made in the species *R. sphaeroides*. The zero-field splitting of the non-heme iron, measured using static magnetisation, yielded values of $D \sim 5\ cm^{-1}$ ($7.6\ K^{-1}$) and $E/D \sim 0.25$. The interaction between the quinone and the iron is axial and of the order of $\sim 0.5\ cm^{-1}$. The structural homology between the PSII and purple bacteria and the strong similarity of the semiquinone iron signals observed suggest that the same theoretical approach is valid. The starting point for all optimized simulations reported here is the parameter set as determined for *R. sphaeroides*.

Table 1 shows the fitted parameters for simulations presented in Fig. 7. As a calibration, the variation amongst different purple bacteria was examined. *R. viridis* has virtually the same quinone–iron acceptor side complex as *R. sphaeroides* with the exception that *R. viridis* contains a menaquinone as Q_A instead of a ubiquinone. Only small differences for the simulated parameters were seen between the two species (Table 1). Both simulations (in *R. viridis* and *R. sphaeroides*) were of samples where *o*-phenanthroline was bound, displacing Q_B from its site. The addition of *o*-phenanthroline and other herbicides slightly narrows the signal of $Q_A^{\bullet-}Fe^{2+}$ and this has a minor affect on the parameters of the fitted lineshape (see [59]).

Simulation of the semiquinone–iron signals ($Q_A^{\bullet-}Fe^{2+}$ or $Q_B^{\bullet-}Fe^{2+}$) seen in formate-treated PSII are also very similar to those seen in purple bacteria with little variation in the coupling between the quinone and the iron and in zero-field splitting of the iron. However, the coupling interaction is rhombic rather than axial. This suggests that there is a small difference in for example the tensor geometries in PSII compared to purple bacteria. An analogous change in the tensor orientations of the system was observed in DFT calculations of iron–quinone model complexes based on crystallographic data from the bacterial reaction center and PSII [34]. No significant change was observed in the magnitude of the zero-field splitting of the iron, but small changes were seen for the orientation of the tensor coupling relative to the zero-field tensor (as estimated by the Fe hyperfine tensor). The $Q_B^{\bullet-}Fe^{2+}$ signal seen in *R. viridis* can also be modeled using the same parameters as used for formate-treated PSII ($Q_A^{\bullet-}Fe^{2+}$ or $Q_B^{\bullet-}Fe^{2+}$). The slightly different parameters used for $Q_B^{\bullet-}Fe^{2+}$ compared to $Q_A^{\bullet-}Fe^{2+}$ may reflect the slight asymmetry in the $Q_AFe^{2+}Q_B$ motif in *R. viridis*, as seen in its crystal structure [11].

A more significant change is observed for the new broad signal attributed to $Q_A^{\bullet-}Fe^{2+}Q_BH_2$. The spectrum of the $Q_A^{\bullet-}Fe^{2+}Q_BH_2$ state shown in Fig. 7 was corrected by subtraction of the unperturbed $Q_A^{\bullet-}Fe^{2+}$ signal (see figure caption). The corrected lineshape is reminiscent of the semiquinone iron signal ($Q_A^{\bullet-}Fe^{2+}$) of purple bacteria rather than those in PSII, with the peak-to-trough splitting the same as observed for *R. viridis* (~310 G). However, the turning point of $Q_A^{\bullet-}Fe^{2+}Q_BH_2$ is shifted to higher field by ~100 G compared to all the other semiquinone signals simulated. The fitted parameters show that this new signal is basically similar to that of "typical" $g \sim 1.8$ semiquinone–iron signals. The exchange interaction between the quinone and the iron is axial, with the x component being the smallest. It appears though that the zero-field splitting of the iron is significantly bigger ($\sim 2\ K^{-1}$). This solution is unlikely to be unique since the changes in the coupling between semiquinone and iron (in particular the J_Y component) and the changes in the zero-field splitting influenced the simulated spectrum in the same way. The fitted parameters presented represent the minimum changes to the *R. sphaeroides* solution that are required to reproduce the new spectrum.

In conclusion these simulations demonstrate that a significant change in the fitted parameters is required to simulate the $Q_A^{\bullet-}Fe^{2+}Q_BH_2$

Table 1
Optimized parameter set for the simulation of the semiquinone–iron complex signals.

	R. sphaeroides ($Q_A^{\bullet-}Fe^{2+}$)[b,c]	*R. viridis* ($Q_A^{\bullet-}Fe^{2+}$)[b]	PSII + formate ($Q_A^{\bullet-}Fe^{2+}$,$Q_B^{\bullet-}Fe^{2+}$) *R. viridis* ($Q_B^{\bullet-}Fe^{2+}$)[a]	PSII + formate ($Q_A^{\bullet-}Fe^{2+}Q_BH_2$)
J_{1X} (K^{-1})	−0.13	−0.154	−0.103	−0.193
J_{1Y} (K^{-1})	−0.58	−0.689	−0.733	−1.003
J_{1Z} (K^{-1})	−0.58	−0.630	−0.496	−1.008
$J_{1(ISO)}$ (K^{-1})	−0.43	−0.491	−0.444	−0.73
D (K^{-1})	7.6	7.560	7.740	9.82
E/D	0.25	0.253	0.250	0.270

[a] *R. sphaeroides* ($Q_A^{\bullet-}Fe^{2+}$) taken from Butler et al. [59].
[b] In the presence of *o*-phenanthroline.
[c] g_{Fe} tensor values fixed to those reported in [59].

Please cite this article as: A. Sedoud, et al., Effects of formate binding on the quinone–iron electron acceptor complex of photosystem II, Biochim. Biophys. Acta (2010), doi:10.1016/j.bbabio.2010.10.019

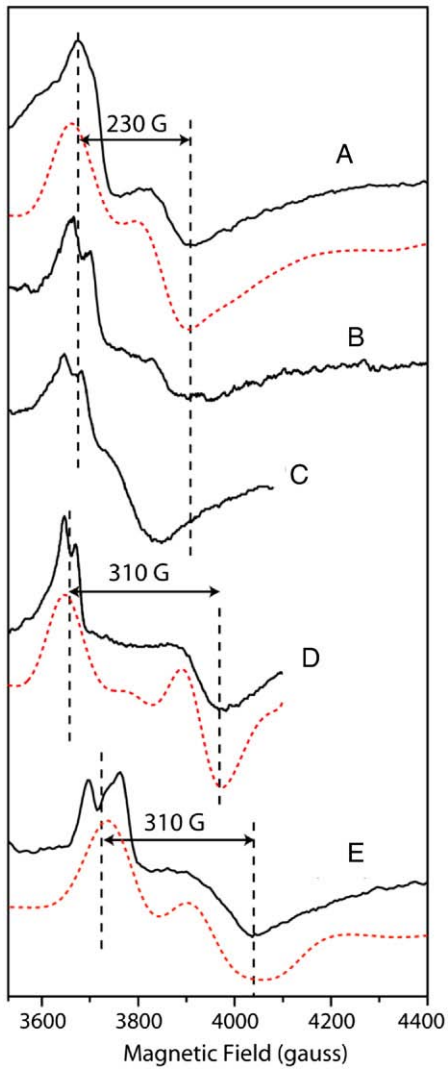

Fig. 7. Simulation of the semiquinone–iron complex signals seen in purple bacteria and PSII. (A) the $Q_A^{\bullet-}Fe^{2+}$ signal seen in PSII; (B) the $Q_B^{\bullet-}Fe^{2+}$ signal seen of PSII; (C) the $Q_B^{\bullet-}Fe^{2+}$ signal in *R. viridis*; (D) the $Q_A^{\bullet-}Fe^{2+}$ signal observed in *R. viridis* were *o*-phenanthroline was added (see [57]); (E) the modified $Q_A^{\bullet-}Fe^{2+}Q_BH_2$ state seen in PSII. This spectrum has been corrected by subtraction of the unperturbed $Q_A^{\bullet-}Fe^{2+}$ signal. It is estimated that the unperturbed $Q_A^{\bullet-}Fe^{2+}$ state accounts for ~20–30% of centers under the conditions where a maximal modified $Q_A^{\bullet-}Fe^{2+}Q_BH_2$ signal was observed. The offset dashed lines show spectral simulations of the EPR lineshape using the Spin Hamiltonian formalism discussed in the text.

quinone–iron complex and this change is much larger than the variation seen in all of the $g \sim 1.8$ semiquinone–iron signals seen in a range of species in the presence and absence of herbicides.

4. Discussion

4.1. An EPR signal from $Q_B^{\bullet-}Fe^{2+}$ in the presence of formate

Here we report an EPR signal that we attribute to formate-modified $Q_B^{\bullet-}Fe^{2+}$ state. This assignment is based on a series of observations and arguments. (i) The signal is similar but not identical to the signal observed for the $Q_A^{\bullet-}Fe^{2+}$ in the presence of formate [38]. (ii) The differences between the new signal and the formate modified $Q_A^{\bullet-}Fe^{2+}$ signal in PSII are similar to those that differentiate the $Q_A^{\bullet-}Fe^{2+}$ and $Q_B^{\bullet-}Fe^{2+}$ signals in purple bacterial reaction centers [59,69,70]. (iii) The EPR signal is formed upon addition of formate to a short dark-adapted sample (Fig. 1) and $Q_B^{\bullet-}$ is known to be stable in the native system (i.e. bicarbonate/carbonate bound) after short dark-adaption [48]. (iv) The formation of the EPR signal does not result in an increase in fluorescence yield (Table 1 in supplementary information) and thus the signal cannot be attributed to a modified form of $Q_A^{\bullet-}$. (v) The new signal is relatively stable but decays after 12 h of dark adaptation (Fig. 1) as expected from $Q_B^{\bullet-}$ [48]. Since we observed that $TyrD^{\bullet}$ decays in a significant fraction of centers during the long dark adaptation (not shown), and since evidence exists for $TyrD^{\bullet}$ $Q_A^{\bullet-}$ recombination at room temperature [73], the slow $Q_B^{\bullet-}$ decay may at least in part reflect $TyrD^{\bullet}$ $Q_B^{\bullet-}$ recombination. (vi) When the signal was absent, a single flash reformed the new signal with double the amplitude of that present in a short (1 h) dark-adapted sample (Fig. 1). (vii) The signal is much smaller on the second flash, as expected of $Q_B^{\bullet-}$ (Fig. 2). Taking into account the usual photochemical miss factor, we estimate that $Q_B^{\bullet-}$ is present in ~80% of centers after 1 flash. Thus the signal present in the short dark-adapted sample is estimated to be approximately 40%. These estimates are similar to those for $Q_B^{\bullet-}Fe^{2+}$ in untreated PSII in comparable conditions [48]. On the third flash however the $Q_B^{\bullet-}Fe^{2+}$ signal did not increase in intensity. Instead a new signal attributed to $Q_A^{\bullet-}Fe^{2+}$ in the presence of a two electron reduced form of Q_B was seen. (viii) The formate-modified $Q_B^{\bullet-}Fe^{2+}$ signal shows a period-of-two oscillation in its amplitude when formate is added *after* photochemical turnovers have occurred (Fig. 3). (ix) The signal can be formed by reduction of a formate-treated sample with DAD/ascorbate, conditions which generate a high concentration of $Q_B^{\bullet-}$ in the native system (Fig. 6).

These lines of evidence present a convincing case for the assignment of this EPR signal to assignment to a formate-modified $Q_B^{\bullet-}Fe^{2+}$ state. This new signal is easy to detect and should be useful for measuring the presence of $Q_B^{\bullet-}$. The maximum signal intensity seen in these studies is less (by around a factor of 2 based on the flash experiments) than that seen for the $Q_A^{\bullet-}Fe^{2+}$ signal in the same samples. This may be partially explained by inefficiencies in electron transfer, (e.g. less than 100% occupancy by Q_B, miss factors…etc.), however it also represents an intrinsically smaller signal from this state. A similar situation was seen for $Q_B^{\bullet-}Fe^{2+}$ in *R. viridis*, where the $Q_B^{\bullet-}Fe^{2+}$ signal also shows a greater splitting of the main peak [70] as shown here for PSII.

4.2. The $Q_A^{\bullet-}Fe^{2+}Q_B^{\bullet-}$ state in formate-treated PSII

In untreated PSII the $Q_A^{\bullet-}Fe^{2+}Q_B^{\bullet-}$ state gives rise to a strong signal at $g = 1.66$ (Fig. 6B) [46–48]. Here we show that when formate is bound, the $Q_A^{\bullet-}Fe^{2+}Q_B^{\bullet-}$ state does not give rise to a signal at $g = 1.66$. Instead the signal intensity at $g = 1.84$ decreases while the shape of the residual signal is attributable to residual $Q_A^{\bullet-}Fe^{2+}$, and perhaps $Q_B^{\bullet-}Fe^{2+}$ present in a very small fraction of centers where $Q_A^{\bullet-}$ is not formed by 77 K illumination [68]. The absence of an EPR signal in this region in the $Q_A^{\bullet-}Fe^{2+}Q_B^{\bullet-}$ state in formate-treated PSII is a further similarity with the purple bacterial reaction centers (see [69,72]). The absence of a signal in this region from the $Q_A^{\bullet-}Fe^{2+}Q_B^{\bullet-}$ state can be understood based on simulations of the spectra and theoretical considerations (Cox et al, in preparation).

4.3. A new formate-modified $Q_A^{\bullet-}Fe^{2+}$ EPR signal: $Q_A^{\bullet-}Fe^{2+}Q_BH_2$?

The second novel EPR signal described here seems to represent $Q_A^{\bullet-}Fe^{2+}$ modified not only by formate but also by the presence of a two-electron reduced form of Q_B. This signal is broader than the usual formate-modified $Q_A^{\bullet-}Fe^{2+}$ signal, with peaks at $g \sim 1.84$ and $g \sim 1.81$ and a marked trough at $g \sim 1.68$. This new state can be generated in several ways in formate-treated PSII: (i) after 3 or more flashes at room temperature (Fig. 2D and E); (ii) by photo-generating $Q_A^{\bullet-}Fe^{2+}$ at low temperature after Q_B has been reduced by two electrons photochemically (Figs. 2 and 3 right panels) or chemically (Fig. 4); (iii) freezing under illumination (Fig. 4B) or immediately after illumination; and (iv) dithionite reduction (Fig. 4C). Furthermore, in the presence of the inhibitor DCMU it

Please cite this article as: A. Sedoud, et al., Effects of formate binding on the quinone–iron electron acceptor complex of photosystem II, Biochim. Biophys. Acta (2010), doi:10.1016/j.bbabio.2010.10.019

was not possible to form the broad signal. These results indicate that the EPR signal from $Q_A^{\bullet-}Fe^{2+}$ is sensitive to the occupation of the Q_B site. It is already known that inhibitor binding in the Q_B site has a marked influence on the $Q_A^{\bullet-}Fe^{2+}$ EPR signal in PSII [74] and in the purple bacterial reaction centers [57,59]. However in the present work the Q_A^{-} site is specifically and significantly modified by the presence of a two-electron reduced form of Q_B in its site. In contrast, in the purple bacterial reaction center, Butler et al. [59] reported that Q_BH_2 had only a small influence on the $Q_A^{\bullet-}Fe^{2+}$ signal.

This modified form of the formate-modified $Q_A^{\bullet-}Fe^{2+}$ signal in dithionite was not seen in earlier reports [38,40,41]. We suggest that this could reflect low occupancy of Q_B in these preparations. Early preparations of *T. elongatus* as used by van Mieghem, [40] lacked Q_B [21]. The small $Q_A^{\bullet-}Fe^{2+}Q_B^{\bullet-}$ EPR signal observed in the PSII preparation of *T. elongatus* [41] compared with our current material (see Fig. 6 and [48]), indicates that the PSII used in [41] had a low $Q_B^{\bullet-}$ concentration. The plant thylakoids used in Ref. [38] would be expected to have had native Q_B levels. However, much lower concentration of formate were used in [38]. An investigation of the concentration dependence of formate on the formation of the new $Q_A^{\bullet-}Fe^{2+}$ state may help understand these effects.

The presence of ANT2p, indigodisulfonate and azide, all resulted in a decrease of the new signal and a relative increase of the standard formate $Q_A^{\bullet-}Fe^{2+}$ signal (Fig. S3). It is not obvious why these diverse chemicals all had a similar effect. Redox, protonation, charge and binding effects can be imagined but further experimentation is required before this can be determined.

Based on the literature [33,75], the most likely candidates for the origin of the new $Q_A^{\bullet-}Fe^{2+}$ signal is the $Q_A^{\bullet-}Fe^{2+}Q_BH_2$ state. This would fit with formate inhibition of electron transfer being due to inhibition of Q_BH_2 release from the site [27,33]. In the most recent crystal structure Q_C is close to the Q_B site (~17 Å) and suggestions have been made for its role in electron transfer as a staging post for Q_BH_2 replacement [23]. If Q_C represents the one-quinone pool reported by Fufezan et al. [48], then it is possible that formate interferes with the exchange process with Q_C. This could occur as a long range influence from its binding to the iron or as a second binding effect closer Q_B and Q_C. It has already been suggested that a second bicarbonate/formate site other than the iron ligation site may be present [32]. This suggestion was mainly based on the observation that DCMU addition inhibited formate binding. Here we suggest it could interfere with Q_B/Q_C exchange. Further experimentation is required in order to address this idea.

If formate interferes with the protonation pathways as suggested earlier [24] and [34] then it is worth considering the two deprotonated forms of the state of $Q_A^{\bullet-}Fe^{2+}Q_BH_2$, that is to say $Q_A^{\bullet-}Fe^{2+}Q_BH^{-}$ and $Q_A^{\bullet-}Fe^{2+}Q_B^{2\bullet-}$ states as a possible origin of the new EPR signal. While we do not rule out these options, in the absence of experimental arguments, the $Q_A^{\bullet-}Fe^{2+}Q_BH_2$ (formate) state is the more conservative assignment and this will be used in the remaining discussion.

Spectral simulations of all the semiquinone–iron signals demonstrate that the modified $Q_A^{\bullet-}Fe^{2+}Q_BH_2$ (formate) state is significantly different from all previously measured signals at around $g=1.84$. The magnitude of the difference is significantly larger than that seen between different species or from the binding of herbicides to the Q_B pocket. Thus Q_BH_2 occupation of the Q_B pocket alone is unlikely to explain the "modified state" of the $Q_A^{\bullet-}Fe^{2+}$. Indeed from the range of semiquinone–iron signals present in the literature, the effects of point mutations and binding of herbicides and the nature of the spectral changes seen, it seems that significant changes in the spectrum of $Q_A^{\bullet-}Fe^{2+}$ reflect changes is the vicinity of the $Q_A^{\bullet-}$ or the Fe^{2+}. In our simulations, the zero-field splitting of the Fe^{2+} was different for the modified state. A similar change was seen for the simulations of the $g\sim1.9$ signal [34] where an increase in the zero-field splitting was inferred of up to 7 K^{-1}. This was interpreted as being due to a change in the first coordination sphere of the iron, i.e. the CO_3^{2-} ligand significantly altered the Fe^{2+}. It is suggested that an analogous modification albeit of lesser magnitude, may occur for the new formate-modified $Q_A^{\bullet-}Fe^{2+}Q_BH_2$ state. Potentially the introduction of a charged group in the 1st/2nd coordination sphere of the iron could induce this effect. One possibility is that formate prevents the re-protonation of a protein residue (close to the iron) after Q_BH_2 formation. An alternative explanation along the same lines is that an additional formate ion is bound (or formed by deprotonation of formic acid) during Q_B reduction.

4.4. Formate-induced inhibition

The EPR study shows that formate inhibits the electron transfer after two electrons arrive on Q_B, as manifest by the formation of the $Q_A^{\bullet-}Fe^{2+}Q_BH_2$ (formate) state on the third flash. This fits with results reported earlier using fluorescence [30] and electronic absorption measurements [27]. In earlier work the $Q_A^{\bullet-}$ oxidation kinetic slowed by more than 2 orders of magnitude, from around 1 ms to 100–200 ms on the third flash [27,30]. Here however the $Q_A^{\bullet-}$ signal is still present in a sample frozen ~1 s second after a laser flash. Possible explanations for this difference include: (i) slower quinone exchange in the thermophile at room temperature (i.e. a species difference); and (ii) some centers lacking Q_C in the isolated PSII (i.e. a biochemical difference). Kinetic experiments on the present material measuring Q_A^{-} decay by using fluorescence or optical absorption changes should resolve this issue.

Overall the data indicate that formate does not greatly modify electron transfer from $Q_A^{\bullet-}$ to Q_B or $Q_A^{\bullet-}$ to $Q_B^{\bullet-}$. We know from the literature that the kinetics is slowed by a factor of 5 and 10 respectively. Given that the uninhibited electron transfer rate ($t_{1/2}$ around 400 and 800 μs) [76] is much faster than the decay of $S_{2/3}Q_A^{\bullet-}$ ($t_{1/2}=1$ s), then this slowing of the rate has little effect on the yield of the final charge separated state. In contrast, on the 3rd flash electron transfer is more drastically affected: (i) $Q_A^{\bullet-}$ begins to get trapped under the conditions of the EPR experiment; (ii) the advance of the charge accumulation states of the water oxidizing complex (S states) becomes less efficient (probably because of the long time for Q_BH_2 exchange compared to the flash spacing); and (iii) a new state is detected by EPR which we suggest is the $Q_A^{\bullet-}Fe^{2+}$ in the presence of a double-reduced form of Q_B. The observation that the main effect of formate on electron transfer occurs on the third turnover, fits with earlier observations in the literature using fluorescence and absorption measurements [27,30]. However the current work indicates that the block occurs with reduced quinone in the Q_B site rather than with an empty site.

The signals reported and characterized here allow the previously elusive $Q_B^{\bullet-}Fe^{2+}$state and the newly discovered, formate-inhibited, $Q_A^{\bullet-}Fe^{2+}Q_BH_2$ state to be easily monitored using EPR. These signals should be useful in future studies aimed at understanding in more detail the nature of the electron transfer inhibition induced by formate and potential regulatory mechanisms involving bicarbonate/carbonate. Indeed the signals are probably distinct enough to be useful for studies in physiologically relevant biological material.

Acknowledgments

This work was supported by the EU/Energy Network project SOLAR-H2 (FP7 contract 212508). We thank Gernot Renger for providing the ANT2p. Arezki Sedoud is supported by the IRTELIS training program of the CEA. Lisa Kastner was funded in part by a grant from the DRI of the CEA. A. Boussac and A. Krieger-Liszkay are acknowledged for helpful discussions. We thank Wolfgang Lubitz for reading the manuscript and for helpful suggestions.

Please cite this article as: A. Sedoud, et al., Effects of formate binding on the quinone–iron electron acceptor complex of photosystem II, Biochim. Biophys. Acta (2010), doi:10.1016/j.bbabio.2010.10.019

Appendix A. Supplementary data

Supplementary data to this article can be found online at doi:10.1016/j.bbabio.2010.10.019.

References

[1] B.A. Diner, G.T. Babcock, Structure, dynamics, and energy conversion efficiency in photosystem II, in: D.R. Ort, C.F. Yocum (Eds.), Oxygenic Photosynthesis: The Light Reactions, Kluwer Academic, Dordecht, The Netherlands, 1996, pp. 213–247.

[2] F. Rappaport, B.A. Diner, Primary photochemistry and energetics leading to the oxidation of the Mn_4Ca cluster and to the evolution of molecular oxygen in Photosystem II, Coord. Chem. Rev. 252 (2008) 259–272.

[3] V. Petrouleas, A.R. Crofts, The iron–quinone acceptor complex, in: T. Wydrzynski, K. Satoh (Eds.), Photosystem II. The light-driven water: plastoquinone oxidoreductase, Springer, Dordecht, The Netherlands, 2005, pp. 177–206.

[4] B. Bouges-Bouquet, Electron transfer between the two photosystems in spinach chloroplasts, Biochim. Biophys. Acta 314 (1973) 250–256.

[5] B.R. Velthuys, J. Amesz, Charge accumulation at reducing side of system 2 of photosynthesis, Biochim. Biophys. Acta 333 (1974) 85–94.

[6] B.R. Velthuys, Electron-dependent competition between plastoquinone and inhibitors for binding to Photosystem II, FEBS Lett. 126 (1981) 277–281.

[7] C.A. Wraight, Oxidation-reduction physical-chemistry of the acceptor quinone complex in bacterial photosynthetic reaction centers—evidence for a new model of herbicide activity, Isr. J. Chem. 21 (1981) 348–354.

[8] C.A. Wraight, Proton and electron transfer in the acceptor quinone complex of photosynthetic reaction centers from *Rhodobacter sphaeroides*, Front. Biosci. 9 (2004) 309–337.

[9] M.Y. Okamura, M.L. Paddock, M.S. Graige, G. Feher, Proton and electron transfer in bacterial reaction centers, Biochim. Biophys. Acta 1458 (2000) 148–163.

[10] A.W. Rutherford, How close is the analogy between the reaction center of PSII and that of purple bacteria? 2. The electron acceptor side, in: J. Biggins (Ed.), Progress in Photosynthesis Research, Martinus Nijhoff, Dordecht, The Netherlands, 1987, pp. 277–283.

[11] H. Michel, J. Deisenhofer, Relevance of the photosynthetic reaction center from purple bacteria to the structure of Photosystem-II, Biochemistry 27 (1988) 1–7.

[12] A.W. Rutherford, Photosystem-II, the water-splitting enzyme, Trends Biochem. Sci. 14 (1989) 227–232.

[13] A. Trebst, The topology of the plastoquinone and herbicide binding peptides of photosystem II in the thylakoid membrane, Z. Naturforsch. C 41 (1986) 240–245.

[14] R.J. Debus, B.A. Barry, G.T. Babcock, L. McIntosh, Site-directed mutagenesis identifies a tyrosine radical involved in the photosynthetic oxygen-evolving system, Proc. Natl Acad. Sci. USA 85 (1988) 427–430.

[15] W.F.J. Vermaas, A.W. Rutherford, O. Hansson, Site-directed mutagenesis in photosystem II of the *Cyanobacterium synechocystis sp* PCC6803—donor-D is a tyrosine residue in the D2-protein, Proc. Natl Acad. Sci. USA 85 (1988) 8477–8481.

[16] B. Svensson, I. Vass, E. Cedergren, S. Styring, Structure of donor side components in photosystem II predicted by computer modelling, EMBO J. 9 (1990) 2051–2059.

[17] R.T. Sayre, B. Andersson, L. Bogorad, The topology of a membrane protein: the orientation of the 32 kd Q_B-binding chloroplast thylakoid membrane protein, Cell 47 (1986) 601–608.

[18] O. Nanba, K. Satoh, Isolation of a photosystem II reaction center consisting of D-1 and D-2 polypeptides and cytochrome b-559, Proc. Natl Acad. Sci. USA 84 (1987) 109–112.

[19] P. Dorlet, A.W. Rutherford, S. Un, Orientation of the tyrosyl D, pheophytin anion, and semiquinone $Q_A^{\bullet -}$ radicals in photosystem II determined by high-field electron paramagnetic resonance, Biochemistry 39 (2000) 7826–7834.

[20] T. Yoshii, H. Hara, A. Kawamori, K. Akabori, M. Iwaki, S. Itoh, ESEEM study of the location of spin-polarized chlorophyll-quinone radical pair in membrane-oriented spinach photosystems I and II complexes, Appl. Magn. Reson. 16 (1999) 565–580.

[21] A. Zouni, H.T. Witt, J. Kern, P. Fromme, N. Krauss, W. Saenger, P. Orth, Crystal structure of photosystem II from *Synechococcus elongatus* at 3.8 angstrom resolution, Nature 409 (2001) 739–743.

[22] K.N. Ferreira, T.M. Iverson, K. Maghlaoui, J. Barber, S. Iwata, Architecture of the photosynthetic oxygen-evolving center, Science 303 (2004) 1831–1838.

[23] A. Guskov, J. Kern, A. Gabdulkhakov, M. Broser, A. Zouni, W. Saenger, Cyanobacterial photosystem II at 2.9-angstrom resolution and the role of quinones, lipids, channels and chloride, Nat. Struct. Mol. Biol. 16 (2009) 334–342.

[24] J.J.S. Van Rensen, W.J.M. Tonk, S.M. Debruijn, Involvement of bicarbonate in the protonation of the secondary quinone electron-acceptor of Photosystem II via the non-heme iron of the quinone–iron acceptor complex, FEBS Lett. 226 (1988) 347–351.

[25] R. Hienerwadel, C. Berthomieu, Bicarbonate binding to the non-heme iron of photosystem II investigated by fourier transform infrared difference spectroscopy and ^{13}C-labeled bicarbonate, Biochemistry 34 (1995) 16288–16297.

[26] P. Jursinic, J. Warden, Govindjee, Major site of bicarbonate effect in system-II reaction evidence from ESR signal-IIvf, fast fluorescence yield changes and delayed light-emission, Biochim. Biophys. Acta 440 (1976) 322–330.

[27] U. Siggel, R. Khanna, G. Renger, Govindjee, Investigation of the absorption changes of the plasto-quinone system in broken chloroplasts. The effect of bicarbonate-depletion, Biochim. Biophys. Acta 462 (1977) 196–207.

[28] H.H. Robinson, J.J. Eaton-Rye, J.J.S. van Rensen, Govindjee, The effects of bicarbonate depletion and formate incubation on the kinetics of oxidation-reduction reactions of the Photosystem II quinone acceptor complex, Z. Naturforsch. C 39 (1984) 382–385.

[29] J.J. Eaton-Rye, Govindjee, Electron-transfer through the quinone acceptor complex of Photosystem-II after one or 2 actinic flashes in bicarbonate-depleted spinach thylakoid membranes, Biochim. Biophys. Acta 935 (1988) 248–257.

[30] M.P.J. Pulles, Govindjee, R. Govindjee, H.J. van Gorkom, L.N.M. Duysens, Inhibition of reoxidation of secondary-electron acceptor of Photosystem-II by bicarbonate depletion, Biochim. Biophys. Acta 449 (1976) 602–605.

[31] J. Farineau, P. Mathis, Effect of bicarbonate on electron transfer between plastoquinones in Photosystem II, in: Y. Inoue, A.R. Crofts, Govindjee, N. Murata, G. Renger, K. Satoh (Eds.), The oxygen evolving system of photosynthesis, Academic Press, Inc., 1983, pp. 317–325.

[32] D.J. Blubaugh, Govindjee, The molecular mechanism of the bicarbonate effect at the plastoquinone reductase site of photosynthesis, Photosynth. Res. 19 (1988) 85–128.

[33] J.J.S. van Rensen, V.V. Klimov, Role of bicarbonate in Photosystem II, in: T.J. Wydrzynski, K. Satoh (Eds.), Advances in photosynthesis and respiration oxygenic photosynthesis: Photosystem II. The light driven water: Plastoquinone oxidoreductase, Springer, Dordrecht, 2005, pp. 329–346.

[34] N. Cox, L. Jin, A. Jaszewski, P.J. Smith, E. Krausz, A.W. Rutherford, R. Pace, The semiquinone–iron complex of photosystem II: Structural insights from ESR and theoretical simulation; evidence that the native ligand to the non-heme iron is carbonate, Biophys. J. 97 (2009) 2024–2033.

[35] J.H.A. Nugent, B.A. Diner, M.C.W. Evans, Direct detection of the electron-acceptor of photosystem-II - evidence that Q is an iron–quinone complex, FEBS Lett. 124 (1981) 241–244.

[36] A.W. Rutherford, P. Mathis, A relationship between the midpoint potential of the primary acceptor and low-temperature photochemistry in Photosystem II, FEBS Lett. 154 (1983) 328–334.

[37] A.W. Rutherford, J.L. Zimmermann, A new EPR signal attributed to the primary plastosemiquinone acceptor in Photosystem II, Biochim. Biophys. Acta 767 (1984) 168–175.

[38] W.F.J. Vermaas, A.W. Rutherford, Electron-paramagnetic-res measurements on the effects of bicarbonate and triazine resistance on the acceptor side of Photosystem II, FEBS Lett. 175 (1984) 243–248.

[39] J.L. Zimmermann, A.W. Rutherford, Photoreductant-induced oxidation of Fe^{2+} in the electron–acceptor complex of Photosystem II, Biochim. Biophys. Acta 851 (1986) 416–423.

[40] F. van Mieghem, K. Brettel, B. Hillmann, A. Kamlowski, A.W. Rutherford, E. Schlodder, Charge recombination reactions in Photosystem II.1. Yields, recombination pathways, and kinetics of the primary pair, Biochemistry 34 (1995) 4798–4813.

[41] F. Mamedov, M.M. Nowaczyk, A. Thapper, M. Rogner, S. Styring, Functional characterization of monomeric Photosystem II core preparations from *Thermosynechococcus elongatus* with or without the Psb27 protein, Biochemistry 46 (2007) 5542–5551.

[42] S. Demeter, C. Goussias, G. Bernat, L. Kovacs, V. Petrouleas, Participation of the $g=1.9$ and $g=1.82$ EPR forms of the semiquinone–iron complex $Q_A^-\cdot Fe^{2+}$ of photosystem II in the generation of the Q and C thermoluminescence bands, respectively, FEBS Lett. 336 (1993) 352–356.

[43] V. Petrouleas, Y. Deligiannakis, B.A. Diner, Binding of carboxylate anions at the non-heme Fe(II) of PS II. II. Competition with bicarbonate and effects on the Q_A/Q_B electron transfer rate, Biochim. Biophys. Acta 1188 (1994) 271–277.

[44] D.F. Ghanotakis, G.T. Babcock, C.F. Yocum, Structural and catalytic properties of the oxygen-evolving complex—correlation of polypeptide and manganese release with the behavior of Z+ in chloroplasts and a highly resolved preparation of the PSII complex, Biochim. Biophys. Acta 765 (1984) 388–398.

[45] A.W. Rutherford, J.L. Zimmermann, P. Mathis, EPR of PSII-interactions, herbicide effects and new signal, in: C. Sybesma (Ed.), Advances in Photosynthesis Research, Martinus Nijhoff, Junk, W., Dordecht, The Netherlands, 1984, pp. 445–448.

[46] B. Hallahan, S. Ruffle, S. Bowden, J.H.A. Nugent, Identification and characterization of EPR signals involving Q_B semiquinone in plant Photosystem II, Biochim. Biophys. Acta 1059 (1991) 181–188.

[47] A.R. Corrie, J.H.A. Nugent, M.C.W. Evans, Identification of EPR Signals from the States $Q_A^-Q_B^-$ and Q_B^- in Photosystem-II from *Phormidium laminosum*, Biochim. Biophys. Acta 1057 (1991) 384–390.

[48] C. Fufezan, C.X. Zhang, A. Krieger-Liszkay, A.W. Rutherford, Secondary quinone in photosystem II of *Thermosynechococcus elongatus*: Semiquinone–iron EPR signals and temperature dependence of electron transfer, Biochemistry 44 (2005) 12780–12789.

[49] J. Kern, B. Loll, C. Luneberg, D. DiFiore, J. Biesiadka, K.D. Irrgang, A. Zouni, Purification, characterisation and crystallisation of photosystem II from *Thermosynechococcus elongatus* cultivated in a new type of photobioreactor, Biochim. Biophys. Acta 1706 (2005) 147–157.

[50] J. Kruk, K. Strzalka, Redox changes of cytochrome b_{559} in the presence of plastoquinones, J. Biol. Chem. 276 (2001) 86–91.

[51] O. Kaminskaya, V.A. Shuvalov, G. Renger, Evidence for a novel quinone-binding site in the photosystem II (PS II) complex that regulates the redox potential of cytochrome b559, Biochemistry 46 (2007) 1091–1105.

[52] U. Muhlenhoff, F. Chauvat, Gene transfer and manipulation in the thermophilic cyanobacterium *Synechococcus elongatus*, Mol. Gen. Genet. 252 (1996) 93–100.

[53] A. Boussac, F. Rappaport, P. Carrier, J.M. Verbavatz, R. Gobin, D. Kirilovsky, A.W. Rutherford, M. Sugiura, Biosynthetic Ca^{2+}/Sr^{2+} exchange in the photosystem II oxygen-evolving enzyme of *Thermosynechococcus elongatus*, J. Biol. Chem. 279 (2004) 22809–22819.

[54] M. Sugiura, Y. Inoue, Highly purified thermo-stable oxygen-evolving photosystem II core complex from the thermophilic cyanobacterium *Synechococcus elongatus* having his-tagged CP43, Plant Cell Physiol. 40 (1999) 1219–1231.

Please cite this article as: A. Sedoud, et al., Effects of formate binding on the quinone–iron electron acceptor complex of photosystem II, Biochim. Biophys. Acta (2010), doi:10.1016/j.bbabio.2010.10.019

[55] J. Cao, Govindjee, Bicarbonate effect on electron flow in a cyanobacterium *Synechocystis* PCC 6803, Photosynth. Res. 19 (1988) 277–285.
[56] S. Stoll, A. Schweiger, EasySpin, a comprehensive software package for spectral simulation and analysis in EPR, J. Magn. Reson. 178 (2006) 42–55.
[57] I. Sinning, H. Michel, P. Mathis, A.W. Rutherford, Characterization of 4 herbicide-resistant mutants of *Rhodopseudomonas viridis* by genetic-analysis, electron-paramagnetic resonance, and optical spectroscopy, Biochemistry 28 (1989) 5544–5553.
[58] J.S. Leigh, P.L. Dutton, Primary electron acceptor in photosynthesis, Biochem. Biophys. Res. 46 (1972) 414-&.
[59] W.F. Butler, R. Calvo, D.R. Fredkin, R.A. Isaacson, M.Y. Okamura, G. Feher, The electronic-structure of Fe2+ in reaction centers from *Rhodopseudomonas sphaeroides*.3. Electron-paramagnetic-res measurements of the reduced acceptor complex, Biophys. J. 45 (1984) 947–973.
[60] J.H.A. Nugent, A.R. Corrie, C. Demetriou, M.C.W. Evans, C.J. Lockett, Bicarbonate binding and the properties of Photosystem II electron-acceptors, FEBS Lett. 235 (1988) 71–75.
[61] B.R. Velthuys, J.W.M. Visser, The reactivation of EPR signal II in chloroplasts treated with reduced dichlorophenol-indophenol: Evidence against a dark equilibrium between two oxidation states of the oxygen evolving system, FEBS Lett. 55 (1975) 109–112.
[62] A.W. Rutherford, A. Boussac, P. Faller, The stable tyrosyl radical in Photosystem II: why D? Biochim. Biophys. Acta 1655 (2004) 222–230.
[63] G.C. Dismukes, Y. Siderer, Intermediates of a polynuclear manganese center involved in photosynthetic oxidation of water, Proc. Natl Acad. Sci. USA 78 (1981) 274–278.
[64] G.W. Brudvig, J.L. Casey, K. Sauer, The effect of temperature on the formation and decay of the multiline electron-paramagnetic-res signal species associated with photosynthetic oxygen evolution, Biochim. Biophys. Acta 723 (1983) 366–371.
[65] Y.M. Feyziev, D. Yoneda, T. Yoshii, N. Katsuta, A. Kawamori, Y. Watanabe, Formate-induced inhibition of the water-oxidizing complex of photosystem II studied by EPR, Biochemistry 39 (2000) 3848–3855.
[66] A. Jajoo, N. Katsuta, A. Kawamori, An EPR study of the pH dependence of formate effects on Photosystem II, Plant Physiol. Biochem. 44 (2006) 186–192.
[67] N. Cox, F.M. Ho, N. Pewnim, R. Steffen, P.J. Smith, K.G.V. Havelius, J.L. Hughes, L. Debono, S. Styring, E. Krausz, R.J. Pace, The S-1 split signal of photosystem II; a tyrosine-manganese coupled interaction, Biochim. Biophys. Acta 1787 (2009) 882–889.
[68] J.L. Hughes, A.W. Rutherford, M. Sugiura, E. Krausz, Quantum efficiency distributions of photo-induced side-pathway donor oxidation at cryogenic temperature in photosystem II, Photosynth. Res. 98 (2008) 199–206.
[69] C.A. Wraight, Iron–quinone interactions in electron-acceptor region of bacterial photosynthetic reaction centers, FEBS Lett. 93 (1978) 283–288.
[70] A.W. Rutherford, M.C.W. Evans, High-potential semiquinone–iron signal in *Rhodopseudomonas viridis* is the specific quinone secondary-electron acceptor in the photosynthetic reaction center, FEBS Lett. 104 (1979) 227–230.
[71] P. Faller, C. Fufezan, A.W. Rutherford, Side-path electrondonnors: cytochrome b559, chlorophyll Z and beta-caroten, in: T.J. Wydrzynski, K. Satoh (Eds.), Photosystem II: The Light-Driven water: Plastoquinone Oxidoreductase, Springer, Dordecht, the Netherlands, 2005, pp. 347–365.
[72] A.W. Rutherford, M.C.W. Evans, High-potential semiquinone–iron type epr signal in *Rhodopseudomonas viridis*, FEBS Lett. 100 (1979) 305–308.
[73] G.N. Johnson, A. Boussac, A.W. Rutherford, The origin of 40-50 °C thermoluminescence bands in Photosystem II, Biochim. Biophys. Acta 1184 (1994) 85–92.
[74] A.W. Rutherford, J.L. Zimmermann, P. Mathis, The effect of herbicides on components of the PSII reaction center measured by electron-paramagnetic-res, FEBS Lett. 165 (1984) 156–162.
[75] J.J.S. van Rensen, C.H. Xu, Govindjee, Role of bicarbonate in photosystem II, the water-plastoquinone oxido-reductase of plant photosynthesis, Physiol. Plant. 105 (1999) 585–592.
[76] R. de Wijn, H.J. van Gorkom, Kinetics of electron transfer from Q_A to Q_B in photosystem II, Biochemistry 40 (2001) 11912–11922.

Please cite this article as: A. Sedoud, et al., Effects of formate binding on the quinone–iron electron acceptor complex of photosystem II, Biochim. Biophys. Acta (2010), doi:10.1016/j.bbabio.2010.10.019

Effects of formate binding on the quinone-iron electron acceptor complex of photosystem II

Arezki Sedoud[a], Lisa Kastner[a], Nicholas Cox[b], Sabah El-Alaoui[a], Diana Kirilovsky[a] and A. William Rutherford[a*]

[a] iBiTec-S, CNRS URA 2096, CEA Saclay, 91191 Gif-sur-Yvette, France.

[b] MPI für Bioanorganische Chemie, Stiftstrasse 34 - 36 / D - 45470 Mülheim an der Ruhr, Germany.

His-tagged CP47 strain construction

The *Thermosynechococcus elongatus* genome region containing the *psbB* and *psbT* genes and flanking regions was amplified by PCR using the *XhoI*-CP47a and the *BamHI*-CP47b oligonucleotides containing the XhoI and BamHI restriction sites (supplementary figure 1). The PCR product of 1.64 kb was cloned in the SK(+) ampicillin-resistant vector. To construct a C-terminal His-tagged CP47 mutant, the His-tag was introduced by site-directed mutagenesis using the Quickchange XL site-directed mutagenesis kit (Stratagene) and synthetic mutagenic oligonucleotides HistagCP47a and HistagCP47b. In addition these primers created an ApaLI restriction site. An HpaI restriction site was created just after the *psbT* gene using the synthetic oligonucleotides CP47aHpa and CP47bHpa. Then a 1.3 kb kanamycin resistance gene was introduced into the *HpaI* restriction site. The plasmid containing the gene coding for the C-terminal His-tagged CP47 was put into wild type *T. elongatus* cells by electroporation according to [1]. Genomic DNA was isolated from *T. elongatus* cells essentially as described by [2]. To verify that the six histidines were present in the transformed *T. elongatus* cells and to confirm the total segregation of the mutant, a PCR analysis was carried out using the oligonucleotides *XhoI*-CP47a and the *BamHI*-CP47b. The amplified fragment was digested by ApaLI. Figure S1C shows that the amplification of the genomic region containing the *psbB* and *psbT* genes and flanking regions gave a 3 kb fragment indicating the presence of the kanamycin resistance. No traces were detected of a 1.6 kb fragment observed in the wild type lacking the antibiotic resistance cassette. The amplified fragment was completely digested by ApaLI giving fragments of 2.2 and 0.6 kb

indicating that the six histidines were present and that complete segregation was achieved in the mutant cells.

Figure S1:

A

XhoI-CP47a: 5'-TAGAATTCGCTCGAGCCACCCTGGAAGAGGCTTGG-3'
BamHI-CP47b: 5'-TCGCGGATCCGCTTCCAGTTGAGCAGGTTGCCGCA-3'

HistagCP47a: 5'-CTCGCCGCAAGGAAGCTGTGCACCACCACCACCACCACTAGTCAT TCCTAGGGGACTA-3'
HistagCP47b: 5'-TAGTCCCCTAGGAATGACTAGTGGTGGTGGTGGTGGTGCACAGC TTCCTTGCGGCGAG-3'

CP47aHpa: 5'-GATCACTAAATAGGTCGTTAACATGTGCCGATCGCGCC-3'
CP47bHpa: 5'-GGCGCGATCGGCACATGTTAACGACCTATTTAGTGATC-3'

B

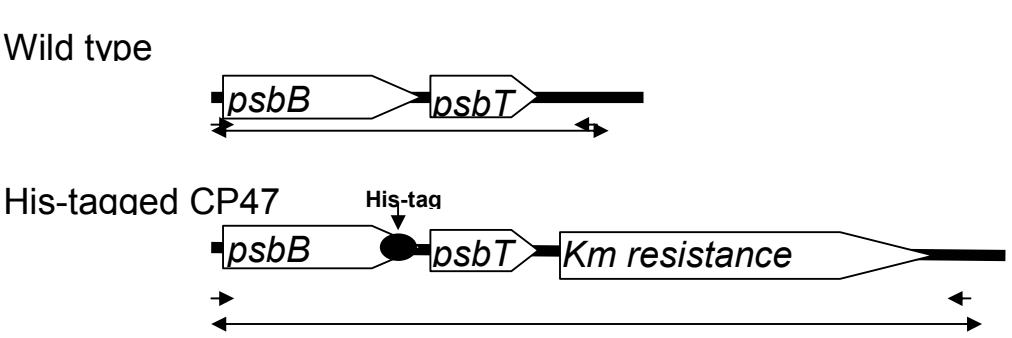

C

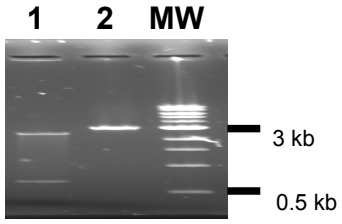

Construction of the His-tagged CP47 *T. elongatus* mutant. A) Oligonucleotides used as primers in the construction of the His-tagged mutant. B) Gene arrangement of the *psbB* and *psbT* genes in wild type *T. elongatus* and His-tagged CP47 mutant cells. C) PCR amplification (2) and ApaLI digestion of the amplified fragment (1) of mutant DNA.

Figure S2:

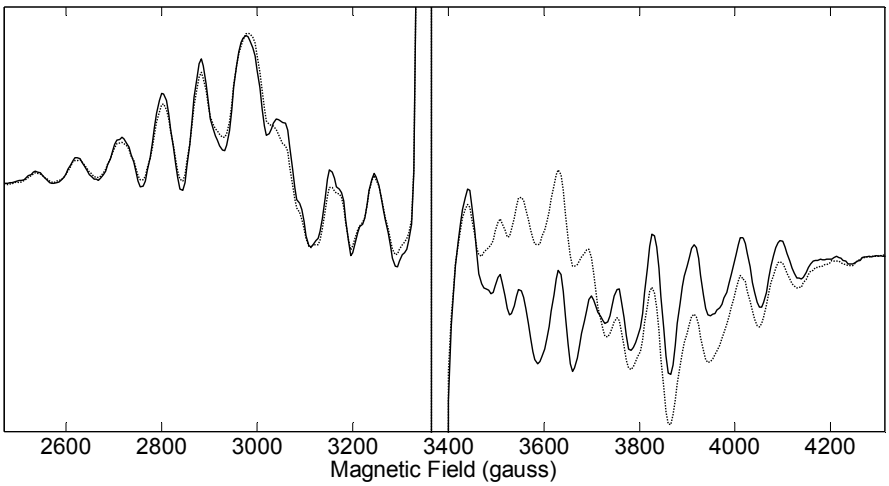

Formate effect on the formation of the S_2 manganese multiline EPR signal. The control (solid line) and formate (dotted line) PSII samples were dark-adapted for 12 h. The S_1 state is expected to be present in virtually 100% of PSII prior to illumination. The S_2 state is generated by illumination at 200 K for 20 sec. Instrument settings: microwave power: 20 mW, modulation amplitude: 25 gauss, temperature: 8.5 K. The main difference in the two spectra arises from the presence of the EPR signal from the formate modified $Q_A^{\bullet-}Fe^{2+}$ signal at around 3600 gauss. However the intensity of the hyperfine lines from the S_2 state itself is slightly smaller in the formate-treated sample.

Table S1:

no addition		Formate addition	
F_0	F_{max}	F_0	F_{max}
10.8	100	11.3	100

The variation of F_0 fluorescence level due to the formate addition is <1 % compared to the F_{max} induced after a pulse of continuous illumination. The F_{max} value was not affected by formate.

Figure S3

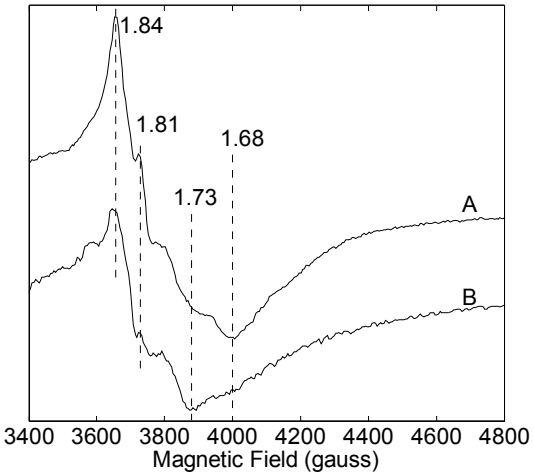

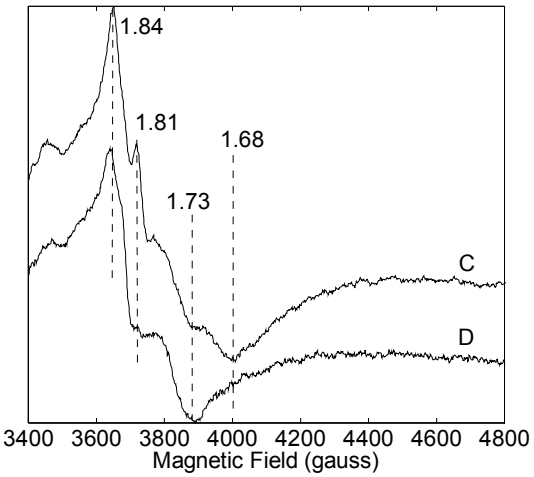

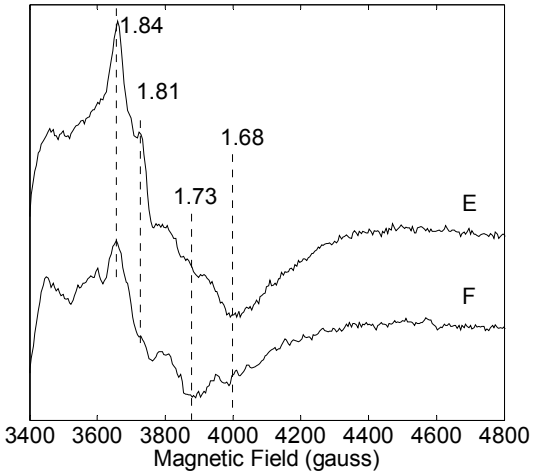

Figure S3: Conversion of the new broad form of the formate-modified $Q_A^{\bullet-}Fe^{2+}$ signal by the addition of sodium azide (panel 1), ANT2p (panel 2) and indigodisulfonate (panel 3). A, C and E: dithionite + 30 min incubation, B: addition of azide (100 mM final concentration, 30

min incubation). D: addition of ANT2p (10 μM final concentration, 10 min incubation). F: addition of indigodisulfonate (20 μM final concentration, 10 min incubation). Instrument settings were the same as in figure S2, except the temperature was 4.5 K.

References

[1] D. Kirilovsky, M. Roncel, A. Boussac, A. Wilson, J.L. Zurita, J.M. Ducruet, H. Bottin, M. Sugiura, J.M. Ortega, A.W. Rutherford, Cytochrome c_{550} in the cyanobacterium *Thermosynechococcus elongatus* - Study of redox mutants, J. Biol. Chem, 279 (2004) 52869-52880.
[2] Y.P. Cai, C.P. Wolk, Use of a conditionally lethal gene in *Anabaena sp-strain PCC-7120* to select for double recombinants and to entrap insertion sequences, J. Bacteriol, 172 (1990) 3138-3145.

ARTICLE 2

(en préparation)

Effect of formate binding on the quinone-iron acceptor complex of photosystem II

Effects of formate binding on the quinone-iron acceptor complex of photosystem II: Thermoluminescence investigation.

Arezki Sedoud[a] and A. William Rutherford[a*].

[a]iBiTec-S, CNRS URA 2096, CEA Saclay, 91191 Gif-sur-Yvette, France.

Abbreviations: PSII, Photosystem II; Q_A and Q_B, primary and secondary quinone electron acceptor of PSII; TL, thermoluminescence.

[*] Corresponding author:
iBiTec-S, CNRS URA 2096, CEA Saclay, 91191 Gif-sur-Yvette, France. Telephone: +33 1 69 08 2940. Fax: + 33 1 69 08 87 17.
E-mail address: alfred.rutherford@cea.fr

Keywords: Photosystem II, quinone, semiquinone, formate, thermoluminescence.

1. Abstract

Thermoluminescence (TL) was used to investigate the energetics and the reduction state of PSII treated with formate. The TL measurements showed inhibition of electron transfer after 2 flashes followed by a progressive shift to lower temperature of the luminescence peak upon flash number. The luminescence seen under these conditions may contain increasing contributions from charge recombination involving S_2 and S_3 and the two-electron reduced form(s) of Q_B. These data provide new insights into the nature of the electron transfer inhibition induced by formate.

2. Introduction

The depletion of bicarbonate/carbonate or its substitution by formate results in a slowing of the electron transfer rate from $Q_A^{\bullet-}$ to Q_B and to $Q_B^{\bullet-}$ by a factors of five and ten respectively [1-4]. The exchange of the Q_BH_2 with the plastoquinone pool is slowed down by more than a two orders of magnitude [2, 5-6]. Some of these inhibitory effects maybe due to the perturbation and/or inhibition of the protonation reactions that are coupled to electron transfer [7]. A specific chemical model explaining how depletion of bicarbonate affects electron transfer in the quinone-iron complex has not yet been established (reviewed in [8-9]).

The main TL peaks in PSII arise from radiative recombination between the positive charge equivalent stored on the Mn_4Ca cluster in the S_2 and S_3 states and the electron stored on $Q_A^{\bullet-}$ or $Q_B^{\bullet-}$ [10]. The amplitude and the temperature maxima of the TL peaks depend on which states are present, their relative concentrations and their relative stability. The latter is dependent on the redox potentials of the cofactors ([10] reviewed in [11] and [12]).

In recent work we have used EPR to study the effect of formate binding on PSII [13]. We have found that the most marked effect of formate appeared to be on Q_BH_2 exchange [13]. In the present work, TL is used to characterize the nature of formate inhibition and its effect on charge recombination.

3. Material and methods

3.1 Culture conditions and PSII preparation

The growth conditions and the PSII preparation (WT) was exactly as described in [13], the PSII was stored in the storage buffer (40 mM MES pH 6.5, 15 mM $CaCl_2$, 15 mM $MgCl_2$, 10 % glycerol and 1 M betaine).

3.2 Thermoluminescence experiments

Thermoluminescence measurements were performed using a lab-built apparatus [14]. PSII samples of concentration 10 µg Chl/ml were first dark-adapted at room temperature for 20 min. Samples were illuminated using a saturating xenon flash lamp (PerkinElmer Optoelectronics) at 5°C. The samples were then frozen to -10°C within 5 s and after an additional 5 s at -10°C; samples were heated at a constant rate (0.33°C/s). Given the relatively long lifetime of the S_2 and S_3 states at room temperature [15], these states can be considered to be stable prior to the start of the measurement, i.e. sample heating.

4. Results

Figure 1 shows the effect of formate on the TL after a series of flashes given at 5°C. The TL was measured after 1, 2, 3, 4 or 20 flashes in control (Fig. 1A) and formate-treated PSII (Fig. 1B).

The peaks observed in the control sample were virtually identical to those reported earlier in this preparation [16-17]. The small peak on the first flash represents $S_2Q_B^{\bullet-}$ recombination [10] which is centered at 57°C in this species [16-17]. The second flash gives a more prominent peak, centered at 50°C assigned to $S_3Q_B^{\bullet-}$ recombination. The $S_3Q_B^{\bullet-}$ peak was at a lower temperature than the $S_2Q_B^{\bullet-}$ peak and showed a more intense signal as expected [10, 18]. The 3rd and 4th flashes gave markedly smaller peaks due to the majority of the centers being in the S_0 and S_1 states which do not give rise to recombination luminescence [10]. After 4 flashes a $S_2/S_3Q_A^{\bullet-}$ recombination peak was observed as a shoulder at 26°C. These data are consistent with the presence of an additional quinone (Q_C) in most centers [16, 19-20]. After 20 flashes, a peak at 26°C, corresponding to $S_2/S_3Q_A^{\bullet-}$ recombination dominated. When DCMU was present a weak peak at low temperature was observed after 1 flash arising from $S_2Q_A^{\bullet-}$ recombination (Fig. 1 A and B).

Formate significantly alters the TL behavior described above (Fig. 1B). After one flash, the TL peak was seen at the same temperature as in the control (57°C) but with a lower intensity. The second flash generated a band with a peak at 46°C, 5°C lower than in the control and its intensity was significantly decreased compared to the control. After the 3rd and 4th flashes, the peak shifted to lower temperatures, 39°C and 36°C respectively, and the intensities of the peaks remained similar to that seen after 2 flashes. 20 flashes induced a band at 29°C. The relatively intense luminescence on the third and fourth flash seem to indicate that the S_0 and S_1 states are not being formed with high yield: *i.e.* there is a large miss factor after two flashes. With increasing flash number, the thermoluminescence peak continues to

shift to lower temperature. However, even after 20 flashes the peak had not shifted to the position of $S_{2/3}Q_A^{\bullet-}$ recombination. Cooling under illumination was required to obtain a TL band at the $S_2/S_3Q_A^{\bullet-}$ recombination temperature (Fig. 2). The peak from $S_2Q_A^{\bullet-}$ recombination was generated after 1 flash when DCMU was present and was at the same temperature (23°C) as the PSII without formate.

The intensity of the TL in the formate-treated PSII is much weaker on the first few flashes but becomes almost comparable to the control after 20 flashes. This may be due in part to formate destabilizing $TyrD^{\bullet}$ [21]. TyrD will diminish TL on the first flash because of electron donation to S_2 and will also cause a S_2/S_3 mixing because reduced TyrD is not present in all centers. Similar experiments were done on long dark-adapted samples (Fig.1 C and D). The results were similar with the main differences attributable to significantly less $Q_B^{\bullet-}$ and a greater fraction of reduced TyrD present after long dark incubations (Fig.1 C and D).

5. Discussion

Effects of formate on thermoluminescence have already been reported [22-23]. The more relevant study [22] used plant thylakoids and several different bicarbonate depletion procedures. This work did describe thermoluminescence peak amplitudes as a function of a flash number. However, the position of the $S_2Q_B^{\bullet-}$ and $S_3Q_B^{\bullet-}$ peaks in the bicarbonate depleted thylakoids were both at slightly higher temperature than in the control. This is different from the present study. However, the peak positions shown in [22] the earlier work were only those for thylakoids that had undergone the mildest depletion procedure, a procedure which was clearly incomplete in terms of electron transfer inhibition. With the more severe bicarbonate depletion treatment, which is more comparable to the conditions used here, although the peak positions were not shown, the flash series showed weak luminescence with only a small flash dependence [22]. Both of these effects are similar to those described here. To resolve the discrepancies and to have access to a system with a full plastoquinone pool, it may be worthwhile revisiting thermoluminescence studies of formate-treated/bicarbonate depleted thylakoids.

The thermoluminescence study reported here shows that the effect of formate is quite marked. The overall level of luminescence is smaller on the first two flashes but comparable to untreated samples after several flashes. The $S_2Q_B^{\bullet-}$ state is almost unaffected in terms of its stability, consistent with the notion that the $Q_A^{\bullet-}$ to Q_B electron transfer step is not greatly

affected by formate [3-4]. The second flash results in a marked change in the TL peak, an increase in its size and a down shift in its position. The position of the TL peak on the second flash in formate-treated material was at a lower temperature than the control. The marked change on the second flash indicates a relatively high quantum yield event. A firm assignment of the charges pair(s) involved is not possible with the present data however the peak on the second flash probably arises mainly from a modified $S_3Q_B^{\bullet-}$ state in those centers that were in the $S_1Q_B^{\bullet-}$ state prior to illumination [10]. For this to occur the Q_BH_2 formed on the first flash must have exchanged before $S_3Q_A^{\bullet-}$ formed on the second flash had time to recombine. This seems feasible given the long incubation during the course of the TL measurement.

On subsequent flashes the TL peaks shifted to gradually lower temperature without the usual diminution of luminescence associated with formation of S_0 and S_1. This indicates a marked formate-induced decrease in the quantum yield on the third and subsequent flashes and the gradual accumulation of an increasingly unstable charge pair or pairs. Given the EPR results discussed above and the current literature, these formate induced effect may arise from S_2/S_3 (but mainly S_3) recombination with Q_BH_2, ($Q_BH^{\bullet-}$, $Q_B^{2\bullet-}$) which might be shifted to lower temperatures compared to $S_3Q_B^{\bullet-}$.

The absence of obvious $S_3Q_A^{\bullet-}$ recombination on the third flash appears to contradict the EPR result (Fig. 2 in Sedoud et al, [13]), which clearly shows $Q_A^{\bullet-}$ trapped in the presence of a double reduced form of Q_B in a significant fraction of centers. However the EPR experiment was measured after being frozen in approximately 1 second after the flash series. Under these conditions $Q_A^{\bullet-}$ may be trapped in the presence Q_BH_2, if as suggested in [13], the Q_BH_2 exchanges with the pool quinone on the several seconds time scale at room temperature. In contrast, TL experiment requires slow warming of the sample which would allow even the slow forward electron transfer to occur during the course of the measurement.

The main difficulty with the TL data is to understand the gradual shift to low temperatures with increasing flashes. The slow accumulation of less and less stable TL recombination seems to indicate a low quantum yield event. This could be due to the gradual, formate-impeded filling of the PQ pool. Given that this pool appears to consist of a single quinone [16], we might have expected this to occur rapidly. Certainly in the control (untreated sample in the absence of formate), $Q_A^{\bullet-}$ recombination does become evident in the TL in samples given three or more flashes.

If the signal seen on flash 2 does represent $S_3Q_B^{\bullet-}$, then this indicates that a reasonable degree of Q_BH_2 exchange can occur in these samples. What then could be the explanation for the low quantum yield when 2 electrons are on the secondary quinones? Consideration of the

kinetics of electron transfer in the formate-treated system provides an explanation for the TL phenomena. Based on the EPR study, we suggested previously [13] that the $Q_A^{\bullet-}$ oxidation rate in the presence of Q_BH_2 in formate-treated PSII was slower in the isolated PSII from the thermophile than was measured earlier for thylakoids of plants (100-200ms). This could put the rate in the seconds time-scale. If so, this could seriously affect multiple flash experiments in which the flash spacing is the usual one per second. This would probably be more marked at 5°C, the flash temperature in the TL experiment. This would result in the drastic drop in quantum yield after formation of the $Q_A^{\bullet-}FeQ_BH_2$ state. In this case the gradual creeping of the TL peak to lower temperatures would represent the rate of Q_BH_2 exchange with (and subsequent reduction of) the plastoquinone pool (in this case Q_C), a process that must be slow compared to the flash rate.

Another option to explain the low quantum yield is to invoke an electron donor side inhibition. In this regard, however we know from the earlier EPR experiments [13] that S_2 formation is not greatly affected by formate. We have also seen formation of the S_3 EPR signal on the second flash [24-25] in formate treated PSII (not shown). Significantly, once formed there is little variation in intensity of the S_3 state on subsequent flashes. This would fit with the slow Q_BH_2 exchange compared to the flash rate as described above, however it could in principle be explained if formate blocked the S_3 to S_0 transition. There is no report of this kind of inhibition in the literature and the absence of formate effects on the Mn EPR signals also argues against an electron donor side inhibition.

It has been reported in plant PSII that the yield of the S_1 split EPR signal, which is thought to arise from a radical (probably $TyrZ^{\bullet}$ interacting magnetically with the Mn_4Ca cluster), was unaffected by the addition of formate [26]. This is consistent with our results. In contrast, from O_2 electrode data Stemler and Lavergne [27] concluded that formate treatment resulted in formation of S_0 at the expense of S_1, a result that is clearly at odds with the present data. As these measurements were performed in PSII isolated from higher plants, we cannot rule out this interpretation since species difference could be responsible for this difference. However we suggest that there may be alternative explanations for their results, the most obvious being the formate-induced destabilization of the $TyrD^{\bullet}$ radical [28]. Given the present state of knowledge we do not favor donor-side inhibition at the level of the water oxidizing complex. The acceptor side mechanism seems sufficient to explain the effects seen.

Overall the data indicate that formate does not greatly modify electron transfer from $Q_A^{\bullet-}$ to Q_B or $Q_A^{\bullet-}$ to $Q_B^{\bullet-}$. We know from the literature that the kinetics is slowed by a factor of 5 and 10 respectively. Given that the uninhibited electron transfer rate ($t_{1/2}$ around 400 and

800 µs) [29] is much faster than the decay of $S_2/_3Q_A^{\bullet-}$ ($t_{1/2}$ = 1 s), then this slowing of the rate has little effect on the yield of the final charge separated state. In contrast, on the 3rd flash electron transfer is more drastically affected: i) $Q_A^{\bullet-}$ begins to get trapped under the conditions of the EPR experiment; ii) the advance of the charge accumulation states of the water oxidizing complex (S states) becomes less efficient (probably because of the Q_BH_2 exchange being slow compared to the flash spacing); iii) recombination luminescence may occur from recombination of S_3 with Q_BH_2 (or a less protonated form) which corresponds to a new state is detected by EPR [13]. The observation that the main effect of formate on electron transfer occurs on the third turnover, fits with earlier observations in the literature using fluorescence and absorption measurements [2, 5]. However the current work indicates that the block occurs with reduced quinone in the Q_B site rather than with an empty site.

Figure 1:

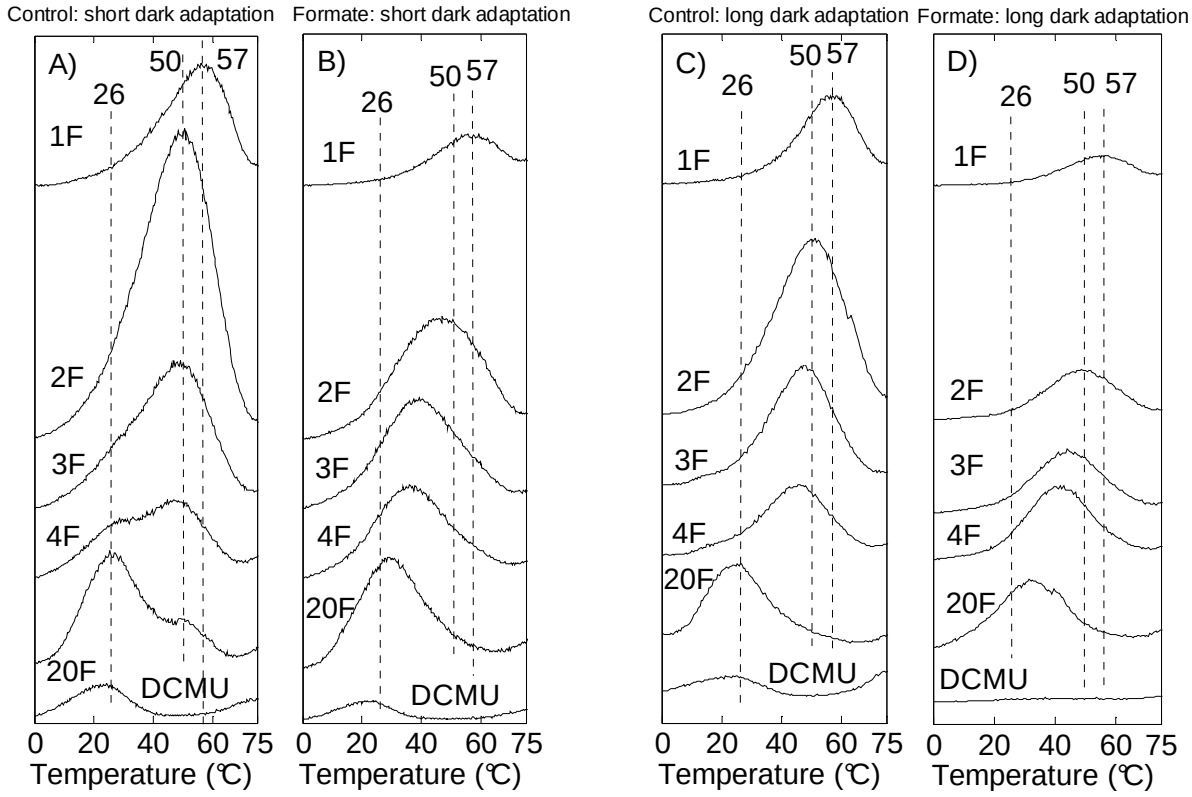

Figure 1: Thermoluminescence measured after 1, 2, 3, 4 and 20 flashes in short-dark adapted PSII, 30 min in dark at room temperature (A and B) and long-dark incubated PSII for 12h in dark at room temperature (C and D) in the control PSII (A and C) and formate-treated PSII (B and D). Samples were previously dark-adapted at room temperature for 30 min before being loaded into the cuvette, cooled to 5 °C and then illuminated with the designated number of flashes. Samples containing DCMU and given 1 flash are also shown. The temperatures of the main peaks in the control are shown in the panels.

Figure 2:

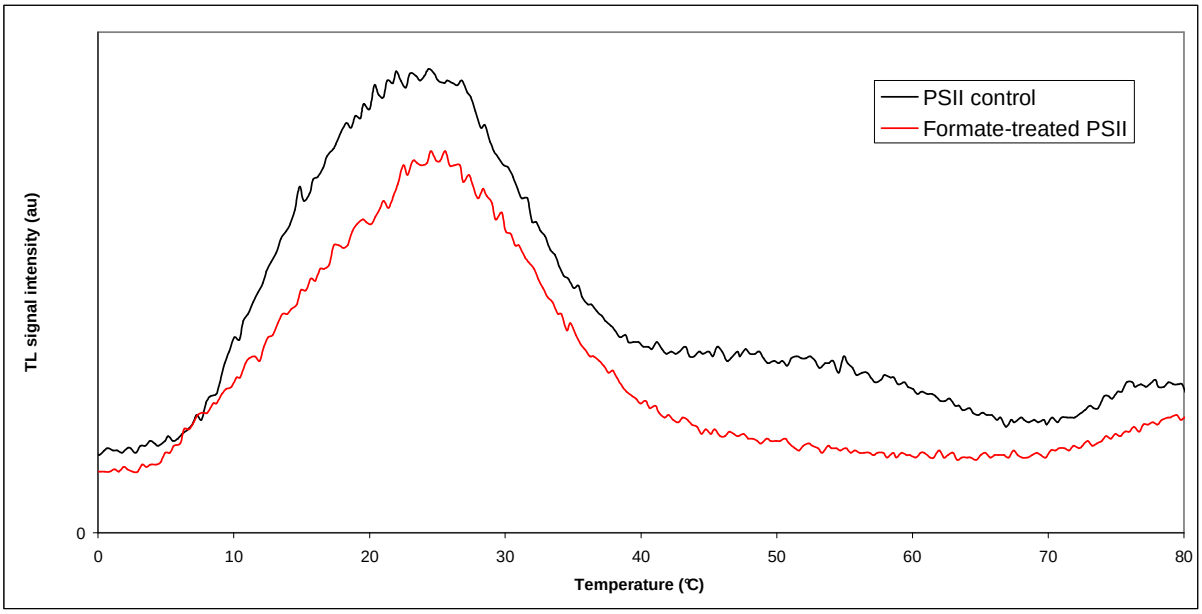

Figure 2: Freezing non-treated PSII (control, black) and formate-treated PSII (red) under illumination. Same experimental conditions as described in Fig. 1 were used expect that the sample was cooling under red-light illumination until -40°C.

References

[1] P. Jursinic, J. Warden, Govindjee, Major site of bicarbonate effect in system-II reaction evidence from ESR signal-II_{vf}, fast fluorescence yield changes and delayed light-emission, Biochim Biophys Acta, 440 (1976) 322-330.
[2] U. Siggel, R. Khanna, G. Renger, Govindjee, Investigation of the absorption changes of the plasto-quinone system in broken chloroplasts. The effect of bicarbonate-depletion, Biochim Biophys Acta, 462 (1977) 196-207.
[3] H.H. Robinson, J.J. Eaton Rye, J.J.S. van Rensen, Govindjee, The effects of bicarbonate depletion and formate incubation on the kinetics of oxidation-reduction reactions of the Photosystem II quinone acceptor complex., Z.Naturforsch.(C), 39 (1984) 382-385.
[4] J.J. Eaton-Rye, Govindjee, Electron-transfer through the quinone acceptor complex of Photosystem-II after one or 2 actinic flashes in bicarbonate-depleted spinach thylakoid membranes, Biochim Biophys Acta, 935 (1988) 248-257.
[5] Govindjee, M.P.J. Pulles, R. Govindjee, H.J. Vangorkom, L.N.M. Duysens, Inhibition of reoxidation of secondary-electron acceptor of Photosystem-II by bicarbonate depletion, Biochim Biophys Acta, 449 (1976) 602-605.
[6] J. Farineau, P. Mathis, Effect of bicarbonate on electron transfer between plastoquinones in Photosystem II, in: Y. Inoue, A.R. Crofts, Govindjee, N. Murata, G. Renger, K. Satoh (Eds.) The oxygen evolving system of photosynthesis, Academic Press, Inc., 1983, pp. 317-325.
[7] J.J.S. van Rensen, W.J.M. Tonk, S.M. Debruijn, Involvement of bicarbonate in the protonation of the secondary quinone electron-acceptor of Photosystem-II via the non-heme Iron of the quinone-iron acceptor complex, Febs Lett, 226 (1988) 347-351.
[8] D.J. Blubaugh, Govindjee, The molecular mechanism of the bicarbonate effect at the plastoquinone reductase site of photosynthesis, Photosynth Res, 19 (1988) 85-128.
[9] J.J.S. van Rensen, V.V. klimov, Role of bicarbonate in Photosystem II, in: T.J. Wydrzynski, K. Satoh (Eds.) Advances in Photosynthesis and Respiration Oxygenic Photosynthesis: Photosystem II. The light driven water: Plastoquinone oxidoreductase, Springer, Dordrecht, 2005, pp. 329-346.
[10] A.W. Rutherford, A.R. Crofts, Y. Inoue, Thermo-luminescence as a probe of Photosystem-II photochemistry - the origin of the flash-induced glow peaks, Biochim Biophys Acta, 682 (1982) 457-465.
[11] F. Rappaport, J. Lavergne, Thermoluminescence: theory, Photosynth Res, 101 (2009) 205-216.
[12] J.M. Ducruet, I. Vass, Thermoluminescence: experimental, Photosynth Res, 101 (2009) 195-204.
[13] A. Sedoud, L. Kastner, N. Cox, S. El-Alaoui, D. Kirilovsky, A.W. Rutherford, Effects of formate binding on the quinone-iron electron acceptor complex of photosystem II, Biochim Biophys Acta, 1807 (2011) 216-226.
[14] J.M. Ducruet, Chlorophyll thermoluminescence of leaf discs: simple instruments and progress in signal interpretation open the way to new ecophysiological indicators, J Exp Bot, 54 (2003) 2419-2430.
[15] A. Boussac, F. Rappaport, P. Carrier, J.M. Verbavatz, R. Gobin, D. Kirilovsky, A.W. Rutherford, M. Sugiura, Biosynthetic Ca^{2+}/Sr^{2+} exchange in the photosystem II oxygen-evolving enzyme of *Thermosynechococcus elongatus*, J Biol Chem, 279 (2004) 22809-22819.
[16] C. Fufezan, C.X. Zhang, A. Krieger-Liszkay, A.W. Rutherford, Secondary quinone in photosystem II of *Thermosynechococcus elongatus*: Semiquinone-iron EPR signals and temperature dependence of electron transfer, Biochemistry, 44 (2005) 12780-12789.

[17] N. Ishida, M. Sugiura, F. Rappaport, T.L. Lai, A.W. Rutherford, A. Boussac, Biosynthetic exchange of bromide for chloride and strontium for calcium in the photosystem II oxygen-evolving enzymes, J Biol Chem, 283 (2008) 13330-13340.
[18] A.W. Rutherford, G. Renger, H. Koike, Y. Inoue, Thermo-luminescence as a probe of Photosystem-II - the redox and protonation states of the secondary acceptor quinone and the O_2-evolving enzyme, Biochim Biophys Acta, 767 (1984) 548-556.
[19] J. Kern, B. Loll, C. Luneberg, D. DiFiore, J. Biesiadka, K.D. Irrgang, A. Zouni, Purification, characterisation and crystallisation of photosystem II from *Thermosynechococcus elongatus* cultivated in a new type of photobioreactor, Biochim Biophys Acta, 1706 (2005) 147-157.
[20] A. Guskov, J. Kern, A. Gabdulkhakov, M. Broser, A. Zouni, W. Saenger, Cyanobacterial photosystem II at 2.9-angstrom resolution and the role of quinones, lipids, channels and chloride, Nat Struct Mol Biol, 16 (2009) 334-342.
[21] R. Hienerwadel, C. Berthomieu, Bicarbonate binding to the non-heme iron of photosystem II investigated by Fourier transform infrared difference spectroscopy and C-13-labeled bicarbonate, Biochemistry, 34 (1995) 16288-16297.
[22] Govindjee, H.Y. Nakatani, A.W. Rutherford, Y. Inoue, Evidence from thermo-luminescence for bicarbonate action on the recombination reactions involving the secondary quinone electron-Acceptor of Photosystem-II, Biochim Biophys Acta, 766 (1984) 416-423.
[23] W. Wiessner, D. Mende, S. Demeter, Thermoluminescence study of the *in-vivo* effects of bicarbonate depletion and acetate formate presence in the 2 Algae *Chlamydobotrys stellata* and *Chlamydomonas reinhardtii*, Photosynth Res, 34 (1992) 279-285.
[24] T. Matsukawa, H. Mino, D. Yoneda, A. Kawamori, Dual-mode EPR study of new signals from the S_3 state of oxygen-evolving complex in photosystem II, Biochemistry, 38 (1999) 4072-4077.
[25] A. Boussac, M. Sugiura, A.W. Rutherford, P. Dorlet, Complete EPR spectrum of the S_3 state of the oxygen-evolving Photosystem II, J Am Chem Soc, 131 (2009) 5050-+.
[26] N. Cox, F.M. Ho, N. Pewnim, R. Steffen, P.J. Smith, K.G.V. Havelius, J.L. Hughes, L. Debono, S. Styring, E. Krausz, R.J. Pace, The S_1 split signal of photosystem II; a tyrosine-manganese coupled interaction, Biochim Biophys Acta, 1787 (2009) 882-889.
[27] A.J. Stemler, J. Lavergne, Evidence that formate destabilizes the S_1 state of the oxygen-evolving mechanism in Photosystem II, Photosynth Res, 51 (1997) 83-92.
[28] R. Hienerwadel, S. Gourion-Arsiquaud, M. Ballottari, R. Bassi, B.A. Diner, C. Berthomieu, Formate binding near the redox-active Tyrosine(D) in Photosystem II: consequences on the properties of Tyr_D, Photosynth Res, 84 (2005) 139-144.
[29] R. de Wijn, H.J. van Gorkom, Kinetics of electron transfer from Q_A to Q_B in photosystem II, Biochemistry, 40 (2001) 11912-11922.

ARTICLE 3

(en préparation)

The semiquinone-iron complex of photosystem II:

a new EPR signal assigned to the low edge of the ground

state doublet

The semiquinone-iron complex of Photosystem II: a new EPR signal assigned to the low field edge of the ground state doublet

Arezki Sedoud[a], Nicholas Cox[c], Miwa Sugiura[b], Wolfgang Lubitz[c], Alain Boussac[a] and A. William Rutherford[a*].

[a]iBiTec-S, CNRS URA 2096, CEA Saclay, 91191 Gif-sur-Yvette, France.

[b]Cell-Free Science and Technology Research Center, Ehime University, Bunkyo-cho, Matsuyama Ehime, 790-8577, Japan.

[c]MPI für Bioanorganische Chemie, Stiftstrasse 34 - 36 / D - 45470 Mülheim an der Ruhr, Germany.

Abbreviations: Cyt b_{559}; cytochrome b_{559}; EPR, electron paramagnetic resonance; PSII, Photosystem II; Q_A and Q_B, primary and secondary quinone electron acceptor of PSII.

[*] Corresponding author:
iBiTec-S, CNRS URA 2096, CEA Saclay, 91191 Gif-sur-Yvette, France. Telephone: +33 1 69 08 2940. Fax: + 33 1 69 08 87 17.
E-mail address: alfred.rutherford@cea.fr

Keywords: Photosystem II, quinone, semiquinone, non-heme iron, EPR.

ABSTRACT

The quinone-iron complex of the electron acceptor side of the water-oxidizing enzyme, photosystem II, was studied by EPR in *Thermosynechococcus elongatus*. New features at g~2 belonging to the EPR signal of the semiquinone forms of the primary and secondary quinone, i.e. $Q_A^{\bullet-}Fe^{2+}$ and $Q_B^{\bullet-}Fe^{2+}$ respectively, are reported. In the earlier literature these signals were missed because they were obscured by the EPR signal arising from the stable tyrosyl radical, $TyrD^{\bullet}$. When the $TyrD^{\bullet}$ signal was removed, either by chemical reduction or by the use of a mutant lacking TyrD, the new signal dominated the spectrum. For $Q_A^{\bullet-}Fe^{2+}$, the signal was formed by illumination at 77 K or by sodium dithionite reduction in the dark. For $Q_B^{\bullet-}Fe^{2+}$ the signal showed the characteristic period-of-two variations in its intensity when generated by a series of laser flashes. The new features showed relaxation characteristics comparable to the well-known features of the semiquinone-iron complexes and showed a temperature dependence consistent with an assignment to the low field edge of the ground state doublet of the spin system. Spectral simulations are consistent with this assignment and with the current model of the spin system. The signal is also present in $Q_B^{\bullet-}Fe^{2+}$ in plant photosystem II but in plants the signal is much less evident in the $Q_A^{\bullet-}Fe^{2+}$ state.

1. INTRODUCTION

The electron acceptor complex of Photosystem II (PSII) is made up of two quinones, Q_A and Q_B, situated symmetrically on either side of a non-heme ferrous ion located at the level of the membrane-water interface of this intrinsic membrane-protein complex. Q_A is tightly bound and acts as a one-electron carrier, while Q_B undergoes two sequential one-electron reduction steps. Q_B is weakly bound in its quinone and quinol form but tightly bound in its one-electron reduced semiquinone form (reviewed in [1]). The non-heme iron is coordinated by four histidines and a bidentate carboxylic acid ligand [1-3]. In the homologous purple bacterial reaction center this ligand is a glutamate of the M subunit [4] while in PSII it is a bicarbonate or carbonate ion [4-7].

The proton-coupled electron transfer reactions that are associated with quinone reduction through the quinone-iron complex have been studied in great detail in purple bacterial reaction centers [8-9]. In PSII however, these reactions remain relatively less well known [1]. While many of the basic features of purple bacterial reaction center are present in the quinone-iron complex of PSII, it seems likely that the different regulatory requirements specific to PSII have led to a range of structural and functional features that are not shared with its purple bacterial cousin.

EPR spectroscopy can contribute to understanding the structure and function of the quinone-iron complex in PSII. As in the purple bacterial reaction center [10], the semiquinone forms of both Q_A and Q_B can interact magnetically with the high spin ferrous iron (Fe^{2+}, S=2) producing similar but not identical EPR signals [1, 5]. In native PSII these signals are slightly shifted (g~1.9 instead of g~1.8) and had much weaker intensities [11-12]. In recent theoretical studies, this difference was attributed to the carboxylic acid ligand being carbonate rather than bicarbonate [7]. When (bi)carbonate was replaced by formate, which unlike bicarbonate cannot undergo a second deprotonation, the EPR signals seen became almost indistinguishable from those naturally present in purple bacterial reaction centers [13]. Given the great enhancement of the intensity of these formate-modified signals, formate is often added to PSII in order to visualize the $Q_A^{\bullet-}Fe^{2+}$ signals (e.g. [14-15]). Recently we demonstrated that an equivalent formate-modified $Q_B^{\bullet-}Fe^{2+}$ signal can be formed [16]. This spectroscopic trick is useful but nevertheless it represents a system that is inhibited and structurally modified by the non-native ligand.

In recent work from our laboratory we noted a new EPR feature that seemed to be associated with the $Q_B^{\bullet-}$ state [16-17]. A similar state is also present in $Q_A^{\bullet-}Fe^{2+}$. Here we report a study aimed at identifying this feature now identified in the complete semiquinones-

iron signals. This new g~2 EPR feature is also found in the $Q_B^{\bullet-}Fe^{2+}$ signal of PSII-enriched membranes from plant.

2. MATERIALS AND METHODS

2.1 Culture conditions and PSII preparation. The photosystem II studied in this article was isolated from 3 different strains of *Thermosynechococcus elongatus* and from spinach. The three *T. elongatus* strains, all His-tagged on the CP43 subunit of PSII were as follows: 1) WT, in which $psbA_1$ was dominantly expressed when grown under normal conditions [18-19]. 2) A3, a strain of cells in which the $psbA_1$ and $psbA_2$ genes were deleted so that only $psbA_3$ was expressed [20], 3) D2-Y160F cells, in which the tyrosine residue known as Tyrosine D [21] was mutated to phenylalanine in the WT strain [22]. PSII core complexes were prepared as described in [5] using a protocol based on [23] with some modifications as described in [16]. The oxygen evolution activity of the PSII core complexes isolated from the WT, A3 and D2-Y160F strains were previously reported [20, 22-23]. Samples were stored in liquid nitrogen in the storage buffer (40 mM MES pH 6.5, 15 mM $MgCl_2$, 15 mM $CaCl_2$, 1 M betaine, 10 % glycerol).

PSII-enriched membranes were isolated from market spinach as described in [24] with the following modification, bicarbonate was added at a final concentration of 1 mM to the thylakoids resuspension buffer, the solubilisation buffer and the storage buffer (25 mM MES pH6.5, 10 mM NaCl, 1 mM bicarbonate, 0.3 M saccharose). The oxygen evolution was ~600 $\mu mol\ O_2 \cdot mg^{-1} \cdot chl \cdot h^{-1}$. This isolation procedure was aimed at maintaining Q_B as functional as possible using milder detergent treatment [24] in the presence of bicarbonate [25].

The presence of Q_B was verified by using thermoluminescence, a single flash produced the typical $S_2Q_B^{\bullet-}$ recombination band, and only a very small $S_2Q_A^{\bullet-}$ band was present, indicating functional Q_B in the vast majority of centers [26]. Thermoluminescence was measured as described earlier [27].

2.2 Chemical reduction treatments. Chemical reduction of PSII with ascorbate was performed as follows: for both *T. elongatus* and PSII-enriched membranes from plant sodium ascorbate from a 300 mM stock solution in storage buffer was added to 120 µL of PSII (~ 1 mg Chl/ml) in the EPR tube in darkness to give a final concentration of 10 mM. The *T. elongatus* sample was then incubated in darkness for 30 min at room temperature prior to

freezing and the PSII-enriched membranes sample was incubated for 60 min at room temperature.

Dithionite reduction of *T. elongatus* PSII was performed at room temperature in darkness by addition of sodium dithionite to the sample in the EPR tube to give a final concentration of 2 mM using a 30 mM sodium dithionite stock solution made up in degassed storage buffer, the reduced sample was immediately frozen at 200 K in solid CO_2/ethanol bath prior to EPR measurements[28].

To eliminate EPR signals around the g~2 region from any free Mn^{2+} ions, EDTA (final concentration 5 mM) was added to EPR samples used in this work, except for the experiments shown in figure 2 and 3.

2.3 EPR measurements. EPR spectra were recorded using a Bruker Elexsys 500 X-band spectrometer equipped with standard ER 4102 resonator and Oxford Instruments ESR 900 cryostat. Instrument settings were: microwave frequency 9.4 GHz, modulation frequency 100 kHz. All other settings were as indicated in the figure legends. 120 µl aliquots of PSII cores (~ 1 mg Chl/ml) in the same buffer used for storage were loaded into 4 mm outer diameter quartz EPR tubes. The samples were manipulated under dim green light and then incubated in complete darkness for 12 hours. For plant PSII, 120 µl aliquots of PSII-enriched membranes (~ 3 mg Chl/ml) in the same buffer used for storage were loaded into 4 mm outer diameter quartz EPR tubes. The samples were manipulated under dim green light and then incubated in complete darkness for 2 hours. The EPR samples were frozen in a solid CO_2/ethanol bath at 200 K. Samples were degassed by pumping (10^{-3} bar) at 200 K and then filled with helium gas. EPR tubes were then transferred to liquid nitrogen prior to the EPR measurements being made. Samples were handled in darkness.

The saturation curves were measured at 4 K after the tubes were degassed at 200 K in a solid CO_2/ethanol bath. The fit used for the saturation curves to estimate the $P_{1/2}$ was as follows: $SI=a*P^{1/2} / (1+P/P_{1/2})^{b/2}$. Where SI represents the signal intensity, a the normalization factor, P the microwave power, $P_{1/2}$ the half saturating microwave power and b is the inhomogeneity factor.

The quantification of the contaminating radical signals was estimated by measuring the area of the double integral of the contaminating radical and comparing it with that of the total $TyrD^{\bullet}$ signal. The total $TyrD^{\bullet}$ was generated by illuminating the PSII sample at room temperature with room light for 1 min, then incubating for 20 seconds in the dark before freezing.

2.4 Illumination conditions. Flashes were performed using a frequency-doubled Nd: YAG laser (Spectra Physics, 7 ns fwhm, 550 mJ, 532 nm) at room temperature. After saturating flash(es), samples were rapidly frozen (1-2 s) in a solid CO_2/ethanol bath at 200 K followed by storage in liquid nitrogen. Low-temperature red-light illumination was performed in an unsilvered dewar containing liquid nitrogen (77 K). Illumination at 77 K was performed for 30 min in order to reduce $Q_A^{\bullet-}Fe^{2+}$ and oxidize Cyt b_{559} to near completion as verified by EPR. Continuous illumination was performed by using an 800 W halogen lamp. The light was filtered through 3 cm of water, calflex IR heat filters and a long-band pass filter (RG-670 nm).

3. RESULTS

3.1. 77 K illumination. Figure 1a shows a 77 K light-*minus*-dark difference spectrum from *T. elongatus* (WT) PSII. Prior to freezing, the sample was dark-incubated for 12 h. This incubation allowed the oxidation of $Q_B^{\bullet-}Fe^{2+}$ and the reduction of $TyrD^{\bullet}$ in a significant fraction of centers [16, 29]. Sodium ascorbate (10 mM) was added 30 minutes before the end of the dark incubation to reduce Cyt b_{559} and residual $TyrD^{\bullet}$. Illumination at 77 K is expected to result in the oxidation Cyt b_{559} and the reduction of Q_A [30]. The near complete reduction of Cyt b_{559} by sodium ascorbate prior to illumination minimizes the appearance of chlorophyll and β-carotene radical cation signals [31-33]. The TyrD does not undergo oxidation at this temperature at this pH [34]. Nevertheless, under these conditions a signal is generated at g~2 (Fig 1a). This signal is accompanied by the well-known broad signals attributable to the $Q_A^{\bullet-}Fe^{2+}$ spin system [7, 11, 29, 35]. The signal at g~2 is not a conventional first derivative Gaussian signal typical of an organic free radical (insets in figure 1, panel A), rather it is a positive spike with a peak maximum at g~2.0057 measured at 4 mW, (see section 3.7 and discussion for the measurements of the g-values).

3.2 $Q_A^{\bullet-}$ to Q_B electron transfer. Electron transfer between $Q_A^{\bullet-}$ and Q_B is blocked at low temperature ([36] and see [29] for a detailed study in *T. elongatus*). When a PSII sample, illuminated at 77 K, is thawed at room temperature, forward electron transfer occurs [26] and this is optimized when the Cyt b_{559} is the electron donor, i.e. when the Cyt b_{559} is fully reduced by ascorbate prior to illumination (see [29] and [16]). Fig. 1b shows the spectrum from the 77 K illuminated sample when thawed and incubated in the dark for 10 minutes. In this case, an intense g~2 feature was still present. Indeed, the new signal was even more clearly spike-like and this small change in shape can be explained by the decay of the small

underlying chlorophyll/β-carotene radical generated at 77 K when the sample was warmed (see [29]). In the thawed sample the peak position of the new signal was somewhat different, with a peak at g~2.0048 (inset b in Fig. 1, panel A, see also below and Fig. 4 for power dependence of the peak position). The thawing procedure also produced changes in the broad signals that are ascribed to the replacement of $Q_A^{\bullet-}Fe^{2+}$ with $Q_B^{\bullet-}Fe^{2+}$, namely slight differences in signals around g~1.9 and g~ 1.7 (data not shown in detail here but see [29] and [16]).

3.3 The biradical-iron complex ($Q_A^{\bullet-}Fe^{2+}Q_B^{\bullet-}$). When the sample containing $Q_B^{\bullet-}Fe^{2+}$ was re-illuminated at 77 K, the $Q_A^{\bullet-}Fe^{2+}Q_B^{\bullet-}$ state was formed giving the characteristic signal at g~1.66 [29, 37]. The g~2 spike significantly decreased under these conditions. A small radical signal was also formed in about 13 % of the centers (g=2.0036), mainly attributable to the chlorophyll radical cation formed in the small fraction of centers in which Cyt b_{559} was oxidized prior to the illumination.

3.4 Plant PSII. Panel B of Fig. 1 shows similar experiments to those in panel A except that the biological material was PSII-enriched membranes from spinach. The plant PSII-enriched membranes were dark-adapted at room temperature for 2 h and then ascorbate was added to reduce the Cyt b_{559} and $TyrD^{\bullet}$. This PSII preparation was based on a protocol aimed at maintaining Q_B integrity (see materials and methods) and one result of this is that there was some contamination by PSI. Illumination at 77 K thus resulted in formation of P_{700}^{+} F_A^{-}/F_B^{-} in the PSI centers and this charge pair is unstable at 200 K [38]. The Cyt $b_{559\ ox}$ $Q_A^{\bullet-}Fe^{2+}$ charge pair in PSII is known to be stable at 200 K. Incubation of the sample at 200 K for 30 minutes allowed the signals from PSI to diminish almost completely before the difference spectrum was taken (Fig. 1d). The light-*minus*-dark spectrum should then correspond to the $Q_A^{\bullet-}$ state in the presence of oxidized Cyt b_{559}. The spectrum obtained in Fig.1d has the typical broad features of the $Q_A^{\bullet-}Fe^{2+}$ state but it shows only a small spike feature at g~2. Given the difficulties with contributions of other radical to the spectra before and after illumination, the exact spectrum in this region still remains unsure. It seems clear however that a strong spike signal from $Q_A^{\bullet-}Fe^{2+}$, like that seen in *T. elongatus* under these conditions, is not present.

Fig. 1e shows the thawed-*minus*-dark difference spectrum from plant PSII-enriched membranes, corresponding to $Q_B^{\bullet-}Fe^{2+}$. Clearly a g~2 "spike" signal is present similar to that seen in *T. elongatus* with a g-value of g~2.0050 measured at 4mW for its peak position (see inset e in Fig. 1, panel B). The $Q_B^{\bullet-}Fe^{2+}$ spike shows a small contamination from a Tyr $D^{\bullet}$

radical signal. Figure 1f shows that re-illumination of this sample produced the $Q_A^{\bullet-}Fe^{2+}Q_B^{\bullet-}$ state showing a signal at g~1.62. This g-value is in agreement with the reported value for this state in plant PSII [25]. The formation of this signal confirms that $Q_B^{\bullet-}Fe^{2+}$ was present in this sample prior to the illumination at 77 K. In this case, the spectrum in Fig. 1f is contaminated with the $P_{700}^{\bullet+}F_A^{\bullet-}/F_B^{\bullet-}$ charge pair. When a 200 K incubation was done to allow this charge pair to recombine, the amplitude of the g~1.62 signal also decreased to some extent. This likely represents $Chl_Z^{+}Q_A^{\bullet-}$ recombination occurring in the presence of $Q_B^{\bullet-}$, and/or some forward electron transfer occurring from $Q_A^{\bullet-}$ to $Q_B^{\bullet-}$ occurring during the 200 K incubation treatment [29].

3.5 Effect of dithionite. The addition of sodium dithionite in the dark is expected to result in the formation of the $Q_A^{\bullet-}$ state in all the centers. Figure 2 shows that sodium dithionite generates the new signal along with the well-known $Q_A^{\bullet-}Fe^{2+}$ signals at around g~1.9 and g~1.73. This is strong support for its assignment as $Q_A^{\bullet-}$. The spectrum in Figure 2, (solid line) is not a reduced-*minus*-oxidized difference spectrum. This is because 12 h of dark adaption still left $TyrD^{\bullet}$ in a significant fraction of centers prior to dithionite addition (Fig. 2 dotted line). Most of the remaining radical was eliminated by addition of dithionite as expected. The inset showed the g-value of the spike was g~2.0036 at 4 mW.

The dithionite-induced $Q_A^{\bullet-}Fe^{2+}$ signal shown in Figure 2 demonstrates that the g~1.9 feature, which is usually reported in samples containing $TyrD^{\bullet}$ and chlorophyll and/or β-carotene cation radicals, is clipped at lower field by the radical (see e.g. [29]). In the absence of the radical the peak of this feature appears at g~1.94 at 5K.

3.6 Effect of a flash series. To test if the g~2 signal arises from the $Q_B^{\bullet-}Fe^{2+}$ state, we looked for the mechanistic behavior typical of this component: the flash-number dependent, period-of-two variation of its intensity [39-40]. For this experiment the Tyrosine D-less mutant of *T. elongatus* [22] was used so that the new signal would not be swamped by the $TyrD^{\bullet}$ radical EPR signal. Fig. 3, panel A shows the result of the flash series given at room temperature using a sample incubated 12 h in darkness to minimize the $Q_B^{\bullet-}$ population prior to illumination. The period of two variations in amplitude is evident; with bigger signals on flashes 1 and 3 (Fig. 3, panel B and C). The pattern however was damped with only a small change occurring between the flashes 3 and 4. This is to be expected in the isolated enzyme with no exogenous electron acceptor added. The fact that the changes occur on the third and 4 flashes is in line with our earlier observation that the isolated enzyme carries an addition

functional quinone [29]. The data of figure 3 constitute strong evidence that the new signal at g~2 arises from $Q_B^{\bullet-}$.

3.7 D1 variants (PsbA1 and PsbA3). It is known that in *T. elongatus* there are three copies of the gene coding for the core reaction center subunit D1 ($PsbA_1$, $PsbA_2$ and $PsbA_3$) [41]. In the growth conditions used here only *psbA*$_1$ is expressed [18, 42]. There are the 21 amino acid differences between $PsbA_1$ and $PsbA_3$; these confer small changes in the redox potentials of some cofactors [18, 43-44]. In Fig. 4, panel A, we asked the question whether these structural changes are manifest as differences seen in the more complete semiquinone-iron spectra reported here. Both $Q_A^{\bullet-}Fe^{2+}$ and $Q_B^{\bullet-}Fe^{2+}$ have the same basic features; g~2, g~1.9, g~1.7. We note that $Q_A^{\bullet-}Fe^{2+}$ has a very small feature at g~1.8 and this may be due to the loss of the native exchangeable carboxylate ligand, which has been suggested to be carbonate [7], in a small fraction of centers. The spectra in figure 4 show no significant difference between WT and A3 mutant in terms of their $Q_A^{\bullet-}Fe^{2+}$ and $Q_B^{\bullet-}Fe^{2+}$ EPR spectra including the new signals.

The peak position in the g~2 region of $Q_A^{\bullet-}Fe^{2+}$ and $Q_B^{\bullet-}Fe^{2+}$ are 2.0030 and 2.0040, respectively (Fig. 4, panel B). These values were measured at higher microwave power (160 mW), in this case the contaminating radical was saturated and the semiquinone-iron spike dominates the spectrum.

3.8 Microwave power and temperature dependence. Figure 5a shows the saturation curves of the new g~2 signals attributed to $Q_A^{\bullet-}Fe^{2+}$ and $Q_B^{\bullet-}Fe^{2+}$. These are compared to the saturation behavior of the g~1.9 feature from $Q_B^{\bullet-}Fe^{2+}$, the g~1.66 signal from $Q_A^{\bullet-}Fe^{2+}Q_B^{\bullet-}$ and as a control the g~4.3 signal generally attributed to a rhombic ferric iron contaminant commonly seen in biological systems. The intensities of the signals were normalized at non-saturating powers. The new g~2 signals had relaxation characteristics similar to each other and their saturation curves fell between the other fast relaxing species (the signals at g ~1.66 and at g~1.9) from the semiquinone-iron complex. All of the signals associated with the semiquinone-iron complex saturated at much higher powers than the g~4.3 rhombic iron signal. The fast relaxation properties of the new g~2 signals are consistent with their attribution to the $Q_A^{\bullet-}Fe^{2+}$ and $Q_B^{\bullet-}Fe^{2+}$ states.

Figure 4B shows the lineshape of the g~2 spike at different microwave powers. At low powers the spectrum of the g~2 spike is contaminated with underlying organic free radical signals. This radical component only has a small contribution at the higher powers. The presence of the radical even in a small amount of centers seems to be responsible for the

apparent g-shift of the semiquinone-iron spike signal. We note that the larger the radical contamination, the larger the apparent g-shift. However the value measured at the highest powers, where the radical contributes very little to the spectrum, does not vary and thus is considered to be the best estimate of the true g-value. It is also of note that the precise position of the new peak at g~2 seemed to be sensitive to O_2 in the sample. All the data presented here were with samples that were degassed at 200 K to remove O_2 [28].

Fig. 5B shows the temperature dependence of the g~2 signal arising from $Q_B^{\bullet-}Fe^{2+}$. The g~2 signal shows ground state behavior (see the next section for more details).

3.9 Simulations of the spectra. Spectral simulations of the g~1.9 semiquinone-iron signal were performed using the Spin Hamiltonian formalism. In earlier work it has been shown that this approach is valid for all semiquinone iron signals in the current literature [7, 10]. A basis set that describes the non-heme iron (S = 2) semiquinone ($Q^{\bullet}$, S_Q = ½) spin manifold can be built from the product of the eigenstates of the two interacting spins. These are expressed in terms of four quantum numbers,

$$\left| S_{Fe} \quad m_{Fe} \quad S_Q \quad m_Q \right\rangle,$$

where S_{Fe} is the total spin of the ground state iron manifold (S = 2), m_{Fe} is the iron magnetic sublevel (m = -S, - S + 1, ……, S – 1, S) and S_Q is the total spin semiquinone (S = ½) and m_Q is the semiquinone sublevel (m_Q = -½ , ½). Thus 10 basis vectors are required to span the spin manifold.

The Spin Hamiltonian appropriate for the $Q_A^{\bullet-}Fe^{2+}$ system includes zero field (D, E), Zeeman ($\mathbf{g}_{Fe}$, $\mathbf{g}_Q$) and anisotropic exchange (***J***):

$$\mathcal{H} = D[(S_{FeZ}^2 - 1/3 S_{Fe}(S_{Fe}+1) + (E/D)(S_{FeX}^2 - S_{FeY}^2)] + \beta H \cdot \mathbf{g}_{Fe} \cdot S_{Fe}$$
$$+ \mathbf{g}_Q \beta H \cdot S - S_{Fe} \cdot \mathbf{J} \cdot S_Q \qquad (1)$$

Subsequent calculations assume the zero-field, Zeeman-iron and exchange tensors to be co-linear and g_Q to be scalar as in [10] and [7]. Estimates for all the Spin Hamiltonian parameters (D, E, $\mathbf{g_{Fe}}$, $\mathbf{g_Q}$ and ***J***) have been made for the g~1.9 semiquinone iron signal: D~10 cm^{-1} (15 K^{-1}) and E/D~0.25. The interaction between the quinone and the iron was axial and of the order of ~0.5 cm^{-1}.

The g~1.9 semiquinone iron signal can be understood as the intersection of two EPR signals that arise from the two lowest Kramer's doublets of the quinone-iron spin manifold (for full discussion see [7]). The ground Kramer’s doublet gives a broad EPR spectrum that is

seen above g~2. The first excited state Kramer's doublet instead appears below g~2 and has approximately a similar width in magnetic field space. A simple description of the system can be made where the two components (ground state and 1st excited state) of the EPR signal are described in terms of two effective spin ½ species (i = 1, 2) of large g-anisotropy.

$$\mathcal{H}_i = \beta H \cdot g_{eff,i} \cdot S_i \qquad (2)$$

Analytical expressions for the effective g positions ($g_{eff,,x}$, $g_{eff,,y}$, $g_{eff,,z}$) of the ground state and 1st excited state species in terms of the real Spin Hamiltonian parameters (D, E, $\mathbf{g_{Fe}}$, $\mathbf{g_Q}$ and $\boldsymbol{J}$) to 3rd order are given in [10]. Of the three effective g-values, $g_{eff,,y}$ is unique and explains the characteristic lineshape of all semiquinone-iron signals. It is the only g-value that has a large 1st order correction, such that $g_{eff,,y}$ decreases for the ground state ($g_{eff,,y}$,~1) and increases for the first excited state ($g_{eff,,y}$,~3-4). This has the effect of spreading the signal across a very large magnetic field range (600 G) and explains why semiquinone-iron signals only give 'weak' EPR signals. The approximate position of the $g_{eff,,y}$ ground and 1st excited state turning points scales with both the J_y component of the exchange coupling tensor and zero-field splitting parameters of the Fe^{2+}. This is in contrast to the other two effective g-values $g_{eff,,x}$, $g_{eff,,z}$. The 1st order corrections to these turning points are small and as such that they are both approximately 2.0. The dependence of $g_{eff,,x}$, $g_{eff,,z}$ on the Spin Hamiltonian parameters (D, E, $\mathbf{g_{Fe}}$, $\mathbf{g_Q}$ and $\boldsymbol{J}$) are as a consequence, far more complicated.

Figure 6 shows spectral simulations of the g~1.9 semiquinone–iron signal based on the Spin Hamiltonian formalism described above. In the Fig. 5B simulation of the temperature dependence of the g ~ 2 spike is shown. As stated above, the temperature dependence of the g~2 spike is consistent with it arising from the ground state of the semiquinone-iron spin manifold; its intensity increases as the temperature decreases. In a previous publication [7] we made an estimate of the fine structure parameters of the Fe^{2+} ion, which defines the zero-field splitting of the quinone-iron complex and thus the temperature dependence of its EPR signal. These values were estimated to be D = 15 K^{-1}, E/D = 0.25. A fitting of the temperature dependence of the g~2 spike yields similar results: D = 16.6 K^{-1}, E/D = 0.25. The component of the ground state of the PSII semiquinone-iron signal that coincides with the g~2 region is the $g_{eff,\,z}$. $g_{eff,\,z}$ defines the low field edge of the ground state and should, when viewed instead as the 1st derivative of the EPR absorption profile, appear as a positive spike, as seen experimentally. Thus these new results would validate the model of the PSII semiquinone-iron signal as published earlier [7].

The exact position of the ground state $g_{eff,\,z}$ is sensitive to the changes in the exchange coupling tensor ***J***. It noted that only small changes of the J_y component (0.1-0.2 K^{-1}) of the exchange coupling tensor is sufficient to shift the position of the g~2 spike over the range of values seen for $Q_A^{\bullet-}Fe^{2+}$ and $Q_B^{\bullet-}Fe^{2+}$ signals (2.0028-2.0040). This is not the case for J_z and J_x. The position of $g_{eff,\,z}$ is insensitive to small changes in J_z. Similarly, while J_x does alter the position of $g_{eff,\,z}$, these changes also lead to modifications of the other turning points: the ground state $g_{eff,x}$ (g~1.7) and excited state turning points ($g_{eff,x}/g_{eff,z}$, g~1.9) etc, the characteristic EPR signals observed for the semiquinone-iron complex. It is thus likely that the small difference seen between the g ~ 2 spike for the $Q_A^{\bullet-}Fe^{2+}$ and $Q_B^{\bullet-}Fe^{2+}$ signals most probably reflects small changes of J_y, possibly the rotation of the exchange tensor in the J_y/J_z plane relative to the fine structure tensor of the Fe^{2+}. Small tensor rotations of this magnitude were inferred for the set of g~1.8 semiquinone iron signals that are seen in plants and purple bacteria [7]. It is noted that small differences between the $Q_A^{\bullet-}Fe^{2+}$ and $Q_B^{\bullet-}Fe^{2+}$ g~2 spike signals must be related to the exchange tensor as opposed to the fine structure tensor/g tensor of the Fe^{2+}. The Fe^{2+} is the same for both complexes.

One final observation is that the EPR linewidth parameter used for the EPR simulations (Figure 6 bottom panel C) must be highly anisotropic to reproduce a 'sharp' $g_{eff,\,z}$ spike at g~2 and relatively broad turning points at g~1.9, g~1.7 etc. It is interesting to note that the apparent EPR linewidth along the three principal axes x, y and z would appear to correlate with the magnitude of the exchange coupling along the three principal directions; the coupling is small along z as is the linewidth whereas the coupling is large along x and y as is the linewidth.

4. Discussion:

In this work, we have identified complete EPR signal arising from the magnetic interaction of the semiquinone with the non-heme high spin (Fe^{2+}, S=2) ferrous iron on the electron acceptor side of PSII. Both $Q_A^{\bullet-}Fe^{2+}$ and $Q_B^{\bullet-}Fe^{2+}$ EPR signals include a sharp feature centred at g~2 with slightly differing g-values. The lines of evidence for the assignment of the signals are as follows. (i) The new feature associated with $Q_A^{\bullet-}Fe^{2+}$ is generated by illumination at 77 K and by reduction with sodium dithionite in darkness, i.e. standard conditions for the formation of $Q_A^{\bullet-}$. (ii) The new signal associated with $Q_B^{\bullet-}Fe^{2+}$ is formed a) upon thawing a sample containing $Q_A^{\bullet-}Fe^{2+}$ and b) upon flash illumination at room temperature, it being bigger on the first and third flashes. These conditions correspond to

those in which $Q_B^{\bullet-}Fe^{2+}$ is formed. (iii) The new features have relaxation properties similar to those of the other signals arising from the semiquinone-iron complex.

In two recent papers from our lab we made observations that also support the assignment of the g~2 signal to $Q_B^{\bullet-}$ Fe^{2+}. We noted that the g~2 feature was present when $Q_B^{\bullet-}Fe^{2+}$ was generated by a chemical reduction (DAD/ascorbate), the g~2 feature disappeared when the sample was illuminated at 77 K upon formation of the $Q_A^{\bullet-}Fe^{2+}Q_B^{\bullet-}$ state [16]. In addition the spike signal was found to be present in about 50 % of centers after 1 h of dark adaptation in the Tyr D-less mutant of *T. elongatus* and disappeared concomitantly with the g~1.94 when an artificial electron acceptor was added. This behavior agrees with that expected of $Q_B^{\bullet-}Fe^{2+}$ [17].

The new features observed here are relatively narrow and thus relatively intense and yet they have escaped detection until now. This is because the EPR signal from $TyrD^{\bullet}$ is still considerably larger than the new signals and it obscures this region of the spectrum. In this work we were able to circumvent these problems by the use of reducing agents or the TyrD-less mutant to eliminate contributions of $TyrD^{\bullet}$ to the spectra. In addition, until relatively recently most of the work on the acceptor side of PSII was done on PSII-enriched membranes from plants, and here we observed that $Q_A^{\bullet-}Fe^{2+}$ has no (or a significantly smaller) g~2 feature. In addition, the light-induced generation of the $Q_A^{\bullet-}Fe^{2+}$ signal at low temperature is usually accompanied by the formation of variable amounts of chlorophyll and β-carotene radical cation signals [31-33, 45] and these also obscure the new photogenerated $Q_A^{\bullet-}Fe^{2+}$ feature at g~2. Here we used sodium ascorbate to reduce any oxidized Cyt b_{559} prior to illumination in order to minimize the formation of these side-path radicals.

We found that a very small fraction of a free radical signal was still present even when efforts had been made to avoid contaminating radicals. This was particularly evident in the relaxation studies (Fig 4, panel B). Depending on the conditions, the identity of the small radical signal can be suggested. In the dithionite reduced $Q_A^{\bullet-}Fe^{2+}$ spectrum a radical with a g-value of g=2.0044 is present and given the low level of resolved hyperfine (not shown), we suggest that this could reflect a small fraction of centers in which the semiquinone is uncoupled from the non-heme iron plus a small contamination from unreduced $TyrD^{\bullet}$. The total number of centers contributing to the radical signal was approximately 4%. Without dithionite, the contaminating radical signal in the photogenerated $Q_A^{\bullet-}Fe^{2+}$ is expected to be due to the side-path radicals formed in the residual centers in which Cyt b_{559} is oxidized prior to illumination. However, the g-values for the signal was g= 2.0040, too high for the side path radicals [31][33] and we attribute this to a mixture of side-path radicals plus a small fraction

of uncoupled $Q_A^{\bullet-}$. The number of centers showing a radical is estimated as approximately 10%. When $Q_B^{\bullet-}Fe^{2+}$ is formed, the radical contamination with a g-value of 2.0044 is attributed to a small fraction of $TyrD^{\bullet}$ plus a fraction of uncoupled $Q_B^{\bullet-}$. The quantitation of the radical indicates approximately 5% of centers exhibit the radical signal.

The g-value of the new signal from $Q_A^{\bullet-}Fe^{2+}$ is g~ 2.0030 while that of $Q_B^{\bullet-}Fe^{2+}$ is g~ 2.0040. These values were obtained at 160 mW, at lower microwave power the apparent g-values shifted to higher values. This shift appeared to be due to contributions from the underlying free radicals and was more marked when the underlying radical was larger. In *T. elongatus* the new signal appeared to be slightly stronger in $Q_B^{\bullet-}Fe^{2+}$ compared to $Q_A^{\bullet-}Fe^{2+}$. In plant PSII, while the signal is clearly present in the $Q_B^{\bullet-}Fe^{2+}$ state, it is very weak or absent in $Q_A^{\bullet-}Fe^{2+}$. The significance of this observation has yet to be understood. We were unable to detect differences in the cw-EPR signals from $Q_A^{\bullet-}Fe^{2+}$ and $Q_B^{\bullet-}Fe^{2+}$ when comparing PSII from the WT (Psb A1) and A3 (Psb A3) strains, although we noted that g~2 signal arising from $Q_A^{\bullet-}Fe^{2+}$ and $Q_B^{\bullet-}Fe^{2+}$ in A3 saturates at slightly lower power levels than the WT (data not shown).

The temperature dependence of the new g~2 signal indicates that it arises from a ground state. Within the context of the current model [7, 10] and given the “spike” –type feature in the first derivative spectrum, these signals would appear to be directly attributable to the low-field edge of the ground state doublet. This is confirmed by the spectral simulations. The new feature provides additional restrictions to the simulation parameters. But, it also shows that the model used and the values obtained in Cox et al, were valid [7]. The decrease in the signal when the $Q_A^{\bullet-}Fe^{2+}Q_B^{\bullet-}$ state is formed is a predictable feature in our on-going attempts to simulate the EPR spectrum from this state (Cox et al in preparation).

The signals from $Q_A^{\bullet-}Fe^{2+}$ and $Q_B^{\bullet-}Fe^{2+}$ in PSII reported here add to the spectroscopic probes with which we can study this enzyme. The strong intensity of the new signals should allow studies to be undertaken that were not previously feasible. Studies of this kind are underway in our laboratories.

5. Acknowledgments:

This work was supported by the EU/Energy Network project SOLAR-H2 (FP7 contract 212508). +CNRS/JSPS (see previous Alains paper). Arezki Sedoud is supported by the IRTELIS training program of the CEA. We would like to thank A. Krieger-Liszkay and D. Kirilovsky for helpful discussion.

Figure 1

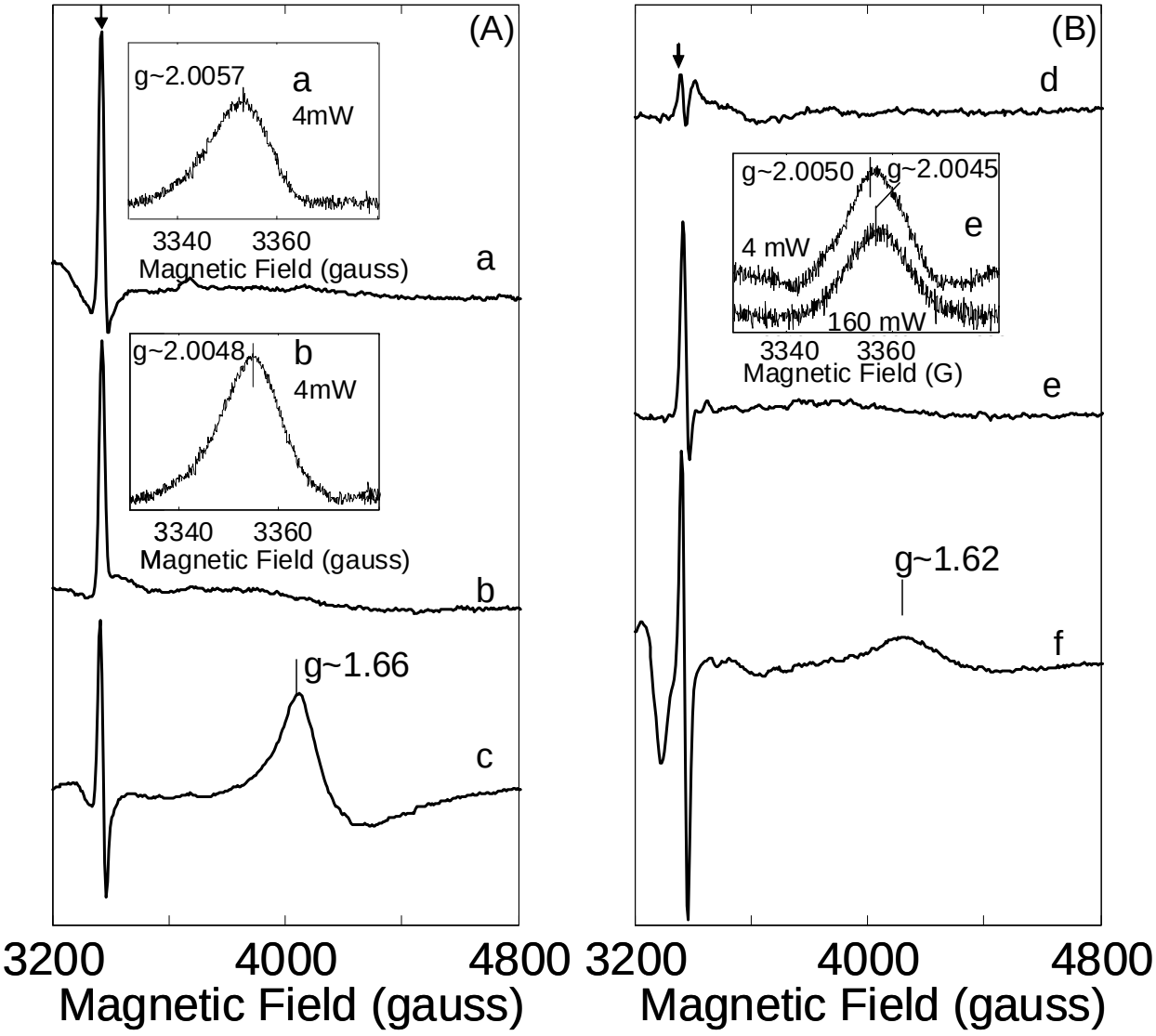

Figure 1: EPR signals attributed to $Q_A^{\bullet-}Fe^{2+}$ and $Q_B^{\bullet-}Fe^{2+}$ in PSII. Panel A shows spectra (a-c) from isolated *T. elongatus* WT PSII, while panel B is from PSII-enriched membranes from spinach. PSII from WT *T. elongatus* was dark-incubated for 12 h, and then treated with ascorbate. The PSII-enriched membranes from spinach were incubated for 2 h at room temperature then treated with ascorbate, See material and methods for ascorbate treatment. Spectrum a: a 77 K-illumination-*minus*-dark spectrum from *T. elongatus* WT PSII attributed to $Q_A^{\bullet-}Fe^{2+}$, the inset a shows the resolution of the g~2 region at 4mW. Spectrum b: a thawed-*minus*-dark spectrum obtained when the sample that had been illuminated at 77 K was thawed at room temperature. This is attributed to $Q_B^{\bullet-}Fe^{2+}$, the inset b shows the resolution of the g~2 region at 4mW. Spectrum c is obtained when the thawed sample containing $Q_B^{\bullet-}Fe^{2+}$ was reilluminated at 77 K. This generates the $Q_A^{\bullet-}Fe^{2+}Q_B^{\bullet-}$ state, which gives rise to the signal at

g~ 1.66. Spectrum e showed the (200 K-incubated sample after the 77 K illumination)-*minus*-dark, this is attributed to the $Q_A^{\bullet-}Fe^{2+}$ state. The plant PSII sample was incubated 30 min at 200 K after the 77 illumination (spectrum d), to allow the decay of $P700^+$ and F_A^-/F_B^- from contaminating PSI. Spectrum e shows the thawed-*minus*-dark sample, representing $Q_B^{\bullet-}Fe^{2+}$, The inset e shows the g~2 region of the $Q_B^{\bullet-}Fe^{2+}$ signal recorded with a microwave of 4 and 160 mW and an expanded magnetic field scale. Upon a further 77 K illumination, the typical g~1.62 signal attributed to $Q_A^{\bullet-}Fe^{2+}Q_B^{\bullet-}$ state was induced (spectrum f). The arrows show the g~2 new feature. Instrument settings: microwave power: 20 mW, modulation amplitude: 25 gauss, temperature: 4 K. For the insets: microwave power: as indicated in the figure, modulation amplitude: 10G, temperature: 4K.

Figure 3

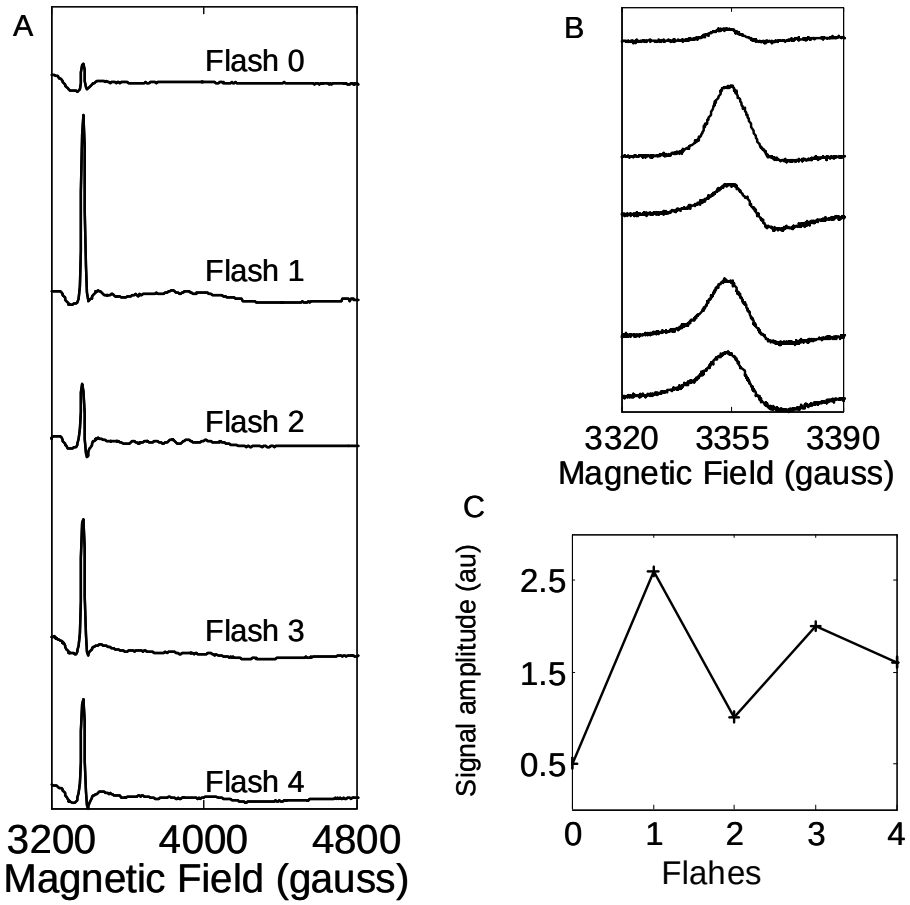

Figure 3: Flash number dependence of the intensity of the g~2 signal attributed to $Q_B^{\bullet-}Fe^{2+}$ in the Tyr D-less mutant PSII from *T. elongatus*. Samples were dark-adapted for ~12 h and then submitted to 0, 1, 2, 3 and 4 flashes at room temperature and frozen. The resulting spectra are shown in panel A. Panel B shows the g~2 region with increase field resolution. Panel C shows a plot of the variation in intensity of the signal with flash number. Instrument settings: microwave power: 20 mW, modulation amplitude: 25 gauss, temperature: 4 K. In panel B: microwave power: 4 mW, modulation amplitude: 10 gauss.

Figure 2

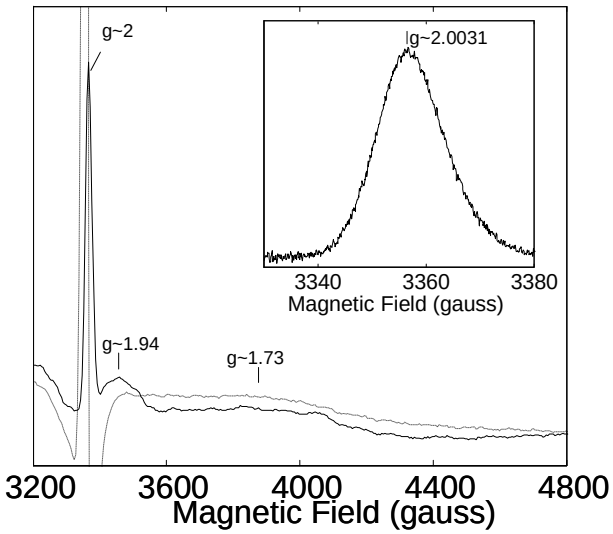

Figure 2: The effect of the addition of sodium dithionite to PSII isolated from *T. elongatus* (WT). The dotted line shows PSII with no additions, this sample was dark-adapted for 12 h prior to dithionite reduction. The solid line shows the PSII at room temperature reduced by dithionite (2 mM) and rapidly frozen after the addition of dithionite. The inset shows the resolved g~2 region. The main g-values are shown in the figure. Instrument settings: microwave power: 20 mW, modulation amplitude: 25 gauss, temperature: 4 K. For the inset, microwave power: 160 mW, modulation amplitude: 10 gauss and the temperature was 4K.

Figure 4:

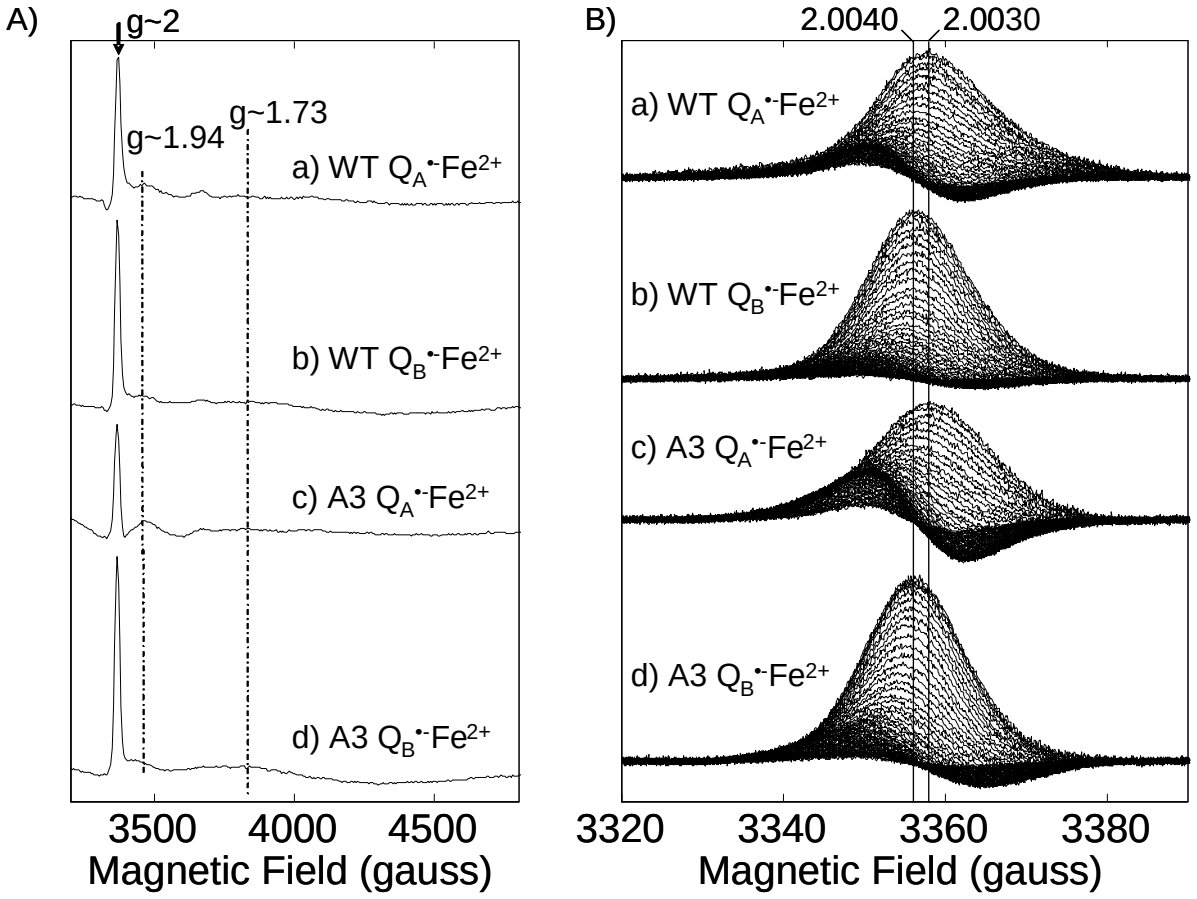

Figure 4: Comparison of the $Q_A^{\bullet-}Fe^{2+}$ and $Q_B^{\bullet-}Fe^{2+}$ EPR signals in PSII isolated from the WT and A3 strains of *T. elongatus*. Left panel, spectrum a and c show the $Q_A^{\bullet-}Fe^{2+}$ in the WT and A3 respectively, spectra b and d show $Q_B^{\bullet-}Fe^{2+}$ in WT and A3 respectively. $Q_A^{\bullet-}Fe^{2+}$ EPR signals were generated by a subtraction of the 77 K illuminated spectrum-*minus*-dark. $Q_B^{\bullet-}Fe^{2+}$ EPR signals were thawed-*minus*-dark spectra in which the 77 K illuminated sample was thawed to allow electron transfer from $Q_A^{\bullet-}$ to Q_B. Instrument settings: microwave power: 20 mW, modulation amplitude: 25 gauss, temperature: 4 K. The right panel show the resolution of the g~2 region and its amplitude versus the microwave power. Spectra e and g showed the $Q_A^{\bullet-}Fe^{2+}$ in the WT and A3 respectively, spectra f and h showed $Q_B^{\bullet-}Fe^{2+}$ in WT and A3 respectively. The main g-values are shown in the figure are those measured at 160 mW microwave power. Instrument settings: modulation amplitude: 10 gauss, temperature: 4 K.

Figure 5:

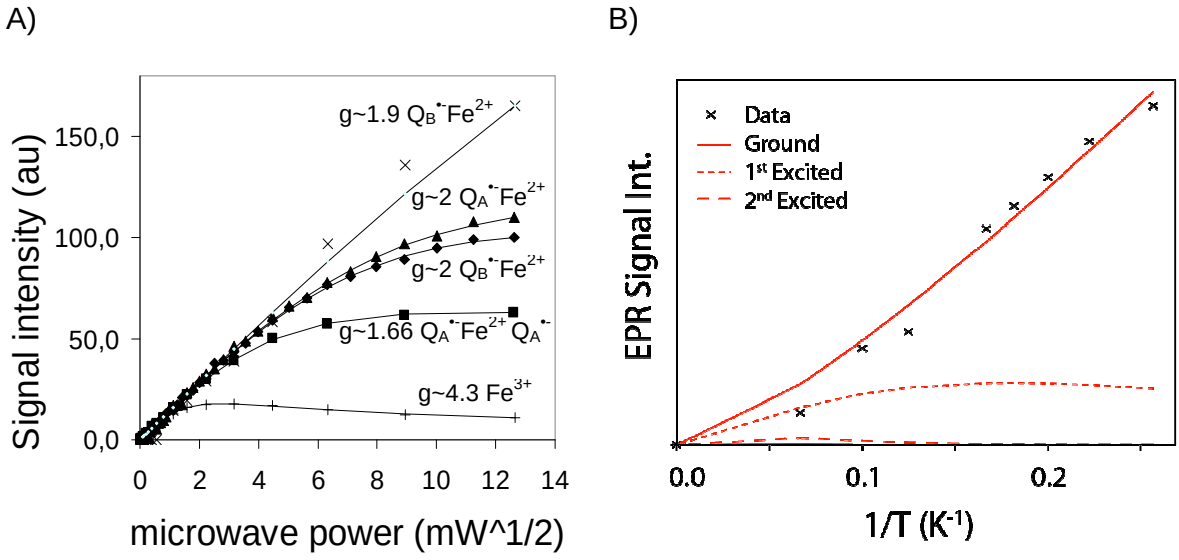

Figure 5: Microwave power saturation (panel A) and temperature dependence (panel B) of the g~2 from $Q_B^{\bullet-}Fe^{2+}$in the WT *T. elongatus* PSII. In panel A, g~2 signals from $Q_A^{\bullet-}Fe^{2+}$ (triangles) and $Q_B^{\bullet-}Fe^{2+}$ (diamonds), the g~1.9 signals arising from $Q_B^{\bullet-}Fe^{2+}$ (crosses), the g~1.66 signal arising from $Q_A^{\bullet-}Fe^{2+}$ $Q_B^{\bullet-}$ (squares) and g~4.3 (plus signs) are shown for comparison as controls. The lines were for the fit. The fits were done according to the equation described in material and methods. $Q_B^{\bullet-}Fe^{2+}$ and $Q_A^{\bullet-}Fe^{2+}$ EPR signals were generated as in figure 1. Amplitudes of the signals were normalized in the low microwave power region. The $P_{1/2}$ and the inhomogeneity factors found were: 180 mW, 1.57 for g~2 $Q_A^{\bullet-}Fe^{2+}$. 160 mW and 1.74 for g~2 $Q_B^{\bullet-}Fe^{2+}$. The g~1.9 $Q_B^{\bullet-}Fe^{2+}$ does not reach saturation. 36.68 mW, 1.28 for g~1.66 $Q_A^{\bullet-}Fe^{2+}Q_B^{\bullet-}$. 3.78 mW and 1.50 for the rhombic iron signal at g~4.3. Instrument settings: for all signals the temperature: 4 K and the modulation amplitude: 25 gauss. Except for the g~2 signals were the modulation amplitude was 10 gauss.

In panel B, the g~2 was measured at 4 mW, the modulation amplitude was 10 gauss, temperature 4K. The underlying radical was subtracted. Lines showed the simulation of the temperature dependence of the g ~ 2 signal based on the spin Hamiltonian formalism (see eq. 2). The red solid line through the data represents the temperature dependence of the ground state of the semiquinone-iron manifold; higher states are shown with red dashed lines. Fit parameters: D = 16. 6 K^{-1} (11.5 cm^{-1}), E/D = 0.25.

Figure 6

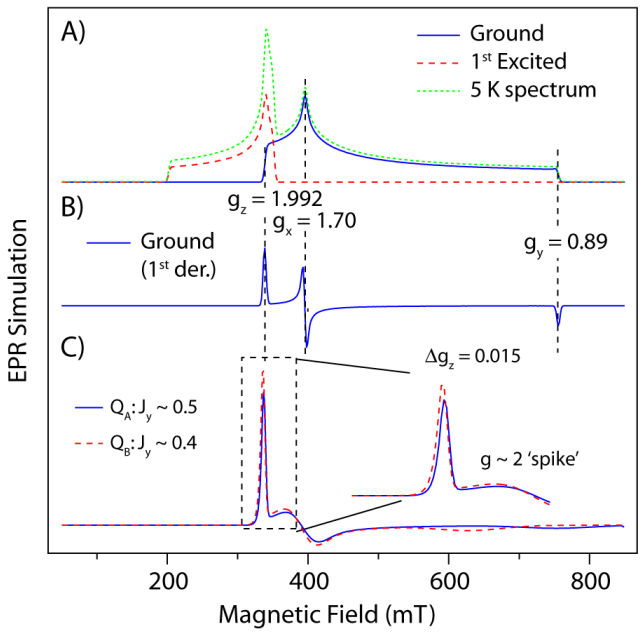

Figure 6: EPR simulation. (A) a simulation of the 5 K absorption lineshape of the g ~ 1.9 semiquinone-iron signal using the Spin Hamiltonian parameters reported in Cox et al [7]. (B) The 1st derivative lineshape of the ground state component of the g ~ 1.9 semiquinone-iron signal as in (A). C): the 1st derivative lineshape of the ground state component of the g ~ 1.9 semiquinone-iron signal as presented in (B) which allows for anisotropic line-broadening. The simulations shown in red and blue demonstrate that the exact position of the $g_{eff,z}$ is dependent on the magnitude of the component of the exchange coupling tensor along y (J_Y).

7. References:

[1] V. Petrouleas, A.R. Crofts, The iron-quinone acceptor complex, in: T. Wydrzynski, K. Satoh (Eds.) Photosystem II. The light-driven water: plastoquinone oxidoreductase, Springer, Dordecht, The Netherlands, 2005, pp. 177-206.
[2] K.N. Ferreira, T.M. Iverson, K. Maghlaoui, J. Barber, S. Iwata, Architecture of the photosynthetic oxygen-evolving center, Science, 303 (2004) 1831-1838.
[3] A. Guskov, J. Kern, A. Gabdulkhakov, M. Broser, A. Zouni, W. Saenger, Cyanobacterial photosystem II at 2.9-angstrom resolution and the role of quinones, lipids, channels and chloride, Nat Struct Mol Biol, 16 (2009) 334-342.
[4] H. Michel, J. Deisenhofer, Relevance of the photosynthetic reaction center from purple bacteria to the structure of Photosystem II, Biochemistry, 27 (1988) 1-7.
[5] A.W. Rutherford, How close is the analogy between the reaction center of PSll and that of purple bacteria? 2. The electron acceptor side, in: J. Biggins (Ed.) In Progress in Photosynthesis Research, Martinus Nijhoff, Dordecht, The Netherlands, 1987, pp. 277-283.
[6] R. Hienerwadel, C. Berthomieu, Bicarbonate binding to the non-heme iron of photosystem II investigated by Fourier transform infrared difference spectroscopy and C-13-labeled bicarbonate, Biochemistry, 34 (1995) 16288-16297.
[7] N. Cox, L. Jin, A. Jaszewski, P.J. Smith, E. Krausz, A.W. Rutherford, R. Pace, The semiquinone-iron complex of Photosystem II: structural insights from ESR and theoretical simulation; evidence that the native ligand to the non-heme iron is carbonate, Biophys. J., 97 (2009) 2024-2033.
[8] C.A. Wraight, Proton and electron transfer in the acceptor quinone complex of photosynthetic reaction centers from *Rhodobacter sphaeroides*, Front Biosci, 9 (2004) 309-337.
[9] M.Y. Okamura, M.L. Paddock, M.S. Graige, G. Feher, Proton and electron transfer in bacterial reaction centers, Biochim Biophys Acta, 1458 (2000) 148-163.
[10] W.F. Butler, R. Calvo, D.R. Fredkin, R.A. Isaacson, M.Y. Okamura, G. Feher, The electronic-structure of Fe^{2+} in reaction centers from *Rhodopseudomonas sphaeroides* .3. Electron-Paramagnetic-Res measurements of the reduced acceptor complex, Biophys. J., 45 (1984) 947-973.
[11] A.W. Rutherford, J.L. Zimmermann, A new Electron-Paramagnetic-Res signal attributed to the primary plastosemiquinone acceptor in Photosystem-II, Biochim Biophys Acta, 767 (1984) 168-175.
[12] J.L. Zimmermann, A.W. Rutherford, Photoreductant-induced oxidation of Fe^{2+} in the electron-acceptor complex of Photosystem-II, Biochim Biophys Acta, 851 (1986) 416-423.
[13] W.F.J. Vermaas, A.W. Rutherford, Electron-paramagnetic-res measurements on the effects of bicarbonate and triazine resistance on the acceptor side of Photosystem-II, Febs Lett, 175 (1984) 243-248.
[14] F. van Mieghem, K. Brettel, B. Hillmann, A. Kamlowski, A.W. Rutherford, E. Schlodder, Charge recombination reactions in Photosystem-II .1. Yields, recombination pathways, and kinetics of the primary pair, Biochemistry, 34 (1995) 4798-4813.
[15] F. Mamedov, M.M. Nowaczyk, A. Thapper, M. Rogner, S. Styring, Functional characterization of monomeric photosystem II core preparations from *Thermosynechococcus elongatus* with or without the Psb27 protein, Biochemistry, 46 (2007) 5542-5551.
[16] A. Sedoud, L. Kastner, N. Cox, S. El-Alaoui, D. Kirilovsky, A.W. Rutherford, Effects of formate binding on the quinone-iron electron acceptor complex of photosystem II, Biochim Biophys Acta, 1807 (2011) 216-226.

[17] A. Boussac, M. Sugiura, F. Rappaport, Probing the quinone binding site of Photosystem II from *Thermosynechococcus elongatus* containing either PsbA1 or PsbA3 as the D1 protein through the binding characteristics of herbicides, Biochim Biophys Acta, 1807 (2011) 119-129.
[18] M. Sugiura, Y. Kato, R. Takahashi, H. Suzuki, T. Watanabe, T. Noguchi, F. Rappaport, A. Boussac, Energetics in Photosystem II from *Thermosynechococcus elongatus* with a D1 protein encoded by either the *psbA1* or *psbA3* gene, Biochim Biophys Acta, 1797 (2010) 1491-1499.
[19] J.L. Hughes, A.W. Rutherford, M. Sugiura, E. Krausz, Quantum efficiency distributions of photo-induced side-pathway donor oxidation at cryogenic temperature in photosystem II, Photosynth Res, 98 (2008) 199-206.
[20] M. Sugiura, A. Boussac, T. Noguchi, F. Rappaport, Influence of histidine-198 of the D1 subunit on the properties of the primary electron donor, P680, of photosystem II in *Thermosynechococcus elongatus*, Biochim Biophys Acta, 1777 (2008) 331-342.
[21] A.W. Rutherford, A. Boussac, P. Faller, The stable tyrosyl radical in Photosystem II: why D?, Biochim Biophys Acta, 1655 (2004) 222-230.
[22] M. Sugiura, F. Rappaport, K. Brettel, T. Noguchi, A.W. Rutherford, A. Boussac, Site-directed mutagenesis of *Thermosynechococcus elongatus* photosystem II: the O2-evolving enzyme lacking the redox-active tyrosine D, Biochemistry, 43 (2004) 13549-13563.
[23] M. Sugiura, Y. Inoue, Highly purified thermo-stable oxygen-evolving photosystem II core complex from the thermophilic cyanobacterium *Synechococcus elongatus* having his-tagged CP43, Plant Cell Physiol, 40 (1999) 1219-1231.
[24] G.N. Johnson, A. Boussac, A.W. Rutherford, The origin of 40-50°C thermoluminescence bands in Photosystem-II, Biochim Biophys Acta, 1184 (1994) 85-92.
[25] B. Hallahan, S. Ruffle, S. Bowden, J.H.A. Nugent, Identification and characterization of EPR signals involving Q_B semiquinone in plant Photosystem-II, Biochim Biophys Acta, 1059 (1991) 181-188.
[26] A.W. Rutherford, A.R. Crofts, Y. Inoue, Thermo-luminescence as a probe of Photosystem-II photochemistry - the origin of the flash-induced glow peaks, Biochim Biophys Acta, 682 (1982) 457-465.
[27] N. Ishida, M. Sugiura, F. Rappaport, T.L. Lai, A.W. Rutherford, A. Boussac, Biosynthetic exchange of bromide for chloride and strontium for calcium in the photosystem II oxygen-evolving enzymes, J Biol Chem, 283 (2008) 13330-13340.
[28] A. Boussac, S. Un, O. Horner, A.W. Rutherford, High-spin states (S >= 5/2) of the photosystem II manganese complex, Biochemistry, 37 (1998) 4001-4007.
[29] C. Fufezan, C.X. Zhang, A. Krieger-Liszkay, A.W. Rutherford, Secondary quinone in photosystem II of *Thermosynechococcus elongatus*: Semiquinone-iron EPR signals and temperature dependence of electron transfer, Biochemistry, 44 (2005) 12780-12789.
[30] D.H. Stewart, G.W. Brudvig, Cytochrome b_{559} of photosystem II, Biochim Biophys Acta, 1367 (1998) 63-87.
[31] J.C. de Paula, J.B. Innes, G.W. Brudvig, Electron-transfer in Photosystem II at cryogenic temperatures, Biochemistry, 24 (1985) 8114-8120.
[32] J. Hanley, Y. Deligiannakis, A. Pascal, P. Faller, A.W. Rutherford, Carotenoid oxidation in photosystem II, Biochemistry, 38 (1999) 8189-8195.
[33] P. Faller, C. Fufezan, A.W. Rutherford, Side-path electrondonnors: cytochrom b_{559}, chlorophyll Z and beta-caroten, in: T.J. Wydrzynski, K. Satoh (Eds.) Photosystem II: The light-driven water: plastoquinone oxidoreductase, Springer, Dordecht, the Netherlands, 2005, pp. 347-365.
[34] P. Faller, A.W. Rutherford, R.J. Debus, Tyrosine D oxidation at cryogenic temperature in photosystem II, Biochemistry, 41 (2002) 12914-12920.

[35] J.H.A. Nugent, D.C. Doetschman, D.J. Maclachlan, Characterization of the multiple EPR line-shapes of iron semiquinones in Photosystem 2, Biochemistry, 31 (1992) 2935-2941.
[36] A. Joliot, Effect of low-temperature (-30 to-60 Degrees C) on reoxidation of Photosystem 2 primary electron-acceptor in presence and absence of 3(34-Dichlorophenyl)-1, 1-Dimethylurea, Biochim Biophys Acta, 357 (1974) 439-448.
[37] A.R. Corrie, J.H.A. Nugent, M.C.W. Evans, Identification of EPR Signals from the States $Q_A^{\cdot-}Q_B^{\cdot-}$ and $Q_B^{\cdot-}$ in Photosystem-II from *Phormidium laminosum*, Biochim Biophys Acta, 1057 (1991) 384-390.
[38] S.K. Chamorovsky, R. Cammack, Effect of temperature on the photo-reduction of center-a and center-b in Photosystem-I, and the kinetics of recombination, Biochim Biophys Acta, 679 (1982) 146-155.
[39] B. Bouges-Bouquet, Electron transfer between the two photosystems in spinach chloroplasts, Biochim Biophys Acta, 314 (1973) 250-256.
[40] B.R. Velthuys, J. Amesz, Charge accumulation at reducing side of system 2 of photosynthesis, Biochim Biophys Acta, 333 (1974) 85-94.
[41] Y. Nakamura, T. Kaneko, S. Sato, M. Ikeuchi, H. Katoh, S. Sasamoto, A. Watanabe, M. Iriguchi, K. Kawashima, T. Kimura, Y. Kishida, C. Kiyokawa, M. Kohara, M. Matsumoto, A. Matsuno, N. Nakazaki, S. Shimpo, M. Sugimoto, C. Takeuchi, M. Yamada, S. Tabata, Complete genome structure of the thermophilic cyanobacterium *Thermosynechococcus elongatus* BP-1, DNA Res, 9 (2002) 123-130.
[42] J.L. Hughes, N. Cox, A.W. Rutherford, E. Krausz, T.L. Lai, A. Boussac, M. Sugiura, D1 protein variants in Photosystem II from *Thermosynechococcus elongatus* studied by low temperature optical spectroscopy, Biochim Biophys Acta, 1797 (2010) 11-19.
[43] P.B. Kos, Z. Deak, O. Cheregi, I. Vass, Differential regulation of *psbA* and *psbD* gene expression, and the role of the different D1 protein copies in the cyanobacterium *Thermosynechococcus elongatus* BP-1, Biochim Biophys Acta, 1777 (2008) 74-83.
[44] B. Loll, M. Broser, P.B. Kos, J. Kern, J. Biesiadka, I. Vass, W. Saenger, A. Zouni, Modeling of variant copies of subunit D1 in the structure of photosystem II from *Thermosynechococcus elongatus*, Biol Chem, 389 (2008) 609-617.
[45] L.K. Thompson, G.W. Brudvig, Cytochrome-b559 may function to protect Photosystem-II from photoinhibition, Biophys. J., 53 (1988) A269-A269.

ARTICLE 4

(en préparation)

Oxidation of the non-heme iron in the quinone-iron complex of Photosystem II

Oxidation of the non-heme iron in the quinone-iron complex of Photosystem II

Arezki Sedoud[a] and A. William Rutherford[a*].

[a]iBiTec-S, CNRS URA 2096, CEA Saclay, 91191 Gif-sur-Yvette, France.

Abbreviations: EPR, electron paramagnetic resonance; PSII, Photosystem II; Q_A and Q_B, primary and secondary quinone electron acceptor of PSII.

[*] Corresponding author:
iBiTec-S, CNRS URA 2096, CEA Saclay, 91191 Gif-sur-Yvette, France. Telephone: +33 1 69 08 2940. Fax: + 33 1 69 08 87 17.
E-mail address: alfred.rutherford@cea.fr

Keywords: Photosystem II, quinone, semiquinone, non-heme iron, EPR.

1. Abstract

EPR is used here to study the oxidation of non-heme iron in Photosystem II from the cyanobacterium *Thermosynechoccus elongatus*. The iron, which is located between the two quinone acceptors, Q_A and Q_B becomes slowly oxidized in the dark when the semiquinone from of Q_B is present. This reaction is slow, occurring in the minutes time scale, occurs only in a fraction (less than 20 %) of centers and occurs in samples from which O_2 was removed. It is suggested that the non-heme iron is oxidized by the Q_B^- forming Q_BH_2. This has repercussion on the current assumptions concerning the redox potentials of the Q_B^-/Q_BH_2 and Q_B/Q_B^- couples.

2. Introduction

A non-heme Fe^{2+} ion is located between the two quinones, Q_A and Q_B, of the electron acceptor complex of the Photosystem II (PSII) [1]. This iron has ligands from four histidines from the protein and a bidentate ligand from an exchangeable bicarbonate [1]. The role of this ion in the electron transfer from Q_A to Q_B is not yet established, despite being present in all type II reaction centers [1]. There are several differences in the properties of the iron in the bacterial system compared to that of PSII. In the bacterial system, the carboxylic acid ligand is from a glutamate 232 of the M subunit and is thus not exchangeable. The Fe region is capped by a globular H subunit which insulates this area from the aqueous phase and controls proton access through channels [2]. In PSII by contrast no such protein has yet been found and the Fe appears to relatively exposed to the aqueous medium. The exchangeable bicarbonate ligand to the iron, represents a significant difference between PSII and the purple bacterial reaction center and it is probably responsible for allowing the iron to undergo oxidation in PSII [1]. The Fe^{2+}/Fe^{3+} couple in PSII has an Em of 400 mV and it is thus oxidizable by ferricyanide [3].

It has also been shown that the semiquinone form of some artificial quinones, commonly used as electron acceptors in vitro, are able to oxidize the iron leading to a typical "photoreductant-induced oxidation" of the iron upon odd numbered flashes, with reduction of the iron occurring on the subsequent (even numbered flashes) [4]. Reports have also been made small amounts of oxidized iron present in dark adapted samples even in the absence of the artificial quinones or exogenous oxidant present [5-7], perhaps reflecting oxidation by O_2^- or peroxide which are both known to be formed in thylakoids. Nugent reported Fe^{2+} oxidation during dark adaptation of pre-illuminated in plant PSII samples in the presence of O_2. It was

suggested that the Fe^{2+} was oxidized “either by oxygen species or semiquinone”, where the semiquinone was Q_B^- when O_2 and present at he same time as Q_B^- formed by dark adaptation after a period of continuous illumination. Recently, it has been shown that the addition of inhibitors (DCMU) induced oxidation of the non-heme iron when Q_B^- is present prior the DCMU addition [7]. The displacement of the Q_BH_2 from its site by the DCMU shifting the following equilibrium to the right:

$$Fe^{2+}Q_B^- + DCMU \rightleftharpoons Fe^{3+}Q_BH_2 + DCMU \rightleftharpoons Fe^{3+}DCMU + Q_BH_2$$

This indicates that the redox potential of Q_B^-/Q_BH_2 couple is not too far away from the potential of Fe^{2+}/Fe^{3+} couple at least in some centers. Thus, Q_B^- may be capable of Fe^{2+} oxidation under some physiologically relevant conditions. Here we report non-heme iron oxidation by Q_B^- in intact untreated PSII monitored by EPR.

3. Materials and methods

PSII preparations were made from 43H *T. elongatus* strain, the procedure was exactly the same as described earlier in Sedoud et al [8].

Chemical reduction of PSII with ascorbate was performed as follows: sodium ascorbate from a 300 mM stock solution in storage buffer was added to 120 µL of PSII (~ 1 mg Chl/ml) in the EPR tube in darkness to give a final concentration of 10 mM. The PSII samples were then incubated in darkness for 30 min at room temperature prior to freezing.

4. Results

Fig. 1 shows the non-heme iron oxidation in the dark by Q_B^-. In this experiment, PSII was first dark incubated for 12 hours, and reduced by ascorbate for 30 min. This treatment diminishes the amount of Q_B^- present in the dark to a level ≤ 5% and reduces the cytochrome b_{559} [6, 8]. The characteristic EPR signals of Fe^{3+} from the non-heme iron were absent in these conditions. Illumination at 77 K led to the reduction of Q_A with the formation of Q_A^- and the oxidation of cytochrome b_{559}, which is the terminal electron donor in the majority of the centers [9]. At this low temperature, the electron transfer from Q_A^- to Q_B is blocked [6, 10]. Fig. 1 shows that no change occurred in the non-heme iron EPR region after the first 77 K illumination: since no Fe^{3+} was present in the dark, then obviously it was not expected to undergo reduction upon illumination. Thawing of this sample in darkness allows transfer of

the electron from Q_A^- to Q_B to occur [8]. Incubation of the sample at room temperature for 10 min led to the appearance of oxidized non-heme iron, which is clearly observable at g~6. The illumination of this thawed sample at 77 K results in the disappearance of the signal, indicating a reduction of the oxidized non-heme iron (by Q_A^-) [1]. Cycles of photoreduction at 77 K of the Fe^{3+}, and its oxidation in the dark were performed, the results is shown in Figure 1B.

Figure 2 shows the time course of the oxidation of the non-heme iron, in different conditions: (i) panel A shows the results obtained in untreated PSII submitted to 1 single saturating flash, (ii) panel B and C showed results obtained in samples with and without ascorbate respectively when submitted to 77 K illumination. The intensities of the g~6 and g~4.3 EPR signals *versus* time are plotted in upper and lower panels in Figure 3, respectively. It is shown that the appearance of g~6 EPR signal has approximately the same time dependence in all samples; the kinetic constant for this component is ~0.2-0.3 min^{-1}. Surprisingly, we found that in addition to the expected g~6 that characterize the non-heme iron, a signal at g~4.3 also increases during incubation in the dark after the illumination have been achieved. It is known that g~4.3 signal arises from rhombic Fe^{3+} that is generally attributed to a possible contamination during the biochemical preparation. In this work however, we show that this signal clearly increased when pre-illuminated-PSII is incubated in the dark. The time course of the g~4.3 is similar that of the g~6 signal. We noted that when ascorbate is absent, the g ~ 4.3 is more intense, and the g ~ 6 is smaller, while when ascorbate is present, the g ~ 6 is more easily detectable and more intense. It is noted also that ascorbate narrows the g~6 signal. In panel C in Fig. 3, it is shown that when the non-heme iron oxidation and the $Q_B^-Fe^{2+}$ EPR signal are monitored, the estimate of the disappearance of Q_B^- may correspond to the amount of the non-heme iron oxidation, in this case 20 % of Q_B^- was decreased, and this may correspond then to the oxidation of the non-heme iron.

5. Discussion

In this work, we show the direct evidence that the non-heme iron undergoes oxidation in dark when Q_B^- is formed in a non-treated PSII. This oxidation is slow (minutes order) compared to the well-known non-heme iron oxidation induced by PPBQ (seconds).

The illumination at 77 K of a sample containing both the g~6 and g~4.3 showed that only the signal at g~6 disappeared, the g~4.3 is thus insensitive to illumination. A similar observation

has already been reported in the literature [5], it was concluded that the g~4.3 may come from the oxidized non-heme iron in a fraction of centers that were denatured due to the strong illumination used during the experiments. In our experiment, we this explanation does not hold, because we could induce the g~4.3 signal even after 1 flash.

The formation of two types of EPR signals arising from the oxidized non-heme iron forms, the g~6 signal, which is sensitive to light, and g~4.3, which is insensitive to light, may indicate that there is two populations of the non-heme iron, one which is photoreducible (the g~6) and one which is not photoreducible (the g~4.3). It was already noted that narrowness of the g~4.3 may mean that it arises in a very small fraction of centers [5]. It is also possible that the g~4.3 iron does not correspond to the non heme Fe but is rather a contaminant in the medium that happens to be oxidizable by Q_B^- in a small fraction of centers.

Previously, a slow formation of the oxidized non-heme iron signal during storage in the dark was reported [7]. This was attributed to the oxidation of Fe^{2+} by semiquinone [7, 11] or oxygen [11]. Nugent has shown that the removal of oxygen inhibited oxidation of the iron [11]. In the results shown here, oxygen was removed by degassing at 200 K, but the thawing procedure was done just by incubating the samples at room temperature in sealed tubes.

McEvoy and Brudvig have recently published a work that was interpreted as indicating non-heme iron oxidation after a charge recombination between Fe^{2+} and Chl^+/Car^+ or $TyrD^\bullet$ in a fraction of centers [12]. In the present work, the non-heme iron oxidation due to such charge recombination is ruled out, and this is because, in the experiment showed in Figure 1 for instance, the final electron donor is not the side pathways Chl^+/Car^+ or $TyrD^\bullet$, but it is the cytochrome $_{b559}$. Also, the experiment showed in Figure 2, panel 1, where PSII was illuminated with 1 flash at room temperature clearly argued against a charge recombination between the Chl^+/Car^+ and $TyrD^\bullet$ and the Fe^{2+}. In the same work, McEvoy and Brudvig proposed the existence of two types of non-heme iron, one population that can undergo photo-reduction at helium cryogenic temperature, and another population of iron that can only undergo photo-reduction above 75 K [12]. In the present work, we found that there are two types of EPR signals, g~6 and g~4.3 originating from the oxidized non-heme iron formed after the incubation in the dark of an illuminated PSII. The g~6 EPR signal can be photo-reduced, while the g~4.3 population is not photo-reducible at 77K. The two populations of the non-heme iron described here are different from the two populations proposed by McEvoy and Brudvig, in that the g~4.3 population is not photoreducible even at room temperature. In

addition the biological material used is different; McEvoy and Brudvig used the PSII-enriched memranes isolated from the plant, while the material used here is PSII core preparations isolated from *T. elongatus*.

The observation of the slow non-heme iron oxidation by Q_B^- in the dark may indicate that the redox potential of the Q_B^-/Q_BH_2 couple is close by or higher than that the non-heme iron. The redox potential of the non-heme iron is ~400 mV at pH 7 [3] in plants, clearly much higher than would be expected for the Q_B^-/Q_BH_2 couple. However, Ishikita and Knapp [13] estimated by theoretical calculations that the Fe^{2+}/Fe^{3+} potential to be ~300 mV at pH 6.5 when Q_B^- is present. This implies that the redox potential of Q_B^-/Q_BH_2 is close to 300 mV.

The redox potential of Q_A/Q_A^- was measured to be -80 mV in intact PSII at pH 6.5 [14] and recently Shibamoto et al, [15] has measured -140 mV, the redox potential difference maybe due to the use of mediators, this will be discussed elsewhere. The redox potential of the plastoquinone/plastoquinol pool was estimated to be around 130 mV at pH 6.5 [16]. The driving force of the Q_A^- to Q_B is estimated to be about 70-83 mV [17-19].

Taking these observations together, two options can be proposed for the potentials of Q_B/Q_B^- and Q_B^-/Q_BH_2. The first option is based on the work presented here and the indications of Fe oxidation by QB- in the literature (Boussac and Nugnet), the redox potential of the Q_B^-/Q_BH_2 is thus suggested to be more oxidizing than the potential of Q_B/Q_B^-. The value of 300 mV as a redox potential of Fe^{2+}/Fe^{3+} in the presence of Q_B^- [13] places thus the potential for Q_B^-/Q_BH_2 to be close to 300 mV (the quantification of the amount of oxidized iron is estimated to be 20 %, see panel C in Fig. 3). By hypothesizing the potential of 300 mV for Q_B^-/Q_BH_2, the potential of Q_B/Q_B^- has to be ~ -40 mV, similar value was deduced by Shibamoto et al, who have found -60 mV as a potential of Q_B/Q_B^- [15]. In this case, the properties of the semiquinone are closer to those predicted for free PQ, with a less marked stabilization of the semiquinone.

The second option is that the potential of Q_B/Q_B^- is more oxidizing than the potential of Q_B^-/Q_BH_2. This option is comparable to the potentials found for Q_B/Q_B^- and Q_B^-/Q_BH_2 in the purple bacterial reaction centers, which were 160 mV and 95 mV for Q_B/Q_B^- and Q_B^-/Q_BH_2, respectively [20]. This model also fits with the observation that reduction of PSII with DAD and ascorbate results in formation of $Q_B^-Fe^{2+}$ in a large fraction of centers. In this option the Q_B^- is greatly stabilized compared to free PQ^-. This model also fits with the observation that under some conditions the $Q_A^-Fe^{2+}Q_B^-$ state can be stabily formed in the dark. This would only occur when the Q_A/Q_A^- couple overlapped with the $Q_B^-Q_BH_2$ couple. This occurs when

the high potential form of Q_A is present (in apo-PSII) at high pH (Rutherford A.W, unpublished), and transiently when treated with strong reductants (not shown).

The two different conditions are very different from each other but should be easily distinguishable by performing redox titrations. The fact that evidence seems to exist for both situations could indicate the existence of both conditions under given circumstances. Whether these circumstances represent physiological relevant conditions of simply damaged centers cannot yet be assessed.

In any case, we describe here the iron oxidation by Q_B^- state in a fraction of centers. In fact, the possibility of getting rid of Q_B^- by its reduction by the iron may stabilizes the PSII in S_2 or S_3 states, which might benefit for water oxidation and photoprotection (decrease in charge recombination and thus decrease in formation of chlorophyll triplet states that can interact with oxygen to form singlet oxygen, harmful for proteins). The titration of the Q_B seems now to be our first priority.

In the present work, we have data for the time course of the non-heme iron oxidation in the S_1 (samples that were illuminated at 77 K, at this temperature no Mn oxidation can occur) and S_2 (sample submitted to 1 flash), in both cases, the time course oxidation of the non-heme iron seemed to be similar. It will be interesting to test this in other S states to see if the S states modulate the potential of the iron and Q_B^-.

Figure 1

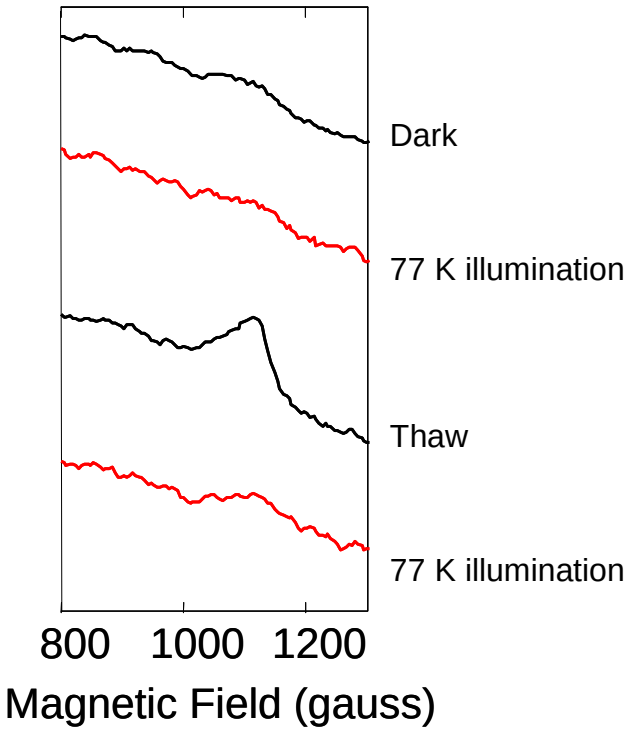

Figure 1: Non-home iron oxidation/reduction oscillation pattern.

PSII was dark-incubated for 12h; then ascorbate was added and incubated for 30 min in the dark, the corresponding spectrum recorded is shown and labeled as dark. A series of 77 K illumination (spectra in red) followed by thawing and incubation in the dark for 10 minutes (spectrum in black) was done. During the illumination at 77 K, the non-heme iron if present in its oxidized form is reduced (red spectra). During the thawing at room temperature for 10 min, the non-heme iron is reoxidized (black spectrum).Instrument settings: microwave frequency: 9.41 GHz, microwave power: 20 mW, modulation amplitude: 25 gauss, temperature: 4.5 K.

Figure 2:

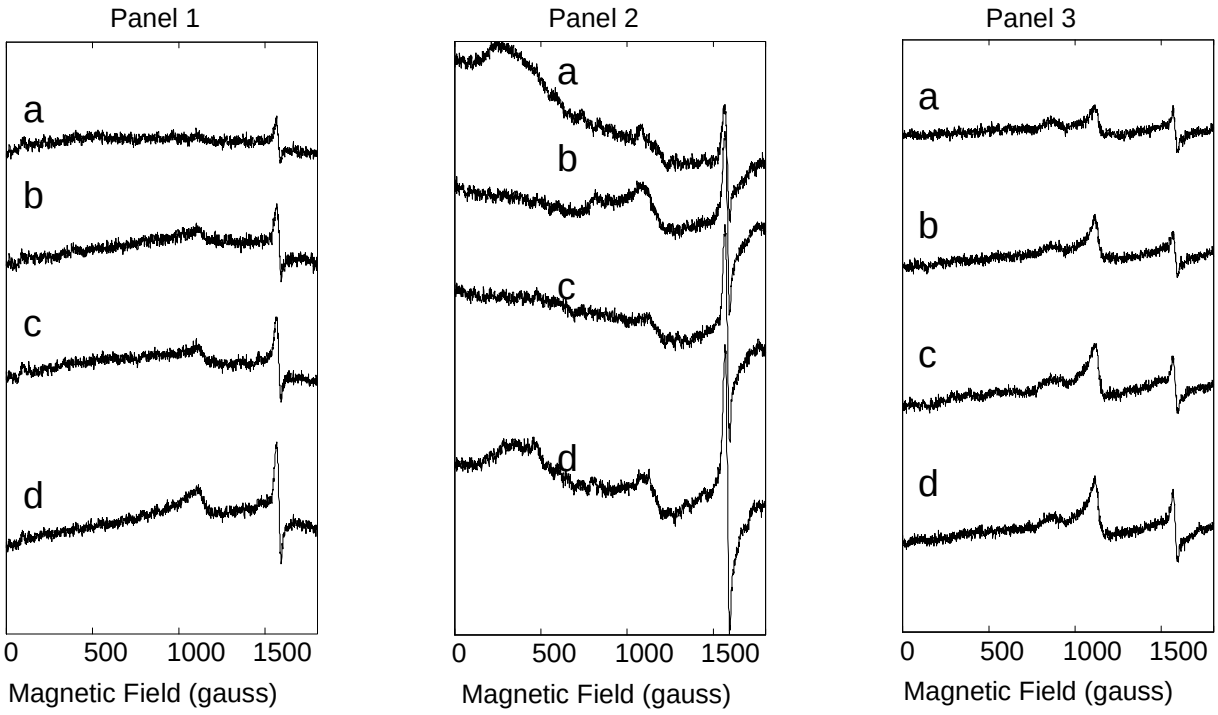

Figure 2: Non-heme iron oxidation time course. The spectra shown are thawn-*minus*-illuminated difference spectra; the thawing was done in the dark at room temperature by incubation of the illuminated sample for 2, 5, 10 and 20 min shown in a, b, c and d respectively. The same concentration of PSII was used (~1 mg Chl / ml), samples were dark incubated for 12 hours, then reduced for 30 min with ascorbate when mentioned. In panel 1, the sample was illuminated by 1 flash at room temperature. Panel 2 and 3, samples were illuminated 30 min at 77 K. Ascorbate was added in the experiment showed in panel 3. Instrument settings as in figure 1.

Figure 3:

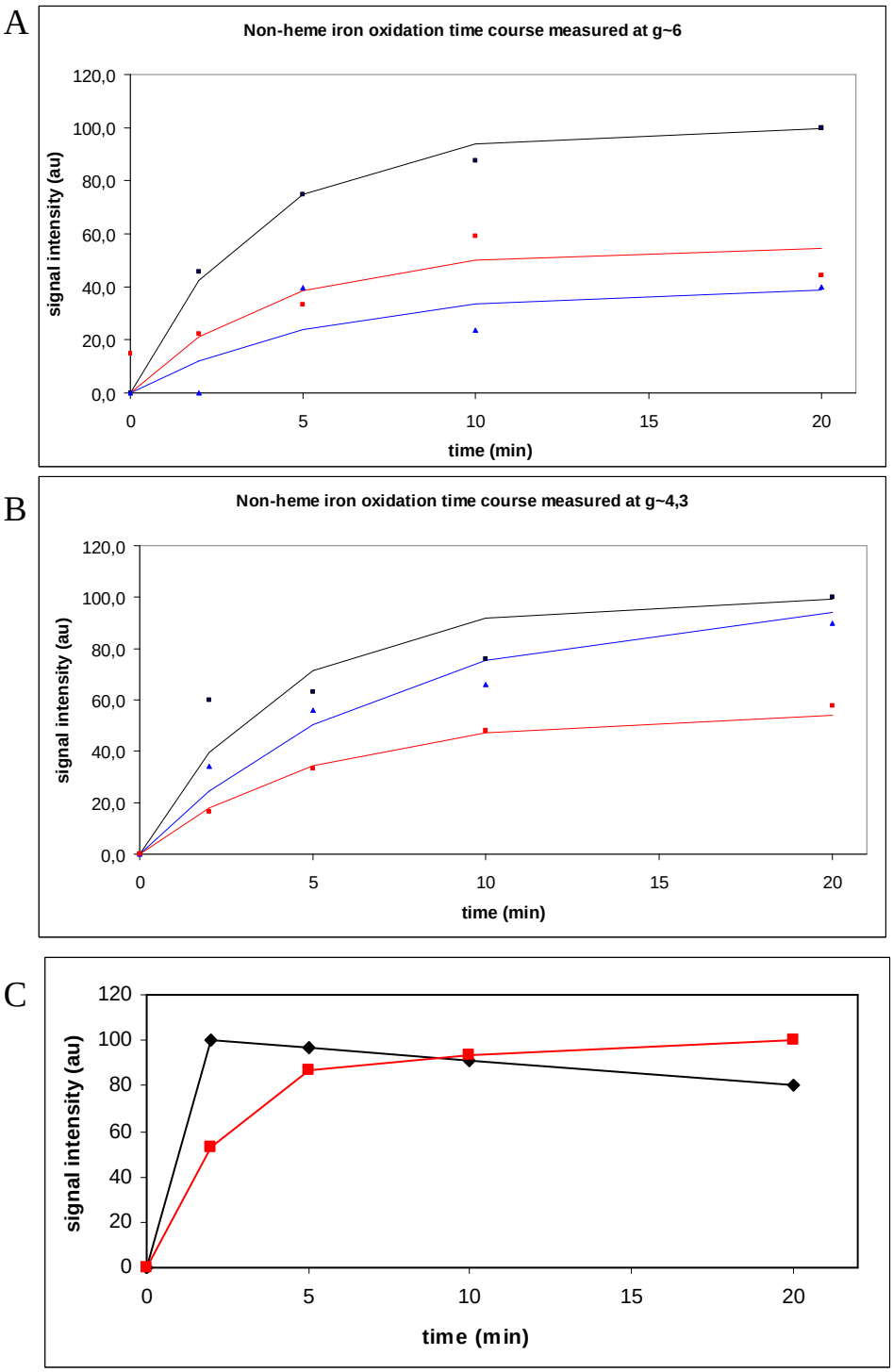

Figure 3: Non-heme iron oxidation kinetic plots. Panel A showed the non-heme iron oxidation measured at g~6. Panel 2 showed the time course of the increase in the g~4.3 signal. In panel 1 and 2, the non-heme iron oxidation induced by 1 flash is shown in black, the blue and red traces show the non-heme iron oxidation induced after 77 K illumination in non-treated and ascorbate-treated PSII respectively. The continuous lines are the fit obtained using the

following equation: y=a[1-exp(-k*t)], where a is an normalization factor, k is the kinetic constant and t is the time in min, see table 1. In panel 3, the red line showed the non-heme iron oxidation time course (the same as the red line in panel A) and in black is shown the Q_B^- EPR signal disappearance quantified by measuring the g~2 and g~1.9 signals, (see article 3 in this thesis).

Table 1:

		1 F	77 K	77 K + asc
g~6	k (min^{-1})	0.2	0.2	0.3
	1/k (min)	5	5	3.3
g~4.3	k (min^{-1})	0.16	0.14	0.25
	1/k (min)	6.2	7.1	4

Table 1: Calculation of the kinetic parameters for the non-heme iron oxidation.

References

[1] V. Petrouleas, A.R. Crofts, The iron-quinone acceptor complex, in: T. Wydrzynski, K. Satoh (Eds.) Photosystem II. The light-driven water: plastoquinone oxidoreductase, Springer, Dordecht, The Netherlands, 2005, pp. 177-206.

[2] C.A. Wraight, Proton and electron transfer in the acceptor quinone complex of photosynthetic reaction centers from *Rhodobacter sphaeroides*, Front Biosci, 9 (2004) 309-337.

[3] B.A. Diner, V. Petrouleas, Q_{400}, the non-heme iron of the Photosystem-II iron-quinone complex - a spectroscopic probe of quinone and inhibitor binding to the reaction center Biochim Biophys Acta, 895 (1987) 107-125.

[4] J.L. Zimmermann, A.W. Rutherford, Photoreductant-induced oxidation of Fe^{2+} in the electron-acceptor complex of Photosystem-II, Biochim Biophys Acta, 851 (1986) 416-423.

[5] Y. Deligiannakis, V. Petrouleas, B.A. Diner, Binding of carboxylate anions at the nonheme Fe(II) of PS-II .1. Effects on the $Q_A^-Fe^{2+}$ and Q_AFe^{3+} EPR spectra and the redox properties of the iron, Biochim Biophys Acta, 1188 (1994) 260-270.

[6] C. Fufezan, C.X. Zhang, A. Krieger-Liszkay, A.W. Rutherford, Secondary quinone in photosystem II of *Thermosynechococcus elongatus*: Semiquinone-iron EPR signals and temperature dependence of electron transfer, Biochemistry, 44 (2005) 12780-12789.

[7] A. Boussac, M. Sugiura, F. Rappaport, Probing the quinone binding site of Photosystem II from *Thermosynechococcus elongatus* containing either PsbA1 or PsbA3 as the D1 protein through the binding characteristics of herbicides, Biochim Biophys Acta, 1807 (2011) 119-129.

[8] A. Sedoud, L. Kastner, N. Cox, S. El-Alaoui, D. Kirilovsky, A.W. Rutherford, Effects of formate binding on the quinone-iron electron acceptor complex of photosystem II, Biochim Biophys Acta, 1807 (2011) 216-226.

[9] D.H. Stewart, G.W. Brudvig, Cytochrome b_{559} of photosystem II, Biochim Biophys Acta, 1367 (1998) 63-87.

[10] A. Joliot, Effect of low-temperature (-30 to-60 Degrees C) on reoxidation of Photosystem 2 primary electron-acceptor in presence and absence of 3(34-Dichlorophenyl)-1, 1-Dimethylurea, Biochim Biophys Acta, 357 (1974) 439-448.

[11] J.H.A. Nugent, Photoreducible high spin iron electron paramagnetic resonance signals in dark-adapted Photosystem II: are they oxidised non-haem iron formed from interaction of oxygen with PSII electron acceptors?, Biochim Biophys Acta, 1504 (2001) 288-298.

[12] J.P. McEvoy, G.W. Brudvig, Redox reactions of the non-heme iron in photosystem II: an EPR spectroscopic study, Biochemistry, 47 (2008) 13394-13403.

[13] H. Ishikita, E.W. Knapp, Oxidation of the non-heme iron complex in photosystem II, Biochemistry, 44 (2005) 14772-14783.

[14] A. Krieger, A.W. Rutherford, G.N. Johnson, On the determination of redox midpoint potential of the primary quinone electron-acceptor, Q_A, in Photosystem-II, Biochim Biophys Acta, 1229 (1995) 193-201.

[15] T. Shibamoto, Y. Kato, M. Sugiura, T. Watanabe, Redox potential of the primary plastoquinone electron acceptor Q_A in Photosystem II from *Thermosynechococcus elongatus* determined by spectroelectrochemistry, Biochemistry, 48 (2009) 10682-10684.

[16] J.H. Golbeck, B. Kok, Redox titration of electron-acceptor Q and the plastoquinone pool in Photosystem II, Biochim Biophys Acta, 547 (1979) 347-360.

[17] H.H. Robinson, A.R. Crofts, Kinetics of the oxidation reduction reactions of the Photosystem II quinone acceptor complex, and the pathway for deactivation, Febs Lett, 153 (1983) 221-226.
[18] W.F.J. Vermaas, G. Dohnt, G. Renger, Binding and release kinetics of inhibitors of Q_A^- oxidation in thylakoid membranes, Biochim Biophys Acta, 765 (1984) 74-83.
[19] F. Rappaport, J. Lavergne, Thermoluminescence: theory, Photosynth Res, 101 (2009) 205-216.
[20] A.W. Rutherford, M.C.W. Evans, High-potential semiquinone-iron signal in *Rhodopseudomonas viridis* is the specific quinone secondary-electron acceptor in the photosynthetic reaction center, Febs Lett, 104 (1979) 227-230.

ARTICLE 5

(en préparation)

Dithionite reduction of Photosystem II:

S_0 state formation and a broad $Q_A^{\bullet -}Fe^{2+}$ EPR signal

Dithionite reduction of Photosystem II: S_0 state formation and a broad $Q_A^{\bullet-}Fe^{2+}$ EPR signal

Arezki Sedoud[a] Laure Michelet[a] and A. William Rutherford[a*].

[a]iBiTec-S, CNRS URA 2096, CEA Saclay, 91191 Gif-sur-Yvette, France.

Abbreviations: Cyt b_{559}; cytochrome b 559; EPR, electron paramagnetic resonance; PSII, Photosystem II; Q_A and Q_B, primary and secondary quinone electron acceptor of PSII.

[*] Corresponding author:
iBiTec-S, CNRS URA 2096, CEA Saclay, 91191 Gif-sur-Yvette, France. Telephone: +33 1 69 08 2940. Fax: + 33 1 69 08 87 17.
E-mail address: alfred.rutherford@cea.fr

Keywords: Photosystem II, quinone, semiquinone, dithionite, EPR, S_0, dithionite.

1. Abstract

Here we have studied the effect of sodium dithionite on Photosystem II from *Thermosynechococcus elongatus* using EPR at cryogenic temperature to monitor the effects. Immediately after addition of dithionite the stable S_1 state of the Mn_4Ca cluster is reduced to form the S_0 state, which is formed in a large fraction of the centers. Reoxidation of this sample and illumination at room temperature, followed by dark adaptation led to a state in which the S_2 multiline signal could be seen in most centers. The enzyme activity was not greatly affected in this sample. Upon further incubation the S_0 EPR signal disappeared presumably because it was further reduced. Reoxidation of the sample incubated for 10 minutes at room temperature in dithionite, followed by illumination, resulted in the recovery of oxygen evolution activity (50 %) and the S_2 multiline EPR signal (30 %) indicating that in this fraction of centers at least, the Mn_4Ca cluster had not disassembled at this time. In addition the $Q_A^{\bullet-}Fe^{2+}$ EPR signal underwent a marked modification when the dithionite-PSII was incubated more than 10 min in dark at room temperature. Possible origins of this change are discussed.

2. Introduction:

The first quinone electron acceptor, Q_A, of PSII exhibits two different redox potentials depending on the intactness of the Mn_4Ca cluster that is located on the other side of the membrane. A change in the redox potential from -80 mV (active form) to +65 mV (inactive form) was determined [1-3], and recently Shibamoto et al, have reported more negative potentials values, -140 and 20 mV for active and inactive PSII, respectively [3]. This effect was correlated to the presence of the Ca^{2+} ion [4], however since the Ca site is provided by the Mn cluster [5-7], the presence of the Mn cluster itself correlates with redox potential change in Q_A [1-2]. This is physiologically relevant since the process of assembling the Mn_4Ca cluster into the photochemical reaction of PSII involves the shift of the redox potential of Q_A and the consequent changes in forward and backward electron transfer properties (reviewed in [8]).

The Mn_4Ca complex even in its most stable redox state in the function enzyme cycle, S_1, consists of Mn ions that have a valence of III or IV (most researchers consider S_1 to be $Mn^{III}_2Mn^{IV}_2$) reviewed in [9]. If so, then this cluster has undergone 6 oxidations, each one expected to occur with potentials around 1 eV, from the starting 4 Mn^{2+} ions. While these oxidations are at least partially compensated by deprotonations etc, the cluster is nevertheless highly oxidizing and out of equilibrium. In the functional enzyme, the cluster is protected from reductive attack by several extrinsic proteins that exclude most soluble reductants. Channels through these and parts of the intrinsic subunits allow the substrate water to enter the active site [10-11].

In redox titrations mediators are generally used to establish equilibrium between the cofactors, the medium and the electrodes. With PSII, redox titrations are problematic because equilibration between the medium and the highly oxidizing Mn_4Ca cluster will inevitably lead to the reduction and of the cluster and its likely disintegration. Loss of the cluster is accompanied by the reversal of the conformation changes that occur during cluster assembly ([12] for recent review) and the shift in the potential of Q_A to its high potential form [1-2]. In the present manuscript, two aspects of the reductive effect of dithionite were studied. First, the effect of dithionite on the Mn_4Ca cluster (see also [13] where some of the results have been published). Second, the effect of dithionite on the electron-acceptor side was also examined and an unexpected effect was seen.

3. Material and methods:

3.1 Culture conditions and PSII preparation

The growth conditions and the PSII preparation (WT) was exactly as described in [14], the PSII was stored in the storage buffer (40 mM MES pH 6.5, 15 mM $CaCl_2$, 15 mM $MgCl_2$, 10 % glycerol and 1 M betaine).

3.2 Chemical reduction treatments

Chemical reduction was done on 120 µL aliquots of PSII (~ 3 mg Chl/ml). Dithionite reduction was performed by addition of sodium dithionite to the sample in the EPR tube to give a final concentration of 2 mM using a 30 mM stock solution made up in degassed storage buffer (the preparation of dithionite in either 500 mM MES pH6.5 or the storage buffer showed exactly the same result). Ferricyanide oxidation was added to give a final concentration of 5 mM using a 25 mM stock solution. All additions were done in anaerobic conditions.

3.3 EPR measurements

EPR spectra were recorded using a Bruker Elexsys 500 X-band spectrometer equipped with standard ER 4102 resonator and Oxford Instruments ESR 900 cryostat. Instrument settings were: microwave frequency 9.4 GHz, modulation frequency 100 kHz. All other settings were as indicated in the figure legends. 120 µl aliquots of PSII cores (~ 1 mg Chl/ml) in the same buffer used for storage were loaded into 4 mm outer diameter quartz EPR tubes. The samples were manipulated under dim-green light and then incubated in complete darkness. The EPR samples were frozen in a dry-ice/ethanol bath at 200 K. Samples were degassed by pumping at 200 K and then filled with helium gas. EPR tubes were then transferred to liquid nitrogen prior to the EPR measurements being made. Samples were handled in darkness.

3.4 Protein gel analysis

PSII dithionite-reduction was followed by SDS-PAGE on 12 % acrylamide gel in non-reductive conditions as described in [15]. PSII samples were denaturated in 2% SDS (m/v), 10 % glycerol (m/v), 50 mM pH6.8 Tris-HCl and 0.1 % (m/v) bromophenol blue, for 30 min at 37°C. 3 µg Chl/ml of PSII were loaded into the gel.

4. Results:

4.1 S_0 state induced by dithionite reduction:

Figure 1 shows the EPR spectrum of PSII frozen less than one minute after the addition of sodium dithionite. A broad signal with many hyperfine lines is present. This is very similar to the S_0 multiline in the literature formed by illumination with three flashes or by reduction with NH_2OH [16-17]. At the same time the intense g~2 signal attributed to the semiquinone-iron signal is observed (Sedoud et al, submitted). The right panel of Fig. 1 showed the decay of S_0. The half-time of S_0 generated by the dithionite reduction is estimated to be around 3 min at room temperature. Mn^{2+}, which is already present in a very small fraction of centers in this preparation, increased slightly after 30 min incubation at room temperature. It seems likely that the S_0 decay represents the further reduction of the cluster. In principle, the states could represent redox states that correspond to S_{-1} to S_{-5}, where S_{-5} represents the fully reduced 4 Mn^{+2} form.

The small Mn^{2+} signal did not diminish when sample was illuminated after re-oxidation with potassium ferricyanide. However ferricyanide is known to precipitate Mn^{2+} ions preventing them from undergoing oxidation by PSII [18]. The small Mn^{2+} signal thus presumably represents a small fraction of centers where the cluster is destroyed by the dithionite treatment. The Mn^{2+} signal was larger in the presence of a mediator (indigodisulfonate, E_m = -125 mV), this indicates that the addition of the mediator reduced the Mn_4Ca cluster further than did the dithionite alone (i.e. S_{-n}, $_{n\leq5}$). Further treatment with a strong white light illumination at room temperature for 12 min, induced an intense Mn^{2+} EPR signal. The light-induced increase could represent direct damage of the Mn_4Ca cluster by light [19] or a further perturbation of the site induced by the double reduction of the Q_A^- to Q_AH_2,which is know to occur under these conditions [20]. It is not clear that this represents the visualization of all the Mn^{2+} ions. Acidification of the sample would be required in order to determine this.

4.2 Oxidation of the dithionite-reduced PSII:

PSII was reduced with dithionite and incubated for 1 min or 10 min and then re-oxidized with potassium ferricyanide (30 min at room temperature). Illumination of such samples at 200 K did not result in formation of the S_2 multiline signal (Fig. 2A,b and 2B,b) indicating that dithionite eliminated the S_1 state as expected from the experiment shown in Fig. 2. Illumination of the samples at room temperature with 3 flashes followed by 1 hour of dark adaptation, generated a state that gave rise to a S_2 multiline signal upon illumination at 200 K (Fig. 2A,c and 2B,c). This indicates that the reduced state formed by dithionite reduction can be reoxidized by light to form the usual S_1 state (or S_2 and S_3 states, which decay back to form S_1).

In principle, centers in S_{-2} would advance to S_1 with 3 flashes, centers in S_{-1} and S_0 would advance to S_2 and S_3 with 3 flashes, respectively. The S_2 and S_3 states are known to recombine or to be reduced by TyrD to form S_1 [21]. Any centers in S_{-3} (and below) would generate S_0 (and lower) with 3 flashes and a 200 K illumination would give no S_2 multiline signal. Thus any centre in S_{-3} and below would not be detectable in our experimental regime. To obtain a complete picture experiments using different illumination regimes (3 flashes, dark adapt, plus 1 flash etc) are required.

Shorter incubation times (1 min) with dithionite also showed no S_2 formation upon re-oxidation with potassium ferricyanide. However nearly 80 % of S_2 formation upon 200 K illumination was seen after 3 flashes and 1 h dark adaptation (Fig. 2B,c). This indicates that the majority of centers were in the S_0, S_{-1} or S_{-2} state after the dithionite treatment. O_2 evolution in such sample was around 70 %.

In the sample incubated with dithionite for 10 minutes (Fig.2A,c), the extent of the multiline seen was around 30 % of that seen in the unreduced control sample (Fig. 2A,a). The 3 flashes illumination means that the S_0, S_{-1} and S_{-2} states sum up to around 30 % of centers. Other experiments directly monitoring S_0 (Fig. 1) indicate that S_0 makes only a small contribution at this incubation time, i.e. the 30 % giving rise to the S_2 signal arise from S_{-1} and S_{-2} (or its formal equivalent S_{-1} TyrD). The other centers are presumably in more reduced forms of the cluster. Measurements of O_2 evolution showed that in this sample the O_2 evolution activity was 50 % of that in untreated samples. The difference between the activity and the centers giving rise to the S_2 signal presumably reflects centers that were further reduced than S_{-2} (or S_{-1}TyrD) but remained rapidly oxidizable and functional. The remaining centers are presumably either irreversibly damaged or require the low quantum yield assembly processes characteristic of photoactivation.

These experiments show that treatment with dithionite results in over-reduction of the Mn_4Ca cluster and that this can be photo-oxidised again when the ambient potential is returned to a potential range that allows reaction centre photochemistry to occur. Future experiments of this kind should allow us to define which states are formed at given times of incubation, so that new redox states formally corresponding to intermediates found in the photoactivation process can be studied spectroscopically.

4.3 Quinone reduction:

Figure 3 shows PSII reduced by dithionite and as expected semiquinone-iron signal is formed. The typical semiquinone EPR signal was generated after a reduction with dithionite for a short time incubation (less than 1 min) (Fig. 3C), with g-values of g~2, g~1.94 and g~1.73 as described in [14, 22] and (Sedoud et al, submitted). This EPR signal is similar to that found in non-treated PSII when $Q_A^{\bullet-}Fe^{2+}$ is generated by light at 77 K (Fig. 3B). This signal is attributed to $Q_A^{\bullet-}Fe^{2+}$ rather than $Q_B^{\bullet-}Fe^{2+}$, which is expected to be doubly reduced (to Q_BH_2) by dithionite. Fig. 3D showed the same sample after 30 min incubation in dark at room temperature. The regular semiquinone EPR signal shown in Fig. 3B is converted to a much broader and more intense signal with g-values of 1.94, 1.83, 1.73 and 1.64 (see stars in left panel of Fig.3). The new broad signal was virtually absent when the sample was re-oxidized with ferricyanide (Fig. 3E). The small residual signal might be from a fraction of centers that had not equilibrated with ferricyanide. Illumination at 200 K is expected to form $Q_A^{\bullet-}Fe^{2+}$. Under these conditions we observed that the final electron donor was the cytochrome b_{559} in the majority of centers, while in small fraction of centers TyrD and Chl_Z radicals were formed (not shown). No S_2 multiline EPR signal was formed, indicating unsurprisingly that S_1 state was absent, probably reflecting an over-reduction, and possibly the loss, of the Mn_4Ca cluster in some centers (see above). The photoinduced $Q_A^{\bullet-}Fe^{2+}$ EPR signal formed in the dithionite-treated PSII (Fig. 3E) resembles the signal found in dithionite-reduced PSII after 30 min incubation (Fig. 3D) and is different from the photoinduced $Q_A^{\bullet-}Fe^{2+}$ in the control without dithionite (Fig. 3B). This result is a further argument in favor of the assigning the new broad semiquinone EPR signal to $Q_A^{\bullet-}Fe^{2+}$.

The right panel of Fig. 3 showed the power saturation curve of the modified form of $Q_A^{\bullet-}Fe^{2+}$ measured at g~1.94 feature present in 30 min incubated dithionite-reduced PSII. This signal has fast relaxation behavior, which is typical of the other semiquinone-iron signals (the signals at g ~1.66, g~1.9 and g~2) (Sedoud et al, submitted). The fast relaxation properties of the new broad g~1.94 signal is consistent with its attribution to the $Q_A^{\bullet-}Fe^{2+}$ state.

4.4 Dithionite reduction seen by protein gel:

Fig. 4 shows the effect of dithionite reduction on PSII protein subunits. A band in the high molecular mass range (~90 kDa) disappears when PSII is reduced by dithionite, while bands appeared at the mass range of ~45 kDa. This indicates that the dithionite treatment affects the

PSII structure, perhaps the splitting of a 90 kDa “homodimer” into its constituents (see discussion).

4.5 An iron-sulfur cluster-type signal generated by dithionite:

Fig. 5 shows another signal induced upon dithionite reduction (Fig. 5B), detected at 15 K. This signal has the following g-values: 2.04, 1.91, with the latter feature showing a shoulder at a slightly lower g-value. This signal is reminiscent of an iron-sulfur cluster. Re-oxidation of the sample with ferricyanide resulted in the loss of this signal (Fig. 5C). The illumination of this reoxidised sample at 200 K did not result in formation of this signal (Fig. 5D) and the signal was never observed as a light induced species in other studies done of PSII. The double reduction of Q_A to Q_AH_2 in a sample (i.e. reduction with dithionite and illuminated strongly for 12 min) [20] did not affect this signal. This signal is detected and unmodified in formate-treated PSII when reduced by dithionite (data not shown). The double reduction of Q_A or the presence of formate as a ligand of the non-heme iron did not affect the presence of the iron-sulfur-like EPR signal. Thus this signal is not related to the semiquinone-iron complex of PSII (data not shown). This signal is also present in the dithionite-reduced Mn-depleted PSII (data not shown) and it was not formed by addition of sodium ascorbate, alone or in the presence of DAD.

5. Discussion:

We have found that at short times after dithionite addition to PSII dithionite the S_0 multiline EPR signal. Until now, the S_0 multiline was formed either photochemically or by NH_2OH reduction [16-17, 23]. The dithionite method represents a new method for generating the S_0 state with high yields and in highly concentrated samples. This should allow improved spectroscopic studies of this state.

We have found that after re-oxidation of the dithionite-reduced PSII by ferricyanide, the semiquinone state was lost due to its oxidation, while the Mn_4Ca cluster remained in an over-reduced state. This is not surprising since chemical oxidation of S-states is expected to require higher potentials than those obtainable with ferricyanide. The over-reduced state could however be efficiently re-oxidized by flashes illumination. Future experiments are needed to characterize the reduced PSII states present. Such experiments should help us clarify the nature of the over-reduced states, their valence and reactivity but also could help understand aspects of the photoassembly process, photoactivation.

The marked change in the Q_A semiquinone EPR signal after incubation in dithionite can be rationalized as reduction-induced structural change in PSII. The reasons for this are as follows. 1) The modified form of the $Q_A^{\bullet-}Fe^{2+}$ signal was generated by illumination when the dithionite treated sample was re-oxidized by ferricyanide. Thus the dithionite-reduction effect is irreversible, at least in our experimental conditions. 2) We know from previous work that the Mn_4Ca cluster when reduced by dithionite can undergo a change that sensed by the electron-acceptor side [8]. The assembly of the Mn_4Ca cluster is associated with conformation changes [12] and this influences the environment of Q_A [2]. The reversal of this process by chemical reduction is expected then to influence the Q_A. 3) The dithionite reduction caused the disappearance of a 90 kDa protein band and appearance of bands around 45 kDa in the SDS PAGE shown in Fig. 5. This could reflect the reduction of a disulfide bride in PSII.

One candidate is the disulfide bridge present in the PsbO subunit [24]. The reduction or mutation of this bridge has been shown to induce changes in the polypeptide structure, and mutation of the cysteins involved in this bridge result in a change of the apparent weight by ~10 kDa (reviewed in [25] and [24]) on SDS PAGE gels. The result shown in Fig. 4 is unlikely to be due to a change in the state of the PsbO bridge.

The 90 kDa protein band may correspond to the core of PSII constituted of D1-D2 with or without Cyt b559. If so then this might be due to a reduction of a disulfide bridge was present between D1 and D2 (D1-C211 and D2-C212), its reduction by dithionite could account for the effect that we report here. The current crystal structure does not show such a bridge, however the two cysteines D1-C211 and D2-C212 are close together (5.6 Å) just beneath the non-heme iron (9-10 Å from the iron and histidines ligands). The distance between those cysteines and the quinones is about 8 Å (see Fig. 6). At the current resolution it may be possible that a disulfide bridge exists under some conditions. We attempted to reproduce the effect of dithionite using reagents specific for disulfide bridge reduction such as dithiothreitol or TCEP, but they had no similar effect (not shown). This however is inconclusive as the putative bridge is hidden in the hydrophobic part of the membrane. The higher resolution crystal structure should answer this question, as well as identification by mass spectroscopy of the 90 kDa band.

The effect of dithionite reduction on the electron acceptor side has been studied for decades. Dithionite reduces Q_A and hence the fluorescence level increases. This gives rise to the change that is most commonly used to monitor the potential of Q_A^-. Some low potential phenomena have remained unexplained. Many researchers (see [1, 26-27]) have reported high redox potential at ~ -275 mV for $Q_A/Q_A^{\bullet-}$ couple in a redox titration measured by either EPR or fluorescence. It seems possible that these effects may correspond to a reduction-induced structural change giving rise to a higher fluorescence level from $Q_A^{\bullet-}$ (e.g. [27]), or a increased trapped Ph^- spilt signal [26]. We note that -275 mV value measured is almost exactly the expected value for a cysteine bridge. A redox titration of the new effect reported here should determine if this signal correlates to the classic -275 mV redox transition.
We note that this -275 mV transition is distinct from the slow and relatively irreversible second reduction step forming Q_AH_2 when PSII is reduced by dithionite and mediator at potentials lower than -400mV or by dithionite and strong illumination, e.g. [28].

The origin of the iron-sulfur like signal is difficult to explain. It seems to be specifically generated by dithionite and not by light. Although we consider it unlikely that the preparation is contaminated by iron-sulfur proteins this has to be the first explanation. A redox titration may help define what this species could be. A very speculative hypothesis is that the iron-sulfur signal may arise from the artefactual formation of an iron-sulfur cluster in PSII formed by cysteines (perhaps the putative bridging cysteines), sulfur from the dithionite and contaminating iron. A single pair of cyteines is not sufficient to complete the coordination of a 2Fe2S centre. It is possible that the centre is more like a Rieske centre with 2 imidazoles completing the coordination e.g [29]. It would be interesting to see if two of the His residues that coordinate the iron in PSII could also coordinate one half of a Rieske like centre in PSII. Should this occur, it is probably in a small fraction of damaged centers.

This is all very speculative but it may be of relevance to the evolution of reaction centers. It is generally agreed that a transition occurred between type I (FeS containing) and type 2 (non-heme iron containing) reaction centers. There have been no clues as to how this might have occurred. Here this gross speculation is presented simply because of the possibility that it provides the first potential clue for understanding this evolutionary of this transition. More experiments are needed to resolve this question and several others raised in this manuscript. The coming high resolution crystal structure will also have a bearing on these questions.

Acknowledgments: This work was supported by the EU/Energy Network project SOLAR-H2 (FP7 contract 212508). Arezki Sedoud is supported by the IRTELIS training program of the CEA. We would like to thank A. Boussac, Pierre Sétif, A. Krieger-Liszkay and D. Kirilovsky for helpful discussion.

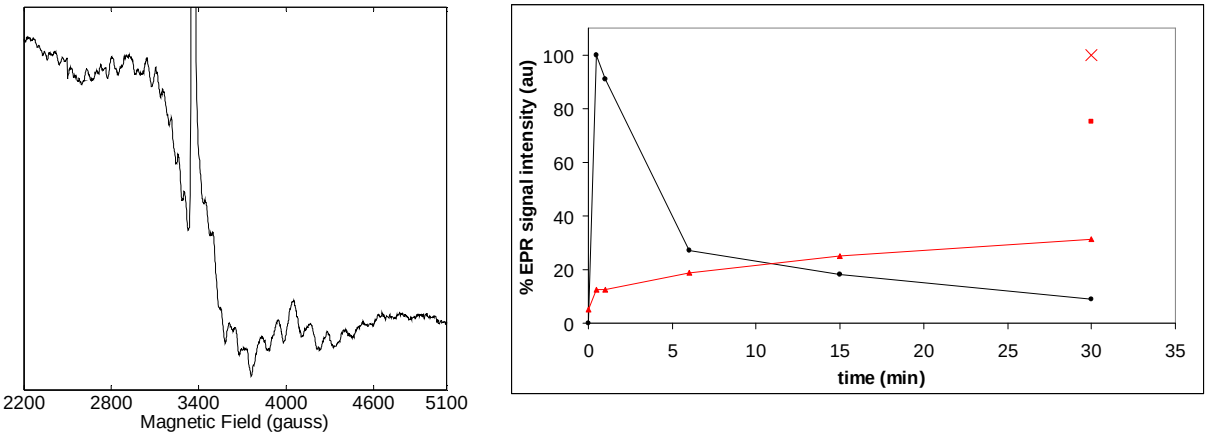

Figure 1: S_0 state induced by dithionite reduction. PSII was reduced by dithionite and frozen right after the dithionite reduction (less than 1 min). Right panel shows the decay of S_0 (black) and Mn^{2+} formation (red). The red square shows the Mn^{2+} level after addition of a redox mediator (indigodisulfonate, E_m = -125 mV). The red cross shows the maximum level of Mn^{2+} that was obtained after 12 min illumination with strong white light at room temperature.

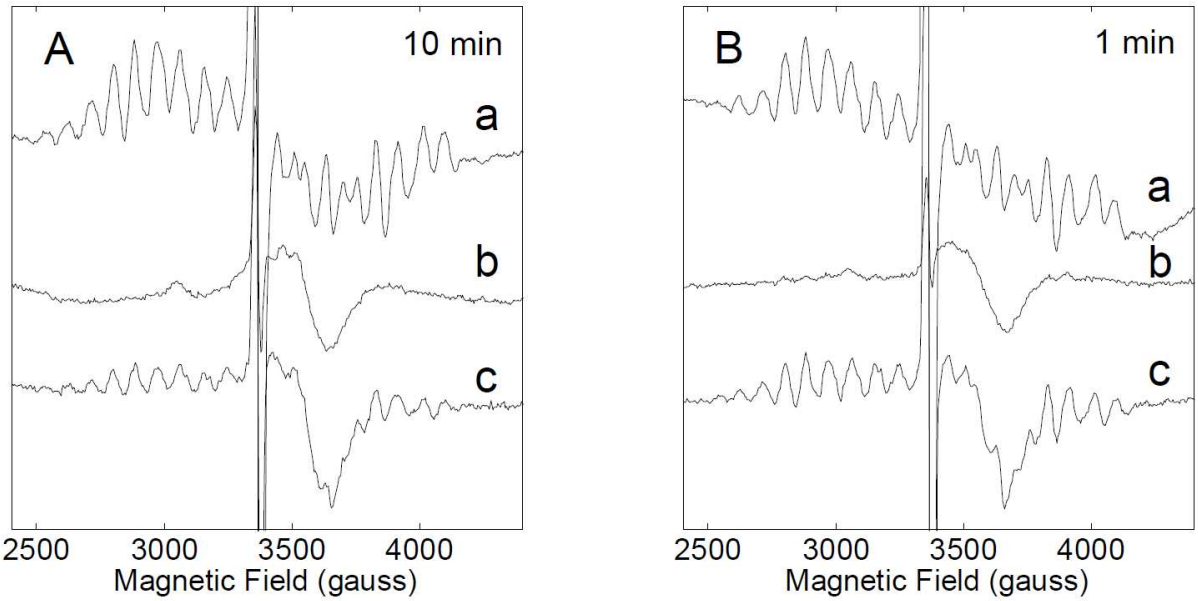

Figure 2: Effect of sodium dithionite on the formation of S_2 multiline EPR signal.

PSII complexes were incubated 10 min (panel A) or 1 min (panel B) in the absence (a) and in the presence of 2 mM of sodium dithionite (b,c). All spectra were difference spectra after 200 K illumination (light-*minus*-dark). (a) Untreated PSII; (b) PSII complexes reduced by sodium dithionite and reoxidized by potassium ferricyanide; (c) sample b was thawed and then was dark adapted at room temperature for 30 min, illuminated by a series of 3 flashes and finally dark adapted for 30 min. Instrument settings: microwave power, 20 mW; modulation amplitude, 25 gauss; temperature, 8.5 K.

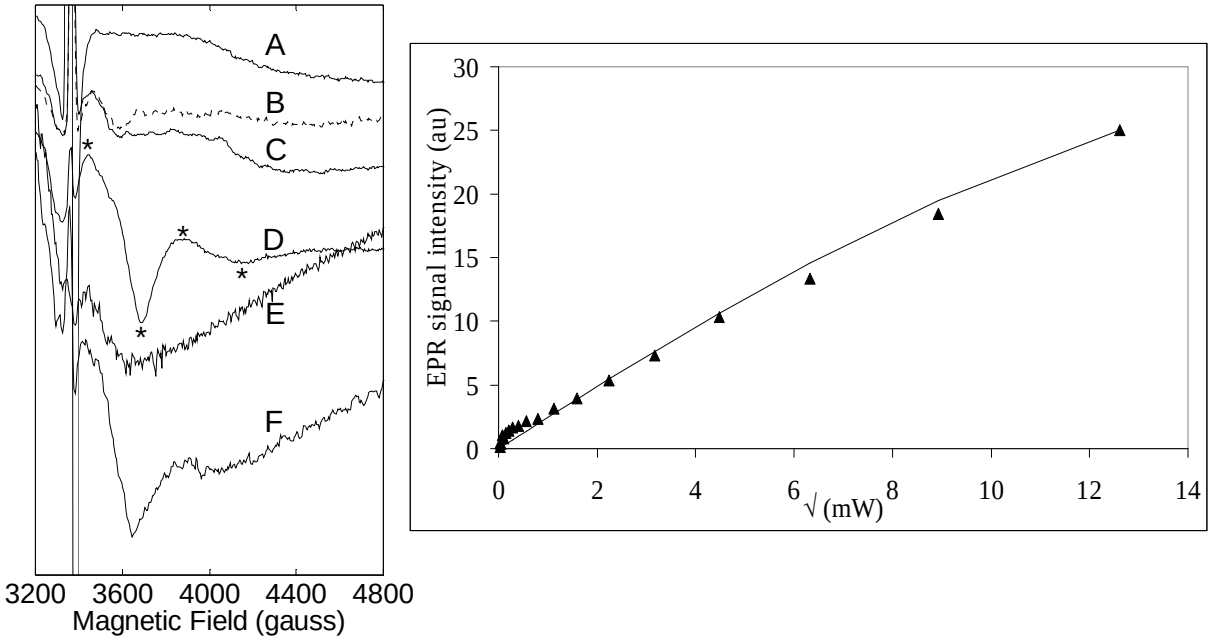

Figure 3: Quinone dithionite-reduction. In left panel; A) Spectrum of long-dark incubated PSII (12h). B) 77 K Light-*minus*-dark representing the photoinduced $Q_A^{\bullet-}Fe^{2+}$ state for comparison. C) Dithionite reduction after 1 min. D) the same sample after 30 min. E) Ferricyanide oxidation (30 min). F) Illumination of the sample presented in (E) at 200 K. Right panel shows the microwave power saturation of the g~1.94 found $Q_A^{\bullet-}Fe^{2+}$ state in the dithionite-reduced PSII that was incubated 30 min. The stars in the left panel labeled the main g-values measured in the $Q_A^{\bullet-}Fe^{2+}$ state in the dithionite-reduced PSII that was incubated 30 min, the g-values were: 1.94, 1.83, 1.73 and 1.64.

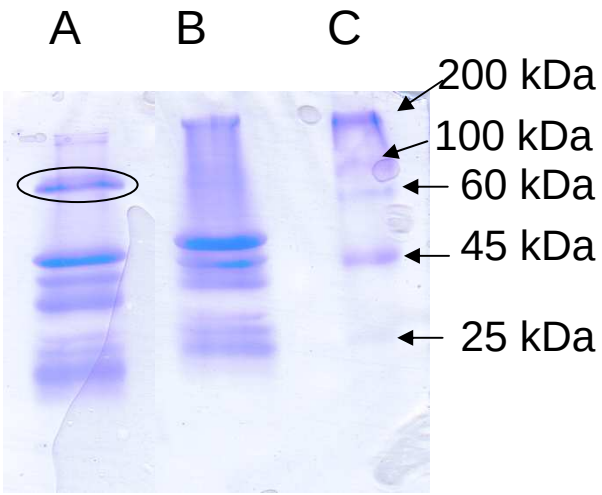

Figure 4: Protein gel. A) PSII control. B) dithionite-reduced PSII. C) Label. 12% SDS non-reducing gel, the circle shows the band that disappears in dithionite-treated PSII.

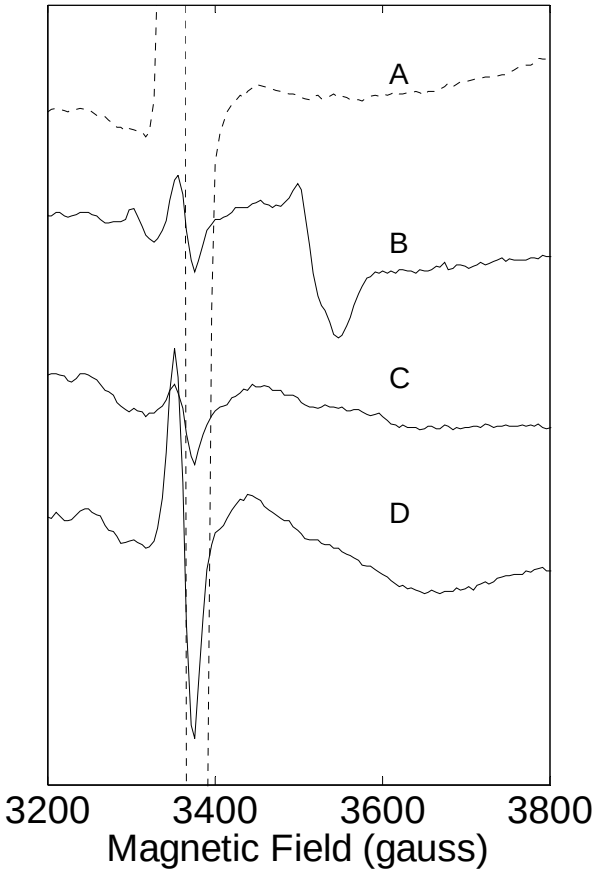

Figure 5: dithionite reduction induces a sulfur-iron EPR type signal. A) PSII long-dark adapted (12h) at room temperature. B) Dithionite reduction for less than 1 min. C) Ferricyanide oxidation. D) Illumination at 200K. Spectra recorded at 15K.

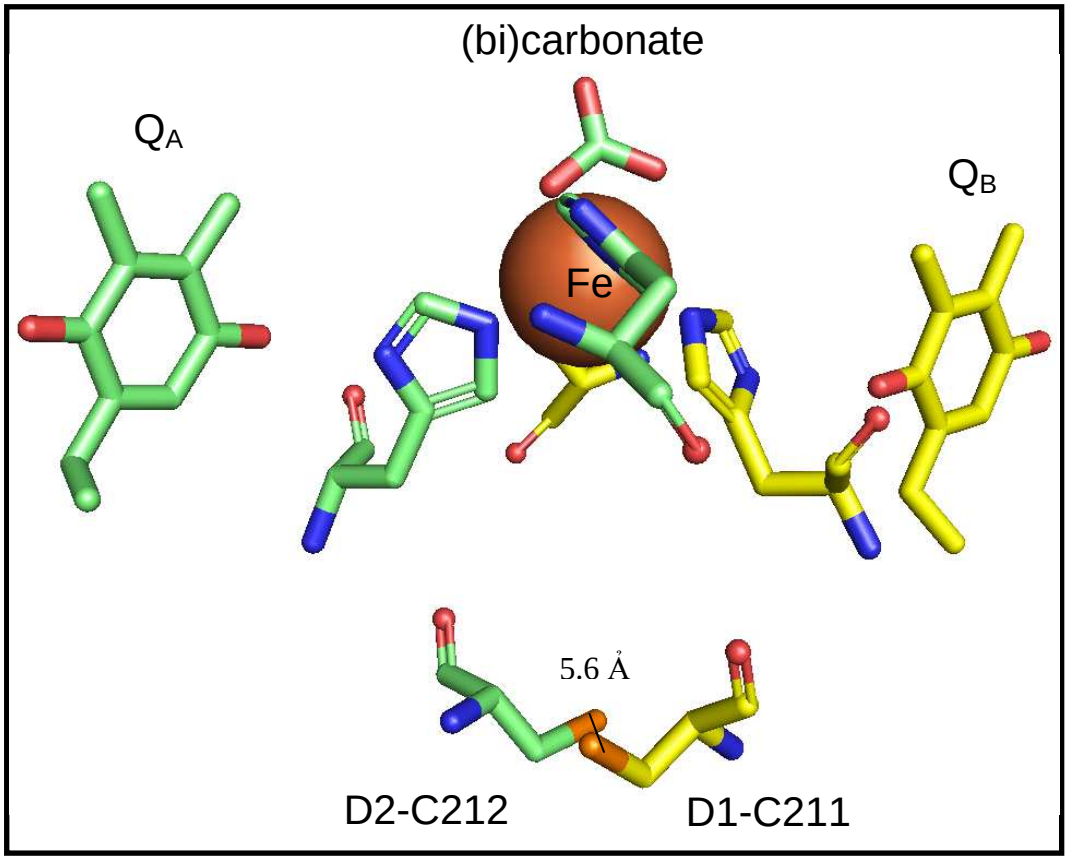

Figure 6: Electron acceptor side structure of PSII (PDB:3BZ1) [30]. Q_A, Q_B, non-heme iron and its hisitidines and (bi)carbonate ligands, D1-C211 and D2-C212 are shown. Figure generated by Pymol.

References

[1] A. Krieger, A.W. Rutherford, G.N. Johnson, On the determination of redox midpoint potential of the primary quinone electron-acceptor, Q_A, in Photosystem-II, Biochim Biophys Acta, 1229 (1995) 193-201.
[2] G.N. Johnson, A.W. Rutherford, A. Krieger, A change in the midpoint potential of the quinone Q_A in Photosystem-II associated with photoactivation of oxygen evolution, Biochim Biophys Acta, 1229 (1995) 202-207.
[3] T. Shibamoto, Y. Kato, M. Sugiura, T. Watanabe, Redox potential of the primary plastoquinone electron acceptor Q_A in Photosystem II from *Thermosynechococcus elongatus* determined by spectroelectrochemistry, Biochemistry, 48 (2009) 10682-10684.
[4] A. Krieger, E. Weis, The role of calcium in the pH-dependent control of Photosystem-II, Photosynth Res, 37 (1993) 117-130.
[5] T. Ono, Y. Inoue, Requirement of divalent-cations for photo-activation of the laten water-oxidation system in intact chloroplasts from flashed leaves, Biochimica et Biophysica Acta (BBA) - Bioenergetics
723 (1983) 191-201.
[6] N. Tamura, G. Cheniae, Photoactivation of the water-oxidizing complex in Photosystem-II membranes depleted of Mn and extrinsic proteins .1. Biochemical and kinetic characterization, Biochim Biophys Acta, 890 (1987) 179-194.
[7] K.N. Ferreira, T.M. Iverson, K. Maghlaoui, J. Barber, S. Iwata, Architecture of the photosynthetic oxygen-evolving center, Science, 303 (2004) 1831-1838.
[8] A. Krieger-Liszkay, C. Fufezan, A. Trebst, Singlet oxygen production in photosystem II and related protection mechanism, Photosynth Res, 98 (2008) 551-564.
[9] A. Haddy, EPR spectroscopy of the manganese cluster of photosystem II, Photosynth Res, 92 (2007) 357-368.
[10] F.M. Ho, Uncovering channels in photosystem II by computer modelling: current progress, future prospects, and lessons from analogous systems, Photosynth Res, 98 (2008) 503-522.
[11] J.W. Murray, J. Barber, Structural characteristics of channels and pathways in photosystem II including the identification of an oxygen channel, J Struct Biol, 159 (2007) 228-237.
[12] J. Dasgupta, G.M. Ananyev, G.C. Dismukes, Photoassembly of the water-oxidizing complex in photosystem II, Coordin. Chem. Rev, 252 (2008) 347-360.
[13] F. Guerrero, A. Sedoud, D. Kirilovsky, A.W. Rutherford, J.M. Ortega, M. Roncel, A high redox potential form of cytochrome c550 in Photosystem II from Thermosynechococcus elongatus, J. Biol. Chem, (2010).
[14] A. Sedoud, L. Kastner, N. Cox, S. El-Alaoui, D. Kirilovsky, A.W. Rutherford, Effects of formate binding on the quinone-iron electron acceptor complex of photosystem II, Biochim Biophys Acta, 1807 (2011) 216-226.
[15] J. Sambrook, E.F. Frirsch, T. Maniatis, Molecular cloning: A laboratory manuel, Cold Spring Harbor: Cold Sping Harbor Laboratory, 2001.
[16] J. Messinger, J.H. Robblee, W.O. Yu, K. Sauer, V.K. Yachandra, M.P. Klein, The S-0 state of the oxygen-evolving complex in photosystem II is paramagnetic: Detection of EPR multiline signal, J Am Chem Soc, 119 (1997) 11349-11350.
[17] K.A. Ahrling, S. Peterson, S. Styring, An oscillating manganese electron paramagnetic resonance signal from the S-0 state of the oxygen evolving complex in photosystem II, Biochemistry, 36 (1997) 13148-13152.

[18] C.W. Hoganson, P.A. Casey, O. Hansson, Flash-Photolysis Studies of Manganese-Depleted Photosystem-Ii - Evidence for Binding of Mn2+ and Other Transition-Metal Ions, Biochim Biophys Acta, 1057 (1991) 399-406.
[19] I. Vass, L. Sass, C. Spetea, A. Bakou, D.F. Ghanotakis, V. Petrouleas, UV-B-induced inhibition of photosystem II electron transport studied by EPR and chlorophyll fluorescence. Impairment of donor and acceptor side components, Biochemistry, 35 (1996) 8964-8973.
[20] F.J.E. van Mieghem, W. Nitschke, P. Mathis, A.W. Rutherford, The Influence of the Quinone-Iron Electron-Acceptor Complex on the Reaction Center Photochemistry of Photosystem-Ii, Biochim Biophys Acta, 977 (1989) 207-214.
[21] A.W. Rutherford, A. Boussac, P. Faller, The stable tyrosyl radical in Photosystem II: why D?, Biochim Biophys Acta, 1655 (2004) 222-230.
[22] N. Cox, L. Jin, A. Jaszewski, P.J. Smith, E. Krausz, A.W. Rutherford, R. Pace, The semiquinone-iron complex of Photosystem II: structural insights from ESR and theoretical simulation; evidence that the native ligand to the non-heme iron is carbonate, Biophys. J., 97 (2009) 2024-2033.
[23] A. Boussac, H. Kuhl, E. Ghibaudi, M. Rogner, A.W. Rutherford, Detection of an electron paramagnetic resonance signal in the S_0 state of the manganese complex of photosystem II from *Synechococcus elongatus*, Biochemistry, 38 (1999) 11942-11948.
[24] A.K. Williamson, Structural and functional aspects of the MSP (PsbO) and study of its differences in thermophilic versus mesophilic organisms, Photosynth Res, 98 (2008) 365-389.
[25] A.J. Wyman, C.F. Yocum, Structure and activity of the photosystem II manganese-stabilizing protein: Role of the conserved disulfide bond, Photosynth Res, 85 (2005) 359-372.
[26] A.W. Rutherford, P. Mathis, A relationship between the midpoint potential of the primary acceptor and low-temperature photochemistry in Photosystem-II, Febs Lett, 154 (1983) 328-334.
[27] A.P.G.M. Thielen, H.J. van Gorkom, Redox potentials of electron-acceptors in Photosystem II-Alpha and II-Beta, Febs Lett, 129 (1981) 205-209.
[28] A.W. Rutherford, D.R. Paterson, J.E. Mullet, A light-induced spin-polarized triplet detected by Electron-Paramagnetic-Res in Photosystem-II reaction centers, Biochim Biophys Acta, 635 (1981) 205-214.
[29] J. Meyer, Iron-sulfur protein folds, iron-sulfur chemistry, and evolution, J. Biol. Inorg. Chem., 13 (2008) 157-170.
[30] A. Guskov, J. Kern, A. Gabdulkhakov, M. Broser, A. Zouni, W. Saenger, Cyanobacterial photosystem II at 2.9-angstrom resolution and the role of quinones, lipids, channels and chloride, Nat Struct Mol Biol, 16 (2009) 334-342.

ARTICLE 6

A high redox potential form of cytochrome *c550* in Photosystem II from *Thermosynechococcus elongatus*.

THE JOURNAL OF BIOLOGICAL CHEMISTRY VOL. 286, NO. 8, pp. 5985–5994, February 25, 2011

A High Redox Potential Form of Cytochrome c_{550} in Photosystem II from *Thermosynechococcus elongatus*[*] [S]

Received for publication, July 30, 2010, and in revised form, December 3, 2010 Published, JBC Papers in Press, December 6, 2010, DOI 10.1074/jbc.M110.170126

Fernando Guerrero[‡§], Arezki Sedoud[§¶], Diana Kirilovsky[§¶], A. William Rutherford[§¶], José M. Ortega[‡], and Mercedes Roncel[‡1]

From the [‡]Instituto de Bioquímica Vegetal y Fotosíntesis, Universidad de Sevilla-CSIC, Américo Vespucio 49, 41092 Sevilla, Spain, the [§]Commissariat à l'Énergie Atomique, Institut de Biologie et Technologies de Saclay (iBiTec-S), 91191 Gif-sur-Yvette, France, and the [¶]Centre National de la Recherche Scientifique, URA 2096, 91191 Gif-sur-Yvette, France

Cytochrome c_{550} (cyt c_{550}) is a component of photosystem II (PSII) from cyanobacteria, red algae, and some other eukaryotic algae. Its physiological role remains unclear. In the present work, measurements of the midpoint redox potential (E_m) were performed using intact PSII core complexes preparations from a histidine-tagged PSII mutant strain of the thermophilic cyanobacterium *Thermosynechococcus* (*T.*) *elongatus.* When redox titrations were done in the absence of redox mediators, an E_m value of +200 mV was obtained for cyt c_{550}. This value is ~300 mV more positive than that previously measured in the presence of mediators (E_m = −80 mV). The shift from the high potential form (E_m = +200 mV) to the low potential form (E_m = −80 mV) of cyt c_{550} is attributed to conformational changes, triggered by the reduction of a component of PSII that is sequestered and out of equilibrium with the medium, most likely the Mn_4Ca cluster. This reduction can occur when reduced low potential redox mediators are present or under highly reducing conditions even in the absence of mediators. Based on these observations, it is suggested that the E_m of +200 mV obtained without mediators could be the physiological redox potential of the cyt c_{550} in PSII. This value opens the possibility of a redox function for cyt c_{550} in PSII.

In all photosynthetic oxygen-evolving organisms, the primary steps of light conversion take place in a large pigment-protein complex named PSII,[2] which drives light-induced electron transfer from water to plastoquinone with the concomitant production of molecular oxygen (for review, see Ref. 1). The reaction center of PSII is made up of two membrane-spanning polypeptides, D1 and D2, which bind four chlorophylls, two pheophytins, two quinones, Q_A and Q_B (the primary and secondary quinone acceptors of the reaction centre of PSII), a non-heme iron atom, and a cluster made up of four manganese ions and one calcium ion. In green algae and higher plants, three extrinsic proteins are associated to reaction center in water-splitting active PSII complexes: 23–24, 16–18, and 33 kDa proteins, whereas in cyanobacteria, red algae and some other eukaryotic algae, cyt c_{550}, 12 kDa and 33 kDa proteins are found. The three-dimensional structure of PSII confirmed that cyt c_{550} binds on the lumenal membrane surface in the vicinity of the D1 and CP43 (2–6).

Cyt c_{550}, encoded by the *psbV* gene, is a monoheme protein with a molecular mass of ≈ 15 kDa and an isoelectric point between 3.8 and 5.0 (7, 8). The recent resolution of the three-dimensional structure of the soluble form of cyt c_{550} from three cyanobacteria, *Synechocystis* sp. PCC 6803 (9), *Arthrospira maxima* (10), and *Thermosynechococcus elongatus* (11) has confirmed a previously proposed bis-histidine coordinated heme that is very unusual for monoheme *c*-type cytochromes (8, 11, 12). Crystal structures of both isolated and PSII-bound forms of cyt c_{550} show that the protein presents a hydrophobic inner core typical of monoheme cytochromes *c*, with three helices forming a nest for the prosthetic group and a fourth helical segment in the N-terminal domain protecting the heme from solvent, indicating that the heme structure is not very different from most *c*-type cytochromes (13).

The exact physiological role of cyt c_{550} is unclear. Extensive research has established that it does not participate in the main photosynthetic reactions despite its close proximity (22 Å) to the water oxidation complex. Cyt c_{550} is thus suggested to play the same role as the other (albeit cofactor-less) extrinsic proteins. By stabilizing the neighboring proteins and protecting the manganese cluster from external reductants, it stabilizes the oxygen-evolving complex (14, 15). Studies of phenotype of the cyt c_{550}-less mutant (ΔPsbV) of *Synechocystis* sp. PCC 6803 have shown that both the cyt c_{550} and the 12-kDa protein stabilize the binding of the Ca^{2+} and Cl^- ions, which are essential for the oxygen-evolving activity of PSII, in a manner analogous to the extrinsic 17 and 24 kDa polypeptides of higher plants (14, 16, 17). The fact that cyt c_{550} can be isolated as a soluble protein (7, 8, 18–20) suggests that other functions not directly related to PSII are possible for this protein. Several nonphotosynthetic roles have been suggested for cyt c_{550}. In fact, a function related to anaerobic disposal of electrons from carbohydrates reserves or fermentation to sustain an organism during prolonged dark and anaerobic conditions have been proposed (19, 21, 22). According to Shen and Inoue (23), cyt c_{550} can accept electron from ferredoxin II in

* This work was supported by grants from the Ministry of Education and Culture of Spain (BFU2007-68107-C02-01/BMC, cofinanced by FEDER), and Andalusia Government (PAI CVI-261) and the EU/Energy Network project SOLAR-H2 (FP7 Contract 212508).

[S] The on-line version of this article (available at http://www.jbc.org) contains supplemental Fig. S1.

[1] To whom correspondence should be addressed: Instituto de Bioquímica Vegetal y Fotosíntesis, Universidad de Sevilla-Consejo Superior de Investigaciones Científicas, Américo Vespucio 49, 41092 Sevilla, Spain. Tel.: 34-954-489525; Fax: 34-954-460065; E-mail: mroncel@us.es.

[2] The abbreviations used are: PSII, photosystem II; cyt b_{559}, cytochrome b_{559}; cyt c_{550}, cytochrome c_{550}; Cm, chloramphenicol; Chl, chlorophyll.

the presence of sodium dithionite and is proposed to remove excess electrons in anaerobically grown cells.

The E_m of cyt c_{550} is one of the key parameters for elucidating the biological role of this cytochrome. An E_m value at pH 7.0 (E_{m7}) of −260 mV was the first to be reported for purified cyt c_{550} from *Anacystis nidulans* (20). Cyt c_{550} from *Microcystis aeruginosa* and *Aphanizomenon flos-aquae* were found to be reducible by sodium dithionite ($E_{m7} = -420$ mV), but not by sodium ascorbate ($E_{m7} = +58$ mV) (7). Later, E_{m7} values from −280 to −314 mV were obtained for purified cyt c_{550} from the same species (12) and an E_{m7} of −250 mV from *Synechocystis* sp. PCC 6803 (8). In previous work, we determined an E_{m6} value of −240 mV for the soluble form of cyt c_{550} from the thermophilic cyanobacterium *T. elongatus* after its extraction from PSII (24). Such low redox potentials are well below the range normally expected for a mono-heme *c*-type cytochrome and seem incompatible with a redox function in PSII electron transfer. Using an electrochemical technique, a value 150 mV more positive ($E_{m7} \approx -100$ mV) was measured for E_m of cyt c_{550} from *Synechocystis* sp. PCC 6803 adsorbed to an electrode surface (13). This higher value was attributed to the exclusion of water from the site due to the protein binding to the electrode (13). The E_m for cyt c_{550} associated with PSII was not established until our group was able to measure it using intact PSII core complexes preparations from *T. elongatus.* Using potentiometric redox titrations, a significantly higher E_m value was obtained for cyt c_{550} when bound to PSII ($E_{m6} = -80$ mV) compared with its soluble form after its extraction from PSII ($E_{m6} = -240$ mV) (24). Moreover, although the E_m of the bound form is pH-independent, the E_m of the soluble form varies from −50 mV at pH 4.5 to −350 mV at pH 9–10 (24). The difference of E_m between the isolated and the PSII-bound forms of cyt c_{550} has been confirmed by theoretical calculations based on crystal structures of the isolated and PSII-bound forms (25). Some authors (13, 24, 26) have proposed that in conditions more native than isolated PSII core complexes, it is possible that the E_m of cyt c_{550} may be even higher than −80 mV, and thus a redox function in the water oxidation complex could be conceivable. Therefore, the precise determination of the redox potential of this protein is of fundamental importance to the understanding its function.

One of the most standard techniques for determining redox potentials of proteins is the redox potentiometry. It involves measuring the ambient redox potential (E_h) while simultaneously determining the concentration of the oxidized and reduced forms of the protein using a spectroscopic technique. Meaningful results will be obtained only if chemical equilibrium is achieved between the various species in solution and electrochemical equilibrium is established at the electrode solution interface (27, 28). Unlike many small inorganic and organic redox couples, most redox proteins do not establish stable potentials because the heterogeneous charge-transfer (electrochemical) rates are low. A predominant reason for this is that the redox center is often shielded by protein and so does not gain proper contact with the electrode surface. Redox mediators are required to act as go-betweens between the measuring electrode and the biological redox couple and thus to get rates of the electron transfer between electrode, mediator and biological component rapid enough to achieve a true equilibrium (*i.e.* one where all redox complexes in the biological electron transfer system are at the same E_h) (29). Therefore, in most redox titrations of proteins, equilibrium is ensured by the addition of a mixture of redox mediators that establishes rapid (heterogeneous) electro-chemical equilibrium with the electrode and rapid (homogeneous) electron transfer with the protein without chemically modifying it in any way.

It has been reported that the E_m of Q_A in PSII-enriched membranes was affected by the presence of redox mediators at low ambient potentials. As consequence of this, a change in the redox potential from −80 mV (active form) to +65 mV (inactive form) has been determined in the potentiometric titrations performed on PSII membranes. This effect was attributed to the loss of the very high potential Mn_4Ca cluster due to reductive attack by the mediators and the sodium dithionite itself under some conditions (30). This was confirmed by the observation that the low potential, active form of the Q_A/Q_A^- couple could be regenerated when the manganese cluster was reconstituted (31). The binding and debinding of the Mn_4Ca cluster and even of the Ca^{2+} ion is considered to be associated with conformational changes that are manifest far from the binding site itself (30, 31).

Based on these observations and taking account that in most of redox titrations of cyt c_{550} bound to PSII, equilibration was ensured by the addition of a mixture of redox mediators (24, 26), it seemed possible that E_m of cyt c_{550} when bound to PSII could suffer from this unexpected technical difficulty. The presence of these mediators could have led to the reduction of the manganese cluster, the consequent loss of the Ca^{2+} and Mn^{2+} ions and associated conformation changes in the protein. The E_m value obtained for cyt c_{550} may not reflect the fully intact form of the PSII-bound cytochrome.

The main objective of this work has been to re-evaluate the redox potential of cyt c_{550} associated with PSII considering the effect of redox mediators. To check for the latter possibility, redox titration experiments were performed using highly active and intact core complexes preparations of PSII from *T. elongatus* testing the presence and absence of redox mediators and different redox mediators.

EXPERIMENTAL PROCEDURES

Strain and Standard Culture Conditions—WT and His-tag CP43 mutant *T. elongatus* cells were grown in a DTN medium (32). Cultures were carried out in 3-liter flasks in a rotary shaker (120 rpm) at 45 °C under continuous illumination from fluorescent white lamps (100 microeinsteins m^{-2} s^{-1}) and CO_2-enriched atmosphere. For maintenance, the His-tag CP43 mutant cells were grown in the presence of chloramphenicol (Cm) (5 μg ml^{-1}) at 45 °C under continuous illumination from fluorescent white lamps (40 microeinsteins m^{-2} s^{-1}).

Construction of Plasmid for His-Tag CP43 T. elongatus Mutant—For constructing a plasmid for expression of His-tagged *psbC* in *T. elongatus*, the genome region containing the *psbD1*, *psbC* and *tlr1632* genes was amplified by PCR.

Genomic DNA of *T. elongatus* as template and the primers *CP43a* (5′-ATGACGATCGCGATTGGACGA-3′) and *CP43b* (5′-GCAATCCAATGATGGACTTAG-3′) were used. The amplified region was digested by KpnI and BamHI, and it was cloned in a pBluescript KS+ plasmid also previously digested by the same restriction enzymes. Then, by site-directed mutagenesis, the bases coding for six histidines were added in the 3′ terminal of the *psbC* gene using the synthetic oligonucleotides *CP43* His-tag a (5′-CCTCTCGATGCCCA-GCCTTGATCACCATCACCATCACCATTAGGGTTACT-GAGTCAACTTAA-3′) and *CP43* His-tag b (5′-TTAAGTT-GACTCAGTAACCCTAATGGTGATGGTGATGGTGATC-AAGGCTGGGCATCGAGAGG-3′). An SmaI site was created between the *psbC* and *tlr1632* genes using the oligonucleotides *CP43SmaIa* (5′-ACCATTAGGGTTCCCGGGT-CAACTTAACTC-3′) and *CP43SmaIb* (5′-GAGTTAAGTT-GACCCGGGAACCCTAATGGT-3′). Finally, a Cm-resistance cassette was introduced in the SmaI site. The Cm resistance cassette was obtained by amplification by PCR of a 1.1-kb fragment of the plasmid pBC SK+ Cm^R using the synthetic oligonucleotides *Cam1.1a* (5′-GCTGTGACGGAA-GATCACTTCGC-3′) and *Cam1.1b* (5′-GCTCCACGGGGA-GAGCCTGAGCA-3′). The construction obtained, pCH-Cm, was a plasmid of 7 kb. To increase the chances for *T. elongatus* transformation, this plasmid was digested by the restriction enzyme EcoRI deleting the *psbD* gene and the beginning of the *psbC* gene. The 5-kb plasmid obtained, named pCH-5.1, was used to transform WT *T. elongatus* cells.

Transformation of T. elongatus Cells and Genetic Analysis of Mutants—The pCH-5.1 plasmid containing the His-tagged psbC gene and the Cm-resistance cassette was introduced into WT *T. elongatus* cells by electroporation according to (32) with slight modifications as described in Ref. 26, creating the His-tag CP43 strain (WT′). After electroporation, cells were rapidly transferred to 2 ml of DTN medium and incubated for 48 h in a rotary shaker at 45 °C under low light conditions. Then, the cells in 0.1–0.2-ml aliquots were spread on agar plates containing Cm (2 μg ml^{-1}) and incubated at 45 °C under dim light and humidified atmosphere. After 2–3 weeks, transformants emerged as green colonies; then, these colonies were spread at least twice on agar plates containing 5 μg ml^{-1} Cm. Genomic DNA was isolated from *T. elongatus* cells essentially as described by Cai and Wolk (33). Total segregation of the mutation was checked by PCR amplification of the genome region containing the *psbC* gene and the gene for Cm resistance. The PCR gave a fragment of 3.6 kb containing the *psbC* and the Cm resistance gene, instead of a fragment of 2.5 kb observed in the WT therefore demonstrating the complete segregation of the mutant. Confirmation of the presence of the His-tag was done by sequencing of the amplified DNA fragment.

PSII Core Complex Preparation—PSII core complexes were prepared from cells of *T. elongatus* as described by Kirilovsky *et al.* (26). The PSII core complexes preparations were resuspended in 40 mM MES, pH 6.5, 15 mM $CaCl_2$, 15 mM $MgCl_2$, 10% glycerol, and 1 M glycinebetaine at ~2–3 mg of Chl ml^{-1} and stored in liquid N_2. The preparations used in this work had an oxygen evolution activity of 2700–3200 μmol O_2 mg Chl^{-1} h^{-1}.

Redox Potential Measurements—Potentiometric redox titrations were carried out basically as described in Roncel *et al.* (24). For titrations, samples contained PSII core complexes (30–50 μg Chl ml^{-1}) were suspended in 2.5-ml buffer containing 40 mM MES, pH 6.5. When indicated, a set of the following eight redox mediators was added: 10 μM *p*-benzoquinone (E_{m7} = +280 mV), 20 μM 2,3,5,6-tetramethyl-*p*-phenylendiamine (also called diaminodurol) (E_{m7} = +220 mV), 10 μM 2,5-dimethyl-*p*-benzoquinone (E_{m7} = +180 mV), 20 μM *o*-naphthoquinone (E_{m7} = +145 mV), 2.5 μM *N*-methylphenazonium methosulfate (E_{m7} = +80 mV), 10 μM *N*-methylphenazonium ethosulfate (E_{m7} = +55 mV), 20 μM duroquinone (E_{m7} = +10 mV) and 30 μM 2-methyl-*p*-naphthoquinone (E_{m7} = 0 mV). Some redox titrations were carried out in the absence of these redox mediators or in the presence of diaminodurol only. Experiments were done at 20 °C under argon atmosphere and continuous stirring.

Reductive titrations were performed by first oxidizing the samples to $E_h \approx +450$ mV with potassium ferricyanide and then reducing it stepwise with sodium dithionite. For oxidative titrations, the samples were first reduced to $E_h \approx -350$ mV with sodium dithionite and then oxidized it stepwise with potassium ferricyanide. In both cases, after the additions of potassium ferricyanide or sodium dithionite, the absorption spectrum between 500 and 600 nm and the redox potential of the solution were simultaneously recorded by using, respectively, an Aminco DW2000 UV-vis spectrophotometer and a Metrohm Herisau potentiometer provided with a combined Pt-Ag/AgCl microelectrode (Crison Instruments, Spain). Differential spectra of cyt b_{559} and cyt c_{550} in PSII core complexes were obtained by subtracting the absolute spectra recorded at each E_h during titrations from the spectra of the fully oxidized state of each cytochrome (reductive titrations) or from the spectra of the fully reduced state of each cytochrome (oxidative titrations). The absorbance differences at 559–570 nm for cyt b_{559} and 549–538 nm for cyt c_{550} obtained from these spectra were normally converted into percentages of reduced cytochrome and plotted *versus* solution redox potentials. The E_m values were then determined by fitting the plots to the Nernst equation for one-electron carrier (n = 1) with 1 or 2 components as needed and using a nonlinear curve-fitting program (Origin version 6.0, Microcal Software).

EPR Measurements—EPR spectra were recorded using a Bruker Elexsys 500 X-band spectrometer equipped with a standard ER 4102 resonator and an Oxford Instruments ESR 900 cryostat. Instrument settings were as follows: microwave frequency, 9.4 GHz; modulation frequency, 100 kHz. All other settings were as indicated in the legend of Fig. 6. 120-μl aliquots of PSII cores (~ 1 mg Chl ml^{-1}) in the same buffer used for storage were loaded into 4-mm outer diameter quartz EPR tubes. The EPR samples were frozen in a dry ice/ethanol bath at 200 K. Samples were degassed by pumping at 200 K and then filled with helium gas. EPR tubes were then transferred to liquid nitrogen prior to the EPR measurements being made. Samples were handled in darkness. Reduction was per-

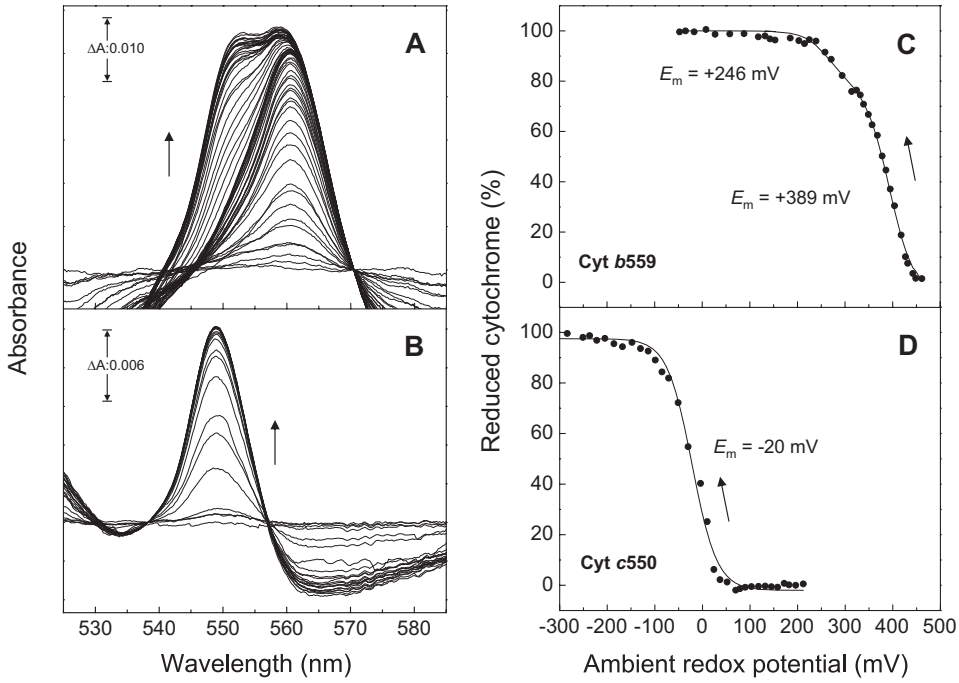

FIGURE 1. **Reductive potentiometric titrations of cyt b_{559} and c_{550} in PSII core complexes in the presence of a mixture of eight redox mediators covering the potential range between +430 and 0 mV.** *A* and *B*, difference absorption spectra in the α-band region of cyt b_{559} and cyt c_{550}. The spectra were obtained by subtracting absolute spectra recorded during the course of the redox titration between +455 and −80 mV minus the spectrum recorded at +455 mV (*A*) and the spectra recorded between +210 mV and −300 mV minus the absolute spectrum recorded at +210 mV (*B*). For simplification, only a set of selected spectra are included in *A* and *B*. *C* and *D*, plot of the percentages of reduced cyt b_{559} and reduced cyt c_{550} obtained from the absorbance differences at 559–570 nm and 549–538 nm *versus* ambient redox potentials, respectively. The *solid curves* represent the best fit of the experimental data to the Nernst equation in accordance with one-electron processes ($n = 1$) for two components (*C*) with an E_m of +246 mV (20%) and +389 mV (80%) and for one component (*D*) with an E_m of −20 mV.

formed by addition of sodium dithionite to the sample in the EPR tube to give a final concentration of 2 mM using a 30 mM stock solution made up in degassed storage buffer. Oxidation was done by addition of potassium ferricyanide to give a final concentration of 5 mM using a 25 mM stock solution. All additions were done in anaerobic conditions.

Spectroscopic Measurements of Cyt c_{550} Binding—To determine the degree of association of cyt c_{550} with PSII after treatment with sodium dithionite, PSII core complexes preparations at a concentration of 25 μg Chl ml^{-1} were incubated in 40 mM MES (pH 6.5) for 30 min in the presence ($E_h \approx -400$ mV) and absence ($E_h \approx +295$ mV) of sodium dithionite (2 mM). The solutions were kept anaerobic in the dark at 20 °C. Samples were then centrifuged in the presence of PEG 8000. Difference spectra of the resuspended precipitate and the supernatant were taken.

RESULTS

Effect of Redox Mediators—Initially potentiometric redox titrations of the isolated PSII core complexes preparations in the presence of a mixture of eight redox mediators (see "Experimental Procedures"), covering the potential range between +430 and 0 mV, were performed. This mixture excluded five mediators with negative redox potential (anthraquinone-2-sulfonate, anthraquinone-2,6-disulfonate, anthraquinone-1,5-disulfonate, 2-hydroxy-*p*-naphthoquinone, and anthraquinone), which were used in our previous work (24). Fig. 1 shows a representative potentiometric titration of PSII core complexes from *T. elongatus* at pH 6.5 under these conditions. Differential absorption spectra in the α-band region of the cytochromes were obtained by subtracting the absolute spectrum recorded at +455 mV from those recorded during the course of the redox titration (Fig. 1*A*). This figure clearly shows that PSII core complexes contain two different components with absorption maxima in the α-band at 559 and 549 nm, which are progressively reduced during the course of titration. The component with an absorption maximum in the α-band at 559 nm that appeared between +455 mV and +210 mV can be assigned to cyt b_{559}, whereas the component appearing between +210 mV and −295 mV can be assigned to cyt c_{550} as has been already described (24). Differential spectra in Fig. 1*A* reveals that both cytochromes can be sequentially titrated observing the change of the α-band of both cyt b_{559} and cyt c_{550}. Consequently, it was first possible to determine the redox potential of cyt b_{559} by measuring the relative content of cyt b_{559} from the absorbance difference between 559 and 570 nm (Fig. 1*A*). A plot of the percentages of reduced cyt b_{559}, obtained from these difference spectra, *versus* E_h could be fitted to a Nernst equation for two $n = 1$ components (Fig. 1*C*). It clearly indicated the existence of two different cyt b_{559} components with E_m values of +389 mV (accounting for ~85% of the total amount of protein) corresponding to the high potential form and +246 mV (~15% of the total amount of protein) corresponding to the intermediated potential form. These values are similar to those obtained in measurements on PSII core complexes of *T. elongatus* where reductive titrations were carried out in the

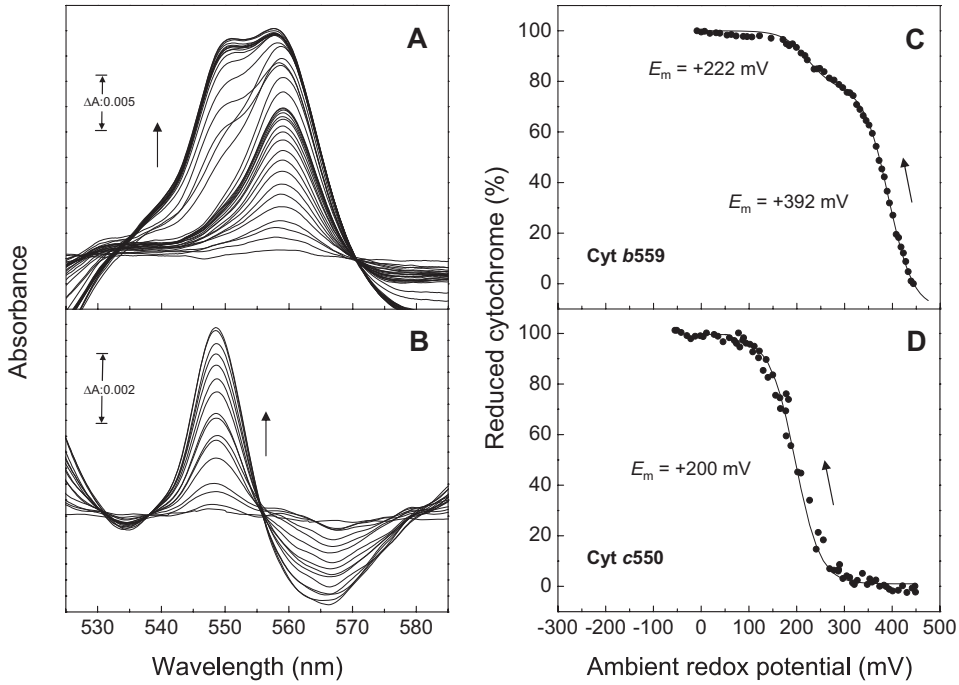

FIGURE 2. **Reductive potentiometric titrations of cyt b_{559} and c_{550} in PSII core complexes without redox mediators in the presence of 25 μM potassium ferricyanide.** *A* and *B*, difference absorption spectra in the α-band region of cyt b_{559} and cyt c_{550}. The spectra were obtained by subtracting absolute spectra recorded during the course of the redox titration between +430 and −80 mV minus the spectrum recorded at +430 mV (*A*) and the spectra recorded between +220 mV and −80 mV minus the absolute spectrum recorded at +230 mV (*B*). For simplification, only a set of selected spectra are included in *A* and *B*. *C* and *D*, plot of the percentages of reduced cyt b_{559} and reduced cyt c_{550} obtained from the absorbance differences at 559–570 nm and 549–538 nm *versus* ambient redox potentials, respectively. The *solid curves* represent the best fit of the experimental data to the Nernst equation in accordance with one-electron processes ($n = 1$) for two components (*C*) with E_m of +222 mV (20%) and +392 mV (80%) and for one component (*D*) with E_m of +200 mV.

presence of low potential mediators (24). When most cyt b_{559} was reduced at E_h of +210 mV, changes in the α-band of cyt c_{550} could be cleanly observed and consequently its E_m determined without any interference from cyt b_{559}. Differential spectra of cyt c_{550} (Fig. 1*B*) were obtained by subtracting the spectrum recorded at +210 mV (cyt c_{550} almost fully oxidized and cyt b_{559} fully reduced) from each spectrum performed at different ambient redox potential (between +210 and −295 mV). The relative content of cyt c_{550} was calculated from the absorbance difference between 549 and 538 nm. Then, the percentages of reduced cyt c_{550} *versus* E_h were plotted and an E_m value of −20 mV was calculated by fitting the experimental points to the Nernst equation for one $n = 1$ component (Fig. 1*D*). This E_m value was significantly higher than those described to date for cyt c_{550} associated with PSII (24, 26).

The E_m of the cyt b_{559} and cyt c_{550} was measured in the absence of redox mediators other than sodium dithionite and potassium ferricyanide. Complete reductive potentiometric titration at pH 6.5 of cyt b_{559} and cyt c_{550} in the PSII core complex was performed with the sample previously oxidized with potassium ferricyanide to an initial redox potential of approximately +450 mV (Fig. 2). Difference absorption spectra in the α-band region of cytochromes obtained during the course of the redox titration between +450 mV and −45 mV are shown in Fig. 2*A*. Fig. 2*C* shows a plot of the percentages of reduced cyt b_{559} *versus* ambient redox potential indicating the presence of two different forms of cyt b_{559} with E_m values of +392 mV (high potential form) and +222 mV (intermediated potential form), each representing ~85 and 15% of the total amount of protein, respectively. This result was similar to those found in the titrations carried out both in the absence (see Fig. 1*C*) and presence of low potential redox mediators (24). However, the plot of percentages of reduced cyt c_{550} obtained from the difference absorption spectra of the cyt c_{550} during the course of the redox titration (Fig. 2*B*) *versus* ambient redox potential clearly showed that cyt c_{550} had a significant higher E_m value (+200 mV) (Fig. 2*D*) than that obtained in the presence of low potential redox mediators (−80 mV) (24) and in the presence of other somewhat higher potential redox mediators (−20 mV) (see Fig. 1*D*). A similar E_m value for cyt c_{550} was obtained if the reductive potentiometric titration of PSII core complex was started from ambient redox potential of the reaction mixture without previous addition of potassium ferricyanide (data not shown).

It has been observed that to get a well defined E_m, most proteins need the presence of mediators with redox potentials within ±30–60 mV of the redox center E_m value and that for a single redox center, one mediator is ordinarily sufficient (27, 28). To verify the new value of E_m obtained for cyt c_{550} in the absence of mediators (Fig. 2*D*), reductive potentiometric titrations were also performed in the presence of a single redox mediator (Fig. 3). We selected the mediator diaminodurol (see "Experimental Procedures") with an E_{m7} of +220 mV, which is very close to the new value obtained for cyt c_{550} bound to PSII (Fig. 2). In these conditions, a value of $E_m = +215$ mV for cyt c_{550} was measured very similar to that obtained in the absence of redox mediators (Fig. 2*D*). Thus, these results show that cyt c_{550} in the absence of redox mediators (other

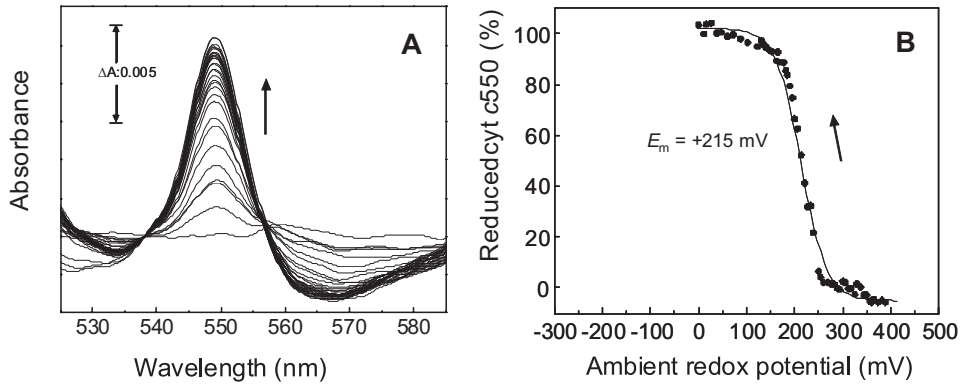

FIGURE 3. **Reductive potentiometric titration of cyt c_{550} in PSII core complexes with 20 μM diaminodurol and 25 μM of potassium ferricyanide.** *A*, difference absorption spectra in the α-band region of cyt c_{550}. The spectra were obtained by subtracting absolute spectra recorded during the course of titration minus the absolute spectrum recorded at +240 mV. For simplification, only a set of selected spectra are included. *B*, plots of the percentages of reduced cyt c_{550} obtained from the absorbance differences at 549–538 nm *versus* ambient redox potentials. The *solid curve* represents the best fits of the experimental data to the Nernst equation in accordance with one-electron processes ($n = 1$) for one component with E_m of +215 mV.

than potassium ferricyanide and sodium dithionite) or with only diaminodurol has an E_m value of ~200 mV higher than that obtained with the mixture of the eight mediators (see "Experimental Procedures") (Fig. 1*D*). These results are consistent with those obtained in redox titrations of Q_A in spinach PSII membranes where it was observed that the addition of redox mediators at low ambient potentials led to a shift of the E_m for Q_A from −80 mV to +65 mV (30).

Hysteresis—To increase confidence that titrations have been successfully performed at equilibrium, it is a common practice to perform redox titrations in both oxidative and reductive sequences, and identical results should be obtained. Oxidative potentiometric titrations were carried out in the same conditions as Figs. 1 and 2. Fig. 4*A* shows the result of an oxidative potentiometric titration of cyt c_{550} in PSII core complexes preparations in the absence of redox mediators. In this case, cyt c_{550} was previously reduced by adding excess sodium dithionite, and once it reached an E_h near −370 mV, the oxidative titration was performed by adding small amounts of potassium ferricyanide. Difference absorption spectra in the α-band region of cyt c_{550} recorded during oxidative titrations in these conditions are shown (Fig. 4*A*, *inset*). From plots of percentage of reduced cyt c_{550} *versus* ambient redox potential obtained from these spectra, it was possible to adjust the oxidative titration curve with a Nernst equation with $n = 1$ (Fig. 4*A*). Fig. 4*A* shows the presence of one component with E_m value of −220 mV, a value very similar to that described for the soluble form of cyt c_{550} (8, 12, 20, 24, 26). One striking feature of this result is that the oxidative titration curve showed considerable differences from those performed in the reductive direction (see Fig. 2*D*). The E_m determined by a reductive or oxidative potentiometric titration is usually identical in most of the biological and non-biological systems. However, cyt c_{550} bound to PSII exhibited anomalous redox chemistry, *i.e.* hysteresis was observed in the reductive and oxidative redox titrations in which an E_m of +200 mV and −220 mV were obtained, respectively.

To test whether the absence of redox mediators was responsible for the differences between reductive and oxidative titrations, an oxidative titration in the presence of eight redox mediators spanning the range between 0 to +300 mV (see "Experimental Procedures") was done. Fig. 4*B* shows difference spectra obtained during the course of this titration (*inset*) and a plot of percentage of reduced cyt c_{550} *versus* ambient redox potential obtained from these spectra. A very similar low redox potential ($E_m = -215$ mV) for cyt c_{550} could be calculated.

The above results suggest the possible existence of at least two states (A and B) corresponding to cyt c_{550} with substantially different E_m. An E_m of +200 mV can be determined by reductive titrations in PSII preparations after oxidation with potassium ferricyanide (state A). But after adding sodium dithionite, the E_m obtained by oxidative titration is −220 mV and correspond to state B. The experiments described below attempt to determine whether these two states could be interconvertible. Fig. 5 shows a cycle of two reductive and one oxidative potentiometric titrations performed on the same sample of PSII core complexes in the absence of redox mediators. The preparation was initially oxidized with potassium ferricyanide to $E_h \approx +450$ mV and a reductive titration was performed, obtaining a value of $E_m \approx +200$ mV for cyt c_{550} (Fig. 5, *curve 1*). After reducing completely the sample and reaching to an $E_h \approx -400$ mV, oxidative titration was performed by reoxidation of the sample with potassium ferricyanide (Fig. 5, *curve 2*) and a value of $E_m \approx -300$ mV was obtained. After complete reoxidation of the sample ($E_h \approx +410$ mV), a second reductive titration was held showing a similar reductive titration curve to the first one and a slightly lower value of $E_m \approx +100$ mV (Fig. 5, *curve 3*). It seems therefore that exist two extremes states for cyt c_{550} in PSII core complexes preparations that could be interconvertible.

Effect of Incubation with Sodium Dithionite—The experiments described above have shown that after addition of excess sodium dithionite and without mediators, the E_m obtained in the oxidative titration of cyt c_{550} is significantly more negative than the E_m from the reductive titration. To clarify the origin of this phenomenon, the effect of incubation with sodium dithionite on PSII and on the association of cyt c_{550} to PSII were studied.

PSII complexes were reduced with an excess of sodium dithionite (2 mM) and incubated for 10 min or 1 min and then reoxidized with potassium ferricyanide. Illumination of such

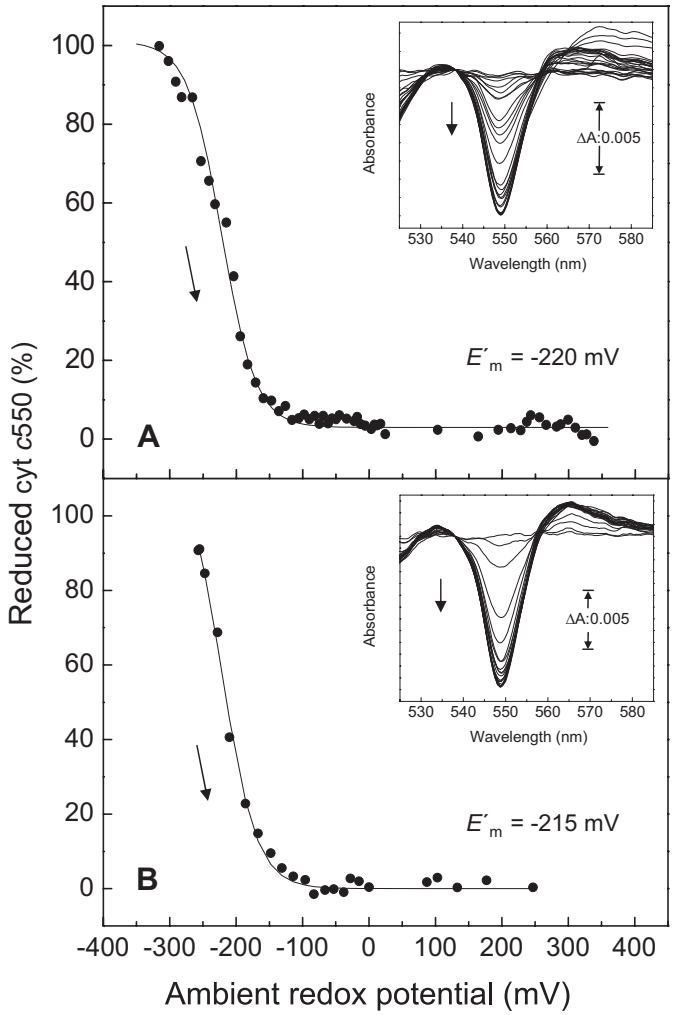

FIGURE 4. **Oxidative potentiometric titrations of cyt c_{550} in PSII core complexes in the absence and presence of redox mediators.** *A* and *B*, plots of the percentages of reduced cyt c_{550} obtained from the absorbance differences at 549–538 nm *versus* ambient redox potentials in PSII core complexes in the absence and in the presence of the mixture of eight redox mediators covering the potential range between +430 and 0 mV, respectively (see "Experimental Procedures"). The *solid curve* represents the best fits of the experimental data to the Nernst equation in accordance with one-electron processes ($n = 1$) for one component with E_m of −220 mV and −215 mV, respectively. *Insets*, difference absorption spectra in the α-band region of cyt c_{550} obtained by subtracting the absolute spectrum recorded at −330 mV from those recorded during the course of the redox titration with potassium ferricyanide in the absence or in the presence of redox mediators, respectively. For simplification, only a set of selected spectra are included.

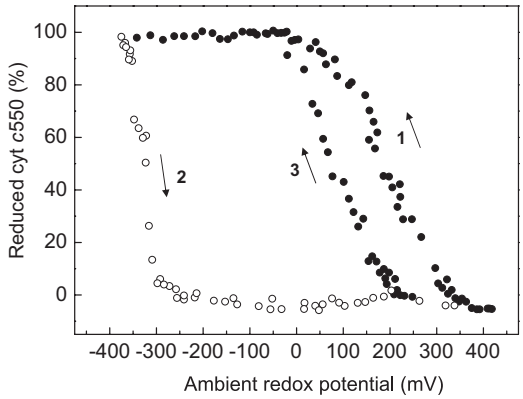

FIGURE 5. **Reversibility of the potentiometric titrations of cyt c_{550} in PSII core complexes in the absence of redox mediators.** The plot represents titration curves corresponding to further cycles of reduction and oxidation (up to three) in the same PSII core complexes preparations. The percentages of reduced cyt c_{550} were plotted *versus* ambient redox potentials in the first reductive titration (*curve 1*), in the first oxidative titration (*curve 2*) and in the second reductive titration (*curve 3*). Each curve was fitted to the Nernst equation in accordance with one-electron processes ($n = 1$) for one component.

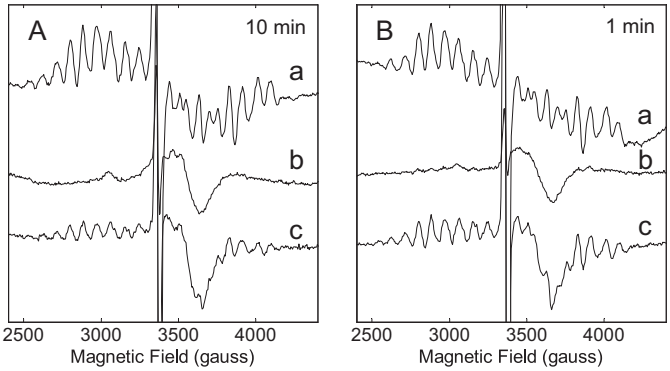

FIGURE 6. **Effect of sodium dithionite on the formation of the S_2 multiline EPR signal.** PSII complexes were incubated 10 min (*A*) or 1 min (*B*) in the absence (*a*) and in the presence of 2 mM of sodium dithionite (*b* and *c*). All spectra were difference spectra after 200 K illumination (light minus dark). *a*, untreated PSII; *b*, PSII complexes reduced by sodium dithionite and reoxidized by potassium ferricyanide; c, sample b was thawed and then was dark adapted at room temperature for 30 min, illuminated by a series of three flashes and finally dark adapted for 30 min. Instrument settings were as follows: microwave power, 20 milliwatt; modulation amplitude, 25 gauss; temperature, 8.5 K.

samples at 200 K did not result in formation of the S_2 manganese multiline signal (Fig. 6, *A*, *b*, and 6, *B*, *b*) indicating that sodium dithionite reduced the manganese cluster. Illumination of the samples at room temperature followed by dark adaptation generated a state that gave rise to a S_2 multiline signal upon illumination at 200 K (Fig. 6, *A*, *c* and 6, *B*, *c*). This indicates that the reduced state formed by sodium dithionite reduction can be reoxidized by light to form the usual S_1 and S_2 states. In the sample incubated with an excess of sodium dithionite for 10 min (Fig. 6, *A*, *c*), the extent of the multiline seen is ~30% of that seen in the unreduced control sample (Fig. 6, *A*, *a*).

The illumination treatment (three flashes) means that the S_0, S_{-1} and S_{-2} states sum up to ~30% of centers. Other experiments directly monitoring S_0 (data not shown) indicate that S_0 makes only a small contribution at this incubation time, *i.e.* the 30% giving rise to the S_2 signal arise from S_{-1} and S_{-2} (or its formal equivalent S_{-1} Tyr-D). The other centers are presumably in more reduced forms of the cluster. Measurements of O_2 evolution showed that in this sample, the O_2 evolution activity was 50% of that in untreated samples. The difference between the activity and the centers giving rise to the S_2 signal presumably reflects centers that were further reduced than S_{-2} but remained rapidly oxidizable and functional. The remaining centers are presumably either irreversibly damaged or require the low quantum yield assembly processes characteristic of photoactivation. We observed that reduction by dithionite also generates the typical Mn^{2+} signals in a small fraction of centers (supplemental Fig. S1*A*). This Mn^{2+} signal does not diminish when sample was illuminated after reoxidation with potassium ferricyanide. Ferricya-

nide is known to precipitate Mn^{2+} ions preventing them from undergoing oxidation by the reaction centers (34). The small Mn^{2+} signal thus presumably represents a small fraction of centers where the cluster is destroyed by the dithionite treatment. The Mn^{2+} signal was larger in the presence of a mediator (indigodisulfonate, $E_m = -125$ mV) indicating greater PSII damage (supplemental Fig. S1*B*).

Shorter incubation times (1 min) with sodium dithionite also showed no S_2 formation upon reoxidation with potassium ferricyanide. However nearly 80% of S_2 formation was seen after three flashes and dark adaptation (Fig. 6, *B*, *c*). This indicates that all the centers were in the S_0, S_{-1} or S_{-2} state after the dithionite treatment. O_2 evolution in such a sample was ~70%.

The EPR experiments show that treatment with excess sodium dithionite results in over-reduction of the manganese cluster and that this can be photo-oxidized again when the ambient potential is returned to a range that allows reaction center photochemistry to occur. Future experiments of this kind should allow us to define which states are formed at given times of incubation and to correlate this more precisely with the binding and redox state of cyt c_{550}.

To test for the release of cyt c_{550} by sodium dithionite treatment, reduced samples were precipitated by PEG, and difference spectra were taken of the supernatant and the pellet (Fig. 7). These were compared with supernatants and pellet from unreduced samples. In the unreduced samples, cyt c_{550} was entirely associated with the PSII (the pellet) (Fig. 7*A*, *spectrum 1*), with no cyt c_{550} present in the supernatant (Fig. 7*A*, *spectrum 2*). However, in the sample incubated with sodium dithionite, the appearance of a typical spectrum cyt c_{550} in the supernatant (Fig. 7*B*, *spectrum 2*) and the corresponding decrease of this cytochrome in the spectrum of the precipitate (Fig. 7*B*, *spectrum 1*), showed that incubation with sodium dithionite had caused the dissociation of a significant fraction of the cyt c_{550} from PSII.

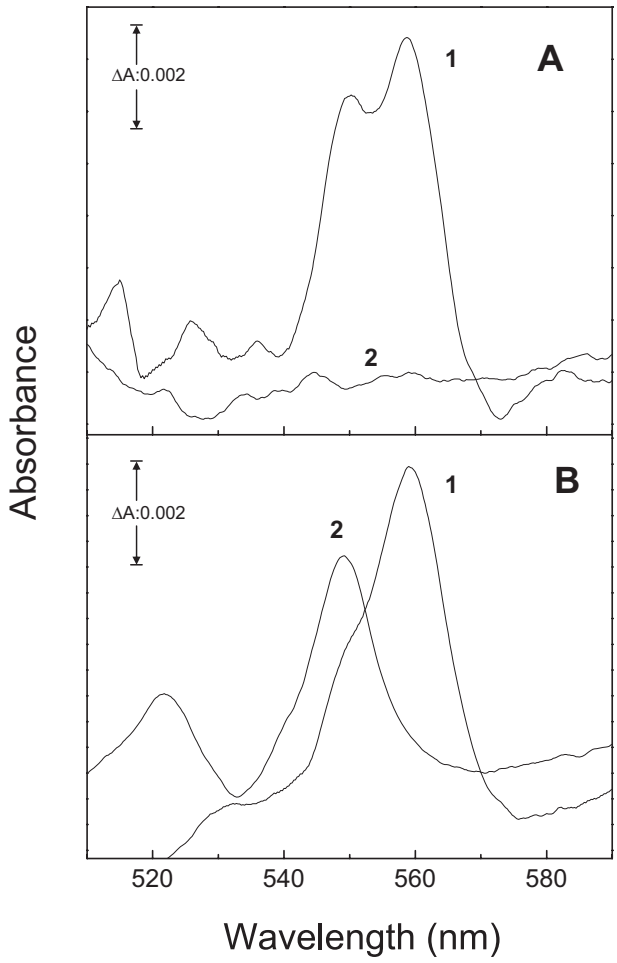

FIGURE 7. **Effect of sodium dithionite on the association of cyt c_{550} to PSII.** Difference absorption spectra of cyt b_{559} and cyt c_{550} were recorded from the pellet (*spectrum 1*) and the supernatant (*spectrum 2*) obtained by precipitation of PSII core complex preparations. The spectra were obtained by subtracting the absolute spectrum at −430 mV (the spectrum of reduced cyt b_{559} and cyt c_{550}) minus at +430 mV (the spectrum of oxidized cyt b_{559} and cyt c_{550}) in PSII core complex preparation untreated (*A*) and treated (*B*) with 2 mM of sodium dithionite during 30 min.

DISCUSSION

Redox titrations of cyt c_{550} performed on PSII core complexes from *T. elongatus* in the absence of low potential redox mediators showed an E_m value for this heme protein that is higher than was obtained previously. This E_m value of +200 mV is ~300 mV more positive than the previously determined when mediators were present ($E_m = -80$ mV) (24). A similar value was obtained in titrations carried out with diaminodurol as a mediator, the potential of which ($E_m = +220$ mV) is quite similar to that determined for cyt c_{550}. The redox potential of the sample during the titration was shown to be reliable under these conditions as demonstrated by (i) the similar E_m values obtained for the cyt b_{559} in the presence or absence of mediators and (ii) the correspondence of the E_m values for cyt b_{559} with those reported in the literature. The good fits of the data sets to one-electron Nernst curves and the large number of measurements allow further confidence in the E_m value obtained for cyt c_{550}.

When titrations were begun at low potentials the values for the E_m were shifted to low potentials, typical of the cyt c_{550} free in solution (26). This effect was specific to the cyt c_{550} and did not affect the cyt b_{559} in the same sample (data not shown). Thus, there was no technical problem in terms of establishing and measuring correct potentials.

The redox potential shift induced by low potentials is reminiscent of earlier reports on the redox potential of Q_A that were reported by Krieger *et al.* (30) and Johnson *et al.* (31). The Mn_4Ca cluster has a very high potential even in the most reduced form of the enzyme cycle. It is protected from reductive attack from the medium by being buried inside a large protein complex with access channels for substrate and products. However, reductants have access to the cluster when highly reducing conditions are used, when mediators are used or when extrinsic polypetides are removed. The reduction of the cluster leads to the weaker binding of the metal ions of the cluster to the site and eventually to their release (35, 36). Reduction of the cluster reverses the assembly process known as photoactivation, which is considered to involve protein conformational changes (37–40). We suggest that these conformational changes are responsible for the increased solvent access and weaker binding of the cyt c_{550} in the presence of

mediators giving E_m values of −80 or −20 mV. Under very reducing conditions, the cyt c_{550} even completely detaches from the PSII (Fig. 7).

Intriguingly when an over-reduced PSII preparation is allowed to become slowly oxidized during the course of a redox titration and then the reductive titration is repeated, the high potential E_m value is recovered. In the context of the explanation given above for the low potential shift, this indicates that the cyt c_{550} rebinds tightly, the protein must have returned to its original conformation and hence the Mn_4Ca cluster also must have returned to its functional state. Reassembly of the Mn_4Ca cluster by binding of free Mn^{2+} ions into the manganese-less PSII, photoactivation (37–40), is a complex process by which Mn^{2+} ions are bound and oxidized one at time by successive turnovers of reaction center photochemistry. A Ca^{2+} ion is also incorporated into the cluster and conformation changes in the protein seem to occur. This process takes place with a relatively low quantum yield. When this is done *in vitro*, high concentrations of Mn^{2+} ions, very high concentrations of Ca^{2+} ions, and the presence of an artificial electron acceptor are required for photoactivation to occur efficiently. Under the conditions of the titrations used here, the medium conditions are clearly not appropriate for this type of photoactivation to occur. Nevertheless, it is still possible to entertain the idea that the cluster "debinds and rebinds" if we propose that the reduced Mn_4Ca cluster is not released from the site upon reduction. The manganese would have to be reduced to a level where the natural geometry of the functional site is lost, and hence the changes in the protein would take place, but the Mn^{2+} and Ca^{2+} ions would not be released into the medium. This is similar to the situation encountered by Mei and Yocum (41) in which reductants were allowed access to the manganese by removal of the 23-kDa polypeptide. Some Mn^{2+} was seen by EPR but was not available to chelators, and the enzyme was rapidly activated by illumination. In the present work, the weak measuring beam used for measuring the spectra during the course of the titration could have been sufficient to reoxidize the manganese and reimpose the protein conformation required to induce the high potential form of the cyt c_{550}.

To test the feasibility of this idea, we did an EPR study that showed (*a*) the Mn_4Ca cluster was indeed reduced by sodium dithionite and upon reoxidation of the electron acceptors in the dark the Mn_4Ca remained in an over-reduced state and (*b*) the over-reduced state could be efficiently reoxidized by flash illumination. The reoxidized PSII showed water oxidation activity in a large proportion of centers. With longer times of incubation in sodium dithionite, the proportion of centers that could be reactivated by illumination diminished. Whether this effect is due to loss of manganese or to the requirement for low quantum yield photoactivation will be the subject of future work. Nevertheless, the EPR experiments are consistent with the proposition that the cyt c_{550} environment reflects conformational changes that are controlled by the redox state of the Mn_4Ca cluster. Further experimentation should allow this to be tested more directly.

The change in the PSII structure associated with the reduction of the Mn_4Ca cluster could lead to a greater accessibility of the heme to the aqueous medium and consequently to a total or partial release of cyt c_{550} from PSII. It seems likely that the increase in solvation energy that occurs when moving the heme out of the low dielectric of the protein environment into the high dielectric of water stabilizes the oxidized state more than the reduced state making the midpoint potential more negative (42–44).

These results lead us to suggest that the E_m of cyt c_{550} in PSII "*in vivo*" may be +200 mV, at least under certain conditions. This opens the possibility of a redox function for this protein in electron transfer in PSII. The nearest redox cofactor is the Mn_4Ca cluster (22 Å) (6). This long distance means that electron transfer would be slow (ms-s time scale) relative to the charge separation events in the reaction center. However, this rate remains potentially significant relative to the lifetime of the reversible charge accumulation states in the enzyme (tens of seconds to minutes) (45). Some kind of protective cycle involving a soluble redox component in the lumen may be envisioned. Before we enter into speculation, an experimental verification that cyt c_{550} does indeed donate electrons to the S_2 and or S_3 states is required.

CONCLUSIONS

We conclude that earlier redox titrations of cyt c_{550} in PSII probably reflected the situation in which the Mn_4Ca cluster is chemically reduced. Conformational changes associated with this resulted in the downshift of the E_m due to solvent access to the heme. Thus, the E_m of +200–215 mV obtained for cyt c_{550} without mediators and with only diaminodurol as a mediator is probably relevant to the most functional form of the enzyme. This E_m value of about +200 mV opens the possibility of a redox function for cyt c_{550} in the PSII as an electron donor to the Mn_4Ca cluster perhaps in some sort of protective cycle. This proposed role has yet to be demonstrated experimentally.

REFERENCES

1. Barber, J. (2009) *Chem. Soc. Rev.* **38,** 185–196
2. Zouni, A., Witt, H. T., Kern, J., Fromme, P., Krauss, N., Saenger, W., and Orth, P. (2001) *Nature* **409,** 739–743
3. Kamiya, N., and Shen, J. R. (2003) *Proc. Natl. Acad. Sci. U.S.A.* **100,** 98–103
4. Ferreira, K. N., Iverson, T. M., Maghlaoui, K., Barber, J., and Iwata, S. (2004) *Science* **303,** 1831–1838
5. Biesiadka, J., Loll, B., Kern, J., Irrgang, K. D., and Zouni, A. (2004) *Phys. Chem. Chem. Phys.* **6,** 4733–4736
6. Guskov, A., Kern, J., Gabdulkhakov, A., Broser, M., Zouni, A., and Saenger, W. (2009) *Nat. Struct. Mol. Biol.* **16,** 334–342
7. Alam, J., Sprinkle, J., Hermodson, M. A., and Krogmann, D. W. (1984) *Biochim. Biophys. Acta.* **766,** 317–321
8. Navarro, J. A., Hervás, M., De la Cerda, B., and De la Rosa, M. A. (1995) *Arch. Biochem. Biophys.* **318,** 46–52
9. Frazão, C., Enguita, F. J., Coelho, R., Sheldrick, G. M., Navarro, J. A., Hervás, M., De la Rosa, M. A., and Carrondo, M. A. (2001) *J. Biol. Inorg. Chem.* **6,** 324–332
10. Sawaya, M. R., Krogmann, D. W., Serag, A., Ho, K. K., Yeates, T. O., and Kerfeld, C. A. (2001) *Biochemistry* **40,** 9215–9225
11. Kerfeld, C. A., Sawaya, M. R., Bottin, H., Tran, K. T., Sugiura, M., Cascio, D., Desbois, A., Yeates, T. O., Kirilovsky, D., and Boussac, A. (2003) *Plant Cell Physiol.* **44,** 697–706
12. Hoganson, C. W., Lagenfelt, G., and Andréasson, L. E. (1990) *Biochim. Biophys Acta* **1016,** 203–206

13. Vrettos, J. S., Reifler, M. J., Kievit, O., Lakshmi, K. V., de Paula, J. C., and Brudvig, G. W. (2001) *J. Biol. Inorg. Chem.* **6,** 708–716
14. Shen, J. R., Qian, M., Inoue, Y., and Burnap, R. L. (1998) *Biochemistry* **37,** 1551–1558
15. Kerfeld, C. A., and Krogmann, D. W. (1998) *Annu. Rev. Plant Physiol. Plant Mol. Biol.* **49,** 397–425
16. Katoh, H., Itoh, S., Shen, J. R., and Ikeuchi, M. (2001) *Plant Cell Physiol.* **42,** 599–607
17. Nishiyama, Y., Hayashi, H., Watanabe, T., and Murata, N. (1994) *Plant Physiol.* **105,** 1313–1319
18. Kienzl, P. F., and Peschek, G. A. (1983) *FEBS Lett.* **162,** 76–80
19. Morand, L. Z., Cheng, R. H., Krogmann, D. W., and Ho, K. K. (1994) in *The Molecular Biology of Cyanobacteria* (Bryant, D. A., ed) pp. 381–407, Kluwer Academic Publishers, Dordrecht, The Netherlands
20. Holton, R. W., and Myers, J. (1963) *Science* **142,** 234–235
21. Krogmann, D. W. (1991) *Biochim. Biophys. Acta* **1058,** 35–37
22. Kang, C., Chitnis, P. R., Smith, S., and Krogmann, D. W. (1994) *FEBS Lett.* **344,** 5–9
23. Shen, J. R., and Inoue, Y. (1993) *Biochemistry* **32,** 1825–1832
24. Roncel, M., Boussac, A., Zurita, J. L., Bottin, H., Sugiura, M., Kirilovsky, D., and Ortega, J. M. (2003) *J. Biol. Inorg. Chem.* **8,** 206–216
25. Ishikita, H., and Knapp, E. W. (2005) *FEBS Lett.* **579,** 3190–3194
26. Kirilovsky, D., Roncel, M., Boussac, A., Wilson, A., Zurita, J. L., Ducruet, J. M., Bottin, H., Sugiura, M., Ortega, J. M., and Rutherford, A. W. (2004) *J. Biol. Chem.* **279,** 52869–52880
27. Clark, W. M. (1960) in *Oxidation–Reduction Potentials of Organic Systems*, Williams and Wilkins, Baltimore
28. Wilson, G. S. (1978) *Methods Enzymol.* **54,** 396–410
29. Dutton, P. L. (1978) *Methods Enzymol.* **54,** 411–435
30. Krieger, A., Rutherford, A. W., and Johnson, G. N. (1995) *Biochim. Biophys. Acta* **1229,** 193–201
31. Johnson, G. N., Rutherford, A. W., and Krieger, A. (1995) *Biochim. Biophys. Acta* **1229,** 202–207
32. Mühlenhoff, U., and Chauvat, F. (1996) *Mol. Gen. Genet.* **252,** 93–100
33. Cai, Y. P., and Wolk, C. P. (1990) *J. Bacteriol.* **172,** 3138–3145
34. Hoganson, C. W., Casey, P. A., and Hansson, O. (1991) *Biochim. Biophys. Acta* **1057,** 399–406
35. Tamura, N., and Cheniae, G. (1985) *Biochim. Biophys. Acta* **809,** 245–259
36. Debus, R. J. (1992) *Biochim. Biophys. Acta* **1102,** 269–352
37. Miyao, M., and Inoue, Y. (1991) *Biochemistry* **30,** 5379–5387
38. Dasgupta, J., Ananyev, G. M., and Dismukes, G. C. (2008) *Coord. Chem. Rev.* **252,** 347–360
39. Cheniae, G. M., and Martin, I. F. (1972) *Plant Physiol.* **50,** 87–94
40. Burnap, R. L. (2004) *Phys. Chem. Chem. Phys.* **6,** 4803–4809
41. Mei, R., and Yocum, C. F. (1991) *Biochemistry* **30,** 7836–7842
42. Mao, J., Hauser, K., and Gunner, M. R. (2003) *Biochemistry* **42,** 9829–9840
43. Wirtz, M., Oganesyanes, V., Zhang, X., Studer, J., and Rivera, M. (2000) *Faraday Discuss.* **116,** 221–234
44. Kassner, R. J. (1972) *Proc. Natl. Acad. Sci. U.S.A.* **69,** 2263–2267
45. Moser, C. C., Page, C. C., and Dutton, P. L. (2005) *Photochem. Phobiol. Sci.* **4,** 933–939

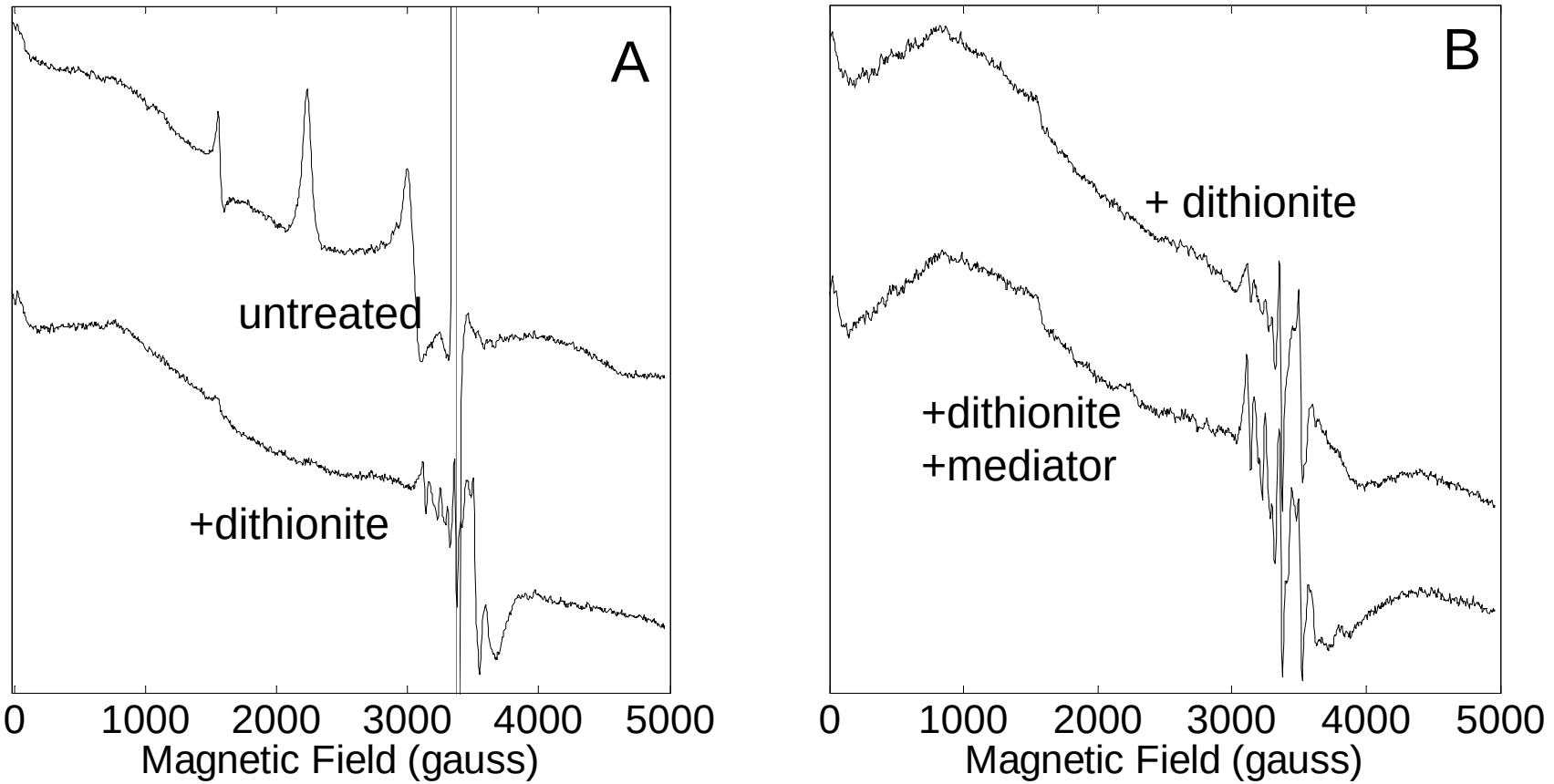

Fig S1. Effect of sodium dithionite reduction and mediator addition on Mn release in PSII.
Panel A shows the effect on PSII of sodium dithionite incubation during 10 min. The upper spectrum showed the PSII before reduction, the lower spectrum showed the reduced PSII. Panel B shows the effect of a mediator (Indigodisulfonate, 20 µM as a final concentration, incubated for 10 min) on the release of Mn^{2+}.The upper spectrum showed the reduced PSII with sodium dithionite for 30 min, while the lower spectrum showed the effect of the mediator addition. Instrument settings: microwave power, 5.6 mW, modulation amplitude, 25 gauss, temperature, 15 K. The signal observed in the presence of mediator is 80% of total signal (maximum released Mn) and in the absence is about 25%.

ARTICLE 7

High and low potential forms of the Q_A quinone electron acceptor in Photosystem II of *Thermosynechococcus elongatus* and spinach

Journal of Photochemistry and Photobiology B: Biology xxx (2011) xxx–xxx

Contents lists available at ScienceDirect

Journal of Photochemistry and Photobiology B: Biology

journal homepage: www.elsevier.com/locate/jphotobiol

High and low potential forms of the Q_A quinone electron acceptor in Photosystem II of *Thermosynechococcus elongatus* and spinach

Kunio Ido [a,b], Christine M. Gross [a], Fernando Guerrero [a,c], Arezki Sedoud [a], Thanh-Lan Lai [a], Kentaro Ifuku [b,d], A. William Rutherford [a], Anja Krieger-Liszkay [a,*]

[a] *Institut de Biologie et Technologies de Saclay (IBiTec-S), CNRS URA 2096, Bât 532, CEA Saclay, 91191 Gif-sur-Yvette, France*
[b] *Graduate School of Biostudies, Kyoto University, Sakyo-ku, Kyoto 606-8502, Japan*
[c] *Instituto de Bioquímica Vegetal y Fotosíntesis, Universidad de Sevilla-CSIC, 41092-Sevilla, Spain*
[d] *PRESTO, Japan Science and Technology Agency (JST), 4-1-8 Honcho Kawaguchi, Saitama 332-0012, Japan*

ARTICLE INFO

Article history:
Available online xxxx

Keywords:
Photosystem II
Oxygen evolving enzyme
Quinone redox potential
Chlorophyll fluorescence

ABSTRACT

The redox potential of Q_A in Photosystem II (PSII) from *Thermosynechococcus elongatus* was titrated monitoring chlorophyll fluorescence. A high potential form (E_m = +60 ± 25 mV) was found in the absence of Mn_4Ca, the active site for water oxidation. The low potential form (E_m = −60 ± 48 mV), which is difficult to measure in conventional titration experiments, could be "locked in" by cross-linking the active enzyme. This indicates that the presence of Mn_4Ca is relayed to the quinone site by significant structural changes in the protein. The presence of high and low potential forms agrees with what has been seen in plants, algae from our lab and in *T. elongatus* (Shibamoto et al., Biochemistry 48 (2009) 10682–10684). In the latter work, the potentials of Q_A were shifted to lower potentials compared to other measurements. The redox potential of Q_A in Mn-depleted PSII from spinach was titrated in the presence of redox mediators and the midpoint potential was shifted by 80 mV towards a more negative value compared to titrations without mediators. The lower values of the midpoint potential of the (Q_A/Q_A^-) redox couple in the literature could be due to a perturbation due to a specific mediator.

1. Introduction

In Photosystem II (PSII), the water oxidising enzyme of plants, the absorption of light results in a chlorophyll-mediated charge separation (for a recent review see [1]). The pheophytin anion formed delivers an electron to a tightly bound quinone co-factor, Q_A, which is H-bonded and shielded from protonation by the protein. This protein environment imposes one-electron redox function on the quinone. Q_A^- passes its electron to a second quinone, Q_B.

The redox potential of Q_A in PSII has been studied for decades and it has turned out to be an unexpectedly complex story. A survey of the literature done in 1995 showed more than 35 values for the Q_A/Q_A^- couple and these values varied over a wide range of potential [2]. The reason for this variation was found to be dependent on the functional (and presumably structural) state of the enzyme. When the Mn_4Ca complex was intact the potential of Q_A was low (−80 mV); without the Mn_4Ca complex the potential was high (65 mV) [3,4]. The same effect was seen when the Ca^{2+} was removed (or put back), but leaving the Mn_4 in place [5,6].

The two potential forms of Q_A are physiologically relevant because PSII is synthesised without the Mn_4Ca cluster and it has to be assembled through a process called photoactivation [7,8]. Mn^{2+} ions are oxidised and assembled into a high valence tetranuclear complex in which Ca^{2+} forms an integral part. The higher potential of Q_A in the PSII reaction centre prior to assembly of the Mn_4Ca cluster is expected to have marked effects on electron transfer both in the forward and backward direction and both are important in protecting against photodamage before the enzyme is fully functional [4,9]. Similarly, alterations of the midpoint potential of the redox couple Ph/Ph^- leads also to variations in the charge recombination pathway and thereby in the protection of PSII against photodamage [10,11]. The redox modulation of the potential of Q_A upon photoactivation has been demonstrated in plants and green algae [4].

Shibamoto and co-workers [12,13] reported midpoint potential for the redox couple (Q_A/Q_A^-) which were −80 mV more negative (−140 mV for the low potential form and +20 mV for the high potential form) than the values reported by us [2,4,6]. In the present study we re-measured the midpoint potentials in PSII-enriched membrane fragments from spinach and in PSII core complexes from *Thermosynechococcus elongatus*.

* Corresponding author. Fax: +33 1 6908 8717.
E-mail address: anja.krieger-liszkay@cea.fr (A. Krieger-Liszkay).

1011-1344/$ - see front matter © 2011 Published by Elsevier B.V.
doi:10.1016/j.jphotobiol.2011.02.010

2. Materials and methods

2.1. Biological material

2.1.1. PSII particles from spinach

PSII-enriched membrane fragments [14] were prepared from market spinach according to [15]. The preparation used in this work had an oxygen evolution activity of 490–500 μmol O_2 mg Chl^{-1} h^{-1}. Where PSII samples were treated to inhibit O_2 evolution, this involved incubation for 1 h on ice in the dark, in a buffer containing 1 mM NH_2OH, 300 mM sucrose, 15 mM NaCl and 50 mM MES, pH 6.5.

2.1.2. PSII core complexes from Thermosynechococcus elongatus

Cells of the transformed strain of *T. elongatus* with a histidine tag on the CP43 protein of PS II (43-H strain) were grown as previously described [16]. PSII core complexes were prepared based on [16] with the modifications described in [17]. The preparations used in this work had an oxygen evolution activity of 3500–3800 μmol O_2 mg Chl^{-1} h^{-1}. Removal of the Mn cluster by TRIS-washing was performed as described in [18].

2.2. Cross-linking

A buffer of 50 mM PIPES, pH 6.9, 5 mM EDTA, 5 mM $MgSO_4$ was adjusted to pH 11 with concentrated KOH and heated to 60 °C. Then 3% *p*-formaldehyde powder was added and completely dissolved. The buffer was cooled to room temperature and the pH was brought back to pH 6.5 by the addition of concentrated H_2SO_4. PSII particles (1.5 mg Chl ml^{-1}) were incubated for 15 min at 25 °C in a ratio of 1:3 in the cross-linking buffer. Then the sample was centrifuged and resuspended in a buffer containing 0.3 M sucrose, 10 mM NaCl, 25 mM MES, pH 6.5.

2.3. Measurements of PSII activity

O_2 evolution was measured at 20 °C using a Clark-type oxygen electrode with saturating white light. O_2 evolution was measured using 20 μg Chl ml^{-1} in the presence of 0.5 mM 2,6-dichloro-*p*-benzoquinone as electron acceptor.

Room temperature chlorophyll fluorescence was measured using a pulse-amplitude modulation fluorimeter (Dual-PAM, Walz, Effeltrich) and 20 μg Chl ml^{-1}. The intensity of the measuring light was sufficiently low (integral intensity about 10^{-8} mol quanta m^{-2} s^{-1}, frequency of modulated light: 1.6 kHz) to prevent the induction of variable fluorescence. Saturating flashes (1 s) were given to measure the maximum fluorescence. Efficiency of the photochemical electron transport was assayed by calculating the ratio of variable fluorescence Fv to maximal fluorescence Fm (Fv/Fm).

2.4. Redox titration of chlorophyll fluorescence

The level of variable fluorescence was used as a measurement of the reduction state of Q_A; the measurements were performed without redox mediators essentially as described in [3]. Only the weak measuring light of the PAM fluorimeter was used. Reversible redox titrations were obtained when the sample is sufficiently diluted (20 μg Chl ml^{-1}). Reductive titrations were performed by gradual addition of sodium dithionite (in 0.5 M MES, pH 6.5), oxidative titrations by the addition of potassium ferricyanide. For one experiment on NH_2OH-treated PSII particles from spinach, the mediators anthraquinone-2-sulfonate (μM; E_m = −195 mV), 2-hydroxy-1,4-naphthoquinone (5 μM; E_m = −100 mV) and *N,N,N′,N′*-tetramethyl-*p*-phenylenediamine (10 μM; E_m = + 300 mV) were added.

3. Results

Fig. 1 shows a redox titration of Q_A monitoring the fluorescence level in Mn-depleted PSII from *T. elongatus*. The E_m of 60 ± 25 mV is close to an earlier value of 84 ± 24 mV [19] obtained using a sample that nominally had a functional Mn_4Ca complex. This is about 160 mV more positive than that measured for Q_A from spinach and is similar to the high potential form seen in algal and plant PSII in the absence of the Ca^{2+} or Mn_4Ca cluster [3–5]. It was suggested earlier that this unexpectedly high redox potential in the "intact" enzyme could reflect the loss of the Mn cluster under the conditions of the titration [19]. The current result is also consistent with that suggestion. Indeed the existence of a lower potential form of Q_A/Q_A^- was evident in redox titrations of intact PSII. Low potential values were seen upon first reducing Q_A, while higher potentials were seen upon the subsequent oxidative and reductive titrations (data not shown). A reversible titration of active PSII from *T. elongatus* showing a low potential Q_A was done recently by Shibamoto et al. [12].

Fig. 2 shows redox titrations done on PSII from *T. elongatus* that had been cross-linked with *p*-formaldehyde prior to the redox titration attempting to "lock-in" the active, low potential conformation. *P*-formaldehyde is a non-specific, short distance (2 Å) cross-linker which is very reactive towards amino and imino groups such as the side-chains of lysine and arginine [20]. SDS–PAGE of the cross-linked PSII shows a loss of a number of protein bands (Supplementary Fig. 1). The cross-linking itself inactivated more than 80% of the O_2 evolution. Parallel to the loss of O_2 evolving activity almost no light-induced variable fluorescence could be measured in the cross-linked PSII. The Fv/Fm value decreased from 0.76 in active PSII core complexes to 0.33 in cross-linked samples. In the presence of dithionite, the Fm value of the cross-linked control was almost completely restored (0.73; Table 1). In addition, in the presence of DCMU, thermoluminescence originating from $S_2Q_A^-$ charge recombination was completely lost after the cross-linking procedure (data not shown).

Redox titrations of cross-linked PSII from *T. elongatus* gave a titration curve with a midpoint potential lower than 0 mV (Fig. 2). The data points are very scattered, most likely caused by heterogeneity of the centres with most being cross-linked but some being non-cross-linked. This sample showed still 18% of the original O_2 evolution activity. Fitting through the points (oxidative and reductive titration) of different titration experiments per-

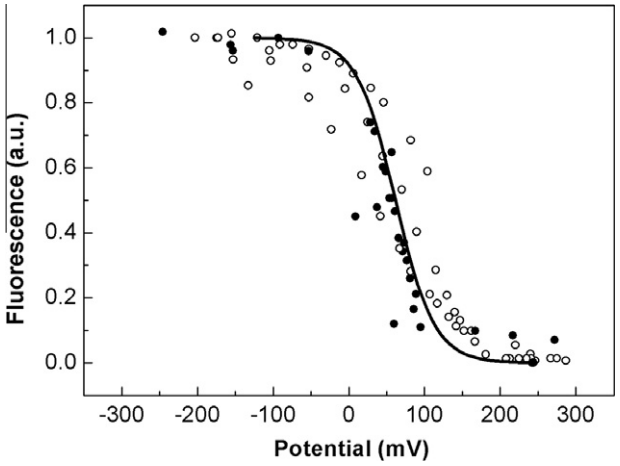

Fig. 1. Redox titration curves of Q_A in TRIS-washed PSII core complexes from *T. elongatus* measured as fluorescence yield. Closed circles, reductive titration; open circles, oxidative titration. The curve shows a one electron Nernst curve. The midpoint potential of the Nernst curve is 60 ± 25 mV.

Please cite this article in press as: K. Ido et al., High and low potential forms of the Q_A quinone electron acceptor in Photosystem II of *Thermosynechococcus elongatus* and spinach, J. Photochem. Photobiol. B: Biol. (2011), doi:10.1016/j.jphotobiol.2011.02.010

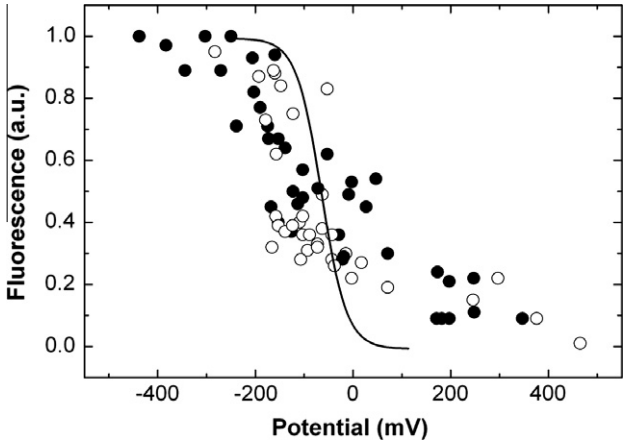

Fig. 2. Redox titration curves of Q_A in cross-linked PSII core complexes measured as fluorescence yield. Closed circles, reductive titration; open circles, oxidative titration. The midpoint potential is −60 ± 48 mV. Points from five independent titrations are shown. The PSII was active (3500–3800 μmol O_2 mg Chl^{-1} h^{-1}) before the cross-linking procedure.

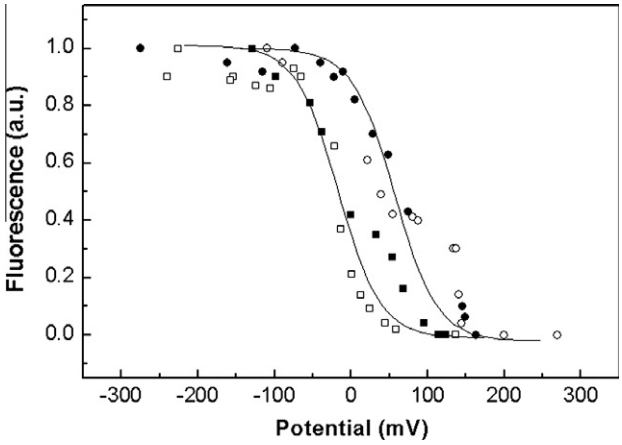

Fig. 3. Redox titration curves of Q_A in NH_2OH-treated PSII-enriched membrane fragments from spinach measured in the presence (squares) and absence of the redox mediators (circles). As redox mediators anthraquinone-2-sulfonate (5 μM), 2-hydroxy-1,4-naphthoquinone (5 μM) and *N,N,N′,N′*-tetramethyl-*p*-phenylenediamine (10 μM) were added. Closed symbols, reductive titration; open symbols, oxidative titration. The curves show one electron Nernst curve. The midpoint potential of the Nernst curve is 60 ± 30 mV in the absence of mediators and −20 ± 30 mV in the presence of mediators. Points from three independent titrations are shown.

Table 1
Midpoint potentials of Q_A obtained from Figs. 1–3 and Fv/Fm values of the corresponding samples.

Sample	E_m (mV)	Fv/Fm Fm obtained with $Na_2S_2O_4$
TRIS-washed PSII core complexes, *T. elongatus*	+60 ± 25	0.71
Cross-linked PSII core complexes, *T. elongatus*	−60 ± 48	0.73
NH_2OH-treated PSII particles, spinach, no mediators	+60 ± 30	0.80
NH_2OH-treated PSII particles, spinach, with mediators	−20 ± 30	0.64

formed on five individual samples resulted in a midpoint potential –60 ± 48 mV (Fig. 2 inset). While the data are rather scattered, they are similar to those reported for active PSII from plants [3]. The data, fits and E_m values for the individual experiments are shown in Supplementary Fig. 2.

The effect of redox mediators on the midpoint potential was investigated using Mn-depleted PSII particles from spinach. We chose spinach for this experiment because we have performed titrations on this material many times [e.g. 2–6]. We have shown earlier that the presence of redox mediators can destroy the Mn Cluster of active PSII under reducing conditions during the long measurements at room temperature, which are required in a classical titration to allow the sample to equilibrate [2]. Shibamoto and co-workers [12,13] reported an Em (Q_A/Q_A^-) of −140 mV for the low potential form and of +20 mV for the high potential form for PSII from *T. elongatus* and an Em (Q_A/Q_A^-) of −160 mV for the low potential form for PSII from spinach. They measured their midpoint potential electrochemically in the presence of high concentrations of the redox mediators using anthraquinone-2-sulfonate (E_m = −195 mV), 2-hydroxy-1,4-naphthoquinone (E_m = −100 mV) and *N,N,N′,N′*-tetramethyl-*p*-phenylenediamine (E_m = +300 mV). Fig. 3 shows titrations done on PSII particles from spinach which had been treated with NH_2OH to remove the Mn_4Ca cluster. In the absence of the redox mediators a midpoint potential of +60 mV was obtained in accordance with earlier measurements [4]. When the redox mediators anthraquinone-2-sulfonate, 2-hydroxy-1,4-naphthoquinone and *N,N,N′,N′*-tetramethyl-*p*-phenylenediamine, were present, the midpoint potential was shifted by 80 mV to a lower value (E_m = −20 mV).

4. Discussion

Here we show that, as we have suggested [19] and as subsequently demonstrated by Shibamoto and co-workers [12], the two redox potential forms of the Q_A, which have been demonstrated in plants and green alga [2,4], exist in cyanobacteria too. The two values (−60 mV, and +60 mV in cyanobacteria vs. −80 mV and +65 mV in plants and algae) and hence the redox difference is approximately the same. Thus the importance of switching between the two redox forms in order to protect against photodamage as described earlier [4] (see also the introduction) applies to cyanobacterial PSII. The low potential form of Q_A was only obtained after cross-linking the sample. The observation made here that multiple cross-linking of the intact enzyme seems to lock it in the active, low potential conformation implies that the structural change is more than a microscopic environmental change such as may be induced by electrostatic effects. The Mn cluster in the non-cross-linked PSII core preparation appears to be more sensitive to reductive release compared to that in thylakoids and PSII-enriched membrane fragments from algae and plants used in our previous experiments [3,4]. Shibamoto and co-workers [12] obtained the low potential form in active PSII core complexes from *T. elongatus* when titrations were performed electrochemically in a thin cell. During the electrochemical titration, no dithionite has to be added so reductive overshoots were eliminated. Also no stirring is required it is possible that the lack of mechanical perturbations may be responsible for the stability difference. In addition, in this thin cell a very high protein concentration is used and this will add to an increased stability of the sample. Whatever the reason for the better stability of the Mn complex, the result of the elelctrochemical titrations was impressive in terms of reversibility and the lack of scatter in the points. However, the values for the midpoint potential of the low and high potential forms of Q_A obtained by Shibamoto and co-workers [12,13] are approximately 80 mV more negative than those reported here and earlier by us [2,4]. As shown in Fig. 3, this effect might be caused by the presence of the redox mediators used by Shibamoto and co-workers. Two of the redox mediators are quinones which are may influence the titration in some way. The variable fluorescence is quenched by anthraquinone-2-sulfonate by 8% and *N,N,N′,N′*-tetramethyl-*p*-

Please cite this article in press as: K. Ido et al., High and low potential forms of the Q_A quinone electron acceptor in Photosystem II of *Thermosynechococcus elongatus* and spinach, J. Photochem. Photobiol. B: Biol. (2011), doi:10.1016/j.jphotobiol.2011.02.010

phenylenediamine by 9% while it is not affected by 2-hydroxy-1,4-naphthoquinone [21]. It seems unlikely however that such fluorescence changes, which are presumably due to direct quenching from PSII chlorophylls, could conspire to shift the measured potential. A more likely explanation is that the mediators bind to the Q_B-binding site and modify thereby the midpoint potential of Q_A. We have shown previously that the herbicide DCMU shifts the midpoint potential of Q_A to a more positive value while the herbicide bromoxynil shifts it to a lower potential [22]. Most likely the discrepancy between the midpoint potentials obtained by Shibamto et al. [12,13] compared to titrations in the absence of mediators shown here and in our previous publications can be explained by specific effects of the redox mediators in their titrations. This problem could be resolved by testing a range of redox mediator mixtures.

Acknowledgements

We thank Kevin Redding (Arizona State University) for useful discussions and the helpful suggestion to cross-link PSII. The authors acknowledge support the Agence Nationale de Recherche reference ANR-09-BLAN-0005-01, Solar H2, and the Deutsche Forschungsgemeinschaft (Li 883/10-1).

Appendix A. Supplementary material

Supplementary data associated with this article can be found, in the online version, at doi:10.1016/j.jphotobiol.2011.02.010.

References

[1] F. Rappaport, B.A. Diner, Primary photochemistry and energetics leading to the oxidation of the $(Mn)_4Ca$ cluster and to the evolution of molecular oxygen in Photosystem II, Coord. Chem. Rev. 252 (2008) 259–272.
[2] A. Krieger, A.W. Rutherford, G. Johnson, On the determination of the redox midpoint potential of the primary quinone electron acceptor, QA, in Photosystem II, Biochim. Biophys. Acta 1229 (1995) 193–201.
[3] A. Krieger, E. Weis, Energy-dependent quenching of chlorophyll-a-fluorescence: the involvement of a proton–calcium-exchange, Photosynthetica 27 (1992) 89–98.
[4] G. Johnson, A.W. Rutherford, A. Krieger, A change in the midpoint potential of QA in Photosystem II associated with photoactivation of oxygen evolution, Biochim. Biophys. Acta 1229 (1995) 202–207.
[5] A. Krieger, E. Weis, S. Demeter, Low pH induced Ca^{2+} ion release in the water splitting system is accompanied by a shift in the midpoint potential of the primary quinone acceptor, Biochim. Biophys. Acta 1144 (1993) 411–418.
[6] A. Krieger, A.W. Rutherford, Comparison of chloride depleted and calcium depleted PSII: the midpoint potential of QA and susceptibility to photodamage, Biochim. Biophys. Acta 1319 (1997) 91–98.
[7] N. Tamura, G.M. Cheniae, Photoactivation of the water-oxidizing complex in Photosystem II membranes depleted of Mn and extrinsic proteins, I. Biochemical and kinetic characterization, Biochim. Biophys. Acta 890 (1987) 179–194.
[8] J. Dasgupta, G.M. Ananyev, G.C. Dismukes, Photoassembly of the water-oxidizing complex in Photosystem II, Coord. Chem. Rev. 252 (2008) 347–360.
[9] A. Krieger-Liszkay, C. Fufezan, A. Trebst, Singlet oxygen production in Photosystem II and related protection mechanism, Photosynth. Res. 98 (2008) 551–564.
[10] I. Vass, K. Cser, Janus-faced charge recombinations in Photosystem II photoinhibition, Trends Plant Sci. 14 (2009) 200–205.
[11] K. Cser, I. Vass, Radiative and non-radiative charge recombination pathways in photosystem II studied by thermoluminescence and chlorophyll fluorescence in the cyanobacterium Synechocystis 6803, Biochim. Biophys. Acta 1767 (2007) 233–243.
[12] T. Shibamoto, Y. Kato, M. Sugiura, T. Watanabe, Redox potential of the primary plastoquinone electron acceptor QA in Photosystem II from *Thermosynechococcus elongatus* determined by spectroelectrochemistry, Biochemistry 48 (2009) 10682–10684.
[13] T. Shibamoto, Y. Kato, R. Nagao, T. Yamazaki, T. Tomo, T. Watanabe, Species-dependence of the redox potential of the primary quinone acceptor QA in Photosystem II verified by spectroelectrochemistry, FEBS Lett. 584 (2010) 1526–1530.
[14] D.A. Berthold, G.T. Babcock, C.F. Yocum, A highly resolved, oxygen-evolving Photosystem II preparation from spinach thylakoid membranes, FEBS Lett. 134 (1981) 231–236.
[15] G.N. Johnson, A. Boussac, A.W. Rutherford, The origin of the 40–50 °C thermoluminescence bands in photosystem II, Biochim. Biophys. Acta 1184 (1994) 85–92.
[16] M. Sugiura, Y. Inoue, Highly purified thermo-stable oxygen-evolving photosystem II core complex from the thermophilic cyanobacterium *Synechococcus elongatus* having His-tagged CP43, Plant Cell Physiol. 40 (1999) 1219–1231.
[17] D. Kirilovsky, M. Roncel, A. Boussac, A. Wilson, J.L. Zurita, J.M. Ducruet, H. Bottin, M. Sugiura, J.M. Ortega, A.W. Rutherford, Cytochrome c550 in the cyanobacterium *Thermosynechococcus elongatus*: study of redox mutants, J. Biol Chem. 279 (2004) 52869–52880.
[18] A. Boussac, F. Rappaport, P. Carrier, J.M. Verbavatz, R. Gobin, D. Kirilovsky, A.W. Rutherford, M. Sugiura, Biosynthetic Ca^{2+}/Sr^{2+} exchange in the photosystem II oxygen-evolving enzyme of *Thermosynechococcus elongatus*, J. Biol. Chem. 279 (2004) 22809–22819.
[19] C. Fufezan, C.M. Gross, M. Sjödin, A.W. Rutherford, A. Krieger-Liszkay, D. Kirilovsky, Influence of the redox potential of the primary quinone electron acceptor on photoinhibition in photosystem II, J. Biol Chem. 282 (2007) 12492–12502.
[20] V. Orlando, H. Strutt, R. Paro, Analysis of chromatin structure by in vivo formaldehyde cross-linking, Methods 11 (1997) 205–214.
[21] K.K. Karukstis, S.C. Boegeman, J.A. Fruetel, S.M. Gruber, M.H. Terris, Multivariate analysis of photosystem II fluorescence quenching by substituted benzoquinones and naphthoquinones, Biochim. Biophys. Acta 891 (1987) 256–264.
[22] A. Krieger-Liszkay, A.W. Rutherford, Influence of herbicides on the redox potential of the quinone acceptor in photosystem II: relevance to photodamage and phytotoxicity, Biochemistry (1998) 17339–17344.

Please cite this article in press as: K. Ido et al., High and low potential forms of the Q_A quinone electron acceptor in Photosystem II of *Thermosynechococcus elongatus* and spinach, J. Photochem. Photobiol. B: Biol. (2011), doi:10.1016/j.jphotobiol.2011.02.010

PHOTOACTIVATION

Photoassembly of the Mn_4Ca cluster in Photosystem II

from *Thermosynechococcus elongatus*.

Photoassembly of the Mn_4Ca cluster in Photosystem II from *Thermosynechococcus elongatus*.

During the course of this work I have taken an interest in the light driven assembly of the Mn_4Ca. I have made several observations that are of interest but remain in a somewhat preliminary phase. In this chapter I present three aspects of this work that seems worthy of being followed up.

1. An Introduction to Photoactivation

Photosystem II (PSII) is synthesized without the Mn_4Ca cluster. The cluster is subsequently assembled via a light-driven process called photoactivation (see [1] for recent review). During the photoactivation, light excitation of the chlorophylls in PSII results in the oxidation of the TyrZ. $TyrZ^{\bullet}$ can then oxidize 4 Mn^{2+} ions up to higher valence states. These high valence Mn ions are bridged by oxo groups. A Ca^{2+} ion is incorporated into the Mn_4Ca cluster. The protein probably undergoes a conformational change during this process. The molecular basis of this process remains to be elucidated.

The current mechanistic model describing photoactivation was first proposed by Cheniae and his co-workers. In this model two light-dependent reactions, separated by a dark rate limiting step, are required to produce a semi-stable intermediate. This intermediate undergoes further light-driven Mn oxidation steps before the final functional enzyme is generated. The experiments done that led to this conclusion were the studies of the photoactivation yield as a function of light intensity and flash interval [2-4]. By varying the time spacing between the flashes, it was found that an optimal spacing was required for the highest yield of photoactivation yield, with lower yields when the flashes were too close together and too far a part. This was interpreted as indicating the presence of a limiting step presumably a protein conformational change occurring in dark ($t_{1/2}$= 125 ms) [5], which was required before the second photoreaction could take place. The two light-dependent reactions were postulated to involve photooxidation of Mn^{2+} by the apo-PSII, with the Mn^{3+} produced on the first light-dependent reaction being unstable, becoming reduced in around $t_{1/2}$= 125 ms. A second Mn^{2+} binds either before or after the dark rate-limiting step, followed by the photooxidation of the $Mn^{3+}Mn^{2+}$ complex to form an $Mn^{3+}Mn^{3+}$. Two more Mn^{2+} ions must bind and be oxidized up to higher valence states before the final functional enzyme is formed.

These steps may include several light and/or dark reaction processes, although details of these reactions are not yet defined mainly because of the low quantum yield of the process leading to scrambling of states.

Support for this basic model of photoactivation has appeared [1, 6-9]. The quantum yield of photoactivation is low, between 0.01 [4] to 0.10 [10]. The reason for the low quantum yield and its range are not fully understood. The percentage of centers reactivated is often low, around 20 % [11] with the highest reported activation being 66 % [12], these values are usually made in comparison to controls depleted of the extrinsic polypeptides.

It is hypothesized that the "dark limiting" step corresponds to a protein rearrangement, this protein rearrangement is influenced by the presence of Ca^{2+} [1, 12]. A deprotonation event may occur during this step, which may explain the rate limitation. The binding of the second Mn^{2+} or the Ca^{2+} may be the structural change or may trigger it.

Ca^{2+} ions are strictly required to restore the O_2 evolution. It was shown that there is competition between Ca^{2+} and Mn^{2+} for the Ca^{2+} binding site and between Ca^{2+} and Mn^{2+} to the Mn^{2+} binding site(s) [6]. Some data indicate that PSII can assemble some $(Mn)_4$-clusters without recovery of O_2-evolution activity in the absence of Ca^{2+}. These non-functional clusters can acquire O_2-evolution activity following dark incubation with Ca^{2+} [4-5]. These authors did not show the experimental data for this observation but some data supporting this idea were subsequently published [13]. However it suggests that photoactivation can proceed in two stages: photoassembly of Mn^{2+} into an inactive $(Mn)_4$-cluster and then binding of Ca^{2+}, and the conversion of the inactive cluster to an active O_2-evolving cluster. According to Tamura and Cheniae [5], one Ca^{2+}-binding site is “created” during the photoassembly of the $(Mn)_4$-cluster and indeed the subsequent crystal structure showed that the Ca ion forms one corner of the cubane part of the clusters [14].

Miyao and coworkers optimized the concentration of chloride to improve the yield of photoactivation [15]. There are two Cl^- found in the PSII crystal structure that have specific sites close to the active site [16], however higher concentrations of Cl^- are required to maintain function when the extrinsic polypeptides are missing [17]. In addition, a specific function for Cl^- may exist during photoactivation, stabilizing the Mn^{3+} in some way. This role may be performed by the extrinsic proteins in native photoactivation [7].

The current model suggests that the first Mn^{2+} atom binds in a high affinity site, and is photo-oxidized to form the Mn_4Ca cluster [1]. The D1Asp170 is thought to contribute to the high affinity site since Mn^{2+} oxidation is strongly affected when D1Asp170 is mutated [18].

Dismukes and his coworkers, showed that there is a requirement for bicarbonate to observe more efficient *in vitro* photoactivation [19-20]. Direct EPR and ESSEM measurements done by the same group showed a possible bicarbonate coordination of the first Mn^{3+} intermediate [21-22]. It was suggested that the stimulating effect of bicarbonate was related to formation of easily oxidizable, electron neutral Mn–bicarbonate complexes [23-24].

Many aspects of the process of photoactivation remain poorly understood. With the exception of the work on the first Mn^{3+} formed then no other intermediates have been studied. Here I present some preliminary studies on difference aspects of photoactivation.

2. Material and methods

Photosystem II preparations: PSII studied in this article was isolated from *Thermosynechococcus elongatus*, that was His-tagged on the CP47 subunit as described in [25].

Manganese-depleted PSII (apo-PSII) Preparation: 2.5 mg Chl/mL to 3 mg Chl/mL of PSII are diluted in 40 ml of either TPA buffer (40 mM MES, pH 6.5; 15 mM $CaCl_2$; 15 mM $MgCl_2$ and 0.03 % βDM) or TPB buffer (20mM MES pH 6.5, 0.03 % βDM) in presence of 10 mM NH_2OH and 0.5 mM EDTA, this preparation is incubated for 1 hour in dark at room temperature. NH_2OH acts as a reductant of Mn_4Ca cluster hence the cluster is reduced and released [26] followed by the release of the extrinsic proteins. The apo-PSII is then washed five to seven times to completely remove NH_2OH and EDTA by a series of concentration using Amicon Ultra-15 concentrator devices (Millipore) with a 100-kDa cutoff. Apo-PSII were stored in liquid nitrogen at a concentration of about 1 mg Chl/mL in either TPA or TPB.

PSII concentration: The PSII concentration was estimated by measuring of the absorbance of the chlorophyll at 665 nm in methanol. 5 µl of the PSII samples were mixed with 995 µL of methanol, the samples were then vortexed for 1 min, and then the absorption was measured at 665 nm. The concentration is then calculated by considering the chlorophyll extinction

coefficient of 79.95 ml/mg cm^{-1}. The concentration was measured for each EPR sample; four measures were done to generate the error and the average.

Chemical treatments: Mn^{2+} was prepared from $MnCl_2$ in TPA or TPB buffer at 1 mM. Mn^{2+} was then added to the apo-PSII and incubated 10 min in the dark at room temperature. When stated, freshly made PPBQ in dimethylsulfoxide was added to the sample at a final concentration of 0.50 mM. When mentioned ferricyanide was added at a final concentration of 5mM, the sample was incubated for 30 min in the dark at room temperature.

Atomic absorption: The Mn concentrations were measured by atomic absorption (4110ZL Perkin-Elmer). Two dilutions with a triplicate for each of the sample were done to generate better accuracy. The standard curve was done with standard Mn in a medium containing the same concentration of the buffer present in the sample. The quantification was done for each EPR samples.

Photoactivation of the apo-PSII: in the presence of 30 µg of apo-PSII, 250 µM $MnCl_2$, 100 mM $CaCl_2$, 1.2 mM bicarbonate, 0.5 mM DCBQ mixed in a final volume of 1.5 ml of TPA. The sample was incubated in the Clark-electrode in the dark at 27°C for 5 min, and then illuminated with weak red light for 90 sec, then illuminated with strong white light and the oxygen evolution was measured. The oxygen evolution measured during the photoactivation was about 15 %. This yield is low, and needs to be optimized by varying the conditions (salt concentration and composition, pH, temperature, light regime etc…).

EPR measurements:

Low temperature 9GHz EPR: 150 µl of the samples were loaded into a standard quartz EPR tubes in complete darkness. EPR spectra were recorded using a Bruker Elexsys 500 X-band spectrometer equipped with standard ER 4102 resonator and Oxford Instruments ESR 900 cryostat. Instrument settings were: microwave frequency 9.4 GHz, modulation frequency 100 kHz. All other settings were as indicated in the figure legends.

Room temperature 9GHz EPR: 200 µl of the samples were loaded into a standard quartz flat cell in complete darkness. The Mn^{2+} oxidation kinetics were measured with Bruker ESP 300 or 500 spectrometer (Bruker, Germany). 9GHz EPR spectra were recorded with 9.7

GHz microwave frequency, modulation frequency 100 kHz, other settings were indicated in the figure legends.

High field high frequency EPR: 100 µl of the samples were loaded into cryogenic tubes (NALGEN in complete darkness. The high field spectrometer has been described in [27]. High fiel EPR spectra were recorded with 285 GHz microwave frequency, other settings were indicated in the figure legends.

3. Mn^{2+} photo-oxidation and stabilization of the Mn^{3+}

- Introduction

The first step of photoactivation should be the easiest to study. According to the literature Mn^{2+} binds to a high affinity site and upon illumination it is oxidised by $TyrZ^{\bullet}$. This state can back react or undergo a change (the dark step) that allows the next photooxidiation of Mn to take place. This dark step has been estimated to occur in 125 ms [5].

Some measurements have been made of a single Mn^{3+} formed under conditions where this state corresponds to the first oxidised Mn^{2+} [18, 28]. Few kinetic studies have been done as far as we are aware. Here we show some preliminary studies of Mn^{2+} oxidation in the PSII from *T. elongatus* after removal of the Mn_4Ca cluster.

- Results

In Figure 1A, the kinetic trace in red shows the flash-induced Mn^{2+} oxidation by Mn-depleted PSII at 20°C. The trace was measured at the field position shown by the arrow in the inset. The flash generates $TyrZ^{\bullet}$ which rapidly oxidises the Mn^{2+}forming Mn^{3+}. Mn^{3+} is EPR silent under these conditions. Mn^{2+} reappears with kinetic two phases: a fast phase with a half time of ~0.30 s and slow phase with a half time of 2-3 s (Figure 1 A and B, red traces). This is attributed to Mn^{3+} reduction probably by charge recombination from the reduced quinone acceptors.

To avoid recombination, an electron acceptor, phenyl benzoquinone (PPBQ), was added. It removes the electron from the acceptor side of PSII by re-oxidizing Q_B^- to Q_B. In addition the semi-reduced form of PPBQ is able to take an electron from the non-heme iron in a significant fraction of centres [29]. It was found that instead of stabilising the Mn^{3+}, the PPBQ had the opposite effect (not shown). The reduced form of PPPQ seems to be able to donate electrons to the Mn^{3+} at a rate that is faster than charge recombination within the reaction centre.

Figure 1 (lower trace) shows that the addition of ferricyanide in addition to PPBQ results in the stable loss of Mn^{2+} upon a flash. Ferricyanide is a stronger oxidant and acts as an electron sink, re-oxidising the reduced form of PPBQ ($PPBQH_2$). In experiments where both acceptors were added, Mn^{3+} was stable, with a halftime of hours (Figure 1A black trace, and see Figure 2).

Figure 1B, shows the effect of continuous illumination on Mn^{2+} oxidation and re-reduction kinetics in a sample without an exogenous electron acceptor. The upper trace is the same trace as in Figure 1A as a control. The lower trace shows that the illumination of PSII in the presence of Mn^{2+} with continuous light leads to more Mn^{2+} undergoing oxidation and a marked stabilisation of Mn^{3+} the state. This is also the case when closely spaced flashes are used (not shown).

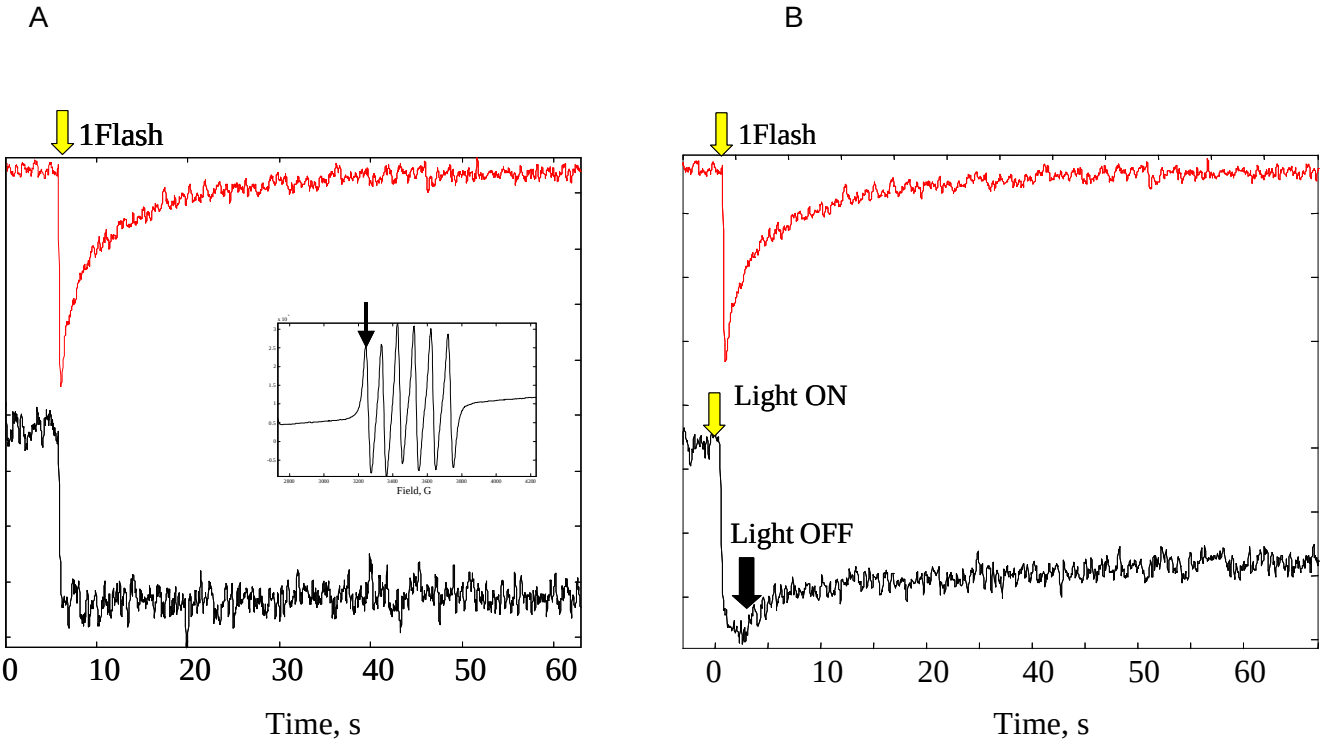

Figure 1: Mn^{2+} oxidation at room temperature induced by illumination of Mn depleted PSII in the presence exogenous Mn^{2+} 4 equivalents of Mn^{2+} were present per PSII. Upper (red) trace induced by one saturating flash. Lower (black) trace, same upper trace but in the presence of the electron acceptors electron acceptors: Phenyl *p* benzoquinone (PPBQ) and ferricyanide. The inset shows the typical room temperature Mn^{2+} EPR signal, the bold arrow shows the position of the field where kinetic traces are measured. Panel B) Red trace same trace as in A), in black the sample was continuously illuminated for approximately 1 second. Setting conditions: Microwave frequency: 9.41GHz, Microwave power: 63 mW, modulation amplitude: 10 gauss, static field: 3239 gauss.

Figure 2 shows an experiment were 4 Mn^{2+} were fully photo-oxidised in the presence of PPBQ and ferricyanide resulting a state that is stable for more than 12 hours. When Ca^{2+} was added to the sample, the Mn^{2+} EPR signal re-appeared and the intensity was close to the Mn^{2+} signal intensity before the photo-oxidation. The full intensity of the Mn^{2+} signal is not entirely recovered upon addition of Ca^{2+} (black).

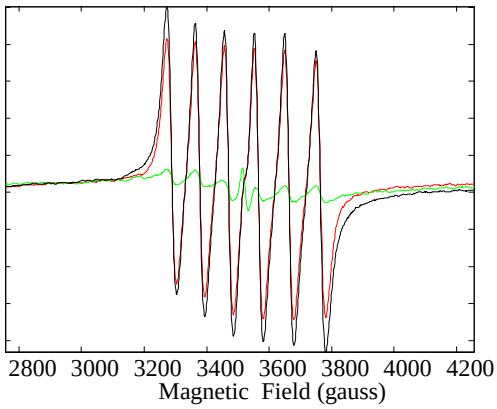

Figure 2: Effect of Ca^{2+} on the stable Mn^{3+} intermediate. Black trace is 4 Mn/Mn-depleted PSII in TPB buffer, with PPBQ/FeCy in the dark. Red, the same sample after continuous illumination, this state was stable for overnight. Red trace is just after addition of $CaCl_2$. Setting conditions: Microwave frequency: 9.41GHz, Microwave power: 63 mW, modulation amplitude: 10 gauss.

- Discussion

It is shown that the stability of the first Mn^{3+} intermediate in photoassembly of the Mn_4Ca cluster can be controlled by adjusting different experimental parameters. The instability of the Mn^{3+} appears to arise from internal charge recombination in PSII. Future experiments to monitor the Q_A^- fluorescence with DCMU are planned attempting to correlate the Q_A^- decay with Mn^{2+} formation.

Scavenging of the electron from the acceptor side using PPBQ and ferricyanide results in a state that is stable for many hours. This stable state should be the subject of spectroscopic and biochemical studies to determine its chemical nature. The fact that it is destabilized by Ca^{2+} is reminiscent of observations in the literature, in which Mn^{2+} can be oxidized in the absence of Ca^{2+} but subsequent Ca^{2+} addition activates a small fraction of correctly assembled clusters and displaces non specifically bound Mn^{2+} [12] and [13]. This could mean that the small fraction of Mn^{2+} that did not reappear in the spectrum upon Ca^{2+} addition represents the formation of the active cluster in a small fraction of centers. This should be easily testable.

In the stabilised system it is clear that ferrocyanide is unable to donate to Mn^{3+}. This could indicate that the Mn^{2+}/Mn^{3+} is at a lower potential than the ferri/ferro cyanide couple, this however seems unlikely based on what is expected from Mn^{2+} chemistry. Alternatively, the $(Fe^{2+}CN_6)^{4-}$ ion may be excluded from the Mn^{3+} environment perhaps because of it negative charge. A third alternative is that the Mn^{2+} is EPR silent rather than oxidised to Mn^{3+}. This seems unlikely but it can be ruled out by doing high field EPR experiments.

The light induced stabilization of the oxidized Mn^{2+} may reflect the rate-limiting dark step of Cheniae [5]. The kinetics of Mn^{2+} formation after a flash may reflect the back reaction occurring at the same time as the dark step. This could explain the biphasicity of the kinetics. By maintaining the Mn^{2+} in an oxidized form using a brief period of continuous light or a number closely spaced flashes (not shown), the stabilized state can be accumulated in all the centers. Figure 1 shows this effect in a sample containing 4 Mn per centre but similar effects are seen when only 1 Mn^{2+} per centre is present. This argues for the effect occurring when a single Mn^{3+} is formed, rather than the formation of Mn dimer, or trimer. The most likely explanation for this stabilization event is that it is a slow deprotonation triggered by Mn^{3+} formation in a site close to TyrZ. It should be possible to test this idea in future research.

4. Mn^{3+} intermediate trapped by illumination at -20°C

- Introduction

In the literature, the most detailed studies of the first intermediate in photoactivation (namely the Mn^{3+} ion) were done by generating this state at -20°C using continuous illumination at low temperature (-20°C) using plant PSII [28]. Parallel mode EPR was used to study this state under various conditions including a range of pH, the presence of Ca^{2+} and bicarbonate ions. Furthermore by difference spectroscopy the spectrum of the Mn^{2+}, which was expected to be in the high affinity site, was studied upon formation of the Mn^{3+} state. ESEEM spectroscopy was used to study the environment of the Mn^{2+} ion and the influence of various ions [21].

We wanted to apply the same methodology to study the same species in PSII from *T. elongatus* which is a much better spectroscopic material and which benefits from having a resolved crystal structure.

- Results

We began our experiments by monitoring Mn^{2+} oxidation upon illumination at -20°C using X-band (9GHz) EPR simply to verify the photo-oxidation of Mn^{2+} in our biological material (*T. elongatus*) at this temperature. Figure 3 (black line) shows the typical six lines Mn^{2+} signal, in a sample containing the Mn-depleted PSII and 4 equivalent of Mn^{2+}. The illumination at -20°C of this sample almost abolished the six lines signal, indicating that the Mn^{2+} was photo-oxidized (Figure 3, red line).

In this experiment, the majority of the Mn^{2+} EPR signal disappeared after the -20°C illumination. When PPBQ was added as an electron acceptor similar results were obtained (not shown). When the number of Mn^{2+} ions per centre was increased, in the presence of PPBQ, these too could be photoxoxidised by illumination at -20°C. Indeed, more than 8 Mn^{2+} could be oxidized per centre. This implies that some Mn^{2+} ions at least were free to diffuse to some extent at -20°C and that in the absence of an exogenous electron acceptor the number of Mn^{2+} oxidized is determined by the capacity of the endogenous electron acceptors.

It is generally considered however that Mn^{2+} EPR when measured at 9GHz is not always a reliable and quantitative probe. We attempted to confirm our findings using high field 295 GHz EPR, a method that is more reliable for detecting Mn^{2+}.

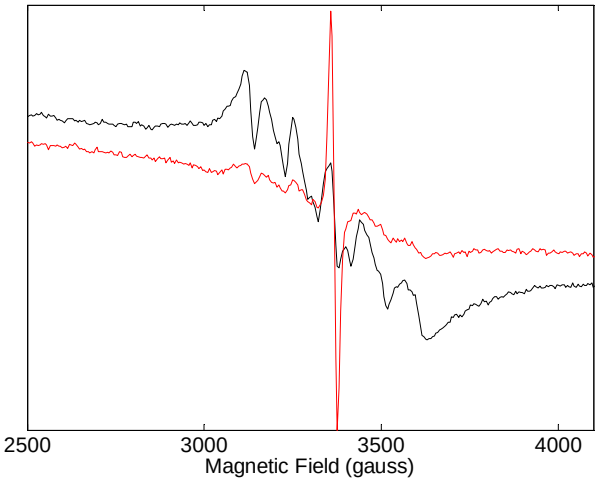

Figure 3: Mn^{2+} photo-oxidation at -20°C by Mn-depleted PSII. The Mn-depleted PSII was incubated for 10 min at room temperature with 4 Mn^{2+} equivalent / Mn-depleted PSII. The black spectrum showed the sample in the dark prior to illumination. The sample was then illuminated for 5 min at -20°C with red light. Instrument setting: Microwave frequency: 9.41GHz, Microwave power: 20 mW, modulation amplitude: 25 gauss, temperature: 15K.

Figure 4a shows a 285 GHz EPR experiment where a sample containing 5.39 Mn^{2+} per centre in the presence of an electron acceptor was illuminated at -20°C. Clearly all the Mn^{2+} were oxidized. In this figure the full oxidation of Mn^{2+} by the Mn-depleted PSII after the illumination at –20°C is shown in both 1.27 Mn^{2+}/Mn-depleted PSII (fig 2, b) in absence of electron acceptor and 5.39 Mn^{2+}/Mn-depleted PSII (fig 2, a) in presence of electron acceptor PPBQ. We clearly show that the illumination at –20°C of the Mn-depleted PSII can oxidize more than one Mn^{2+} per Mn-depleted PSII centre. In fact, Mn-depleted PSII can photo-oxidize more than 8 equivalents Mn^{2+} per Mn-depleted PSII centre (not shown), the limitation is the electron acceptors, this is clear from the experiment in Fig. 2a, where almost 5.39 Mn^{2+} were photo-oxidized in presence of electron acceptor.

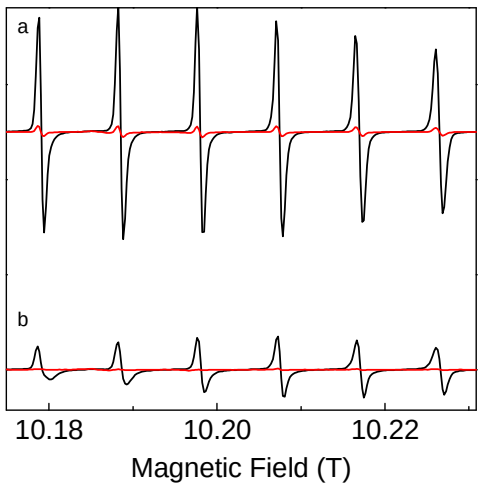

Figure 4: High field EPR spectroscopy of Mn^{2+} photooxidation at low temperature. In black is the spectrum taken before illumination, in red after illumination at –20°C for the indicated time in the text bellow. The Mn-depleted PSII was mixed with Mn^{2+} and TPA (40 mM MES pH 6.5, 15 mM $CaCl_2$, 15 mM $MgCl_2$, 0.03% β-DM) in presence or absence of the electron acceptor PPBQ in the dark at room temperature. (a) The ratio of Mn^{2+}/ Mn-depleted PSII was 5.39. The illumination time was 15 minutes. (b) The ratio of Mn^{2+}/ Mn-depleted PSII was 1.27. The illumination time was 3 minutes. Setting conditions: Microwave frequency: 285 GHz, modulation amplitude: 2 gauss, temperature: 23 K.

Figure 5 shows the photooxidized Mn^{2+} after illumination at –20°C, showing thus a full oxidation of Mn^{2+} to Mn^{3+} by the Mn-depleted PSII, as shown in Figure 3 and 4. After thawing at room temperature of the sample for 10 minutes, the original spectrum was obtained (Figure 5, blue spectrum). The re-illumination of this sample showed the full re-photooxidation of the Mn^{2+}, showing the reversibility of Mn^{2+} photooxidation (data not shown). This shows that, first as expected, the Mn^{3+} intermediate generated is unstable. Second, Mn^{3+} is reduced to Mn^{2+} that has exactly the same absorption spectrum as it was before illumination, thus, Mn^{2+} returns to the same environment and symmetry after 10 minutes in the dark.

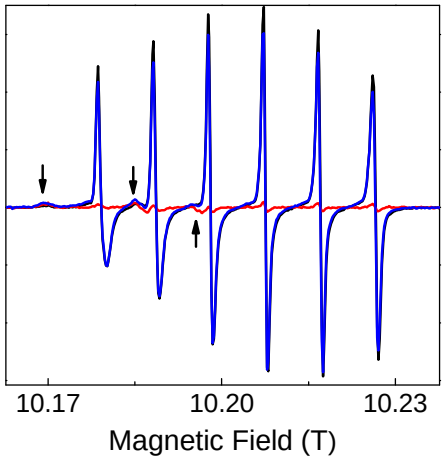

Figure 5: High field EPR spectroscopy showing reduction of the oxidized Mn (reappearance of $Mn^{2+)}$ upon thawing the sample in darkness. The Mn-depleted PSII was mixed with Mn^{2+} and TPA in dark at room temperature. The ration of Mn^{2+}/ Mn-depleted PSII was 1.27. In black is the spectrum before illumination, in red is the spectrum after illumination for 3 minutes at –20°C and in blue is the sample after 10 minutes of thawing at room temperature in the dark. Arrows show the special signature feature of $TyrD^{\cdot+}$ signal. Setting conditions as in figure 4.

- Discussion

In our conditions it seems clear that continuous illumination at -20°C results in multiple oxidations of Mn^{2+} by PSII if they are present. This will result in a mixture of sites/states, which will complicate the spectroscopic studies. To study the specific Mn^{3+} state (or by difference the Mn^{2+} undergoing oxidation), it will be necessary to work with substoichiometric quantities of Mn^{2+} or to find different conditions. In order to saturate the

site, a superstoichiometric number Mn^{2+} can be used provided a single saturating flash is used. To allow the Mn^{3+} state to be trapped, the PPBQ plus ferricyanide acceptor system should be appropriate.

In earlier studies, the method used to trap the first Mn^{3+} was by using illuminating at -20°C samples containing 6 Mn^{2+} equivalents for one Mn-depleted PSII, in those conditions, Tyryshkin et al, claimed that only one Mn^{2+} is oxidized at the high affinity site [28]. This is in clear disagreement with the present work. It is possible that species difference could be responsible for this discrepancy. This should be testable using plant PSII membranes under our experimental conditions.

5. The Mn^{2+} environments with PSII studied by high-field EPR

- Introduction

High field EPR is very good at detecting Mn^{2+} ions. The greatly enhanced resolution can also provide unique insight on the environment of the metal ion. Here we looked at the high field EPR spectra of Mn^{2+} ions that are photoxodisable by the manganese-depleted PSII under a range of conditions.

- Results

Figure 6 shows the Mn^{2+} high field EPR signal in the presence and absence of the Mn-depleted PSII . The EPR signal of Mn^{2+} in the TPA buffer (40 mM MES, pH 6.5; 15 mM $CaCl_2$; 15 mM $MgCl_2$ and 0.03 % βDM) shows broader and more complex six line spectrum corresponding to the Mn^{2+} interacting with the Cl^- anion [30] (see article 9 in the annexes of this thesis). In contrast, in presence of Mn-depleted PSII, only six sharp lines are seen. Also, the shape of the Mn^{2+} EPR signal in presence of the Mn-depleted PSII is not as regular as it is in the TPA buffer alone. Hence, the Mn^{2+} in the presence of Mn-depleted PSII is in a different environment and symmetry than the one found in the TPA buffer alone. This indicates that the Mn^{2+} molecules do not interact with the chloride ions in the buffer but interact with the Mn-depleted PSII protein instead. The illumination at -20°C of the Mn-depleted PSII added to the Mn^{2+} in TPA buffer shows complete oxidation of Mn^{2+} (Fig 4a). Thus the Mn^{2+} ions were either bound close enough to TyrZ to be photo-oxidizable, or they diffused during the illumination process that generates $TyrZ^{\bullet}$.

Ca^{2+} and Mg^{2+} are competitors of Mn^{2+} in its binding site [6]. In figure 6, the typical Mn^{2+}-Cl^- broad signal described by [30] is not detectable when the Mn-depleted PSII was

present. Thus even in the presence of 15 mM Ca^{2+} and 15 mM of Mg^{2+} none of the 4 Mn^{2+} per PSII were interacting with Cl^- ions. This may indicate that the 4 Mn^{2+} are bound to the Mn-depleted PSII in a special environment (cavity, channel or close to a surface) that prevents binding of the Cl^- ions.

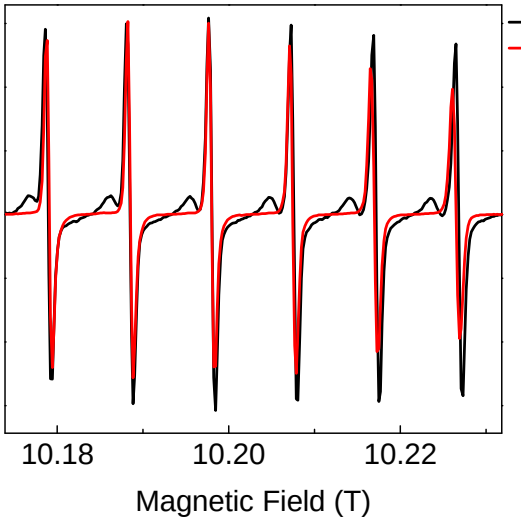

Figure 6: High-field high-frequency EPR spectra of 4 Mn^{2+} with Mn-depleted PSII in TPA buffer (in red) compared to the free Mn^{2+} in TPA buffer (in black). Measuring conditions were as in figure 4.

Figure 7 shows the high field EPR signal of Mn^{2+} in absence and presence of the Mn-depleted PSII in TPB buffer, which lacks Mg^{2+}, Ca^{2+} and Cl^- ions (20 mM MES pH 6.5, 0.03% β-DM). The high field EPR signal of Mn^{2+} in the TPB buffer shows a regular six lines shape, while the EPR signal of the Mn^{2+} in the presence of Mn-depleted PSII has a different shape where the six lines are not equal. The hyperfine value for the Mn^{2+} control in the TPB buffer is 0.965 T, while it decreases in the presence of Mn-depleted PSII to 0.943 T. The hyperfine is smaller in the presence of Mn-depleted PSII, indicating that the Mn^{2+} ions interact to a greater extent with Mn-depleted PSII and less free to interact with the buffer.

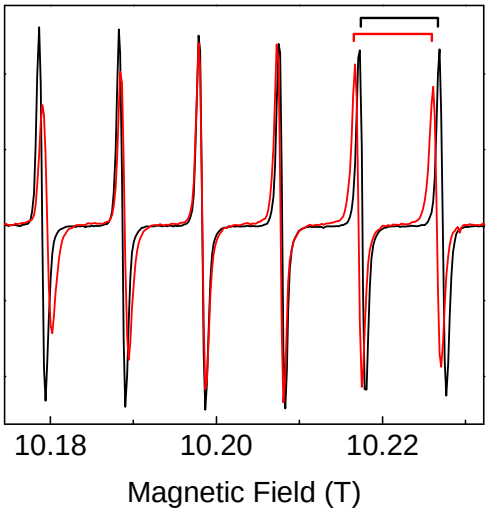

Figure 7: High-field high-frequency EPR spectra of one equivalent Mn^{2+} in Mn-depleted PSII in TPB buffer (in red) compared to Mn^{2+} in the TPB buffer control (in black). Black bracket is the hyperfine value 0.965 T of the Mn^{2+} EPR signal in TPB buffer, and the red bracket is the hyperfine value 0.943T of Mn^{2+} in Mn-depleted PSII. Setting conditions as in figure 2.

Figure 8 shows that Ca^{2+} and Mg^{2+} can change the high-field EPR signal arising from the Mn^{2+} interacting with the Mn-depleted PSII. The change consists of a distortion of the shape of the six lines and an increase in the hyperfine splitting when Ca^{2+} and Mg^{2+} are present. The hyperfine value is slightly bigger in the presence of Ca^{2+} or Mg^{2+} showing that a population of Mn^{2+} is in a different environment. The Mn^{2+}-Cl^- signal is still undetectable in figure 8. This might be explained by the fact that the Mn^{2+} is in an environment where Cl^- is unable to bind. The Mn^{2+} might be in a negatively charged cavity or surface, in which Cl^- ions are excluded. The fact that even, in the presence of Ca^{2+} and Mg^{2+}, the Mn^{2+} can be photo-oxidized (figure 3, 4 and 5) may indicate that this environment is near the TyrZ.

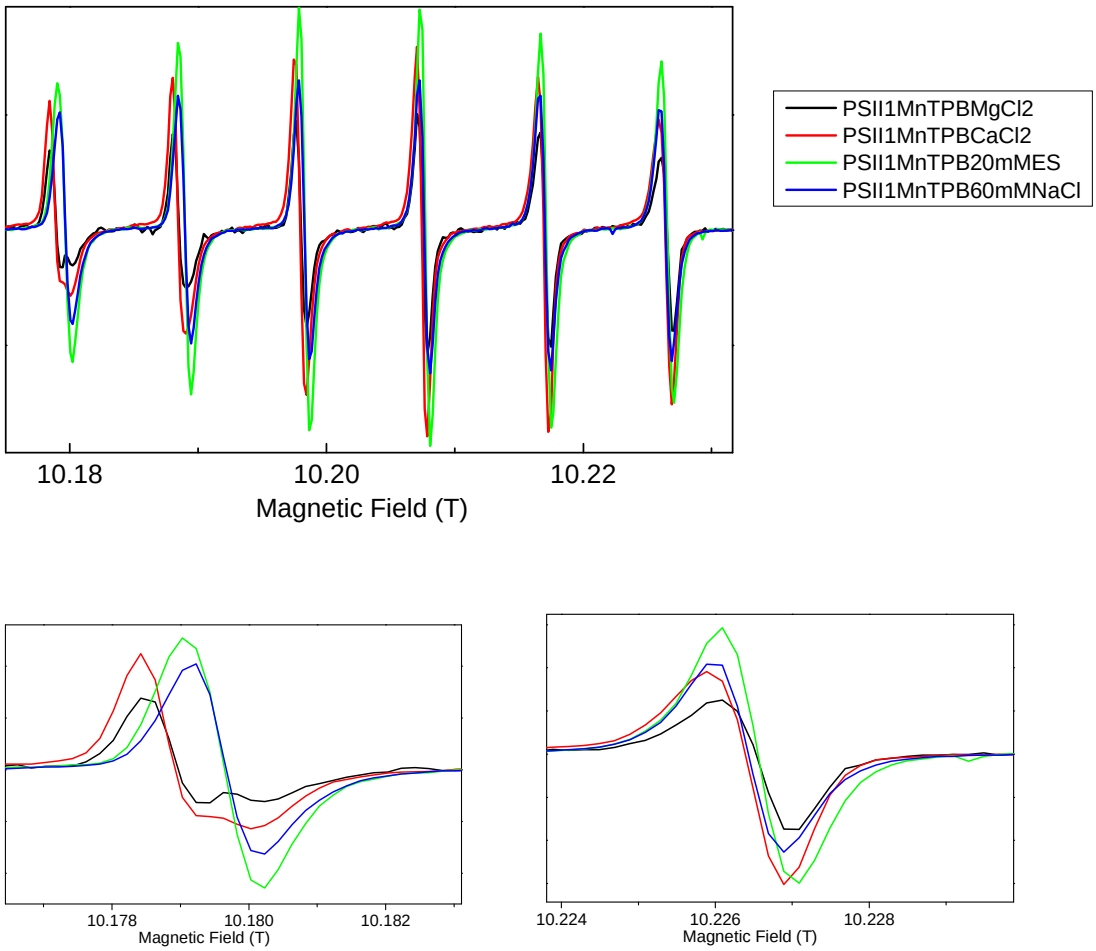

Figure 8: Effect of divalent cations on Mn^{2+} high-field high frequency EPR signal in presence of Mn-depleted PSII. In green, no adds. Black, 15 mM $MgCl_2$. Red, 15 mM $CaCl_2$. Blue, 60 mM NaCl. 1 equivalent Mn^{2+} per Mn-depleted PSII was added to all samples, the buffer was TPB. Setting conditions as in figure 4.

- Conclusions:

In the present work, we cannot distinguish unambiguously whether the Mn^{2+} ions are bound to the protein or free in the buffer. Given the literature we expect to have a specific high affinity site, however the high field EPR does not distinguish this site from those occupied by other oxidizable Mn^{2+} ions. It is possible that several Mn^{2+} bind to the Mn-depleted PSII in similar environments and all in proximity to the TyrZ. Given the large vacant ligands that hold together the Mn_4Ca cluster, this is not too difficult to accept. It is possible that the Mn^{2+} ions are relatively loosely bound in a channel or cavity close to the binding site. We suppose that the Mn^{2+} maybe bound to the Mn-depleted PSII in a special

environment, it can be a cavity mainly made by carboxylic acids negatively charged, channel or close to the protein surface, this may explain the lack of Cl^- ion binding and the inability of ferrocyanide to donate to Mn^{3+}.

6. General Conclusion

These short unfinished studies on aspects of photoactivation represent only a small part of the data I obtained working on this complicated subject. Several observations are intriguing and provide some directions that future research may follow. Photoactivation remains one of the areas of PSII research that has still to give up its secrets of how the water is oxidized. I imagine that resolving the photoassembling process will help the scientists working in the artificial photosynthesis. I hope that this small contribution will be useful for future researchers who take up the challenge.

7. References

[1] J. Dasgupta, G.M. Ananyev, G.C. Dismukes, Photoassembly of the water-oxidizing complex in photosystem II, Coordin. Chem. Rev, 252 (2008) 347-360.
[2] R. Radmer, G.M. Cheniae, Photoactivation of manganese catalyst of O2 evolution .2. 2-Quantum mechanism, Biochim Biophys Acta, 253 (1971) 182-&.
[3] G.M. Cheniae, I.F. Martin, Photoactivation of manganese catalyst of O_2 evolution .1. Biochemical and kinetic aspects, Biochim Biophys Acta, 253 (1971) 167-&.
[4] N. Tamura, G. Cheniae, Photoactivation of the water-oxidizing complex in Photosystem-II membranes depleted of Mn and extrinsic proteins .1. Biochemical and kinetic characterization, Biochim Biophys Acta, 890 (1987) 179-194.
[5] N. Tamura, Y. Inoue, G.M. Cheniae, Photoactivation of the water-oxidizing complex in Photosystem II membranes depleted of Mn, Ca and extrinsic proteins .2. Studies on the functions of Ca^{2+}, Biochim Biophys Acta, 976 (1989) 173-181.
[6] A.F. Miller, G.W. Brudvig, Manganese and calcium requirements for reconstitution of oxygen-evolution activity in manganese-depleted Photosystem II membranes, Biochemistry, 28 (1989) 8181-8190.
[7] M. Miyao, Y. Inoue, An improved procedure for photoactivation of photosynthetic oxygen evolution - effect of artificial electron-acceptors on the photoactivation yield of NH2OH-treated wheat Ohotosystem II membranes, Biochim Biophys Acta, 1056 (1991) 47-56.
[8] R.L. Burnap, M. Qian, S. AlKhladi, C. Pierce, Photoactivation and S-state cycling kinetics in Photosystem II mutants in *Synechocystis sp* PCC 6803, Photosynthesis: From Light to Biosphere, Vol II, (1995) 443-446
988.
[9] T. Ono, Metallo-radical hypothesis for photoassembly of Mn_4-cluster of photosynthetic oxygen evolving complex, Biochim Biophys Acta, 1503 (2001) 40-51.
[10] M. Miyao-Tokutomi, Y. Inoue, Improvement by benzoquinones of the quantum yield of photoactivation of photosynthetic oxygen evolution - direct evidence for the 2-quantum mechanism, Biochemistry, 31 (1992) 526-532.
[11] N. Bondarava, P. Beyer, A. Krieger-Liszkay, Function of the 23 kDa extrinsic protein of photosystem II as a manganese binding protein and its role in photoactivation, Biochim Biophys Acta, 1708 (2005) 63-70.
[12] C.G. Chen, J. Kazimir, G.M. Cheniae, Calcium modulates thephotoassembly of Photosystem-II Mn_4-Clusters by preventing ligation of nonfunctional high-valency states of manganese, Biochemistry, 34 (1995) 13511-13526.
[13] A. Krieger, A.W. Rutherford, I. Vass, E. Hideg, Relationship between activity, D1 loss, and Mn binding in photoinhibition of photosystem II, Biochemistry, 37 (1998) 16262-16269.
[14] K.N. Ferreira, T.M. Iverson, K. Maghlaoui, J. Barber, S. Iwata, Architecture of the photosynthetic oxygen-evolving center, Science, 303 (2004) 1831-1838.
[15] M. Miyao, Y. Inoue, Enhancement by chloride-Ions of photoactivation of oxygen evolution in manganese-depleted Photosystem II membranes, Biochemistry, 30 (1991) 5379-5387.
[16] J.W. Murray, K. Maghlaoui, J. Kargul, N. Ishida, T.L. Lai, A.W. Rutherford, M. Sugiura, A. Boussac, J. Barber, X-ray crystallography identifies two chloride binding sites in the oxygen evolving centre of Photosystem II, Energ Environ Sci, 1 (2008) 161-166.
[17] C.F. Yocum, The calcium and chloride requirements of the O_2 evolving complex, Coordin. Chem. Rev, 252 (2008) 296-305.
[18] K.A. Campbell, D.A. Force, P.J. Nixon, F. Dole, B.A. Diner, R.D. Britt, Dual-mode EPR detects the initial intermediate in photoassembly of the photosystem II mn cluster: The

influence of amino acid residue 170 of the D1 polypeptide on Mn coordination, J Am Chem Soc, 122 (2000) 3754-3761.
[19] S.V. Baranov, G.M. Ananyev, V.V. Klimov, G.C. Dismukes, Bicarbonate accelerates assembly of the inorganic core of the water-oxidizing complex in manganese-depleted photosystem II: A proposed biogeochemical role for atmospheric carbon dioxide in oxygenic photosynthesis, Biochemistry, 39 (2000) 6060-6065.
[20] S.V. Baranov, A.M. Tyryshkin, D. Katz, G.C. Dismukes, G.M. Ananyev, V.V. Klimov, Bicarbonate is a native cofactor for assembly of the manganese cluster of the photosynthetic water oxidizing complex. Kinetics of reconstitution of O_2 evolution by photoactivation, Biochemistry, 43 (2004) 2070-2079.
[21] J. Dasgupta, A.M. Tyryshkin, G.C. Dismukes, ESEEM spectroscopy reveals carbonate and an N-donor protein-ligand binding to Mn^{2+} in the photoassembly reaction of the Mn4Ca cluster in photosystem II, Angew Chem Int Edit, 46 (2007) 8028-8031.
[22] J. Dasgupta, A.M. Tyryshkin, S.V. Baranov, G.C. Dismukes, Bicarbonate coordinates to Mn^{3+} during photo-assembly of the catalytic Mn_4Ca core of photosynthetic water oxidation: EPR characterization, Appl. Magn. Reson., 37 (2010) 137-150.
[23] V.V. Klimov, S.V. Baranov, Bicarbonate requirement for the water-oxidizing complex of photosystem II, Biochim Biophys Acta, 1503 (2001) 187-196.
[24] Y.N. Kozlov, S.K. Zharmukhamedov, K.G. Tikhonov, J. Dasgupta, A.A. Kazakova, G.C. Dismukes, V.V. Klimov, Oxidation potentials and electron donation to photosystem II of manganese complexes containing bicarbonate and carboxylate ligands, Phys Chem Chem Phys, 6 (2004) 4905-4911.
[25] A. Sedoud, L. Kastner, N. Cox, S. El-Alaoui, D. Kirilovsky, A.W. Rutherford, Effects of formate binding on the quinone-iron electron acceptor complex of photosystem II, Biochim Biophys Acta, 1807 (2011) 216-226.
[26] G.M. Cheniae, I.F. Martin, Effects of hydroxylamine on Photosystem II .1. Factors affecting decay of O2 evolution, Plant Physiol., 47 (1971) 568-&.
[27] S. Un, P. Dorlet, A.W. Rutherford, A high-field EPR tour of radicals in photosystems I and II, Appl. Magn. Reson., 21 (2001) 341-361.
[28] A.M. Tyryshkin, R.K. Watt, S.V. Baranov, J. Dasgupta, M.P. Hendrich, G.C. Dismukes, Spectroscopic evidence for Ca^{2+} involvement in the assembly of the Mn_4Ca cluster in the photosynthetic water-oxidizing complex, Biochemistry, 45 (2006) 12876-12889.
[29] J.L. Zimmermann, A.W. Rutherford, Photoreductant-induced oxidation of Fe^{2+} in the electron-acceptor complex of Photosystem-II, Biochim Biophys Acta, 851 (1986) 416-423.
[30] S. Un, A. Sedoud, High-field EPR Study of the effect of Chloride on Mn^{2+} ions in frozen aqueous solutions, Appl. Magn. Reson., 37 (2010) 247-256.

CONCLUSION

et

DISCUSSION

1. Spécificité du côté accepteur du PSII comparé à celui des centres réactionnels bactériens :

Malgré les similitudes structurales du côté accepteur d'électrons entre le PSII et le centre réactionnel des bactéries pourpres (voir introduction), des différences existent. Ces différences peuvent refléter la fonctionnalité du PSII.

(1) Le fer non-hémique peut être oxydé ou réduit dans certain cas. La réduction du Fe^{3+} en Fe^{2+} peut se faire après une réduction par Q_A^-, et peut être aussi réalisée chimiquement avec des réducteurs tels que le dithionite. L'oxydation de ce fer peut se faire par ajout d'oxydants tel que le ferricyanure [1], ou encore par certaines semiquinones telles que PPBQ [2]. D'autres observations sont décrits dans la littérature ; Nugent a montré l'oxydation du fer non-hémique dans le noir après un éclairement du PSII [3] ; La présence d'une quantité résiduelle de fer oxydé dans le noir [4] ; Boussac et al [5], ont montré l'oxydation du fer dans le noir lors de l'ajout de DCMU dans les centres ayant Q_B^- présent à l'obscurité [5]. Cette dernière observation a été expliquées par un déplacement de l'équilibre de la réaction ci-dessous vers la droite par le DCMU, mais peut indiquer qu'une oxydation du fer non-hémique par Q_B^- présente de manière naturelle peut être possible.

$$Fe^{2+}Q_B^- + DCMU \rightleftharpoons Fe^{3+}Q_BH_2 + DCMU \rightleftharpoons Fe^{3+}DCMU + Q_BH_2$$

Dans l'article 4, j'ai montré l'oxydation du fer non-hémique en présence de Q_B^- dans le PSII non-traité dans 20 % des centres approximativement. La capacité de Q_B^- à oxyder le fer non-hémique nous permet de proposer un potentiel redox pour le couple Q_B^-/Q_BH_2 qui doit être assez proche du potentiel du Fe^{3+}/Fe^{2+}, lui même calculé par Ishikita et Knapp à ~300 mV à pH 6,5 en présence de Q_B^- [6]. L'oxydation du fer non-hémique dans une fraction des centres de PSII peut avoir un effet protecteur, en effet, le fer pourrait jouer un rôle de réducteur de Q_B^-, diminuant ainsi les chances d'une recombinaison de charges entre Q_B^- et les états S_2/S_3.

(2) Au niveau du côté donneur, le cluster de Mn_4Ca est absent dans le centre réactionnel des bactéries pourpres. Or dans le PSII la présence ou l'absence du cluster de Mn_4Ca induit un changement dans le potentiel redox du couple Q_A/Q_A^- [7-8].

Cet effet de l'augmentation de potentiel redox est proposé avoir un effet protecteur lors de recombinaisons de charges entre Q_A^- et P_{680}^+ en favorisant une recombinaison directe entre Q_A^- et P_{680}^+, évitant ainsi la recombinaison indirecte en passant par la $Pheo^-$ qui peut produire l'état triplet $^3P_{680}$ et $^1O_2$ [9-10]. Il est à noter que le cluster de Mn_4Ca est situé au niveau de la sous unité D1 et que Q_A et Q_B sont localisées sur les sous unités D2 et D1, respectivement. On

prédit donc un possible changement de potentiel redox de Q_B lorsque le cluster de Mn_4Ca est absent, cela n'a jamais été mesuré dans la littérature.

(3) La sous-unité H présente au dessus du fer non-hémique dans le centre réactionnel bactérien est absente dans le PSII, ce qui laisse prévoir ainsi une plus grande accessibilité. Dans le centre réactionnel des bactéries pourpres, la sous-unité H possède les canaux nécessaires pour l'acheminement de protons [11] alors, que dans le PSII, le côté accepteur est exposé à l'extérieur (stroma). L'accessibilité du côté accepteur du PSII pourrait donc faciliter l'accès pour une régulation de type pH, accès d'acides carboxyliques pouvant influencer sur la vitesse du transfert d'électrons entre Q_A et Q_B.

(4) La présence d'un ligand échangeable (bicarbonate) lié au fer dans le PSII pourrait être impliqué dans les régulations de transfert d'électrons entre Q_A et Q_B ou encore dans le mécanisme peu connu de la protonation de Q_B. J'ai montré dans cette thèse que le formate peut remplacer le bicarbonate et induire un signal RPE $Q_B^-Fe^{2+}$ différent de celui de $Q_A^-Fe^{2+}$ et plus facilement détectable. Cela facilite la détection de $Q_B^-Fe^{2+}$ en RPE. Les signaux RPE de $Q_A^-Fe^{2+}$ et $Q_B^-Fe^{2+}$ en présence de formate sont similaires aux signaux RPE de $Q_A^-Fe^{2+}$ et $Q_B^-Fe^{2+}$ trouvés dans les centres réactionnels des bactéries pourpres [12]. L'échange du bicarbonate par le formate provoque un ralentissement dans le transfert d'électrons entre Q_A et Q_B comme il est décrit dans la littérature [13]. On a aussi montré que le formate pouvait bloquer l'échange de Q_BH_2 [12-14]. Le ralentissement du transfert d'électrons entre Q_A et Q_B et le blocage de l'échange de Q_BH_2 lorsque le formate remplace le bicarbonate indiquent une implication du bicarbonate dans l'efficacité de transfert d'électrons et peut être un rôle dans les mécanismes de protonation de Q_B^- et/ou Q_B^{2-}. Il est à rappeler que le CO_2 est l'accepteur final d'électrons de la chaine de photosynthèse, donc une régulation du transfert d'électrons entre Q_A et Q_B due à la concentration de CO_2 peut être possible. Petrouleas et al, [15-16] ont rapporté les effets de ralentissement de transfert d'électrons entre Q_A et Q_B lorsque le bicarbonate est échangé par des acides carboxyliques (glyoxylate, oxalate, glycolate) et ont exclu un possible rôle de régulation du transfert d'électrons dans le PSII par les acides carboxyliques, car pour déplacer le bicarbonate il faudra utiliser de fortes concentrations d'acides carboxyliques (il faut utiliser 30 fois la concentration d'acides carboxyliques pouvant échanger le bicarbonate afin de commencer à voir un ralentissement du transfert d'électrons entre Q_A et Q_B).

L'accessibilité du fer (due à l'absence de la sous-unité H) et le ligand échangeable dans le PSII peuvent expliquer pourquoi le fer non-hémique peut être une espèce redox active en comparaison avec le fer non-hémique du centre réactionnel bactérien.

2. Sur la voie de la détermination du potentiel redox de Q_B:

Le potentiel redox de Q_B est difficile à mesurer et donc très peu reporté dans la littérature, cela dit des estimations basées sur les cinétiques de transfert d'électrons entre Q_A et Q_B et d'expériences de thermoluminescence existent. En prenant en compte (1) de la valeur de -80 mV comme potentiel du couple Q_A/Q_A^- [8] (2) une différence de potentiel de 70-83 mV permettant un transfert d'électrons efficace entre Q_A et Q_B [17-20] (3) un potentiel de 130 mV pour le couple Q_B/Q_BH_2 [21]. En supposons que la moyenne du potentiel de Q_B/Q_B^- et Q_B^-/Q_BH_2 est égale au potentiel du PQ/PQH_2.

Plusieurs options peuvent être envisagées (voir le schéma 1):

La première option : $E_m\ Q_B/Q_B^- \geq E_m\ Q_B^-/Q_BH_2$

En considérant le potentiel de -80 mV pour le couple Q_A/Q_A^-, on suppose que le potentiel du couple Q_B/Q_B^- est ~260 mV et le potentiel de Q_B^-/Q_BH_2 est ~ 0 mV. Si on prend la valeur de -140 mV comme potentiel du couple Q_A/Q_A^-, le potentiel de Q_B/Q_B^- est ~ 320 mV et le potentiel de Q_B^-/Q_BH_2 est ~ -60 mV. Dans cette option, la capacité de Q_B^- est incapable d'oxyder le fer non-hémique. Ce cas de figure est similaire aux potentiels reportés dans *Bl. viridis*; $E_m\ Q_A/Q_A^-$ = -80 mV [22], et le potentiel de Q_B/Q_B^- est plus oxydant que le potentiel de Q_B^-/Q_BH_2 ($E_m\ Q_B/Q_B^-$ = 160 mV et $E_m\ Q_B^-/Q_BH_2$ = 95 mV [23]). J'ai montré dans l'article 1 [12] que Q_B est réduit lorsque le PSII est traité par le DAD/ascorbate. Ce résultat peut être expliqué par le fait que le potentiel de Q_B/Q_B^- est plus oxydant que celui du couple Q_B^-/Q_BH_2 et donc correspondrai plus cette l'option où $E_m\ Q_B/Q_B^- \geq E_m\ Q_B^-/Q_BH_2$. Cette option justifie aussi une observation reproductible où les deux espèces Q_A^- et Q_B^- sont présent en même temps et stable pendant quelques minutes à température ambiante (résultats non montrés ici).

La deuxième option : $E_m\ Q_B/Q_B^- \leq E_m\ Q_B^-/Q_BH_2$

La deuxième option consiste à satisfaire la différence de potentiel de 70-83 mV entre Q_A/Q_A^- et Q_B/Q_B^- et donc de proposer un $E_m\ Q_B/Q_B^-$ aux environs de 0 mV (en prenant -80 mV pour Q_A/Q_A^- [8]), et $E_m\ Q_B^-/Q_BH_2$ ~260 mV. Cette valeur de ~260 mV pour le couple Q_B^-/Q_BH_2 pourrait expliquer l'observation réalisée au cours de cette thèse concernant l'oxydation du fer-non hémique par Q_B^- dans une fraction des centres. Dans ce cas, le couple Q_B^-/Q_BH_2 a un potentiel suffisant pour oxyder le fer non-hémique. Petrouleas et al, [15] ont proposé une valeur de 310-430 mV pour le couple Q_B^-/Q_BH_2, ce qui consolide cette option.

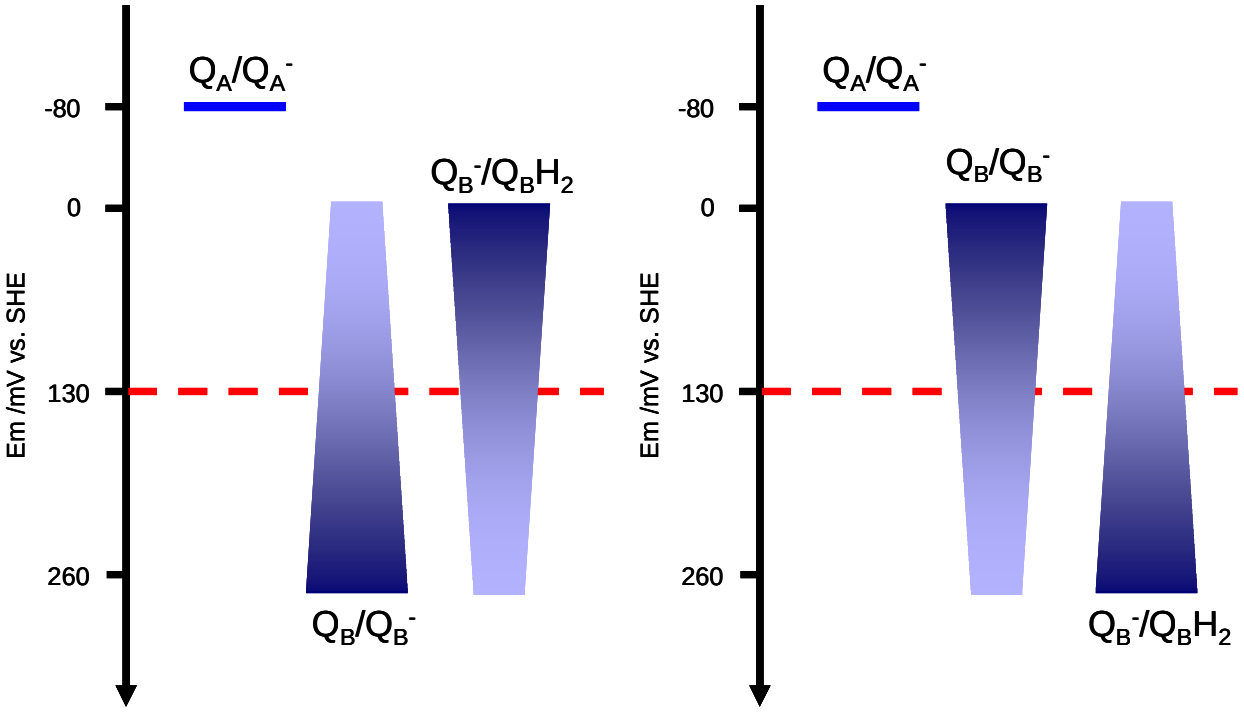

Schéma 1 : Proposition du diagramme énergétique de Q_B. A gauche, schéma basé sur l'option 1: E_m Q_B/Q_B^- ≥ E_m Q_B^-/Q_BH_2. A droite, le schéma énergétique basé sur l'option 2 : E_m Q_B/Q_B^- ≤ E_m Q_B^-/Q_BH_2. Le potentiel de -80 mV est pris comme référence [8]. La valeur de 130 mV représente le potentiel redox du pool membranaire de plastoquinone PQ/PQH_2 [21]. Potentiels proposées à pH 6,5. Dans ce schéma, on suppose que la moyenne du potentiel de Q_B/Q_B^- et Q_B^-/Q_BH_2 est égale au potentiel du PQ/PQH_2.

Pour répondre clairement à cette question et sortir des spéculations parfois contradictoires, le titrage potentiométrique semble primordial. La RPE pourrait servir de technique de premier choix afin d'acquérir cet objectif. Les résultats obtenus au cours de ma thèse concernant les spectres RPE de $Q_A^-Fe^{2+}$ et $Q_B^-Fe^{2+}$ complètement résolus (article 3) et l'évolution du signal de $Q_A^-Fe^{2+}$ au cours du temps en présence de dithionite (article 5) découvert ici (bien que l'origine exacte du changement de signal RPE de Q_AFe^{2+} réduit par la dithionite en fonction du temps est jusqu'à présent obscure) seront pris en compte lors de la réalisation du titrage de Q_B. Le titrage de Q_B par RPE a été tenté par Corrie et al, [24], un potentiel de 150 mV et 80 ont été trouvé à pH 6,5 pour les couples Q_B/Q_B^- et Q_B^-/Q_BH_2, respectivement. Ces valeurs sont proches des valeurs trouvées dans les centres bactériens et correspondants à la première option. Sauf que dans ces travaux [24], la réversibilité du titrage n'a pas été effectué et le potentiel redox trouvé pour les couples Q_B/Q_B^- et Q_B^-/Q_BH_2 coïncide

avec les potentiels redox de deux médiateurs utilisés lors du titrage. C'est en partie pourquoi ces valeurs ne sont pas reprises dans la littérature.

3. Photoactivation de l'apo-PSII:

L'assemblage du cluster de Mn_4Ca reste jusqu'à présent un mécanisme inconnu. L'élucidation de ce mécanisme pourra aider à la compréhension de la réaction d'oxydation de l'eau.

Pendant cette thèse, j'ai mis au point un protocole de photoactivation de l'apo-PSII isolé de *T. elongatus*, un matériel de choix pour la RPE. Le rendement de photoactivation reste faible (~15%) et pourrait être optimisé. J'ai utilisé ce matériel pour explorer la première étape de la photoactivation consistant à photo-oxyder un Mn^{2+}. La première étape de photoactivation consistant en l'oxydation du Mn^{2+} en Mn^{3+} est piégée par l'éclairement à basse température (-20°C). Il a été conclu qu'à cette température seul un Mn^{2+} est photo-oxydé par l'apo-PSII [25]. Les auteurs ont interprété la diminution de moitié du signal RPE X-band de Mn^{2+} lorsque l'échantillon contenant 6 Mn^{2+} / apo-PSII est éclairé à -20°C, par la photo-oxydation d'un seul Mn^{2+} lié au site de haute affinité. Ce résultat a été la base d'une série d'articles visant à caractériser la première étape de photoactivation par différentes techniques et dans des conditions différentes [25-28]. Or, J'ai démontré qu'à -20°C l'apo-PSII peut photo-oxyder plus qu'un ion Mn^{2+}, la photo-oxydation à -20°C du Mn^{2+} est limitée par la disponibilité d'un accepteur d'électrons. Je suggère donc, que dans les conditions expérimentales dans ces papiers, plusieurs Mn^{2+} ont été photo-oxydés et non pas un seul Mn^{2+} spécifique lié à son site de haute affinité. Cela a une grande répercussion sur l'interprétation des résultats spectroscopiques.

J'ai mis au point deux méthodes afin de stabiliser la première étape de la photoactivation, la première consiste à l'utilisation d'une mélange PPBQ/ferricyanure, la deuxième méthode consiste à l'éclairement pendant quelques secondes. Ces deux méthodes doivent être étudiées encore plus.

J'ai aussi mis en évidence en collaboration avec le Dr. Sun Un une méthode qui pourra être utilisée pour les études de Mn^{2+} lié à une protéine ou libre, et cela par le fait que le Mn^{2+} libre lie le Cl^- en changeant le spectre RPE à haut champ [29].

Références:

[1] B.A. Diner, V. Petrouleas, Q_{400}, the non-heme iron of the Photosystem-II iron-quinone complex - a spectroscopic probe of quinone and inhibitor binding to the reaction center Biochim Biophys Acta, 895 (1987) 107-125.
[2] J.L. Zimmermann, A.W. Rutherford, Photoreductant-induced oxidation of Fe^{2+} in the electron-acceptor complex of Photosystem-II, Biochim Biophys Acta, 851 (1986) 416-423.
[3] J.H.A. Nugent, Photoreducible high spin iron electron paramagnetic resonance signals in dark-adapted Photosystem II: are they oxidised non-haem iron formed from interaction of oxygen with PSII electron acceptors?, Biochim Biophys Acta, 1504 (2001) 288-298.
[4] C. Fufezan, C.X. Zhang, A. Krieger-Liszkay, A.W. Rutherford, Secondary quinone in photosystem II of *Thermosynechococcus elongatus*: Semiquinone-iron EPR signals and temperature dependence of electron transfer, Biochemistry, 44 (2005) 12780-12789.
[5] A. Boussac, M. Sugiura, F. Rappaport, Probing the quinone binding site of Photosystem II from *Thermosynechococcus elongatus* containing either PsbA1 or PsbA3 as the D1 protein through the binding characteristics of herbicides, Biochim Biophys Acta, 1807 (2011) 119-129.
[6] H. Ishikita, E.W. Knapp, Oxidation of the non-heme iron complex in photosystem II, Biochemistry, 44 (2005) 14772-14783.
[7] G.N. Johnson, A.W. Rutherford, A. Krieger, A change in the midpoint potential of the quinone Q_A in Photosystem-II associated with photoactivation of oxygen evolution, Biochim Biophys Acta, 1229 (1995) 202-207.
[8] A. Krieger, A.W. Rutherford, G.N. Johnson, On the determination of redox midpoint potential of the primary quinone electron-acceptor, Q_A, in Photosystem-II, Biochim Biophys Acta, 1229 (1995) 193-201.
[9] A.W. Rutherford, A. Krieger-Liszkay, Herbicide-induced oxidative stress in photosystem II, Trends Biochem Sci, 26 (2001) 648-653.
[10] A. Krieger-Liszkay, C. Fufezan, A. Trebst, Singlet oxygen production in photosystem II and related protection mechanism, Photosynth Res, 98 (2008) 551-564.
[11] C.A. Wraight, Proton and electron transfer in the acceptor quinone complex of photosynthetic reaction centers from *Rhodobacter sphaeroides*, Front Biosci, 9 (2004) 309-337.
[12] A. Sedoud, L. Kastner, N. Cox, S. El-Alaoui, D. Kirilovsky, A.W. Rutherford, Effects of formate binding on the quinone-iron electron acceptor complex of photosystem II, Biochim Biophys Acta, 1807 (2011) 216-226.
[13] J.J.S. van Rensen, V.V. klimov, Role of bicarbonate in Photosystem II, in: T.J. Wydrzynski, K. Satoh (Eds.) Advances in Photosynthesis and Respiration Oxygenic Photosynthesis: Photosystem II. The light driven water: Plastoquinone oxidoreductase, Springer, Dordrecht, 2005, pp. 329-346.
[14] U. Siggel, R. Khanna, G. Renger, Govindjee, Investigation of the absorption changes of the plasto-quinone system in broken chloroplasts. The effect of bicarbonate-depletion, Biochim Biophys Acta, 462 (1977) 196-207.
[15] V. Petrouleas, Y. Deligiannakis, B.A. Diner, Binding of carboxylate anions at the non-heme Fe(II) of PS II .
II. Competition with bicarbonate and effects on the Q_A/Q_B electron transfer rate, Biochim Biophys Acta, 1188 (1994) 271-277.
[16] Y. Deligiannakis, V. Petrouleas, B.A. Diner, Binding of carboxylate anions at the nonheme Fe(II) of PS-II .1. Effects on the $Q_A^-Fe^{2+}$ and Q_AFe^{3+} EPR spectra and the redox properties of the iron, Biochim Biophys Acta, 1188 (1994) 260-270.

[17] B.A. Diner, Dependence of the deactivation reactions of photosystem II on the redox state of plastoquinone pool A varied under anaerobic conditions; Equilibria on the acceptor side of photosystem II, Biochim Biophys Acta, 460 (1977) 247-258.
[18] H.H. Robinson, A.R. Crofts, Kinetics of the oxidation reduction reactions of the Photosystem II quinone acceptor complex, and the pathway for deactivation, Febs Lett, 153 (1983) 221-226.
[19] A.R. Crofts, C.A. Wraight, The electrochemical domain of photosynthesis, Biochim Biophys Acta, 726 (1983) 149-185.
[20] F. Rappaport, J. Lavergne, Thermoluminescence: theory, Photosynth Res, 101 (2009) 205-216.
[21] J.H. Golbeck, B. Kok, Redox titration of electron-acceptor Q and the plastoquinone pool in Photosystem II, Biochim Biophys Acta, 547 (1979) 347-360.
[22] P.L. Dutton, R.C. Prince, D.M. Tiede, Reaction center of photosynthetic bacteria, Photochem Photobiol, 28 (1978) 939-949.
[23] A.W. Rutherford, M.C.W. Evans, High-potential semiquinone-iron type epr signal in *Rhodopseudomonas viridis*, Febs Lett, 100 (1979) 305-308.
[24] A.R. Corrie, J.H.A. Nugent, M.C.W. Evans, Identification of EPR Signals from the States $Q_A^{\cdot-}Q_B^{\cdot-}$ and $Q_B^{\cdot-}$ in Photosystem-II from *Phormidium laminosum*, Biochim Biophys Acta, 1057 (1991) 384-390.
[25] A.M. Tyryshkin, R.K. Watt, S.V. Baranov, J. Dasgupta, M.P. Hendrich, G.C. Dismukes, Spectroscopic evidence for Ca^{2+} involvement in the assembly of the Mn_4Ca cluster in the photosynthetic water-oxidizing complex, Biochemistry, 45 (2006) 12876-12889.
[26] J. Dasgupta, A.M. Tyryshkin, G.C. Dismukes, ESEEM spectroscopy reveals carbonate and an N-donor protein-ligand binding to Mn^{2+} in the photoassembly reaction of the Mn4Ca cluster in photosystem II, Angew Chem Int Edit, 46 (2007) 8028-8031.
[27] J. Dasgupta, G.M. Ananyev, G.C. Dismukes, Photoassembly of the water-oxidizing complex in photosystem II, Coordin. Chem. Rev, 252 (2008) 347-360.
[28] J. Dasgupta, A.M. Tyryshkin, S.V. Baranov, G.C. Dismukes, Bicarbonate coordinates to Mn^{3+} during photo-assembly of the catalytic Mn_4Ca core of photosynthetic water oxidation: EPR characterization, Appl. Magn. Reson., 37 (2010) 137-150.
[29] S. Un, A. Sedoud, High-field EPR Study of the effect of Chloride on Mn^{2+} ions in frozen aqueous solutions, Appl. Magn. Reson., 37 (2010) 247-256.

ANNEXES

ARTICLE 9

High-field EPR study of the effect of chloride on Mn^{2+} ions

in frozen aqueous solutions

Appl Magn Reson (2010) 37:247–256
DOI 10.1007/s00723-009-0062-y

Applied
Magnetic Resonance

High-field EPR Study of the Effect of Chloride on Mn^{2+} Ions in Frozen Aqueous Solutions

Sun Un · Arezki Sedoud

Received: 12 May 2009 / Revised: 2 June 2009 / Published online: 16 November 2009

Abstract The effect of chloride concentration on Mn^{2+} ($S = 5/2$, $I = 5/2$) ions in frozen aqueous solutions is studied by high-field high-frequency electron paramagnetic resonance (HFEPR). The usually six sharp lines characteristic of Mn^{2+} ions, arising from the $m_s = -1/2 \rightarrow 1/2$ transition, is modified by the addition of Cl^- anions and the six resonances become much broader and more complex. This new feature likely arises from the ligation of one Cl^- anion to a hydrated Mn^{2+} ion forming a $[Mn(H_2O)_5Cl]^-$ complex. This complex increases linearly with Cl^- concentration with an association constant of $K_{a,\,\mathrm{apparent}} = 61\ M^{-1}$. The structure of the putative chloride complex was studied using density functional theory calculations and the expected zero-field interaction of such a manganese center was calculated using the superposition model. The predicted values were similar to those determined from the simulation of the spectrum of the $m_s = -5/3 \rightarrow -3/2$ transition of the chloride complex. This effect of Cl^- anions occurs at biologically relevant concentration and can be used to probe the Mn^{2+} ions in cellular and protein environments.

1 Introduction

Many important biological processes depend on manganese ranging from photosynthetic oxygen production to control of oxidative stress as well as other enzymatic processes [1]. Although manganese takes on a variety of oxidation states in these processes, most, if not all, originates as Mn^{2+}. As such, its acquisition, transport and homeostasis are important to cells. There are few techniques capable of selectively detecting and characterizing manganese ions. Electron paramagnetic resonance

S. Un (✉) · A. Sedoud
Service de Bioénergétique, Biologie Structurale et Mécanismes,
Institut de Biologie et Technologies de Saclay, CNRS URA 2096,
Pièce 210, Bâtiment 532, CEA Saclay, 91191 Gif-sur-Yvette, France
e-mail: sun.un@cea.fr

(EPR) spectroscopy is one of such methods that is capable of probing the electronic states and structure of manganese ions and their binding sites.

The EPR spectroscopy of Mn^{2+} ($S = 5/2$, $I = 5/2$) is essentially determined by the spin Hamiltonian

$$H = \beta\vec{B}\cdot\mathbf{g}\cdot\vec{S} + \vec{I}\cdot\mathbf{A}\cdot\vec{S} + \frac{D}{3}\left(3S_z^2 - S(S+1)\right) + E\left(S_+^2 - S_-^2\right) \quad (1)$$

where the first term describes the electronic Zeeman interaction and the second the hyperfine interaction between the unpaired electrons and the manganese nucleus ($I = 5/2$), and the last two terms describe the zero-field interaction. For most Mn^{2+} ions, the Zeeman and hyperfine interactions are essentially isotropic which greatly simplifies the spin Hamiltonian and spectral analysis.

Due to the zero-field interaction, which can range from essentially 0 to beyond 10 GHz, conventional 9 GHz EPR has proven to be of limited value due to poor resolution and high spectral complexity. Recently, several experiments have been carried out using high magnetic-field high-frequency EPR (HFEPR) [2–5] that suggest that this approach not only circumvents these two limitations, but also allows accurate measurement of the magnetic spin parameters of an Mn^{2+} ion from which valuable information about its electronic structure and interactions with the environment can be extracted. The essence of HFEPR spectroscopy of Mn^{2+} ions is shown in Fig. 1. There are two notable features of Mn^{2+} HFEPR. In general, the zero-field interaction does not affect the $m_s = -1/2 \rightarrow 1/2$ resonances to first order; nonetheless, it does contribute to higher orders resulting in line broadening. When modest, these higher-order line broadening effects can be exploited to determine the zero-field parameters, D and E, from line shape analysis, but they also inevitably lead to loss of resolution. It is possible to suppress or reduce such effects by using higher magnetic field that also requires higher microwave frequencies. An ideal situation is one where these zero-field effects can be "tuned" by using variable magnetic fields and microwave frequencies. We have demonstrated such an approach by using 95, 190, and 285 GHz microwave frequencies and a 10 T magnet to study manganese centers in superoxide dismutases that have zero-field interactions ranging from 1 to 10 GHz [6]. A second feature of Mn^{2+} HFEPR is the ability to observe clearly and easily the spectrum of the $m_s = -5/2 \rightarrow -3/2$ transition even in frozen solutions. This is accomplished by reducing the observation temperature to that of liquid helium, where only $m_s = -5/2$ and $-3/2$ levels are significantly occupied (for 10 T and $g = 2$, $\nu = 285$ GHz at 13 K). The zero-field parameters can be directly determined from such a liquid-helium-temperature spectrum with the added advantage that for cases, where the E/D ratio is not close to 1/3, the algebraic sign of D can be unambiguously determined (Fig. 1).

We and others have been exploiting HFEPR spectroscopy to study Mn^{2+} in enzymes, but recently we have turned our attention to the so-called "free" Mn^{2+}, that is, ions not bound to enzymes. They have been implicated in nonenzymatic, but nonetheless catalytic, dismutation of superoxide [7] and conversion of peroxide to oxygen, and water [8]. Little is known about what chemical form the free Mn^{2+} takes. This is important, for example, because the reduction potential of the Mn^{3+}/Mn^{2+} couple in water is too high to carry out catalytically the dismutation of superoxide. We have shown that the Mn^{2+} zero-field parameters are sensitive to the

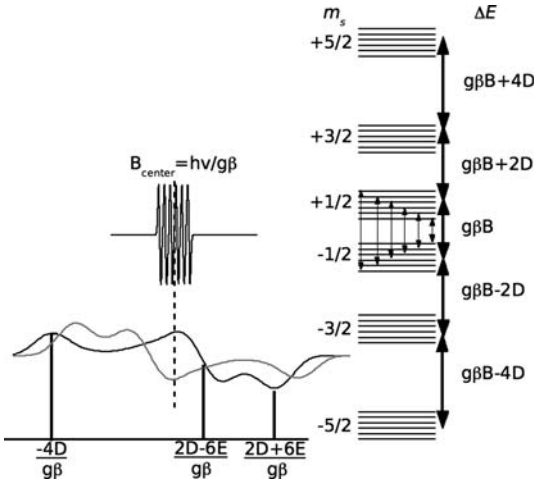

Fig. 1 The EPR spectra (*left*) and energy levels (*right*) of a Mn^{2+} ion when the Zeeman interaction ($g\beta B$) is the dominant interaction. The energy diagram is for the case where $E = 0$ and the *heavy arrows* denote the five formally allowed electronic spin transitions. The powder spectrum of the $m_s = -5/2 \rightarrow -3/2$ transition is shown for $D < 0$ (*gray*) and $D > 0$ (*black*). The $m_s = -1/2 \rightarrow 1/2$ spectrum and the associated electron-nuclear hyperfine transitions (*fine arrows*) are also shown. Both, the $m_s = -5/2 \rightarrow -3/2$ and $m_s = -1/2 \rightarrow 1/2$ spectra are centered $B_{\text{center}} = h\nu/g\beta$. The labeled field positions are relative to B_{center}

electrostatic environment of the metal binding site and, at least in certain synthetic complexes, the Mn^{2+} zero-field interaction is proportional to the Mn^{3+}/Mn^{2+} redox potential [9, 10]. Hence, HFEPR provides an effective chemical probe. A different approach has been the use of high-field pulsed electron-nuclear double resonance [11]. In this study, we describe HFEPR spectroscopic study of Mn^{2+} ions in frozen buffered solutions and the effect of chloride on them. The concentrations of metal and chloride used were well within biologically relevant range and the results of this study should have direct implications to what happens in the cellular milieu.

2 Materials and Methods

2.1 Chemicals

Standard reagent-grade $MnCl_2 \cdot 2H_2O$ and NaCl were used and dissolved in 10 mM 2-(*N*-morpholino)ethanesulfonic acid (MES) buffer (pH 6.3). Manganese concentrations were verified by atomic absorption spectrometry (Perkin-Elmer).

2.2 HFEPR Spectrometer

The HFEPR spectrometer has been described in detail elsewhere [12]. Field calibration was based on a Mn^{2+}-doped MgO standard sample ($g = 2.00101$ [13]) and the absolute error in field measurements was 1 G (0.1 mT). Spectra of the $m_s = -1/2 \leftrightarrow 1/2$ transition were taken at 23 K with 2 G resolution and 2 G

modulation amplitude. With these parameters, sufficiently accurate amplitudes and line shapes were obtained. All $m_s = -1/2 \leftrightarrow 1/2$ spectra were obtained under non-saturating conditions and could be readily double integrated. The $m_s = -5/2 \leftrightarrow -3/2$ spectra were obtained at 4.2 K—with a modulation amplitude of 20 G.

2.3 Spectrum Simulations

Simulations of the spectra of the $m_s = -1/2 \leftrightarrow 1/2$ transitions were carried out as previously described [6, 14]. It has been previously shown that the estimated error limits of the fitting procedure can be as small as ±0.06 GHz for the two zero-field parameters. Simulations of the 4-K spectra were based on standard second-order perturbation solutions to the spin Hamiltonian Eq. (1). The **g**- and hyperfine tensors were assumed to be isotropic. Only the formally "allowed" transitions were considered. The amplitudes of the transitions were properly weighed to take into account the quantum mechanical transition probabilities, as well as populations of the six levels as defined by Boltzmann's equation.

3 Results and Discussion

Figure 2 shows the HFEPR spectrum $m_s = -1/2 \leftrightarrow 1/2$ of 15 μM Mn^{2+} in 10 mM MES buffer as a function of the NaCl concentration added. Below 3 mM chloride concentration, the $m_s = -1/2 \leftrightarrow 1/2$ spectra consisted simply of six relatively sharp lines, one of which is labeled "B" in Fig. 2. These spectra were essentially identical to the spectrum in the absence of chloride. The six lines are due to the hyperfine interaction and the sharpness of the lines indicated that the zero-field interaction was relatively small. From here on, the Mn^{2+} ions that give rise to such simple spectrum will be referred to as Mn^{2+}_{free}. Above 3 mM NaCl, a different six-line spectrum (one of the lines is labeled "A" in Fig. 2) that had a much more complex line shape appeared. This more complex spectrum grew with increasing concentration of NaCl until 150 mM. The width of each of the new hyperfine lines was much broader than those observed in the absence of chloride and, for a given NaCl concentration, the width of these resonances increased with increasing magnetic field, that is, the hyperfine line corresponding to the +5/2 nuclear spin state was the widest. These observations were indicative of Mn^{2+} centers that had a much larger zero-field interaction than that of the Mn^{2+}_{free} ions. The same effect was seen when $CaCl_2$ and $MgCl_2$ were added as the source of chloride anions, indicating the changes in the spectra were predominately, if not solely, determined by chloride.

The Cl^- concentration dependence of the Mn^{2+} spectra was examined (Fig. 3). The Mn^{2+} spectra for a given chloride concentration could be readily decomposed into the components corresponding to the Mn^{2+}_{free} and the chloride complexed species. The simplest chemical equilibrium that describes the observed changes was

$$(Mn(H_2O)_6)^{2+} + Cl^- \rightleftharpoons (Mn(H_2O)_5Cl)^+ + H_2O. \quad (2)$$

Here, we assumed that the Mn^{2+}_{free} was $(Mn(H_2O)_6)^{2+}$ and the chloride-bound species results from the displacement of one water molecule by a chloride anion.

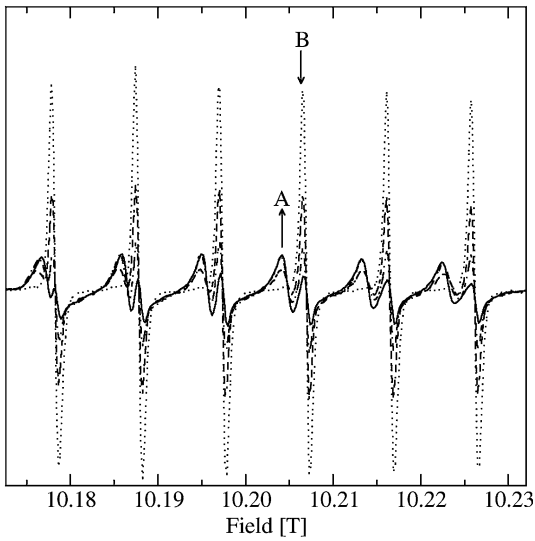

Fig. 2 The 285 GHz Mn^{2+} EPR spectra ($m_s = -1/2 \leftrightarrow 1/2$) of frozen solution of 15 μM Mn^{2+} in 10 mM MES (pH 6.2) buffer as a concentration of NaCl is increased: 3 mM (*dotted*), 30 mM (*dashed*), 60 mM (*dot-dashed*), and 150 mM (*solid*). "*A*" indicates one of the six hyperfine lines of the chloride-complexed ions and "*B*" that of the Mn^{2+}_{free}. The directions of the *arrows* show the direction of the amplitude change with increasing chloride concentration

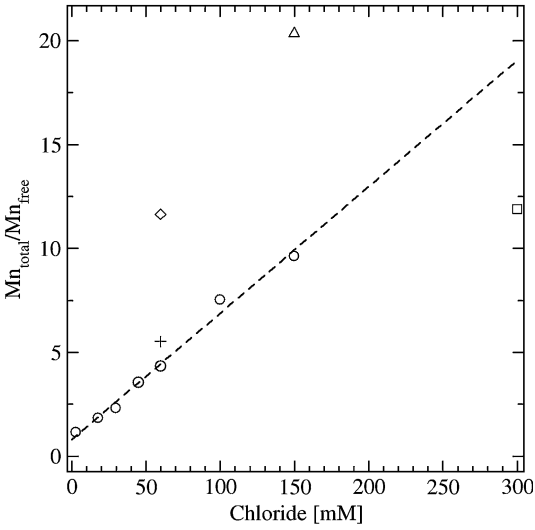

Fig. 3 Ratio of the intensity of the total spectrum to that of the free manganese as a function of chloride concentration with total Mn^{2+} concentrations of: 15 (*circles* and *square*), 150 (*triangle* and *cross*), and 300 (*diamond*) μM. The *dashed line* is the linear regression fit of the *circle* points only. See text for details

In the detail, the line shape of the broad component appeared to depend on the specific conditions (Figs. 4 and 5). Hence, the species that we denote $(Mn(H_2O)_5Cl)^+$ may not have been a unique chemical species. Nonetheless, at relatively low Mn^{2+} and chloride concentrations the spectra appeared to be consistent with the above simple equilibrium, which can be described by the equation

$$K_a = \frac{[(Mn(H_2O)_5Cl)^+]}{[(Mn(H_2O)_6)]^{2+}[Cl^-]}$$
$$K_a[Cl^-]_0 + 1 = \frac{[Mn^{2+}]_0}{[(Mn(H_2O)_6)^{2+}]} \quad (3)$$

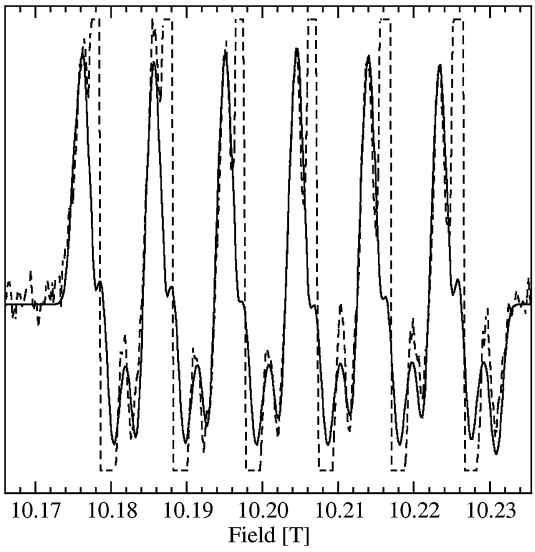

Fig. 4 Simulation (*solid line*) of the 285 GHz EPR spectrum (*dashed line*) of chloride complex species obtained at 23 K for solution of 15 μM Mn^{2+} and 18 mM NaCl in MES (pH 6.2). The six lines corresponding to Mn^{2+}_{free} have been truncated. The fitting was constrained to the broad component. The zero-field parameters were: $|D| = 2.79$ and $E = 0.57$ GHz

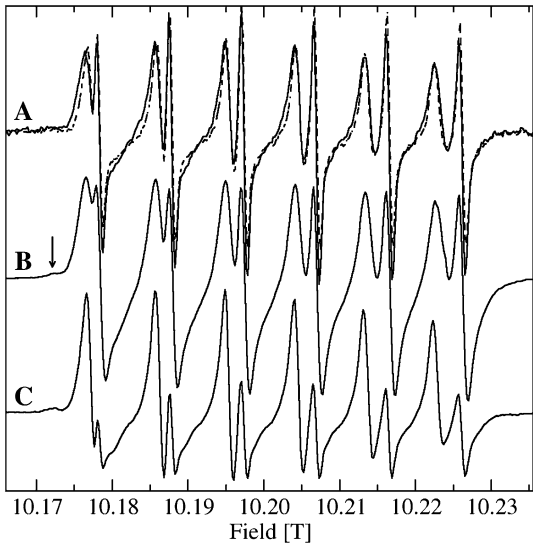

Fig. 5 The 285-GHz Mn^{2+} EPR spectra ($m_s = -1/2 \leftrightarrow 1/2$) of a solution with: (*a*) 15 μM Mn^{2+} and 60 mM NaCl (*solid*) and 15 μM Mn^{2+} and 300 mM NaCl (*dashed*); (*b*) 300 μM Mn^{2+} and 60 mM NaCl; and (*c*) 150 μM Mn^{2+} and 300 mM NaCl. All samples were in 10 mM MES (pH 6.2) buffer. The *arrow* indicates a large zero-field species that grows with Mn^{2+} concentration

in which K_a is the association constant, $[Cl^-]_0$ and $[Mn^{2+}]_0$ are the total manganese and chloride contents. The latter a proportional to the double integral of the total spectrum, while $[(Mn(H_2O)_6)^{2+}]$ is proportional to the double integral of the contribution of the sharp free manganese component. Equation (3) is only valid when $[Cl^-]_0$ is much greater than $[Mn^{2+}]_0$, which is true in our case. Hence, a plot of the ratios of these double integrals as a function of chloride concentration should be linear with intercept of 1 and slope of K_a. At least for a Mn^{2+} concentration of 15 μM and chloride concentrations below 150 μM, this was in fact what was seen

(Fig. 3). The linear regression fit of the measured data yielded: $K_{a,apparent} = 61 \pm 3\ M^{-1}$ and an intercept of 0.8 ± 0.2. Since the HFEPR measurements were carried out in frozen solution, this association constant cannot be considered a true measurement of the equilibrium constant, but should be considered as an "apparent" one, most likely reflecting the equilibrium concentrations immediately before freezing (i.e., $\sim$0°C). There is no rigorous proof for this, but a series of subsequent competitive binding experiments (unpubl. data) with other anions, such as adenosine triphosphate and other phosphates, for which the association constants are known, suggests that the low value of the chloride $K_{a,apparent}$ that we have obtained is entirely consistent with these other values.

The situation is unlikely to be as simple as depicted by the above equilibrium. At chloride concentration above 150 μM, the ratio of total to free Mn^{2+} appeared to level-off and the line shape of the broad component also subtly changed (Figs. 4 and 5). Equation (3) only depends on the ratio of total to free Mn^{2+}. The intensity ratios for the 150-μM Mn^{2+} and 60 mM chloride combination were approximately the same as for the case of 15 μM Mn^{2+} in 60 mM chloride. However, for the much larger concentration of 300 μM Mn^{2+} in 60 mM chloride, a significantly different ratio was found (Fig. 3). This suggested that there might have been other equilibria involved such as the formation of other molecular species induced by high ion concentration or increased ionic strengths.

This heterogeneity in the chloride-complexed species was evident in the line shapes of the resonances corresponding to these species, which appeared to depend on the chloride concentration. At 18 mM chloride, the resonances were well resolved (Fig. 4). At higher concentrations (>300 mM), the high-field side of each of the six resonances became less resolved, indicative of a distribution in the zero-field parameters. There also appeared to be a slight narrowing indicating a small reduction in the zero-field interaction (Fig. 5). Also with increasing manganese concentration a small resonance, indicated by an arrow in Fig. 5, became more noticeable. The extent of this signal indicated a Mn^{2+} center with zero-field interaction almost twice as large as in the dominant species.

To quantify the zero-field interactions of the chloride complexed species, the spectra were fitted. Figure 4 shows the simulation of the $m_s = -1/2 \leftrightarrow 1/2$ spectrum of this component. The 18-mM chloride sample was used since it exhibited the highest overall resolution. As can be seen the fit was good and yielded a $|D|$ value of 2.79 and E of 0.57 GHz. The g_{iso} and $|A_{iso}|$ values for the chloride complexed ion were 2.0003 and 0.263 GHz, respectively. The same values for Mn^{2+}_{free} were 2.0003 and 0.267 GHz, respectively. By comparison, the manganese center in concanavalin-A has $g_{iso} = 2.0001$ and $|A_{iso}| = 0.260$ GHz [6, 15]. Although all three g-values are within the experimental error, the 7-MHz difference in the isotropic coupling is significant, possibly indicating greater ionicity in the chloride complexed and free species compared to the protein case [16].

We also examined the 4-K spectrum of the sample containing 150 μM Mn^{2+} and 60 mM chloride (Fig. 6). This was the lowest Mn^{2+} concentration for which we have been able to record the $m_s = -5/2 \leftrightarrow -3/2$ component. What was immediately evident is that the spectrum was, in fact, composed of at least three contributions: one from the narrow Mn^{2+}_{free}, another due to the chloride complexed

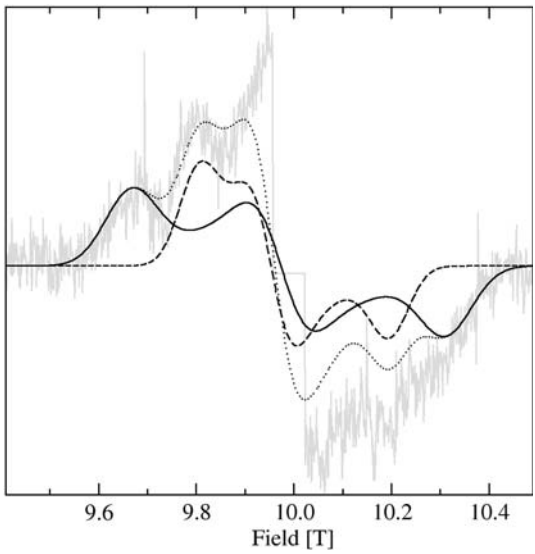

Fig. 6 The 4.2-K 279 GHz spectrum of $m_s = -5/2 \leftrightarrow -3/2$ transition for the frozen solution of 150 μM Mn^{2+} and 60 mM NaCl in MES (pH 6.2) buffer (*gray*). The two components that make up the spectrum, determined from simulations, are also shown (*solid and dashed lines*), as well as the sum of these two contributions (*dotted line*). The fitted zero-field parameters were: $D = -2.22$ and $E = 0.784$ GHz (*solid line*), and 1.49 and 0.346 GHz (*dashed*). The six-shape lines corresponding to the $m_s = -1/2 \leftrightarrow 1/2$ transition have been omitted for clarity

species ($D = -2.22$ and $E = 0.78$) that was similar to the one simulated in Fig. 4, and a third component that had an intermediate zero-field interaction ($D = +1.49$ and $E = 0.35$). We noted that the passing that the "free" manganese did not give a well-defined $m_s = -5/2 \leftrightarrow -3/2$ transition (the contribution between 9.9 and 10.1 T in Fig. 6) and hence, determination of its zero-field parameters was not possible, except that the magnitude of the zero-field interaction was less than 1 GHz. It is likely that the third component is the one responsible for apparent loss of resolution when one compares spectra in Figs. 4 and 5a.

Given the relatively high chloride concentrations required to observe the broader spectral component (Fig. 4), it seemed chemically reasonable that the species from which it arose was indeed $(Mn(H_2O)_5Cl)^+$. It is known that a chloride ligand will significantly increase the Mn^{2+} zero-field interaction compared to an oxygen-based ligand [17, 18]. The structure and energetics of the formation of $(Mn(H_2O)_5Cl)^+$ were examined using quantum chemical calculations. Geometry optimization and frequency calculations were carried out using the B3LYP exchange–correlation functional and the QZVPP basis-set [19] for the metal center and 6-31G + (d) basis-set for all other atoms. The manganese complexes were embedded in water using the polarizable continuum model as implemented in Gaussian-03 [20]. The optimized structure (Fig. 7) had C_{2v} symmetry, with two opposing equatorial water ligands perpendicular to the chloride ligand with a Mn–O bond length of 2.153 Å and the other two bent away with a Mn–O bond length of 2.183 Å. The Mn–Cl bond length was 2.577 Å and the axial Mn-(OH_2) 2.160 Å. Normal-mode analysis confirmed that the structure was at a true energy minimum (that is no mode had imaginary frequencies). From this analysis, the enthalpy and Gibbs free energy for the complex were also obtained. The same parameters were also obtained for $(Mn(H_2O)_6)^{2+}$, water and chloride anion using the same methods. The change in enthalpy for the equilibrium given by Eq. (2) was −6.4 kcal/mol and the Gibbs free

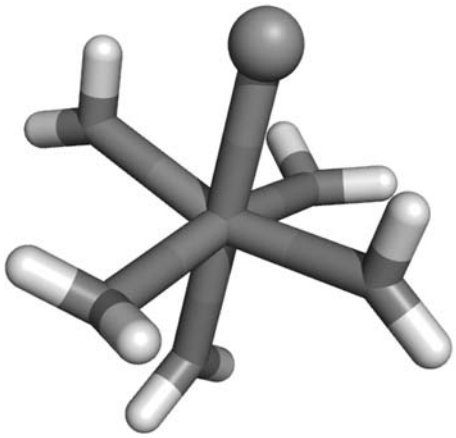

Fig. 7 The B3LYP/QZVPP/6-31G+(d) optimized geometry of the $Mn(H_2O)_5Cl)^+$. The round sphere is the chloride atom

energy, −9.4 kcal/mol. Using the TZVPP basis-set yielded values that were about 0.5 kcal/mol lower. These values showed that formation of the chloride complex was indeed favorable, but energies were relatively small (for example, comparable to hydrogen bonding energies).

The superposition model (SPM) is one method for predicting the zero-field interaction parameters of the Mn^{2+} site on the basis of its structure [18, 21]. Application of the SPM to the optimized geometry, discussed above, yielded $D = +3.21$ and $E = 0.15$, assuming the zero-field axis was along the Mn–Cl bond. The measured values indicated a nearly completely rhombic tensor, while these calculated values predicted an intermediate rhombicity. Nonetheless, the magnitudes of the zero-field interaction, as defined by $(D^2 + 3E^2)^{1/2}$, differ only by 0.5 GHz between the measured and calculated. A complete ab initio quantum chemical treatment is underway.

4 Conclusion

Our HFEPR experiments show that chloride anions bind Mn^{2+} at concentrations that are physiologically relevant (blood plasma chloride concentration is about 150 mM). The association is low ($K_{a,apparent} = 61\ M^{-1}$). The zero-field interaction of the chloride complexed Mn^{2+} species is considerably larger than that of the water-solvated ions, indicating that, not surprisingly, the electronic structure of the metal ion was different. Nonetheless, these observations suggest the possibility that the electrochemical potential of chloride complexed species may be different from that of free manganese ions [9, 10]. Another intriguing possibility is that the chloride anions can be used to label or contrast those Mn^{2+} ions in solution from those interacting with proteins. These and other aspects of this simple chemical system are being pursued.

Acknowledgments We thank A. W. Rutherford for support and encouragement, T. L. Lai for technical assistance and F. Leach for valuable help in preparing this manuscript. A.S. is grateful for financial

support from the IRTELIS (international research training for excellence in life science) graduate program. This research was supported by the (EU COST) European Cooperation in Science and Technology) P15 action on "Advanced paramagnetic resonance methods in molecular biophysics".

References

1. N.S. Jakubovics, H.F. Jenkinson, Microbiology **147**, 1709–1718 (2001)
2. B.J. Gaffney, C. Su, E.H. Oliw, Appl. Magn. Reson. **21**, 413–424 (2001)
3. S. Un, P. Dorlet, G. Voyard, L.C. Tabares, N. Cortez, J. Am. Chem. Soc. **123**, 10123–10124 (2001)
4. D. Goldfarb, K.V. Narasimhulu, R. Carmieli, Magn. Reson. Chem. **43**, S40–S50 (2005)
5. A. Angerhofer, E.W. Moomaw, I. Garcia-Rubio, A. Ozarowski, J. Krzystek, R.T. Weber, N.G. Richards, J. Phys. Chem. B. **111**, 5043–5046 (2007)
6. L.C. Tabares, N. Cortez, I. Agalidis, S. Un, J. Am. Chem. Soc. **127**, 6039–6047 (2005)
7. K. Barnese, E.B. Gralla, D.E. Cabelli, J.S. Valentine, J. Am. Chem. Soc. **130**, 4604–4606 (2008)
8. M.J. Horsburgh, S.J. Wharton, M. Karavolos, S.J. Foster, Trends. Microbiol. **10**, 496–501 (2002)
9. J. Gätjens, M. Sjodin, V.L. Pecoraro, S. Un, J. Am. Chem. Soc. **129**, 13825–13827 (2007)
10. M. Sjodin, J. Gatjens, L.C. Tabares, P. Thuery, V.L. Pecoraro, S. Un, Inorg. Chem. **47**, 2897–2908 (2008)
11. A. Potapov, D. Goldfarb, Inorg. Chem. **47**, 10491–10498 (2008)
12. S. Un, P. Dorlet, A.W. Rutherford, Appl. Magn. Reson. **21**, 341–361 (2001)
13. O. Burghaus, M. Plato, M. Rohrer, K. Moebius, F. MacMillan, W. Lubitz, J. Phys. Chem. **97**, 7639–7647 (1993)
14. S. Un, L.C. Tabares, N. Cortez, B.Y. Hiraoka, F. Yamakura, J. Am. Chem. Soc. **126**, 2720–2726 (2004)
15. E. Meirovitch, Z. Luz, A.J. Kalb, J. Am. Chem. Soc. **96**, 7538 (1974)
16. O. Matumura, J. Phys. Soc. Jpn. **108**, 108 (1959)
17. C. Duboc, T. Phoeung, S. Zein, J. Pecaut, M.N. Collomb, F. Neese, Inorg. Chem. **46**, 4905–4916 (2007)
18. M. Heming, S. Remme, G. Lehmann, J. Magn. Reson. **69**, 134–143 (1986)
19. F. Weigend, F. Furche, R. Ahlrichs, J. Chem. Phys. **119**, 12753–12762 (2003)
20. M.J. Frisch, G.W.T.H.B. Schlegel, G.E. Scuseria, M.A. Robb, J.R.C.J.A. Montgomery, Jr., T. Vreven, K.N. Kudin, J.C.B.J.M. Millam, S.S. Iyengar, J. Tomasi, V. Barone, B.M.M. Cossi, G. Scalmani, N. Rega G.A. Petersson, H.N.M. Hada, M. Ehara, K. Toyota, R. Fukuda, J.H.M. Ishida, T. Nakajima, Y. Honda, O. Kitao, H. Nakai, M.K.X. Li, J.E. Knox, H.P. Hratchian, J.B. Cross, C. Adamo, J.J.R. Gomperts, R.E. Stratmann, O. Yazyev, A.J. Austin, R.C.C. Pomelli, J.W. Ochterski, P.Y. Ayala, K. Morokuma, G.A.V.P. Salvador, J.J. Dannenberg, V.G. Zakrzewski, S.D.A.D. Daniels, M.C. Strain, O. Farkas, D.K.M.A.D. Rabuck, K. Raghavachari, J.B. Foresman, J.V.O.Q. Cui, A.G. Baboul, S. Clifford, J. Cioslowski, B.B.S.G. Liu, A. Liashenko, P. Piskorz, I. Komaromi, R.L.M.D.J. Fox, T. Keith, M.A. Al-Laham, C.Y. Peng, A.N.M. Challacombe, P.M.W. Gill, B. Johnson, W.C.M.W. Wong, C. Gonzalez, J.A. Pople, Gaussian 03, Revision B.05 (2003)
21. D.J. Newman, W. Urban, Adv. Phys. **24**, 793–844 (1975)

ARTICLE 10

(en préparation)

The biradical ($Q_A^{\bullet -}Fe^{2+}Q_B^{\bullet -}$) complex of Photosystem II

TITLE: The bi-radical ($Q_A^-Fe^{2+}Q_B^-$) complex of Photosystem II

AUTHORS: Nicholas Cox[*], Arezki Sedoud[§], Adrian Jaszewski[#], Ron Pace[#], Wolfgang Lubitz[*], Raphael Calvo[%], A. William Rutherford[§].

AFFILIATIONS: [*]MPI für Bioanorganische Chemie, Stiftstrasse 34 - 36 / D - 45470 Mülheim an der Ruhr, Germany, [%]INTEC (CONICET-UNL) Güemes 3450, 3000 Santa Fe, Argentina, [#]Research School of Chemistry, Australian National University, Canberra, ACT 0200, Australia. [§]iBiTec-S, CNRS URA 2096, Bât 532, CEA Saclay, 91191 Gif-sur-Yvette, France.

CORRESPONDING AUTHOR: Email address: cox@mpi-muelheim.mpg.de; Telephone: +49-208-306-3865

ABSTRACT

The bi-radical ($Q_A^-Fe^{2+}Q_B^-$) signal of Photosystem II (PS II) was studied using ESR/EPR spectroscopy. This signal is characterized by a turning point at g~1.66. In this work we have further characterized this signal, identifying its low and high field edges and its temperature dependence. The g~1.66 EPR signal was simulated using the theoretical approach used previously for the bacterial reaction center (BRC) and PS II semiquinone-iron complex ($Q_A^-Fe^{2+}$), a spin Hamiltonian formalism in which the two semiquinone radicals magnetically interact (J ~ 1 cm^{-1}) with the near by high spin Fe^{2+} [Butler et al. 1984 *Biophys. J.* 45, 947, Cox et al. 2009 *Biophys. J.* (in press)]. In the latter it was shown that the two forms of the semiquinone-iron signal (Q_AFe^{2+}) differed mainly by an axis rotation of the exchange coupling tensor (J) relative to the fine structure tensor and a small increase in the zero-field parameter D (~6 cm^{-1}). Together with DFT calculations, these inferred changes in the coupling environment of the two complexes suggested the native exogenous ligand to the Fe^{2+} center of PS II was a carbonate (CO_3^{2-}) rather than bicarbonate in the 'dark state' ($Q_AFe^{2+}Q_B$).

Here we provide evidence that the g~1.66 bi-radical ($Q_A^-Fe^{2+}Q_B^-$) signal generated at 5 K is heterogeneous, with a fraction of centers in which the exogenous ligand to the Fe^{2+} is a carbonate and a fraction of centers with a bicarbonate. As a homogenous g~1.9 ($Q_B^-Fe^{2+}$) signal (carbonate) was observed prior to illumination (5 K), reduction of the Q_A is proposed to induce protonation of the exogenous (carbonate). This observation suggests a possible protonation pathway via the Fe^{2+} center for Q_B in PS II.

INTRODUCTION

Proton coupled electron transfer (PCET) reactions are a common feature of many biological enzymes including Photosystem II (PS II). The PS II enzyme (plastoquinone oxidoreductase), a pigment-protein complex, performs a proton coupled two electron reduction of an exchangeable plastoquinone (Q_B). Quinone reduction is a light driven process. Photo-excitation of the primary electron donor P680 of PS II, a $chlorophyll_a$ complex located near the lumenal membrane interface, initiates the transfer of an electron to the neighboring $pheophytin_a$ ($pheo_{D1}$). From there the electron is rapidly passed to the primary plastoquinone (Q_A) on the stromal side (for a recent review see (1)). Q_A is a tightly bound species that undergoes a one-electron reduction forming the semiquinone (Q_A^-).

(Scheme 1 (2))

Electrons leave PS II via the secondary plastoquinone acceptor (Q_B), the mobile electron acceptor of PS II. Q_A^- reduces Q_B, first to the semiquinone (Q_B^-), and then the quinol (Q_BH_2) after a second photochemical turnover (2). This two-electron gate mechanism was discovered in PS II by (3, 4) in PS II, and later in purple bacterial reaction centers (BRC) (5, 6). The secondary quinone (Q_B) and quinol (Q_BH_2) bind weakly (dissociation constants, ~1-2 mM, (2, 7)), in contrast to the semi-quinone (Q_B^-), which has a dissociation constant (~0.5 μM) that is 2000 times less than the quinol. The relative stability of the bound semiquinone is thought to arise from coulombic interactions with the surrounding protein/metal environment and H-bonding to residues in the Q_B pocket. The mechanism of electron transfer through the two quinones and the structure of their sites are similar in PS II and BRC (2, 8-10).

In the BRC the electron transfer between Q_A^- and Q_B ($k_{AB(1)}$ in Scheme 1) is limited by a conformational gating process rather than by the driving force (11). The subsequent electron transfer step Q_A^- to Q_B^- ($k_{AB(2)}$) appears to be rate limited by the uptake of a proton (12). After a second protonation, the Q_BH_2 exchanges with a quinone from the pool in the membrane, completing the two electron reaction cycle (for reviews see (2, 12)).

In PS II Q_A and Q_B are positioned on either side of a non-heme iron center (Fe^{2+}), which is within ~7.5 Å of either quinone (center to center). The Fe^{2+} adopts a near-octahedral ligand geometry (9, 10, 13, 14). Four coordination sites are provided by histidine residues, two from D1 (H215 and H272) and two from D2 (H214 and H268). An exogenous bi-dentate bicarbonate/carbonate fills the remaining two coordination sites (15, 16). A homologous quinone–iron complex is present in the BRC (8, 17) with an almost identical geometry, a 6-coordinate Fe^{2+} center, with 4 histidine ligands (provided by the L and M subunits, the bacterial D1/ D2 analogs). The remaining co-ordination site is however occupied by a glutamate residue of the M subunit (M234 in R. sphaeroides) rather than the exchangeable bicarbonate. In the BRC the H subunit encloses the quinone-iron complex, isolating it from the external environment (8, 17). In PS II there is no corresponding H subunit.

The role of the non-heme iron in BRC and PS II is not fully understood. In BRC other divalent transition metal ions (Mn^{2+}, Co^{2+}, Ni^{2+}, and Cu^{2+}) and even Zn^{2+} can replace the iron and show identical electron transfer rates i.e. $1/k_{AB}$ = ~150 μs^{-1} (18). Indeed Mn^{2+} has been found to be naturally present is some strains (19). Similarly, metal free BRC have been shown to be functional, with the observed rate of the electron transfer between Q_A and Q_B approximately half that of the native system (18). These studies suggest that the Fe^{2+} center has a marginal role in electron transfer between Q_A and Q_B in BRC.

In contrast to BRC, electron transfer in PS II is more strongly influenced by changes at the non-heme iron site. The relative 'openness' of the Fe^{2+} center in PS II allows the exogenous bicarbonate/carbonate ligand to be displaced by various other small molecules including: formate, cyanide, nitric oxide etc ((2) and refs. therein). The electron transfer rate between Q_A and Q_B is often significantly reduced in these ligand perturbed systems.

The 'bicarbonate effect' – an enhanced electron transfer rate between Q_A and Q_B seen when the non-heme iron binds bicarbonate/carbonate – is a topic of substantial interest in PS II research. Experiments show that electron transfer between Q_A and Q_B slows after the *second* actinic flash in samples where bicarbonate/carbonate has been exchanged (formate-treated etc) (20). As the second electron transfer step (scheme 1) requires protonation of the Q_B, it has been proposed that bicarbonate/carbonate facilitates this process. It is unclear whether it donates protons to Q_B (via a protein side-chain network) or influences protonation events by modifying the pK_a environment of the Q_B protein scaffold ((21) and ref. therein).

The ESR spectrum of the semiquinone (Q_A^- or Q_B^-) observed in either BRC appears as a broad resonance with turning point at g~1.84 (22-28). A similar but not identical signal has been observed in PS II with a turning point at g~1.9 (29, 30). Both signals have been simulated using the spin Hamiltonian formalism, where the semiquinone Q^- interacts magnetically with an Fe^{2+} center (16, 31). It has been shown that the two signals differ mainly by an axis rotation of the exchange coupling tensor (J) relative to the fine structure tensor and a small increase in the zero-field parameter D (~6 cm^{-1}). Together with DFT calculations, these inferred changes in the coupling environment of the two complexes suggested that the native exogenous ligand to the Fe^{2+} center of PS II was a carbonate (CO_3^{2-}) rather than bicarbonate in the 'dark state' ($Q_AFe^{2+}Q_B$).

The ESR spectrum of the bi-radical signal ($Q_A^-Fe^{2+}Q_B^-$), as yet only observed in PS II, appears as a broad resonance with turning point at g~1.66 (32, 33). It is formed by either: 1) reducing the Q_A at low temperatures (<200 K), followed by annealing of the sample to above 270 K to allow single electron transfer to Q_B and a subsequent second low temperature illumination (<100 K) to reform Q_A^- (33). 2) By single flash illumination at room temperature to form the Q_B^- and a subsequent low temperature illumination (<100 K) to form Q_A^- (33). The $Q_A^-Fe^{2+}Q_B^-$ state is only stable at low temperature. Upon warming the sample above 200 K all semi-quinone signals are lost; the electron on Q_A^- is passed to the Q_B^-, protonation occurs and the EPR silent quinol (Q_BH_2) is exchanged for a quinone (Q_B).
These measurements are often done in the presence of an electron mediator to reduce high oxidation S-states (S_2) of the water oxidizing complex (WOC), the stable electron donor to P680. S_2 exhibits a strong EPR resonance that overlays the semi-quinone iron signals.

Here we use the basic theoretical model established earlier (31) for describing the semiquinone iron signal in BRC in order to model the corresponding bi-radical signal in native PS II. A specific simulation package was written to calculate the theoretical absorbance ESR spectra at different temperatures. Two solutions corresponding to the optimized parameter set for each semiquinone signal (g~1.81 and g~1.9) were examined. Using an admixture of these two theoretical spectra a fitting on the experimental $Q_A^-Fe^{2+}Q_B^-$ signal was achieved.

MATERIAL AND METHODS

Sample preparation

PSII preparations were made from 43H *T. elongatus* strain, the procedure was exactly the same as described earlier in Sedoud et al [44].

ESR/EPR measurements

EPR sample loading was performed under dim green illumination. PS II core samples (~2 mg/mL chl, 60 μmol) were treated with ANT-2P (60 μmol) dissolved in DMSO (final conc. 2-3%) in the dark. ANT-2P, an electron mediator, facilitates the rapid reduction high oxidation S-states (S_2). Samples were dark adapted overnight to remove any long lived Q_B^- signal. Samples at 20°C were pumped using a Turbo-pump for 1-2 minutes. The EPR tube was then filled with He gas to minimize O_2 signals.

To generate the semiquinone iron signal samples were illuminated with a 125 W halogen lamp. The beam was focused to a 20 mm diameter spot directly onto the front grate

of the EPR cavity after passing through a water filter (path length 3cm) and a long-band pass filter (RG-670 nm).

ESR measurements were performed on a Bruker ESP300E spectrometer with an Oxford ESR9 liquid helium flow cryostat using a gold-chromel thermocouple directly below the sample position.

ESR/EPR Simulations

Spectral simulations were performed numerically from a Hamiltonian (20 x 20 matrix) using Scilab-4.4.1, an open source vector-based linear algebra package (www.scilab.org). A complete description of the EPR simulations can be found in the supporting information.

RESULTS

$Q_A^-Fe^{2+}$/$Q_A^-Fe^{2+}Q_B^-$ signals of PS II.

Fig. 1 shows the derivative ESR semiquinone-iron signals (Q_A^- and Q_B^-) and bi-radical-iron signal observed in *T. Elongatus* PS II core complexes. Characteristic of these signals are turning points in the g ~ 1.6-1.9 region. As a consequence, semiquinone/bi-radical signals are identified by the position of this spectral feature. In native PS II the turning point semiquinone–iron signal is at g~1.9, whereas the bi-radical signal appears at g~1.66.

The g~1.9 signal ($Q_A^-Fe^{2+}$) was photo-induced by illumination with visible light for ~ 10 minutes at cryogenic temperatures (5-20 K) (Fig. 1). Incubation in ANT-2p fully oxidized the Cyt_{b559} in the dark. The oxidized electron donor (D^+) for the system appears as a narrow (10-15 G p–p) featureless radical centered at g~2.0 which is assigned to an admixture of chlorophyll (chl^+) and carotenoid (car^+) radicals (39).

The g~1.9 signal ($Q_B^-Fe^{2+}$) was generated by first forming the g~1.9 ($Q_A^-Fe^{2+}$) signal at 200 K. Here the electron donor (D^+) for the system was the Mn-cluster; an S_2 state multiline signal was readily observed. Upon annealing to 270-280 K for ~10 s, the electron was passed from the Q_A^- to Q_B (33). ANT-2p re-reduced the S_2 state back to the S_1 state. Rapid freezing to <200 K trapped the $Q_B^-Fe^{2+}$ state in a majority of centers (Fig.1).

The g~1.9 signals (Q_A^- and Q_B^-) observed in *T. Elongatus* are similar to those seen from PS II membranes (29, 30) and in core complex sources from higher plants. Two pseudo-derivative features were resolved at 5 K: at g~1.9 and g~1.7 (Fig. 1 B). The latter was lost at higher temperatures (15 K), whereas the former narrows (Fig. 1 C) (see (30)).

The corresponding g~1.66 bi-radical signal ($Q_A^-Fe^{2+}Q_B^-$) was formed in a sample where the Q_B had already been reduced by the method described above (also see introduction) (32, 33). Upon illumination at 5 K with visible light for ~10 minutes, a second stable charge separated state was formed (Q_A^-) in a large fraction of centers (>50%). As before, the low temperature donor (D^+) for the system appears as a narrow (10-15 G p–p) featureless radical centered at g~2.0 which is assigned to an admixture of chlorophyll (chl^+) and carotenoid (car^+) radicals (39).

The g~1.66 signals ($Q_A^-Fe^{2+}Q_B^-$) observed in *T. Elongatus* is similar to those seen from PS II membranes (29, 30). Its dominant turning point appears at g~1.66, an asymmetric-derivative feature that extends to high field (g<1.0). This turning point significantly decreases at higher temperatures (15 K). A second weaker derivative-like feature is observed g~2.0. Its temperature dependence is less marked.

Absorption ESR spectra of the $Q_A^-Fe^{2+}Q_B^-$ resonance in PS II

Fig. 2 displays the ESR absorption spectra of the bi-radical-iron signal seen in *T. Elongatus* at 5 and 15 K. The absorption spectrum of the g~1.66 signal was generated by integration of

data presented in Fig. 1. It is experimentally difficult to resolve such a broad ESR signal since the baseline is inherently variable over large field ranges. To minimize this problem the g~1.66 semi-quinone iron signal was generated by direct illumination of the sample in the cavity at 5 K. This avoided moving the sample. The difference between a spectrum taken under (or after) the 5 K illumination minus a spectrum taken immediately before illumination effectively eliminated baseline features and yielded a well-defined semi-quinone iron signal. This also canceled Cyt_{b559}^{OX} signals, tyrosyl radical ($Y_D^{\bullet}$) etc. Even with these measures, a baseline correction had to be subtracted to remove a signal offset. Consequently there is a degree of uncertainty in the position of the edges of the signal. A high spin (g~5) Cyt_{b559} signal was also subtracted from the data presented in Fig. 2.

The absorbance spectrum of the g~1.66 signal is similar to its corresponding g~1.9 signal (16). It is strongly temperature dependent. The high field component of the spectrum (g <1.8) is more readily observed at low temperatures (5 K), whereas the low field component remains virtually unchanged over the 5-20 K region. This behavior is similar to that observed for both semiquinone-iron signals (g~1.81 and g~1.9) (16, 31).

MODELING AND ANALYSIS

Simple Picture - Iron (Fe^{2+}), quinone energy levels

The non-heme iron center of PS II and BRC is high spin d^6 (Fe^{2+}, S = 2) (31). The number of distinct electronic configurations (210) that the system can adopt is large and as previously(15, 16) the problem can be simplified by assuming the ground state is a quintet (2S+1), energetically well removed from higher electronic states. (e.g. see (31) for a justification of this).

The energy level splittings within the ground state orbital manifold can be well described using the spin Hamiltonian formalism with quadratic zero-field parameters; the axial (D) and rhombic (E) terms. For the BRC, the D and E terms were estimated as 7.6 and 1.9 K respectively, using bulk magnetization measurements (40). Similar values were estimated for the PS II, D = 15 K, E = 4 K (16).

When weakly coupled to the Q_A^- center, each singlet sublevel of the iron manifold becomes a Kramer's doublet, which splits in the presence of a magnetic field. Allowed ESR transitions occur within these doublets (i.e. 5 observable spin-allowed transitions, all contributing to the observed ESR semiquinone-iron signal). In these studies the microwave frequency (9 GHz, 0.43 K) is too low to induce transitions between doublet states. Over the temperature range (5-20 K) used here the ESR signal is dominated by the two lowest doublet transitions.

In a similar way, coupling of both the Q_A^- and Q_B^- centers to each singlet sublevel of the iron manifold results in a quartet of energy-levels, which unlike the $Q_A^-Fe^{2+}$ spin manifold are non-degenerate at zero-field. The spin transitions that contribute to the observed at X-band (9 GHz, 0.43 K) spectrum, as with the Q_AFe^{2+} signal, are confined to each quartet level and the EPR signal (5-20 K) is dominated by transitions within the two lowest quartets.

Spin Hamiltonian Formalism – $Q_A^-Fe^{2+}$/ $Q_B^-Fe^{2+}$

This has been previously described(15, 16) The effective spin Hamiltonian $\mathcal{H}$ is

$$\mathcal{H} = D[(S_{Fe\,Z}^2 - 1/3\,S_{Fe}(S_{Fe}+1) + (E/D)(S_{Fe\,X}^2 - S_{Fe\,Y}^2)] + \beta H \cdot \mathbf{g}_{Fe} \cdot S_{Fe}$$
$$+ \mathbf{g}_Q \beta H \cdot S - S_{Fe} \cdot \mathbf{J} \cdot S_Q \qquad (1)$$

It includes zero field (D, E), Zeeman ($\mathbf{g}_{Fe}$, $\mathbf{g}_{Q}$) and anisotropic exchange ($\boldsymbol{J}$) terms. Subsequent calculations assume the zero-field, Zeeman-iron and exchange tensors to be co-linear and g_Q to be scalar.

Spin Hamiltonian Formalism –$Q_A^-Fe^{2+}Q_B^-$

Similarly, a description of the non-heme iron (S = 2) and bi-semi-quinone, Q_A^-, Q_B^- (S = ½, ½) system requires a spin Hamiltonian of the form:

$$\mathcal{H} = D[(S_{FeZ}^2 - 1/3 S_{Fe}(S_{Fe}+1) + (E/D)(S_{FeX}^2 - S_{FeY}^2)] + \beta H \cdot g_{Fe} \cdot S_{Fe} + g_{Q_A}\beta H \cdot S_{Q_A} + g_{Q_B}\beta H \cdot S_{Q_B} - S_{Fe} \cdot J \cdot S_{Q_A} - S_{Fe} \cdot J \cdot S_{Q_B} \quad (2)$$

It is solved in terms of basis vectors. $|S,\ m,\ s_1,\ s_2,\rangle$,

where S is the total spin of the ground iron manifold (S = 2), m is the iron magnetic sub-level (m = -S, - S + 1, ……, S – 1, S) and s is a semi-quinone sublevel (s = - ½ , ½). Similar assumptions regarding the relevant tensors are made, as above.

.

Computational simulation of the semiquinone-iron signals

The program employed to simulate the system using the above Hamiltonian (Eq. 2) is described in the supporting information (SX). It outputs the ESR spectrum for transitions within the three lowest quartets.

The iron-quinone complex of PS II (and BRC) is structurally well characterised (8-10, 13, 14, 17). The mean iron-quinone distance for both Q_A and Q_B is nominally the same (8, 13, 14, 17). The iron-quinone complex has a pseudo C_2-axis of symmetry, with the histidine ligands of the Fe^{2+} occupying similar positions between the iron center and the two quinones (9, 10, 13, 14). The corresponding $Q_A^-Fe^{2+}$ and $Q_B^-Fe^{2+}$ ESR signals (g~1.9) are very similar (see above and (30)), suggesting the quinone-iron interaction for both Q_A and Q_B is approximately the same i.e. the exchange, fine structure and g tensors are assumed to be identical for both the $Q_A^-Fe^{2+}$ and $Q_B^-Fe^{2+}$ complex.

The above Hamiltonian (Eq. 2) has 11 independent variables: g_X, g_Y, g_Z, J_{1X}, J_{1Y}, J_{1Z}, J_{2X}, J_{2Y}, J_{2Z}, D and E. The procedure used to generate the bi-radical ($Q_A^-Fe^{2+}Q_B^-$) signal suggests several restrictions can be placed on this parameter set, limiting the number of free variable to three. The formation of the bi-radical signal requires the initial reduction of the Q_B at high temperatures (see introduction). A second low temperature illumination (5 K), reducing the Q_A, then gives rise to the $Q_A^-Fe^{2+}Q_B^-$ state. Q_A reduction takes place under conditions where significant protein relaxation cannot occur (5 K). As a consequence, Q_A^- formation is unlikely to strongly influence the $Q_B^-Fe^{2+}$ interaction. A reasonable assumption is that the exchange (J_{2X}, J_{2Y}, J_{2Z}), fine structure (D, E), g (g_X, g_Y, g_Z) tensors of the quinone-iron complex are the same prior to and post Q_A^- formation. This reduces the number of free parameters to three.

It is also noted that no structural rearrangement at the Q_A site upon reduction. The $Q_A^-Fe^{2+}$ (g~1.9) signal is identical when formed at either low temperature or at room temperature in samples where electron transfer to Q_B is blocked i.e. in the presence of DCMU. Similarly, the Q_B^- state has been shown not to induce any conformational change of the Q_A in BRC using X-ray crystallography (41). This then suggests the exchange tensor (J_{1X}, J_{1Y}, J_{1Z}) describing the $Q_A^-Fe^{2+}$ interaction should be nominally the same for both the semiquinone ($Q_A^-Fe^{2+}$, g~1.9) and bi-radical ($Q_A^-Fe^{2+}Q_B^-$, g~1.66) complexes.

Guided by this, the input parameters used initially to simulate the g~1.66 signal were the same as used for the original semiquinone-iron simulations. Two 'theoretical spectra' were calculated, one using the g~1.9 parameters, one using the g~1.84 parameters. These are shown in Fig. 3. The simulation using the g~1.9 fit parameters bears a strong resemblance to the absorption spectrum of the g~1.66 signal. It resolves a strong turning point at g~1.61, nearly the same position as seen in the experimental spectrum. The temperature dependence of the simulation also broadly fits the observed behavior of the g~1.66 signal; the high field (ground quartet) signal provides a smaller (relative) contribution to the total signal at higher temperatures (15 K). However, the low field (1^{st} excited quartet) component of the simulation, while similar to the experimental spectrum, lacks several features seen in the data and is of insufficient width.

Although it is stated above that no large change in the quinone-iron coupling environment is expected upon Q_A^- formation at low temperature, current literature suggests the g~1.84 and g~1.9 signal may only differ by the protonation state of the exogenous ligand i.e. bicarbonate/carbonate, see discussion and (16). Interestingly, several features seen in the experimental spectrum do seem to be reproduced in the second theoretical simulation; the simulation using the g~1.84 parameters. Relative sharp features seen at g~13.5, g~3.55 and g~1.36 all seem to match well the structures (if not the exact g position) of the g~1.84 simulation. This observation invites a simple rationale for the g~1.66 bi-radical signal within current literature models. It may be an admixture of two signal types, resembling the above two theoretical spectra. With this assumption, the g~1.66 signal can be readily modeled using a 4:1 addition of the two theoretical spectra. To correctly reproduce the relative intensities of the major features seen, the isotropic linewidth of the transitions from the 1^{st} excited state quartet (using the g~1.9 fit parameters) was increased by a factor of 5 relative to that of the ground state quartet. Small changes (<0.1 K) in the exchange tensor (J_{2Y}) were also made to reproduce the exact positions of key features.

Decomposition of the semi-quinone iron/bi-radical iron signal: effective g_X, g_Y, g_Z positions

The ESR spectrum of the isolated semi-quinone radical is near isotropic at g~2. Addition of the Fe^{2+} center introduces a magnetization (*effective* internal magnetic field) principally along the molecular y axis. For the ground state, as the magnetization of the Fe^{2+} sublevel is negative, the effective field is decreased, shifting the ESR transition to higher external field. Similarly, for the 1^{st} excited state the total effective field is raised, shifting the ESR transition to lower external field. A pictorial representation of the powder pattern spectra corresponding to the ground and 1^{st} excited state transitions is shown in Fig. 5 A. 2^{nd} order effects lead to a breaking of the x, z degeneracy as seen in the real systems as indicated in Fig. 5 B, C. The maxima of the ground and first excited state appear symmetrically about g~1.8 for the BRC signal. Their sum yields the relatively sharp prominent feature of the ESR signal. The absorbance spectrum of the g~1.9 signal is very similar. Compared to the g~1.84 signal, the maximum for each doublet (nominally the average of the effective g_X and g_Z positions) separate; the ground state maximum shifts to high field, the first excited state maximum to low field. This decomposition is consistent with the temperature dependence of the signal - the high field edge is lost as the observation temperature increases.

The addition of the second quinone (Q_B^-, S = ½) can be considered as a perturbation of the original system. As the iron-quinone coupling is weak, it is expected that there are only two ESR/EPR transitions within each quartet of the spin manifold with a large transition probability. These two transitions correspond to $\left|-\frac{1}{2}\right\rangle \rightarrow \left|\frac{1}{2}\right\rangle$ for each semiquinone. While no

explicit interaction between the two semi-quinones is considered in the Spin Hamiltonian, the coupling of the two semi-quinones to the *same* iron center yields an effective interaction. This can be best observed from looking at the decomposition of the bi-radical signal along the three principle directions (x, y, z), (Figs. 6 and 7)

As stated above, the semiquinone iron signal can be consider as an effective spin ½ system with anisotropic g-tensor g_X, g_Y, g_Z. The corresponding bi-radical signal resolves two transition split about the effective g-positions of the semi-quinone iron signal. This is shown in Figs. 6 and 7. The splitting along the three principle directions differs. The new bi-radical signal can then simply be considered a triplet state; here two spin ½ couple with anisotropic exchange interaction:

$$H = \beta H \cdot g_{eff} \cdot S_{Q_A} + \beta H \cdot g_{eff} \cdot S_{QB} - S_{Q_A} \cdot J_{eff} \cdot S_{Q_B} \qquad (3)$$

A) g~1.9 signal (D=15 K, E/D=0.27)

$$J_{GRO} = \begin{bmatrix} 100 & 0 & 0 \\ 0 & 570 & 0 \\ 0 & 0 & 570 \end{bmatrix} \qquad J_{1st} = \begin{bmatrix} 500 & 0 & 0 \\ 0 & 360 & 0 \\ 0 & 0 & 360 \end{bmatrix}$$

$$J_{ISO} = 420\text{MHz} \qquad J_{ISO} = 400\text{MHz}$$

B) g~1.81 signal (D=7.6 K, E/D=0.25)

$$J_{GRO} = \begin{bmatrix} 1000 & 0 & 0 \\ 0 & 290 & 0 \\ 0 & 0 & 890 \end{bmatrix} \qquad J_{1st} = \begin{bmatrix} 1070 & 0 & 0 \\ 0 & 710 & 0 \\ 0 & 0 & 1430 \end{bmatrix}$$

$$J_{ISO} = 730\text{MHz} \qquad J_{ISO} = 1070\text{MHz}$$

(Note: 2.8 MHz = 1 G)

The effective interaction between the two quinones is axial, mirroring the iron-quinone interaction. The smallest tensor component for the ground state is along the axis where the iron-quinone coupling is largest (x for g~1.9 signal, y for the g~1.84 signal). This then reverses for the 1st excited quartet. The magnitude of the splitting scales with the inverse of the D. This seems intuitively reasonable as the relative magnitude of the 'perturbation' increases as the energy level separation between the quartet states decreases.
It is noted that an effective exchange interaction of ~400 MHz (ground quartet) is approximately 40 times larger than the direct dipole-dipole interaction between the two quinones Q_A and Q_B measured in Fe^{2+} substituted (with Zn^{2+}, S = 0) samples (42).

DISCUSSION

The two forms of the bi-radical signal: the bi-radical signal reports on the protonation state of the carbonate/bicarbonate ligand

Previous work (16) suggested that the two forms of the semiquinone iron signal (g~1.84 and g~1.9) corresponded to the two protonation states of the exogenous ligand, a bicarbonate/carbonate. This assignment was based on a comparison between ESR fit

parameters (fine structure, exchange tensor) and DFT calculations on a model of quinone-iron complex. The g~1.84 and g~1.9 signals differed by a rotation of the relative orientation of the exchange and zero-field tensors and an increase in the central iron D value (by up to 10 K), which was supported by computation

The bi-radical (g~1.66) simulation (shown above) is consistent with current models of the quinone-iron interaction (16, 31) and current X-ray structural data of the acceptor side complex (13, 14). The dominant feature of the signal, namely the g~1.66 turning point, can be explained by two semi-quinones interacting (in an identical way) with a Fe^{2+} center. The parameters used in this simulation are approximately the same as used for the g~1.9 semi-quinone iron signal. This then suggests that in a majority of centers the exogenous ligand to the Fe^{2+} is a carbonate in the $Q_A^-Fe^{2+}Q_B^-$ state.

Additional features are seen in the experimental g~1.66 signal however, that cannot be explained using the simulation described above. These correspond to features arising from the same general three center model, but with parameters corresponding to the g~1.84 semi-quinone iron signal, suggesting a fraction of centers where the exogenous Fe^{2+} ligand is bicarbonate. As only the g~1.9 signal (Q_B^-) was observed prior to light induced (5 K) formation of the bi-radical ($Q_A^-Fe^{2+}Q_B^-$) signal, the subsequently observed signal heterogeneity suggests that Q_A^- formation may induce partial protonation of the carbonate ligand.

It was proposed (16) that a lysine residue (D2-K264) may interact directly with the bicarbonate/carbonate ligand. The ε-amino group of the lysine is within 4 Å of the oxygen of the carbonate (see Fig. 8). The carbonate ligand could be stabilized by forming a hydrogen bond/salt bridge to this residue. Mutation of this residue leads to a 40-fold drop in bicarbonate binding affinity (43). Thus Q_A^- formation may cause the proton of the lysine (NH_3^+) group to migrate to the carbonate ligand, although the mechanism of this simulated proton movement is at present unclear.

Mechanistic role of carbonate/bicarbonate: protonation of the reduced Q_B

Bicarbonate has been proposed to be involved in: i) the protonation step(s) of the reduced Q_B and ii) stabilization of the structure of the quinone-iron complex ((21) and ref. therein).

Electron transfer between Q_A and Q_B dramatically slows after the *second* actinic flash in PS II when bicarbonate has been exchanged (formate-treated etc, reviewed in (20)). As the second electron transfer step (see introduction, scheme 1), requires protonation of the reduced forms of Q_B, it has been suggested (21) that bicarbonate somehow facilitates this process. Recent work (16) has suggested that the native ligand to the Fe^{2+} is a carbonate ion rather than bicarbonate and thus the ligand cannot act as the terminal H^+ donor to Q_B. Here though, the authors did suggest that the carbonate ligand could be part of a protonation pathway consistent with earlier suggestions for the role of bicarbonate (21). Here the carbonate would be involved in picking up a proton(s) and passing it on to the reduced quinone. In such a model bicarbonate could form transiently during the Q_A^- to Q_B^- electron transfer step. The results here on simulation of the bi-radical (g~1.66) signals are consistent with this mechanism. A fraction of centers (~25%), initially carbonate ligated, appear to have a bicarbonate bound to the Fe^{2+} following low temperature Q_A^- formation.

The simulation presented here will require a re-evaluation of the kinetics of Q_A^- Q_B^- electron transfer (Fufezan et al. (33)). Here the temperature dependant decay of the g~1.66 signal was examined. The loss of the bi-radical signal, as judged by the g~1.66 field position was interpreted as monitoring forward electron transfer from Q_A^- to Q_B^- (forming Q_BH_2). This work suggests that the loss of the g~1.66 signal (the turning point dominated by the carbonate population) may also reflect the protonation of the carbonate ligand. Thus the

observed temperature dependent decay of the g~1.66 signal should resolve two phases, one associated with proton movement, one with electron movement.

This work was financially supported by the EU/Energy Network project SOLAR-H2 (FP7 contract 212508). A.R.J. thanks the University of Wroclaw for a two year sabbatical to allow a post-doctoral fellowship at ANU. The computations were performed using the Wroclaw Center of Networking and Supercomputing (Grant No. 48) facility.

REFERENCE LIST

1. Diner, B. A., and F. Rappaport. 2002. Structure, Dynamics, and Energetics of the Primary Photochemistry of Photosystem II of Oxygenic Photosynthesis. Annu Rev Plant Biol. 53:551-580.
2. Petrouleas, V., and A. R. Crofts. 2005. The Iron-Quinone Acceptor Complex. Springer, Dordrecht.
3. Bouges-Bocquet, B. 1973. Electron transfer between the two photosystems in spinach chloroplasts. Biochim. Biophys. Acta 314:250-256.
4. Velthuys, B. R., and J. Amesz. 1974. Charge accumulation at the reducing side of system 2 of photosynthesis. Biochim. Biophys. Acta 333:85-94.
5. Vermeglio, A., and R. K. Clayton. 1977. Kinetics of electron transfer between the primary and secondary electron acceptors in reaction centers from Rhodopseudomonas Sphaeroides. Biochim Biophys. Acta 461:159-165.
6. Wraight, C. A. 1977. Electron acceptors of photosynthetic bacterial reaction center. Direct observation of oscillatory behaviour suggesting two closely equivalent ubiquinones. Biochim Biophys. Acta 459:525-531.
7. Crofts, A. R., H. H. Robinson, and M. Snozzi. 1984. Reactions of quinols at catalytic sites; a diffusional role in H-transfer. -In Advances in Photosynthesis Research. The Hague, Martinus.
8. Deisenhofer, J., O. Epp, K. Miki, R. Huber, and H. Michel. 1985. Structure of the protein subunits in the photosynthetic reaction centre of *Rhodopseudomonas viridis* at 3 Å resolution. Nature 318:618-624.
9. Diner, B. A., V. Petrouleas, and J. J. Wendoloski. 1991. The Iron-quinone electron-acceptor complex of photosystem II. Physiol. Plant. 81:423-436.
10. Rutherford, A. W. 1987. In Progress in Photosynthesis Research. J. Biggins, editor. Martinus Nijhoff Publishers, Dordrecht. 277-283.
11. Graige, M. S., G. Feher, and M. Y. Okamura. 1998. Conformational gating of the electron transfer reaction $QA^{-\cdot}QB \rightarrow QAQB^{-\cdot}$ in bacterial reaction centers of *Rhodobacter sphaeroides* determined by a driving force assay. Proc. Natl. Acad. Sci. USA 95:11679-11684.
12. Feher, G., and M. Y. Okamura. 1999. The Primary and Secondary Acceptors in Bacterial Photosynthesis: II. The Structure of the Fe2+-Q- Complex. Appl. Magn. Reson. 16:63-100.
13. Ferreira, K. N., T. M. Iverson, K. Maghlaoui, J. Barber, and S. Iwata. 2004. Architecture of the Photosynthetic Oxygen-Evolving Center. Science 303:1831-1838.
14. Loll, B., J. Kern, W. Saenger, A. Zouni, and J. Biesiadka. 2005. Towards Complete Cofactor Arrangement in the 3.0 Å Resolution Crystal Structure of Photosystem II. Nature 438:1040-1044.

15. Hienerwadel, R., and C. Berthomieu. 1995. Bicarbonate binding to the non-heme iron of photosystem II, investigated by Fourier transform infrared difference spectroscopy and 13C-labeled bicarbonate. Biochemistry 34:16288-16297.
16. Cox, N., L. Jin, A. Jaszewski, P. J. Smith, E. Krausz, A. W. Rutherford, and R. J. Pace. 2009. The semiquinone-iron complex of Photosystem II: structural insights from ESR and theoretical simulation. Evidence that the native ligand to the non-heme iron is carbonate. Biophys. J. (Accepted).
17. Allen, J. P., G. Feher, T. O. Yeates, H. Komiya, and D. C. Rees. 1988. Structure of the Reaction Center from *Rhodobacter sphaeroides* R-26: Protein-Cofactor (Quinones and Fe2+) Interactions. Proc. Natl. Acad. Sci. USA 85:8487-8491.
18. Debus, R. J., G. Feher, and M. Y. Okamura. 1986. Iron-depleted reaction centers from Rhodopseudomonas sphaeroides R-26.1: characterization and reconstitution with iron(2+), manganese(2+), cobalt(2+), nickel(2+), copper(2+), and zinc(2+). Biochemistry 25:2276-2287.
19. Rutherford, A. W., I. Agalidis, and F. Reiss-Husson. 1985. Manganese-quinone interactions in the electron acceptor region of bacterial photosynthetic reaction centres. FEBS Lett. 182:151-157.
20. Van Rensen, J. J. S., C. Xu, and Govindjee. 2002. Role of bicarbonate in photosystem II, the water-plastoquinone oxido-reductase of plant photosynthesis. Physiol. Plant. 105:585-592.
21. Van Rensen, J. J. S., and V. V. Klimov. 2005. Bicarbonate Interactions. In Photosystem II. The Light driven Water: Plastoquinone Oxidoreductase T. J. Wydrzynski, and K. Satoh, editors. Springer, Dordrecht. 329-346.
22. Wraight, C. A. 1978. Iron-quinone interactions in the electron acceptor region of bacterial photosynthetic reaction centers. FEBS Lett. 93:283-288.
23. Okamura, M. Y., R. A. Isaacson, and G. Feher. 1978. EPR signals from the primary and secondary quinones in reaction centers from *R. sphaeroides* R-26. Biophys. J. 21:8a (Abstr.).
24. McElroy, J. D., G. Feher, and D. C. Mauzerall. 1970. Observation of a second light induced EPR signal from reaction centers of photosynethic baterica. Biophys. Soc. Abstr. 10:204a.
25. Leigh, J. S., and P. L. Dutton. 1972. The primary electron acceptor in photosynthesis. Biochem. Biophys. Res. Commun. 46:414-421.
26. Feher, G. 1971. Some chemical and physical properties of a bacterial reaction center particle and its primary photochemical reactants. Photochem. Photobiol. 14:373-388.
27. Dutton, P. L., J. S. Leigh, and D. W. Reed. 1973. Primary events in reactions centers from *Rhodopseudomonas sphaeroides* strain R-26: Triplet and oxidation states of bacteriochlorophyll and the identification of the primary electron acceptor Biochim. Biophys. Acta 292:654-664.
28. Rutherford, A. W., and M. C. W. Evans. 1979. The high potential semiquinone-iron signal of *Rhodopseudomonas viridis* is the specific quinone secondary electron acceptor in the photosynthetic reaction center FEBS Lett. 104:227-230.
29. Rutherford, A. W., and J. L. Zimmermann. 1984. A new EPR signal attributed to the primary plastosemiquinone acceptor in Photosystem II. Biochim. Biophys. Acta 767:168-175.
30. Nugent, J. H. A., D. C. Doetschman, and D. J. MacLachan. 1992. Characterization of the Multiple ESR Line Shapes of Iron-Semiquinones in Photosystem 2. Biochemistry 31:2935-2941.
31. Butler, W. F., R. Calvo, D. R. Fredkin, R. A. Isaacson, M. Y. Okamura, and G. Feher. 1984. The electronic structure of Fe2+ in reaction centre's from *Rhodopseudomonas*

sphaeroides. III. EPR measurements of the reduced acceptor complex. Biophys. J. 45:947-973.
32. Hallahan, B., S. Ruffle, S. Bowden, and J. H. A. Nugent. 1991. Identification and Characterisation of EPR signals involving Q_B semiquinone in plant Photosystem II. Biochim. Biophys. Acta 1059:181-188.
33. Fufezan, C., C. Zhang, A. Krieger-Liszkay, and A. W. Rutherford. 2005. Secondary Quinone in Photosystem II of Thermosynechococcus elongatus: Semiquinone-Iron EPR Signals and Temperature Dependence of Electron Transfer. Biochemistry 38:12780-12789.
34. Frisch, M. J., and et al. 2004. Gaussian 03. Gaussian Inc, Wallingford
35. Becke, A. D. 1993. Density-functional thermochemistry. III. The role of exact exchange. J. Chem. Phys. 98:5648-5652.
36. Wachters, A. J. H. 1970. Gaussian Basis Set for Molecular Wavefunctions Containing Third-Row Atoms. J. Chem. Phys. 52:1033-1036.
37. Bauschlicher, C. W., Jr., S. R. Langhoff, H. Partridge, and L. A. Barnes. 1989. Theoretical studies of the first- and second-row transition-metal methyls and their positive ions. J. Chem. Phys. 91:2399-2411.
38. Dunning, T. H., Jr., and P. J. Hay. 1976. Modern Theoretical Chemistry. Plenum, New York.
39. Hanley, J., Y. Deligiannakis, A. Pascal, P. Faller, and A. W. Rutherford. 1999. Carotenoid Oxidation in Photosystem II. Biochemistry 38:8189-8195.
40. Butler, W. F., R. Calvo, D. R. Fredkin, R. A. Isaacson, M. Y. Okamura, and G. Feher. 1980. The electronic structure of Fe2+ in reaction centers from *Rhodopseudomonas sphaeroides* I. Static magnetization measurements. Biophys. J. 45:947-973.
41. Stowell, M. H. B., T. M. McPhillips, D. C. Rees, S. M. Soltis, E. Abresch, and G. Feher. 1997. Light-Induced Structural Changes in Photosynthetic Reaction Center: Implications for Mechanism of Electron-Proton Transfer. Science 276:812-816.
42. Calvo, R., E. C. Abresch, R. Bittl, G. Feher, W. Hofbauer, R. A. Isaacson, W. Lubitz, M. Y. Okamura, and M. L. Paddock. 2000. EPR Study of the Molecular and Electronic Structure of the Semiquinone Biradical $Q_A^-Q_B^-$ in Photosynthetic Reaction Centers from Rhodobacter sphaeroides. J. Am. Chem. Soc. 122:7327-7341.
43. Diner, B. A., P. J. Nixon, and J. W. Farchaus. 1991. Site-directed mutagenesis of photosynthetic reaction centers. Curr. Opin. Struct. Biol. 1:546-554.
44. Sedoud, A. Kastner, L. Cox, N. El-Allaoui, S. Kirilovsky, D. Rutherford, A. W. 2011. Effects of formate binding on the quinone-iron acceptor complex of photosystem II. Biochim. Biophys. Acta 1807: 216-226.

TABLES

	g~1.84 (K, BRC) (see (31))	g~1.9 (K, PSII)*
J_{1X}	-0.13	-0.90
J_{1Y}	-0.58	-0.50
J_{1Z}	-0.58	-0.10
$J_{1(ISO)}$	-0.43	-0.50
J_{2X}	-0.13	-0.90
J_{2Y}	-0.50	-0.45
J_{2Z}	-0.58	-0.10
$J_{2(ISO)}$	-0.40	-0.48
D	7.6	15.0
E/D	0.25	0.27
Width (FWHM)	600 (G)	300 (G)

*g_{Fe} tensor values as per Bulter et al. (31)

Table 1: Optimized parameter set for the simulation of the bi-radical (g~1.66) signal shown in Fig. 4.

REACTION SCHEMES

Scheme 1: Acceptor-side electron transfer pathways in PS II and BRC; the two electron gate (2).

FIGURE CAPTIONS

Figure 1: Derivative ESR spectra of the semiquinone-iron and bi-radical observed in *T. Elongatus*. Panel A: g~1.9 $Q_A^-Fe^{2+}$ signal (5 K). Panel B: g~1.9 $Q_B^-Fe^{2+}$ signal (5 K). Panel C: g~1.66 $Q_A^-Fe^{2+}$ Q_B^- signal (5 and 15 K).

Figure 2: Absorption ESR spectra of the g~1.66 bi-radical ($Q_A^-Fe^{2+}$ Q_B^-) signal observed in *T. Elongatus*: (i) 5 K (black trace) ;(ii) 15 K (grey trace). The radical region about g = 2 is dominated by light-induced radicals (D^+) and has been omitted for clarity (as indicated by the grey column).

Figure 3: Pictorial representation of the energy-levels of the bi-radical ($Q_A^-Fe^{2+}$ Q_B^-) system

Figure 4: Simulation of the bi-radical signal (g~1.66) using the spin Hamiltonian formalism; comparison of experimental and theoretical results. Parameter values as in Table 1. Panel A: bi-radical simulation using the g~1.9 fit parameters (5 K) (16). Panel B: bi-radical simulation using the g~1.84 fit parameters (5 K) (31). Panel C: Simulation of the g~1.66 signal of *T. Elongatus* (5 K), see text. Panel D: Simulation of the g~1.66 signal of *T. Elongatus* (15 K). Free radical region omitted in panels B and C. Black lines:- total simulation, grey lines:- doublet transitions.

Figure 5: Decomposition of the semiquinone-iron signal into its two lowest ESR transitions. Marked g positions (g_X, g_Y, g_Z) show the effective g tensor values as calculated by third order perturbation theory (see (16, 31)). Panel A: simple theory; panel B: g~1.84 signal; panel C: g~1.9 signal.

Figure 6: The energy-levels of the two lowest quartets of the bi-radical signal (using the g~1.9 fit parameters) long the three principle directions. Also shown are the two ESR/EPR transitions observed for the ground (black) and 1st excited (grey) quartets. These two transitions appear for the two quartets symmetrically about the effective g tensor positions (see Fig. 5) of the g~1.9 semi-quinone iron signal (shown using dashed lines).

Figure 7: The energy-levels of the two lowest quartets of the bi-radical signal (using the g~1.84 fit parameters) long the three principle directions. Also shown are the two ESR/EPR transitions observed for the ground (black) and 1st excited (grey) quartets. These two transitions appear for the two quartets symmetrically about the effective g tensor positions (see Fig. 5) of the g~1.84 semi-quinone iron signal (shown using dashed lines).

Figure 8: The quinone-iron complex of PS II. Residues in the immediate vicinity of the carbonate/bicarbonate ligand to the non-heme iron (Loll et al. (14)).

Figure 1

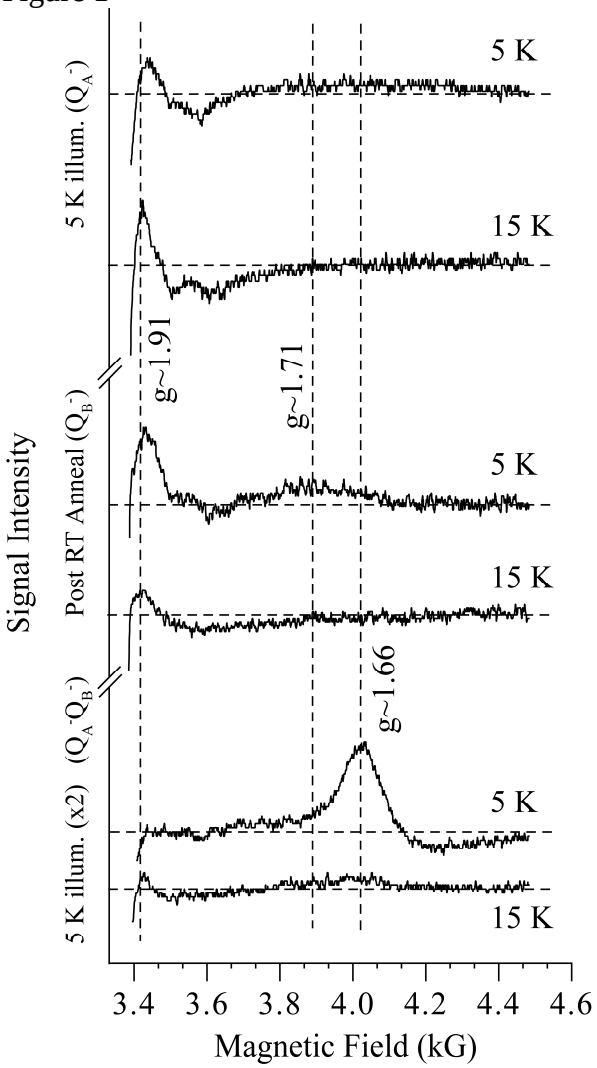

Figure 2

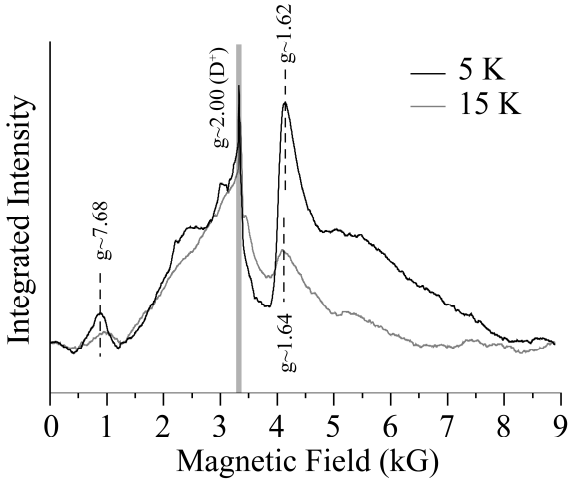

Figure 3

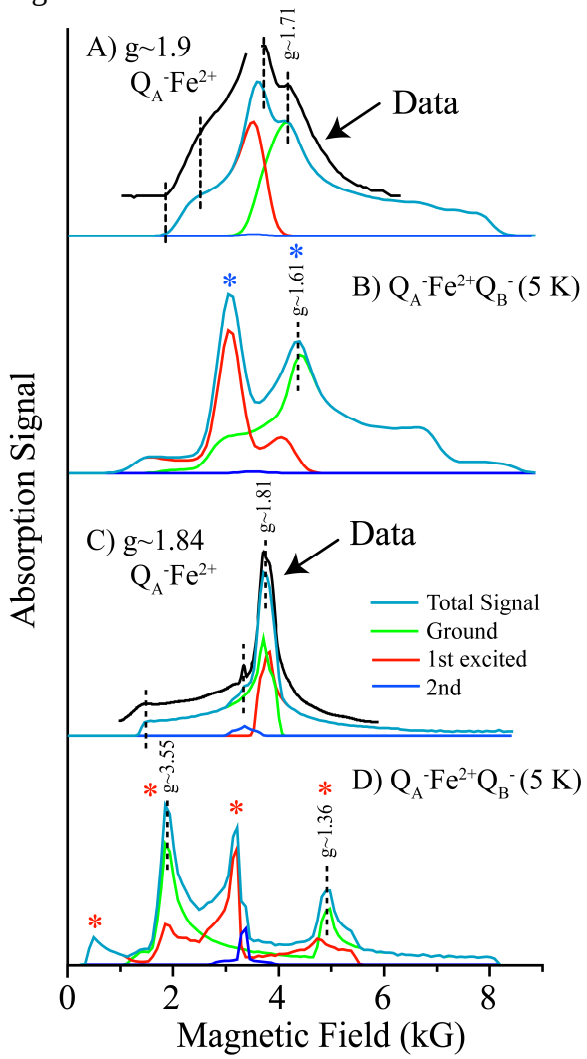

Figure 4

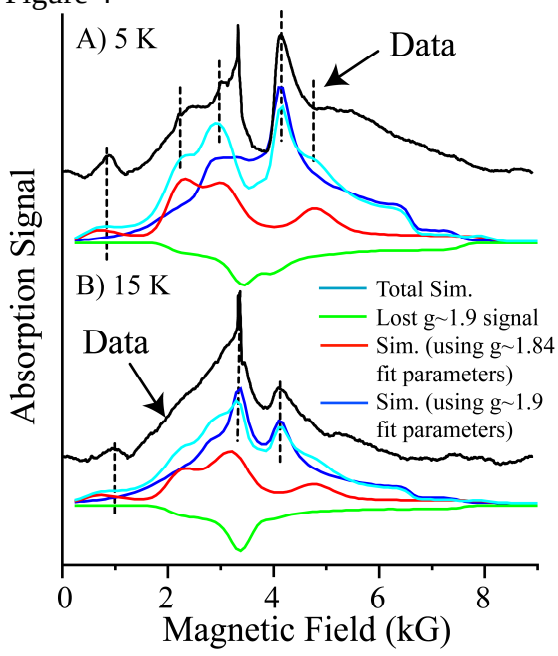

Figure 5

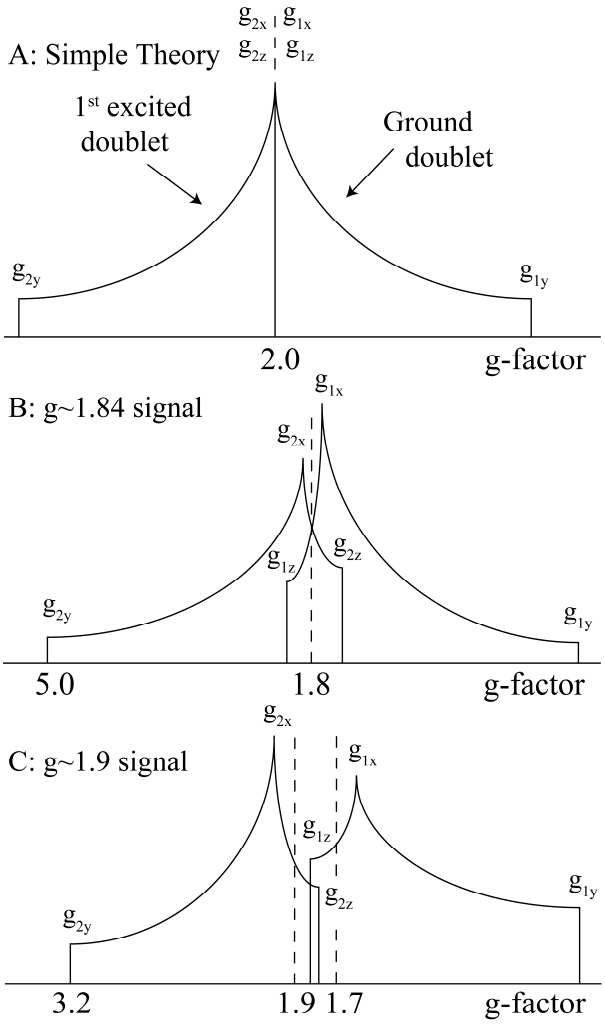
A: Simple Theory
g2x g1x
g2z g1z
1st excited doublet
Ground doublet
g2y
g1y
2.0
g-factor
B: g~1.84 signal
g1x
g2x
g1z
g2z
g2y
g1y
5.0
1.8
g-factor
C: g~1.9 signal
g2x
g1x
g1z
g1y
g2z
g2y
3.2
1.9 1.7
g-factor

Figure 6

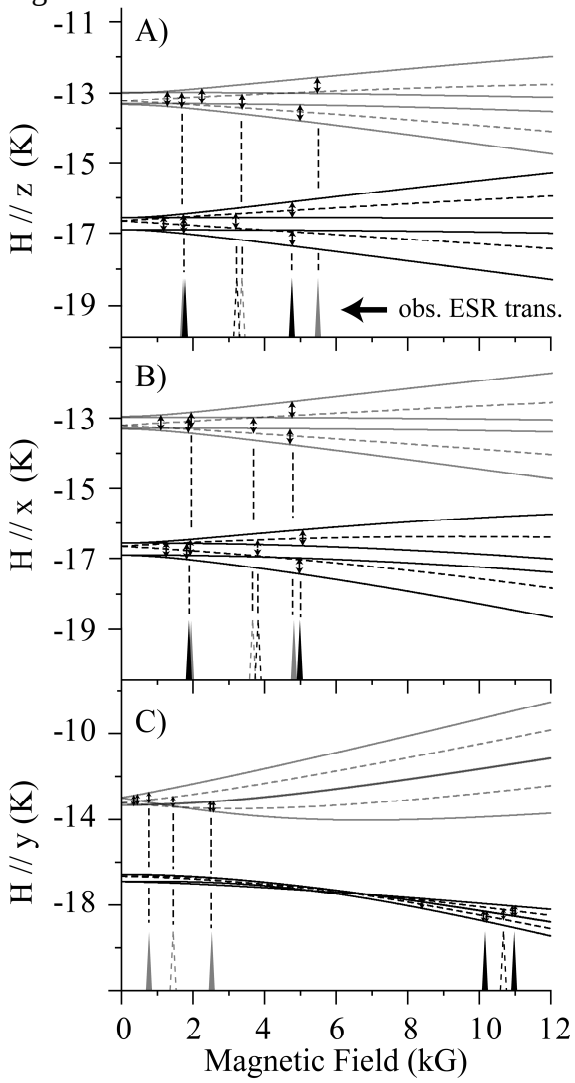
A)
B)
C)
H // z (K)
H // x (K)
H // y (K)
-11
-13
-15
-17
-19
-10
-14
-18
obs. ESR trans.
0
2
4
6
8
10
12
Magnetic Field (kG)

Figure 7

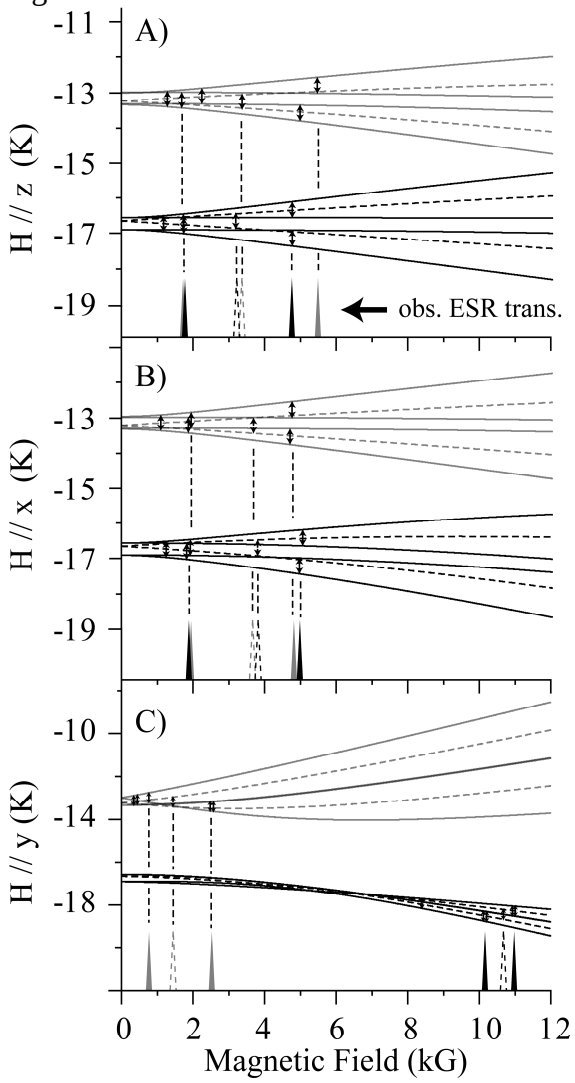
A)
B)
C)
H // z (K)
H // x (K)
H // y (K)
-11
-13
-15
-17
-19
-10
-14
-18
obs. ESR trans.
0
2
4
6
8
10
12
Magnetic Field (kG)

Figure 8

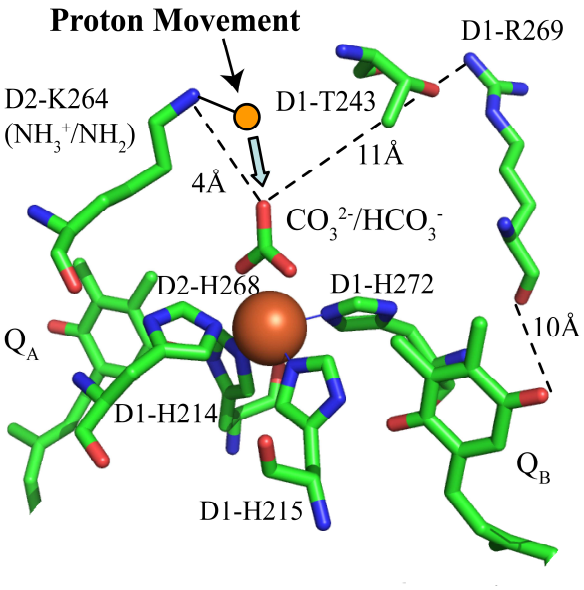
Proton Movement
D1-R269
D2-K264
(NH3+/NH2)
D1-T243
11Å
4Å
CO3 2-/HCO3-
D2-H268
D1-H272
10Å
QA
D1-H214
QB
D1-H215